DEVELOPMENT OF CELLULOSE, HEMICELLULOSE AND CYCLODEXTRIN BASED HYDROGELS FOR THE IN VITRO RELEASE OF BIOMOLECULES AND METAL ION ADSORPTION

A Thesis Submitted in Partial Fulfillment of the

Requirements for the Degree of

DOCTOR OF PHILOSOPHY

By

DEBASHIS KUNDU

DEPARTMENT OF CHEMICAL ENGINEERING

INDIAN INSTITUTE OF TECHNOLOGY GUWAHATI

MARCH, 2019

Indian Institute of Technology Guwahati

Department of Chemical Engineering

Statement

I, hereby declare that the content embodied in this thesis entitled "**Development of Cellulose, Hemicellulose and Cyclodextrin Based Hydrogels for the In Vitro Release of Biomolecules and Metal Ion Adsorption**" is the result of investigations carried out by me at the Department of Chemical Engineering, Indian Institute of Technology Guwahati, Guwahati, India, under the supervision of **Prof. Tamal Banerjee**.

In keeping with the general practice of reporting scientific observations, due acknowledgements have been made wherever the work described is based on the findings of other investigators.

Guwahati,
March, 2019

Debashis Kundu

Indian Institute of Technology Guwahati

Department of Chemical Engineering

Certificate

It is certified that the work presented in the thesis entitled **"Development of Cellulose, Hemicellulose and Cyclodextrin Based Hydrogels for the In Vitro Release of Biomolecules and Metal Ion Adsorption"**, is a bonafide work of **Mr. Debashis Kundu (Roll No. 156107001),** has been carried out in the Department of Chemical Engineering, Indian Institute of Technology Guwahati, under my supervision and this work has not been submitted elsewhere for any other degree.

Prof. Tamal Banerjee,
Professor,
Department of Chemical Engineering,
Indian Institute of Technology Guwahati,
Guwahati-781039, Assam, India.

Dedicated

To

My Late Grand Mother

Mrs. Jyotikana Dutta

1st January, 1942 - 4th January, 2017

Acknowledgement

I take the opportunity to express my sincere gratitude to all without whom my Ph.D. work would not be completed.

At first, I sincerely thank to **Prof. Tamal Banerjee Sir**, Department of Chemical Engineering, IIT Guwahati, for his encouragement, support in bringing fresh idea into the research work. His motivation, constructive suggestions and positive mentorship, encourage me to perform an in depth research during my Ph.D. tenure. Further, his mental support helps me to overcome the social stress during my stay at IIT Guwahati. However, it is impossible to write within a few lines about all the efforts Prof. Banerjee made to complete my research work. I do feel blessed to become a doctorate under his guidance.

I further acknowledge the contribution of my Doctoral Committee members, Prof. Gopal Pugazhenthi Sir (Chairman), Prof. Pallab Ghosh Sir (member, internal) and Prof. Sandip Paul Sir (member, external) for their constructive suggestions and one-on-one discussions regarding my research work. The constructive criticisms they made, during my State of the Art Seminar, Annual Progress Seminars are actually the key moments to explore the in depth research in hydrogel. The criticism regularly followed by the constructive discussions about the future research plan which eventually helped to solidify the research output. Further, I thank my Comprehensive Examination Committee members Prof. Gopal Pugazhenthi Sir, Prof. Pallab Ghosh Sir and Prof. Amit Kumar Sir for a structured comprehensive examination.

I acknowledge the support of my parents, sister and relatives throughout my Ph.D. tenure. I am indebted to my sisters Debjani , Richita, Piku di and Luci di; brothers Soumik and Souvik for bringing smile on my face every time. Word is not enough to mention the contribution of my best friend Anindita during this time. Further, the support of Anindita's family was instrumental in troubled moments of Ph.D. I am blessed to have my little beloved friends Ujjayinee, Chirantan, Aisani and Aishika who always bring happiness into my life with their smile.

I am especially indebted to Supriyo, Abhik, Dr. Abir Ghosh, Piyal, Dr. Prince Kumar Baranwal, Shatrudhan, Nilanjan and Sirshendu for their constant cooperation, motivational talk and mental support in my research carrier. I particularly enjoy the tea time discussion with Supriyo and Abhik which are refreshing moments in the busy

schedule of day to day life. Further, I acknowledge the technical support of Dr. Sankar Chakma, Dr. Sujoy Bose, Dr. Randeep Singh and Dr. Rupak Kishore towards the completion of the work. Further, I acknowledge the support of my undergraduate friends Amit, Gorachand, Partha, Subrata, Arpan, Sandipan and Kamalesh. I acknowledge the cooperation of Dr. Subham Dastidar and Dr. Richa Singhal and happy to express that, I am deeply influenced by their work ethics in research. I thank to my fellow research group mates and fellow researchers of RL-I, II and III for their cooperation and constructive suggestions to my work. I am especially indebted to Dr. Mood Mohan and Papu Kumar Naik for their tireless suggestions and help in understanding various technical features of research. Further, I acknowledge the cooperation of my colleagues, Gaurab, Harish, Priyotosh, Pratik, Dilip, Raunak, Sainiwetha in my research.

Last but not the least, I acknowledge the technical support of faculties and staffs of the Department of Chemical Engineering, staffs and teaching assistants of the Central Instrument Facility, IIT Guwahati, my fellow research scholars, seniors and juniors for their kind help and cooperation towards the successful completion of my Ph.D. tenure. I wish to thank to all well-wishers for being a constant support in my life. I thank to Ministry of Human Resource Development (MHRD) and IIT Guwahati for providing fellowship throughout the PhD program.

Above all, I am grateful to **MOTHER INDIA** who nurture me to be able to emerge as a doctorate.

BHARAT MATA KI JAY

JAI HIND

(DEBASHIS KUNDU)

Synopsis

Hydrogel is a three dimensional polymeric network with high degree of flexibility and contains large amount of water. The polymeric structure originates due to the physical or chemical crosslinking of the precursors. It retains water by hydration, osmotic or capillary forces which are counterbalanced by the forces exerted by the crosslinked structure to retain the network. It resembles extracellular matrix due to the biocompatible nature of constituents, soft and rubbery structure and high water retention capacity. For that, hydrogels are widely used in tissue engineering, cell encapsulation, controlled delivery of drug and biomolecules. Apart from the biomedical applications, the functional moieties of hydrogel poses active binding sites for metal ions and dyes, leading to its application as biosorbent.

Hydrogels are primarily divided into seven classes, namely; (i) origin of precursors, (ii) method of preparation, (iii) nature of crosslinking, (iv) net ionic charge, (v) degradability in the environment as well as various media, (vi) physical properties and (vii) response to external stimuli. As synthesis of hydrogels, selection of precursors and reaction environment are governed by the potential application, the external stimuli is further classified into three categories, namely; physical, chemical and biochemical responsive. Among these classifications, most prominent classification is nature of crosslinking which leads to the tunable physical and chemical properties of hydrogel. The degree of crosslinking is primarily controlled by the feed to crosslinker ratio and amount of solvent.

Cellulose, hemicellulose belong to the polysaccharide family whereas cyclodextrin is an oligosaccharide. The ease of functionalization or chemical crosslinking of hydroxyl moieties present in the backbone of polysaccharides, make them attractive precursor for hydrogel. Microcrystalline cellulose (MCC) is a variant of cellulose, having a degree polymerization approximately 100. MCC has characteristic properties such as non-toxicity, high mechanical strength, low density, large surface area, biodegradability, biocompatibility etc. However, MCC suffers drawback due to incompatibility with most polymeric matrices, poor wettability, insolubility in water and other organic solvents due to inherent crystallinity which limits its use as hydrogel precursor. The various strategies of solubilization of MCC open up the possibility of forming hydrogels from MCC. Carboxymethyl cellulose (CMC) is water soluble derivative of cellulose and is obtained

by partial substitution of hydroxyl moieties with carboxymethyl moiety. Low immunogenicity, high biocompatibility and biodegradability make it potential carrier for controlled release or site specific drug delivery and stimuli responsive hydrogel. Xylan is a heteropolysaccharide consisting of pentoses and hexoses and belongs to the hemicellulose family. It consists of 80-200 β-xylopyranose residues as backbone which are connected by β-(1→4) glycosydic bonds. The xylan based hydrogels have been used as a carrier for drugs and biological macromolecules, biosorbent for organic dyes and metal ions. β-Cyclodextrin (βCD) is a toroid shaped oligosaccharide with seven D-glucose units covalently connected by α-1, 4 - glucosidic linkages. This structural formation makes the exterior of βCD hydrophilic and interior as hydrophobic. These classes of materials have wide applications in sustained and targeted delivery of biomolecules, tissue engineering and medical diagnostics. Copolymerized hydrogels are synthesized using a difunctional crosslinker, namely, Ethylene glycol diglycidyl ether (EGDE). The highly strained epoxide moieties react with the hydroxyl moieties of pyranose ring at high basic medium. However, both the opening of the epoxide ring and crosslinking with pyranose ring must happen simultaneously for a successful crosslinking.

Summary of chapters

Cephalexin is first generation cephalosporin drug and is having similar fundamental structural requirements like penicillin. It is almost completely absorbed from the gastrointestinal tract with a bio availability of 95%. MCC based homopolymerized gel and copolymerized gels with CMC and xylan are synthesized using EGDE crosslinker. MCC-CMC gel has swelling ratio of 160%, 468%, 651% and 664% in artificial gastric fluid (AGF, pH=1.2), artificial intestinal fluid (AIF, pH=6.8), Phosphate Buffer Saline (PBS, pH=7.4) and deionized (DI) water respectively which are higher among the three gels in the respective mediums. The swelling ratio is shown to increase with the pH. The gel fraction follows the opposite trend of swelling ratio whereby MCC gel has the highest gel fraction of 96.98%. A coarse nature is observed in the morphological observation for all hydrogels. Further, the hydrogels produce shear thinning behavior with increasing shear rate. A longer gel point at 64 Hz is observed for MCC-CMC hydrogel, whereas MCC-xylan produces a shorter gel point of 20 Hz. Upto the gel point, elastic nature of hydrogel prevails as determined from the loss tangent. The longer gelation point of MCC-CMC reflects the suitability of MCC-CMC among the three gels. Further MCC-CMC gel shows

a drug loading capacity of 26.48% (±1.15%) which is highest among the three gels. Further, MCC-CMC releases 15% Cephalexin in AGF, 86% in AIF and 98% in PBS respectively. The *in vitro* release study in AIF and PBS reveal initial burst release of Cephalexin due to the swelling of gels followed by a steady release.

Vitamin B_{12} (VB_{12}) is the largest as well as most complex vitamin in the vitamin family and is considered as essential nutrient to human body. It alleviates the symptoms of megaloblastic anemia, allergic asthma and allergic rhinitis. EGDE crosslinked CMC and xylan based homopolymerized hydrogels as well as copolymerized CMC-xylan based gels are synthesized in alkaline medium. Among the five gels, CMC gel possesses highest swelling ratio and xylan gel has the least swelling ratio in AGF, AIF, PBS buffer and DI water. The swelling ratio of CMC gel is 146.58% in AGF buffer and steadily increases to 659.34% in DI water. However, gel fraction follows the opposite trend of swelling ratio i.e. highest gel fraction of 98.63% is obtained with xylan gel while CMC gel produces 85.64% gel fraction. Morphology of CMC and xylan gel appear to be coarse in nature whereas copolymerized CMC-xylan gels are porous in nature. All five hydrogels produce shear thinning behavior upon increasing rate upto 1000 s^{-1}. Further, CMC-xylan gel (1:1 molar ratio) has lower gel point than CMC gel and xylan gel. The longer gel point proves that the copolymerized structure can withstand more stress than pure hydrogels. Further the loss tangent values are less than unity until gel point signifying the elastic nature of hydrogels which dominates over the viscous nature. The dominance of elastic nature concludes the successful crosslinking with EGDE whereby hydrogels can relax the crosslinking structure upto gel point with an influence of external stimuli. CMC-xylan gel (1:1 molar ratio) has least gelation temperature of 317 K and gelation process starts after 5 min. After the gelation, stable hydrogel network is observed upto 353 K. This hydrogel is further proved to have higher VB_{12} loading of 36.59%. Further, the copolymerized gels release 24-28% VB_{12} in AGF, 82-88% in AIF and 96-98% in PBS which are higher than homopolymerized gels. The *in vitro* release profile reflects the initial burst release of VB_{12} followed by the steady release upto 8 hour.

Industrial wastes contain a large quantity of heavy metals which have adverse effect on human and animal health. Nickel (Ni (II)) and cadmium (Cd (II)) are two such toxic contaminants that can cause severe damage in human and aquatic life after being accumulated in high concentrations. *β*CD based four hydrogels are synthesized from *β*CD, CMC, xylan and MCC oligosaccharides, using EGDE crosslinker in alkaline conditions.

The swelling study of synthesized hydrogels are carried out in pH = 2-8 and DI water where water absorbance increases with pH. A highest swelling ratio of 362.53% is observed with *β*CD-CMC gel at pH = 8. All the hydrogels are shown to have better adsorption abilities toward Cd (II) than Ni (II). Overall the *β*CD-CMC hydrogel has proven to be better candidate for adsorbing Cd (II) and Ni (II) among all studied hydrogels. The parameters of adsorption are studied with the variation of adsorbent dosage, concentration of metal ion solution, pH and temperature. The order of adsorption capacity for both the metals is *β*CD-CMC > *β*CD-xylan > *β*CD-MCC > *β*CD gel with all studied parameters. For Cd (II), *β*CD-CMC based hydrogel gives adsorbent capacities of 13.81 mg g^{-1} at 80 mg adsorbent dosage; 24.61 mg g^{-1} at 100 mg L^{-1} initial metal ion concentration; 24.66 mg g^{-1} at the pH = 6 of metal ion solution; 26.42 mg g^{-1} at the 328 K temperature. Similarly, for Ni (II), *β*CD-CMC based hydrogel gives adsorbent capacities of 10.58 mg g^{-1} at 80 mg adsorbent dosage; 15.89 mg g^{-1} at 100 mg L^{-1} initial metal ion concentration; 15.93 mg g^{-1} at the pH = 6 of metal ion solution and 17.29 mg g^{-1} at the 328 K temperature. The toroid shape of *β*CD prevents it from large swelling and thus giving it lesser amount of surface i.e. active binding sites for adsorption. The surface adsorption of metal ions is confirmed by the Langmuir isotherm model with R_L values are less than 1 for all cases, reflecting favorable condition for adsorption. Pseudo second order is proved to be better fitted model for the adsorption process. Further lower amount of increment in the change in enthalpy values lead to conclude the adsorption process is physisorption process involving weak interaction of complex, formed among metal ions and active binding sites.

Apart from these applications, the hydrogels can be used for cationic dye removal and cell encapsulation. A step further of establishing these laboratory scale synthesis procedure is to scale up for possible industrial production by process simulation. Further, molecular level understanding of hydrogel network as well as host-guest interactions with various biomolecules can better be explored with molecular dynamics simulation. These can be taken as future direction from this thesis.

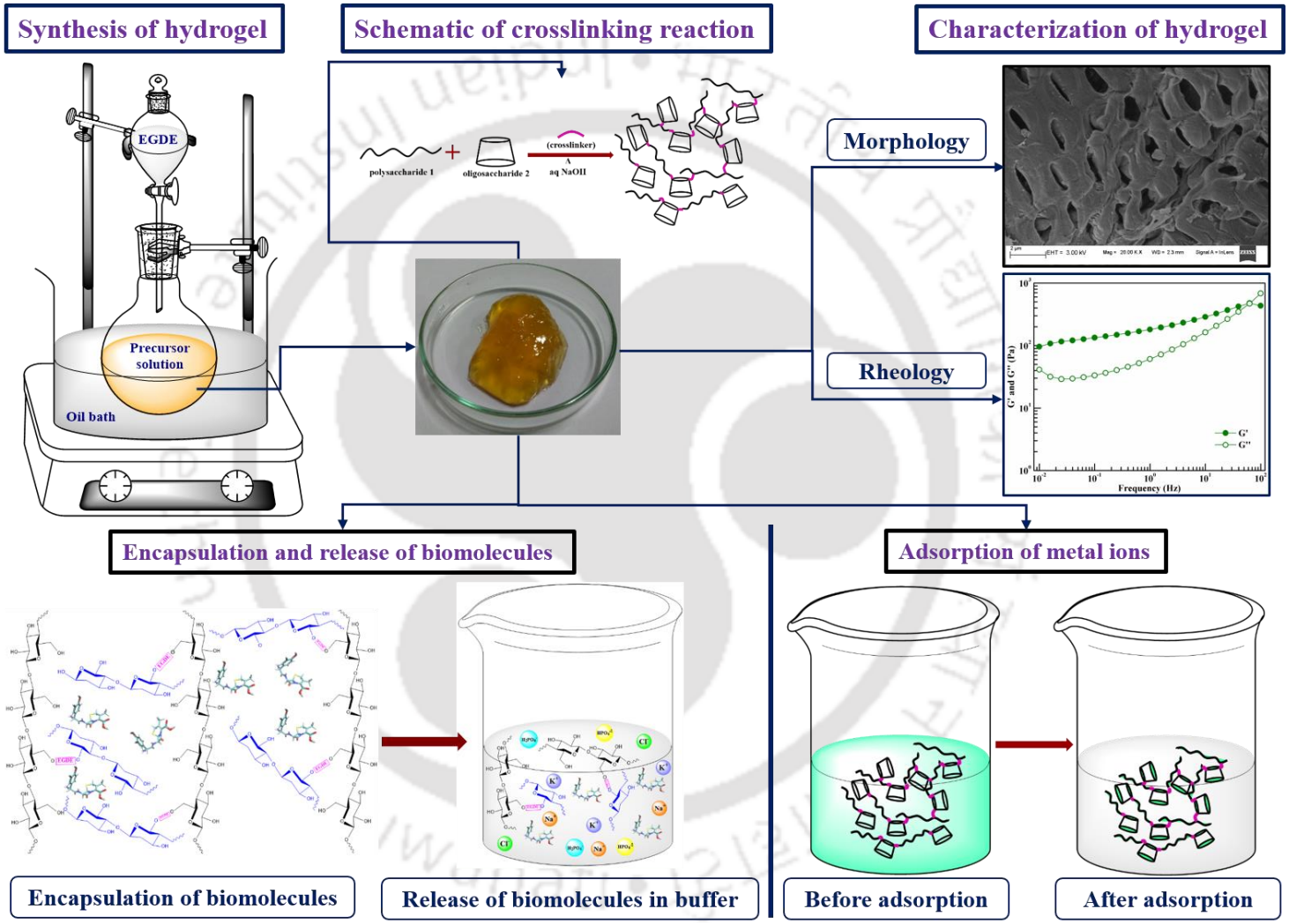

Synopsis Figure. Overview of the thesis

Table of Content

List of Figures

List of Tables

List of Symbols

$G^{'}$	storage moduli (Pa)
$G^{''}$	loss moduli (Pa)
$\tan\delta$	loss tangent
Drug loading	Amount of drug loaded (%)
VB_{12} loading	Amount of Vitamin B_{12} loaded (%)
F_t	The fraction of Cephalexin / Vitamin B_{12} release at any certain time (%)
M_t	Amount of Cephalexin / Vitamin B_{12} release from hydrogel at a certain time (mg)
M_0	Total amount of Cephalexin / Vitamin B_{12} loaded initially (mg)
η	Viscosity (mPa s)
$\dot{\gamma}$	Shear rate
n	Power-law index
m	Consistency index
R^2	correlation coefficient
SR	Swelling ratio (%)
W_{eq}	Equilibrium weight of hydrogel (gm)
W_i	Weight of freeze dried hydrogel (gm)
W_0	Constant weight of hydrogel (gm)
W_1	Measured weight of hydrogel after 72 hour, 333 K (gm)
C_0	Initial concentration of metal ions in solutions (mg L^{-1})
C_e	Equilibrium concentration of metal ions in solutions (mg L^{-1})
C_t	Time resolved concentration of metal ions in solutions (mg L^{-1})
C_{ad}	Concentration of adsorbed metal ions inside hydrogel matrix (mg L^{-1})
V	Volume of metal ions in solution (L)
m	Dry weight of hydrogel (gm)
Removal	Removal efficiency (%)
q_e	Equilibrium adsorption capacity (mg g^{-1})
q_t	Time resolved adsorption capacity (mg g^{-1})
q_m	Maximum adsorption capacity (mg g^{-1})

b	Energy of adsorption and affinity to binding sites (L mg^{-1})
R_L	Equilibrium parameter for Langmuir isotherm (Dimensionless constant)
K_f	Freundlich constants relates to the adsorption capacity
n_f	Freundlich constants relates to the adsorption intensity
R	Ideal gas constant (8.314 J mol^{-1} K^{-1})
T	Temperature (K)
k_1	Pseudo first order rate constant (L min^{-1})
k_2	Pseudo second order rate constant (g mg^{-1} min^{-1})
k_{ad}	Equilibrium constant
ΔH	Change in enthalpy (kJ mol^{-1})
ΔG	Gibbs free energy (kJ mol^{-1})
$\Delta H_{T_1 \to T_2}$	Change in enthalpy from T_1 to T_2 temperature (kJ mol^{-1})
pH_i	Initial pH of the system
pH_f	Final pH of the system
ΔpH	Change in pH of the system
Regeneration efficiency	Ratio of amount of metal ion released by the metal ion loaded hydrogel to the amount of metal ion loaded during desorption phase (%)

List of Abbreviations

MCC	Microcrystalline cellulose
CMC	Carboxymethyl cellulose sodium salt
*β*CD	*β*-cyclodextrin
EGDE	Ethylene glycol diglycidyl ether
CPX	Cephalexin
VB_{12}	Vitamin B_{12}
AGF	Artificial gastric fluid
AIF	Artificial intestinal fluid
PBS	Phosphate Buffer Saline
Ni(II)	Nickel ion
Cd(II)	Cadmium ion
FT-IR	Fourier Transform Infra-Red
FESEM	Field Emission Scanning Electron Microscope
AAS	Atomic Absorption Spectroscopy
DI	Deionized
LVR	Linear viscoelastic region
XPS	X-ray Photoelectron Spectroscopy

Chapter 1

Introduction

Highlights

- Overview of hydrogels
- Overview of precursors
- Potential applications
- Overview of chapters

1.1. Hydrogel

Hydrogels are three dimensional hydrophilic polymer network that can swell due to the presence of large amount of water. They do not dissolve in water rather swell and hold up water more than 90-99% of its mass when placed in an aqueous solution. Natural or synthetic biopolymers often initiate via physical or chemical crosslinking to create network gel. High retention capacity of water and interconnected three dimensional network of hydrogel mimic the extracellular matrix. Additionally, the biocompatible and biodegradable nature of hydrogel makes it suitable for tissue engineering [1], drug delivery [2] and biomedical applications [3]. The shape and volume of hydrogel can be reversibly changed upon various external stimuli such as pH, temperature, light, electric and magnetic fields. Apart from the conventional applications, hydrogels are used in sensors and actuators [4], metal removal [5] and dye removal [6]. Wichterle and Lim first introduce hydrogel in 1960s with the novel paper on poly(2-hydroxyethyl methacrylate) [7].

1.1.1. Hydrogel forming materials

Polysaccharide and oligosachharide are considered as suitable materials for hydrogels because of abundance of hydroxyl groups which can be either physically crosslinked via van der Waals and hydrogen bonding interaction or functionalized by chemical crosslinking. Being naturally abundant, biocompatible and biodegradable, polysaccharides hold advantages over synthetic polymers with respect to the preparation of hydrogel [8]. The well-known natural hydrogel forming materials are cellulose, chitosan and gelatin. Cellulose, the main structural component of plant cell walls, is insoluble in water due to strong hydrogen bonding between hydroxyl groups. Chenite et al. introduced chitosan based thermally responsive hydrogels [9]. Chitosan is derived from the deacetylation process of chitin found in skeletons of invertebrates. Denaturation process of collagen yields gelatin which can be chemically crosslinked with other polymers that are stable at 37 ºC i.e. physiological temperature [10, 11].

Naturally occurring Hyaluronic acid (HA), a high molecular weight linear polysaccharide is often applied in cosmetics and medicine due to its excellent rheological properties, biocompatibility, biodegradability and nontoxicity [12]. Synthetic hydrogels like poly(ethylene-glycol) (PEG) based hydrogels have advantages over natural hydrogels, such

as the ability for photopolymerization, adjustable mechanical properties, and easy control of scaffold architecture and chemical compositions, but PEG hydrogels alone cannot provide an ideal environment to support cell adhesion and tissue formation due to their bio-inert nature [13]. Poly(vinyl alcohol) (PVA) based hydrogels are typically synthesized via freeze-thaw method to densify the macromolecular structure. These hydrogels are widely used in cardiovascular surgery and various other blood-handling procedures [14].

1.1.2. Classification of Hydrogel

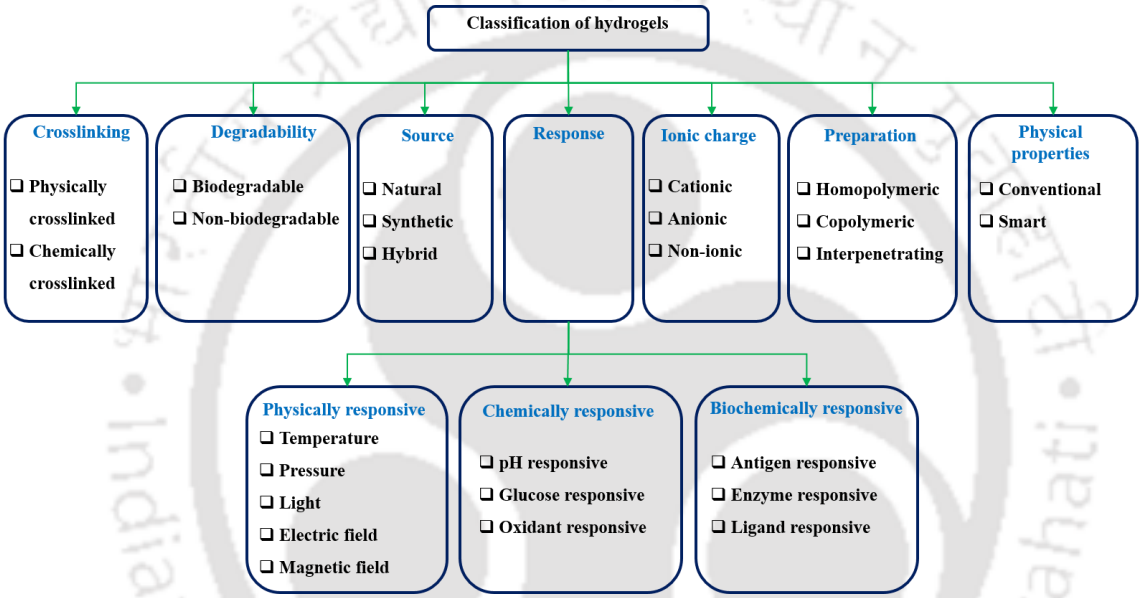

Figure 1.1. Classification of hydrogel

Figure 1.1 represents various classifications of hydrogels based on their source of precursors, preparation procedure, nature of crosslinking, physical properties, net charge of hydrogels, response to external stimuli and ease of degradability [15]. Although seven different types of classifications are shown above, typically hydrogels are classified based on their crosslinking procedure. The degree of crosslinking, which is controlled by the chosen feed to crosslinking ratio and solvent content during preparation, is the most important factor affecting the swelling property of hydrogels. The crosslinking ratio is defined as the ratio of one mole of crosslinking agent to one mole of polymer repeating units. The greater the incorporation of the crosslinking agent into the hydrogel structure, the greater the crosslinking ratio. Highly crosslinked hydrogels have a tighter structure and swell less than the same hydrogels of lower crosslinking

ratio. Crosslinking hinders the mobility of the polymer chain, thereby lowering the swelling ratio. The swelling ratio of hydrogel is also affected by the chemical structure of the polymer. Hydrogel containing hydrophilic groups swell more than those are composed of hydrophobic groups. Hydrophobic groups aggregate, and this leads to collapse of hydrogel structure in the presence of water thereby minimizing their exposure to the water molecule. Physical crosslinking occurs when strong non-covalent bonds i.e. ionic, van der Waals or hydrogen bond interactions are present between constituent macromolecules. Physical hydrogels are mechanically weak and may not be ideal for applications where high mechanical strength is required. Chemical crosslinking involve formation of covalent bond among functional moieties and provide mechanical stability *in vivo* condition.

For the *in vivo* applications, swelling of hydrogels can be controlled by specific stimuli. Temperature-sensitive hydrogels are gels whose properties, especially their equilibrium swelling ratio, vary in response to the change in the temperature of the environment. The influence of temperature on the swelling ratio varies according to the sensitivity of a given hydrogel. Temperature-sensitive hydrogels can be classified into positive and negative thermosensitive types. Positive thermosensitivity hydrogels contain mostly hydrophilic monomers; they increase in swelling with rise in temperature. Negative thermosensitivity hydrogels are composed of monomers such as N-methylacrylamide, N, N-dimethylacrylamide, and N-isopropylacrylamide, which contain hydrophobic substituents; they increase in swelling with decline in temperature. Ionic hydrogels are swollen polymer networks containing pendent groups, such as carboxylic or sulfonic acid, which show sudden or gradual change in their dynamic and equilibrium swelling behavior with the change in external pH. As ionization increases (increased system pH), the number of fixed charges increases, resulting in increased electrostatic repulsions between the chains. This, in turn, results in (i) increased hydrophilicity of the network, and (ii) electrostatic repulsion, and hence greater swelling ratios. In a low pH environment, ionization increases causing increased electrostatic repulsions; as a result, the hydrogel becomes increasingly hydrophilic and swells to an increased level.

1.1.3. Applications of hydrogel

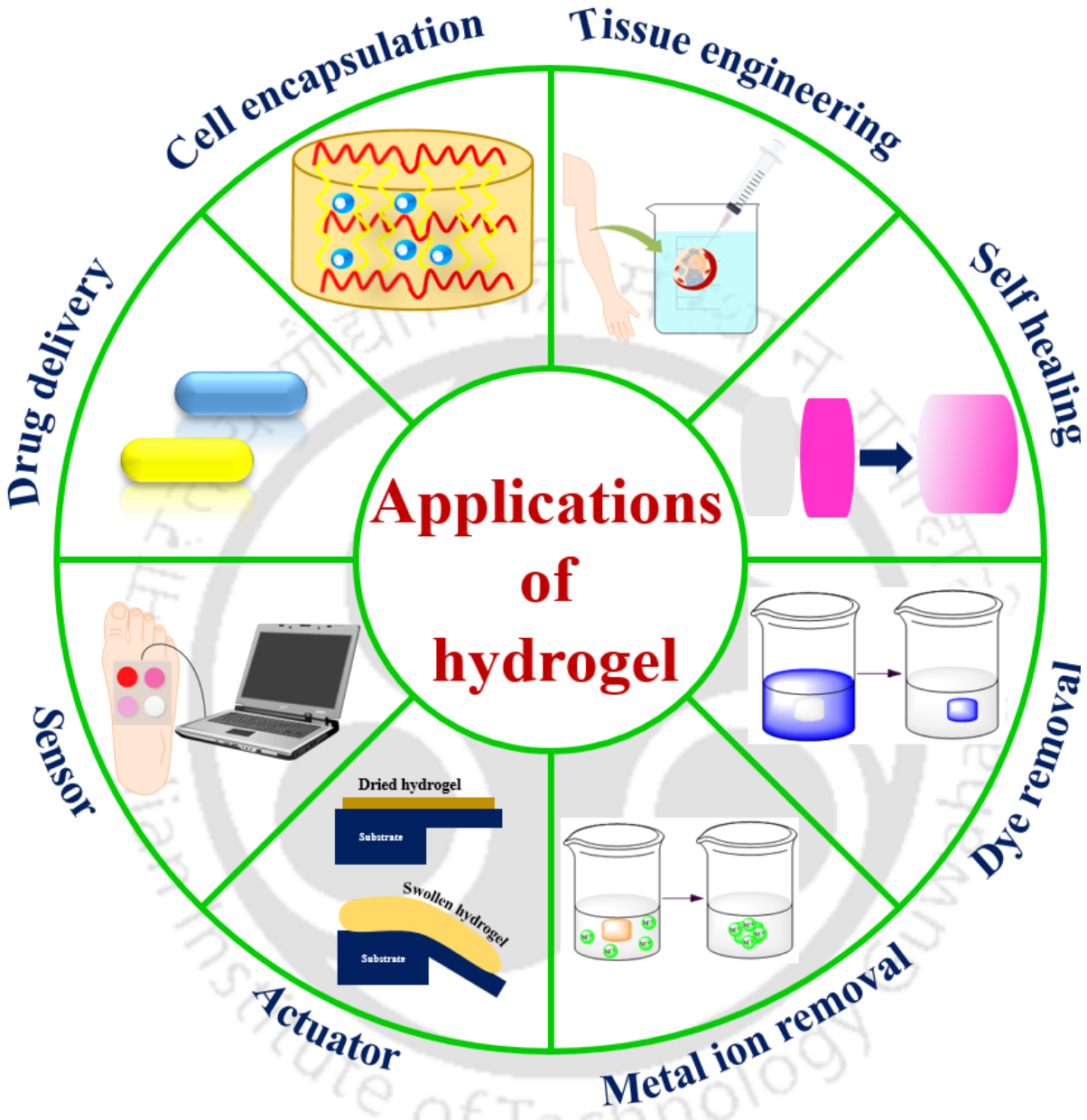

Figure 1.2. Potential applications of hydrogel

Figure 1.2 represents the potential applications of hydrogel. Drug-delivery systems are designed to protect sensitive therapeutic agents such as proteins so as to maintain their integrity until release. The swelling kinetics of hydrogel makes them excellent candidates for the controlled release of drugs or targetable devices of therapeutic agents. It can be classified

as either diffusion controlled or relaxation controlled. When water diffuses into the hydrogel more rapidly than relaxation of polymer chains, the swelling kinetics is diffusion controlled.

Biomolecules such as proteins, peptides are bioconjugated with hydrogels to create biomimetic and functional hydrogels [16]. The bioconjugated hydrogels tune or improve various cellular behavior; thus viewing them for prospective use in tissue engineering and regenerative applications. Polyacralamide based hydrogels have similar properties to that of living tissue, resulting its use as artificial muscles [17], although it suffers the problem of sluggish response. Hydrogels are capable of delivering neurotropic factors and can act as scaffolds to bridge the gap between lesions [18, 19]. These prompted hydrogels use in repair of spinal cord injury. Self-healing is a fundamental property of tissues but most human tissues have limited capacity for regeneration. Applying non-covalent supermolecular chemistry, self-healing hydrogels can be prepared. The self-healing hydrogel has reversible cross-linking network which is initiated via various driving forces such as thermally reversible reaction, ionomeric arrangements and hydrogen bonding interaction [20].

Hydrogels are used in sensing devices such as pH sensor [15], temperature sensor [21]. Further it is used in many indirect sensors such as CO_2 sensor [22], sensors for rheochemical characterization for solutions [23], ion sensors [24] etc. However, hydrogel based sensors suffer problem of selectivity. The biomedical sensors get affected due to the various parameters of human body which are not fully controlled. Ion sensors are also affected by temperature. Hydrogels are also used as actuators employing a combination of sensing-actuating mechanism. The swelling characteristics and soft nature of hydrogels are applied to control the fluid flow and minimize the leakage [25].

Hydrogels have abundance of hydrogel and amine moieties which can easily bind with the transition metals. Thus hydrogels are widely used as biosorbent for wastewater treatment. The adsorption mechanism is governed by the various phenomena such as adsorption on surface, diffusion, complexation etc. The metal ions typically bind with the active binding sites of hydrogel and thus are removed. Common metal pollutants such as lead, copper, zinc, nickel, cadmium are adsorbed by cellulose, chitosan, polyacrylamide, pectin and graphene

oxide based hydrogels [5]. Like heavy metal ions, industrial dyes cause significant damages in human, animal and aquatic lives. Hydrogels are successfully employed for the removal of dyes such as methylene blue, congo red, crystal violet etc [26].

1.2. Cellulose, hemicellulose and cyclodextrin

Plant biomass is widely considered as the potential bio-factory for the generation of various types of polysaccharides [27]. Cellulose, hemicellulose belong to polysaccharide family whereas cyclodextrin is an oligosaccharide. Polysaccharides are renewable natural polymer possessing the advantages such as being nontoxic, biocompatible, biodegradable and naturally abundant. Monosaccharide subunits connected with intermediate linkages form polysaccharides. They are essentially an elaborate form of carbohydrate polymers, naturally found in plants, microbes and animal sources. The ease of functionalization or chemical crosslinking of hydroxyl moieties present in the backbone of polysaccharides, make them attractive precursor for hydrogel. Cellulose is a natural biopolymer, homopolysaccharide in nature with linearly ordered β-(1→4)-linked D-anhydroglucopyranose repeating units and found in plants, bacteria, fungi and sea animals [28]. It is water insoluble, stable and fibrous polysaccharide and plays a vital role in structural organization, tensile strength and plant growth. Plant cellulose possess a degree of polymerization of on order of 10,000 and approximately 40-45% of wood by weight.

Like cellulose, hemicellulose with hydroxyl groups is considered to play a central role in mechanical properties of plant cell wall and is the second most abundant material found in woods after cellulose. Hemicellulose is soluble in alkali and has lower degree of polymerization (~200 residues) than cellulose. They are heteropolysaccharides with various types of hexose and pentose sugar and are amorphous in nature. There are four subclasses of hemicellulose, namely; xyloglycans (xylans), mannoglycans (mannans), xyloglucans and mixed-linkage β-glucans [29]. Among the four, xylan constitutes of 25-35% of hemicellulose class [30] and is found in hard wood species. Cyclodextrins are also known as cellulosine because of similar chemical behavior to cellulose i.e. the absence of reducing power and resistance towards hydrolysis. [31] It is first reported by Schardinger et al. [32] and generally produced by the bacterial enzymatic degradation of starch [33].

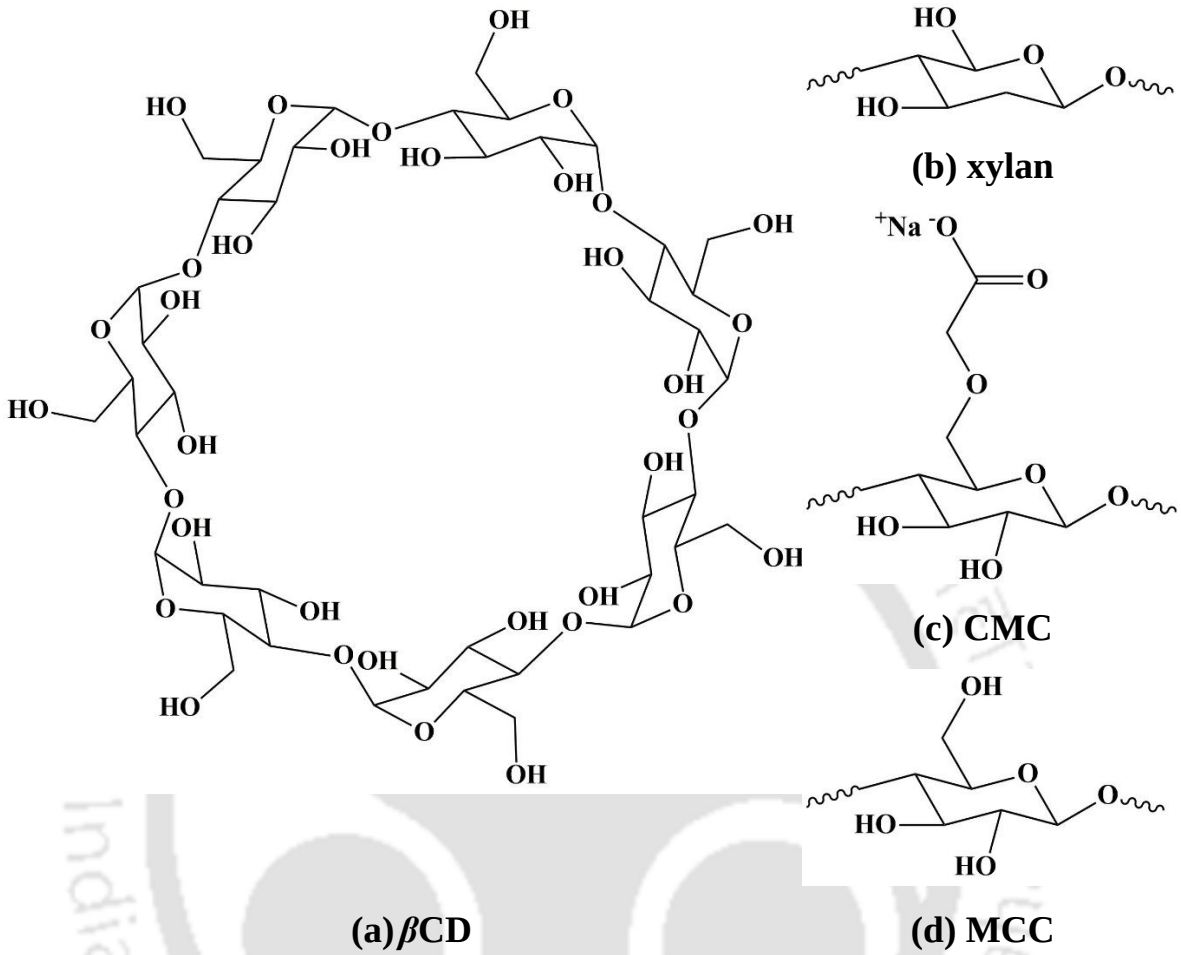

Figure 1.3. Structure of polysaccharides. (a) *β*CD [31], (b) xylan [34], (c) CMC [35], (d) MCC [36].

1.2.1. Microcrystalline cellulose

A prominent class of cellulose is microcrystalline cellulose (MCC), having a degree polymerization of approximately 100. The treatment of alpha cellulose with excess amount of mineral acids, yields MCC which has a reduced number of degree of polymerization of cellulose and hence has shorter polymeric chains. MCC has characteristic properties such as non-toxicity, high mechanical strength, low density, large surface area, biodegradability and biocompatibility. The fascinating mechanical and chemical properties drew attention from scientific community as well as various industries. MCC is widely used as thickener, binder

and adsorbent in pharmaceutical and cosmetic industries; gelling agent, stabilizer and anticaking agent in food and beverage industries [37]. In addition to the advantages, MCC suffers drawback due to incompatibility with most polymeric matrices, poor wettability, insolubility in water and other organic solvents due to inherent crystallinity. However, crystallinity of cellulose limits its application because of insolubility in water and common organic solvents. However, various polar solvents such as ionic liquid, deep eutectic solvent and alkali aqueous system [38] can potentially solubilize MCC. The various strategies of solubilization of MCC open up the possibility of forming hydrogel from MCC. This enables cellulose based hydrogels to be prepared from cellulose solution via chemical or physical crosslinking process. Another approach to prepare cellulose based hydrogels is too partially or fully substitute hydroxyl groups with water soluble moieties like carboxymethyl etc.

1.2.2. Carboxymethyl cellulose

Carboxymethyl cellulose (CMC) is water soluble derivative of cellulose and is a linear polymer. It is obtained by partial substitution of hydroxyl groups with carboxymethyl groups [39]. It is conveniently produced by the alkali-catalyzed reaction between cellulose and chloroacetic acid. Low immunogenicity, high biocompatibility and biodegradability make it a potential carrier for controlled release or site specific drug delivery [40, 41]. For that, it has approval from FDA for biomedical applications [42]. CMC is also used as precursor for stimuli-responsive hydrogel. CMC is neither a part of human cell signaling cascade nor degradable by human enzymes. The CMC based hydrogels are long been used as carrier for drugs and biological macromolecules [43]. Crosslinked CMC is known to absorb large amount of water to form biocompatible and pH sensitive hydrogel [44]. CMC based hydrogels are further known to show excellent dynamic viscoelasticity [45]. Apart from biocompatible and pH sensitive hydrogels, CMC is used in food products (as thickener and emulsion stabilizer), non-food products such as diet pills, tooth pastes, laxatives, water based paints, paper products, detergents (as binder) and biomedical domain [46].

1.2.3. Xylan

Xylan is a heteropolysaccharide consisting of pentoses and hexoses. It belongs to the hemicellulose family and found in most abundant quantity in the family. Xylan consists of 80-

200 β-xylopyranose residues as backbone which are connected by β-(1→4) glycosydic bonds [47]. Further it contains 10% 4-O-methyl-D-glucoronic acid and β-1,4-D-xylopyranosyl units as backbone [48]. Xylan is obtained from hard wood by alkali extraction method. Like cellulose, hemicellulose as well as xylan can be easily functionalized due to abundance in hydroxyl moiety. It creates suspension in water but are soluble in hot alkaline water. The gel and film forming properties of hemicellulose coupled with the biocompatible and biodegradable nature, find wide range of application in biomedical applications, drug delivery and as adhesive, coating and additive in pharmacy, food industries [49]. Additionally, multiple stimuli, such as organic solvent, ion and pH sensitive xylan-based gels have gained recent attention [50]. The xylan based hydrogels have been used as a carrier for drugs and biological macromolecules [51], bioadsorbent for organic dyes and metal ions [52, 53]. The various subclasses of hemicellulose are used as thickener, emulsifier, coatings and additives in paper, food and pharmaceutical industries [54, 55].

1.2.4. β-Cyclodextrin

Cyclodextrins (CD) are toroid shaped oligosaccharides with a six, seven, eight D-glucose units, and are covalently connected by α-1, 4-glucosidic linkages. Depending upon the number of units, they are classified as α- (6 units), β- (7 units) and γ- (8 units) CD. Primary hydroxyl groups of CD are located at the narrower i.e. primary face and secondary hydroxyl groups are located at the wider i.e. secondary face [56]. This structural formation makes the exterior of CD hydrophilic and interior as hydrophobic. Unmodified βCD has lower aqueous solubility than αCD and γCD. CDs are found as extensive uses in pharmacy, textile, food and packaging industry. Due to its economic benefits it is used in analytical sciences, separation processes and catalysis due to their capability in forming inclusion complexes [31]. CDs and its derivatives are often employed to build polymeric building blocks and assemblies such as nano and microparticles, hydrogels and micelles etc [31]. These classes of materials have wide applications in sustained and targeted delivery of biomolecules, tissue engineering and medical diagnostics [56].

1.3. Crosslinker

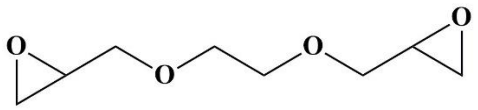

Figure 1.4. Structure of ethylene glycol diglycidyl ether [57].

Ethylene glycol diglycidyl ether (EGDE) is a difunctional crosslinker having two epoxide moieties at both ends [57]. Due to the presence of high strains in the epoxide ring, these ethers are more reactive than other ethers. The opening of the epoxide ring and reaction with hydroxyl moieties of pyranose ring occur in high basic medium [35]. However for successful crosslinking, both the opening of epoxide ring and crosslinking with polysaccharide/oligosaccharide must happen simultaneously. Alsheri et al. reported the synthesis of CMC-PVA based hydrogel using EGDE crosslinker [58]. The same crosslinker has been used by Kono et al. to synthesize βCD-CMC based hydrogel [35]. A number of gelatin based hydrogels are also reported using EGDE [57, 59].

1.4. Hydrogels based on cellulose, hemicellulose and cyclodextrin

MCC based hydrogels are relatively less explored in the literature whereas abundant literature is found with CMC based hydrogels. Choe et al. reported pure MCC based hydrogel after dissolving in tetrabutylammonium fluoride/dimethyl sulfoxide solvent and subsequent adjustment in viscosity [60]. Conductive hydrogel is being reported by dissolving MCC in ionic liquid and further aided by polypyrrole [61]. Thiol-ene click chemistry based MCC hydrogels are prepared by exposing the allyl functionalized MCC into UV exposure [36]. However, to this date, the applications of MCC based hydrogels are not explored in the literature.

However, CMC based database of hydrogel is enormous and is difficult to shorten the entire literature in a single paragraph. Therefore, a handful number of them are discussed here. Apart from the conventional drug delivery, biomedical applications and pollutant removal, CMC based hydrogels are used in targeted delivery of fertilizers [62], release of insecticide [63], shape memory [64] and self-healing material etc. [65]. CMC based hydrogels can be

formed by both physical as well as chemical crosslinking. With γ-ray irradiation, CMC based hydrogels are prepared with high degree of substitution [66]. The electron beam irradiation mediated supersorbent CMC-acrylamide based hydrogels are reported by Ibrahim et al [67]. Apart from high energy radiation, blending of CMC with other polymers such as PVA, have been proven as an effective strategy to synthesize hydrogel. Due to the presence of carboxymethyl moiety, CMC is a negatively charged polyelectrolyte. CMC-Chitosan is reported to be crosslinked with glutaraldehyde to form conducting hydrogel [68]. CMC based semi-IPN hydrogels are prepared with poly(acrylic acid), as a second network gel [69].

Hemicellulose based hydrogels have drawn renewed attention in recent years despite being first reported by Gabrieli and Gatenholm almost two decades ago [70]. They are prepared by both physical and covalent crosslinking. Freeze-thaw technique is applied to prepare hemicellulose-PVA hydrogel for tissue engineering applications [71]. However, hemicellulose based hydrogels suffer from relatively poor mechanical integrity [72]. To overcome this, Maleki et al. synthesized full interpenetrating hemicellulose hydrogel by free-radical polymerization and thiol-ene click reaction [73]. Daz et al. have employed trans-estarification reaction to synthesize hydrogel with hemicellulose and glycidyl methacrylate for the removal of arsenic and chromium from aqueous solution [53]. Hemicellulose based hydrogels are further prepared by thiol-ene click chemistry [74].

The CD based hydrogels are prepared in three major ways, namely; i) grafting of CDs to preformed polymer networks, ii) direct crosslinking of CDs,and iii) copolymerization of CDs with vinyl and acrylic co-monomers [75]. Further, the crosslinking is divided into physical, covalent and sliding-ring i.e. topologically interlocked. CDs form inclusion complex with the guest molecules (drug, biomolecule, metal ions etc.) The crosslinked mesh of hydrogel prevents the leaching of CD upon entering into the physiological fluids. Therefore the covalently linked CDs have limited flexibility and the delivery of drugs or biomolecules is thus depends on the interaction of drugs with physiological buffers. The adsorption of metal ions by CD is typically performed by ion exchange process. The abundance of hydroxyl moieties put water molecules and metal ions in competition to bind with the adsorption sites.

1.5. Applications in the field of delivery of biomolecules and removal of metal ions

1.5.1. Delivery of Cephalexin

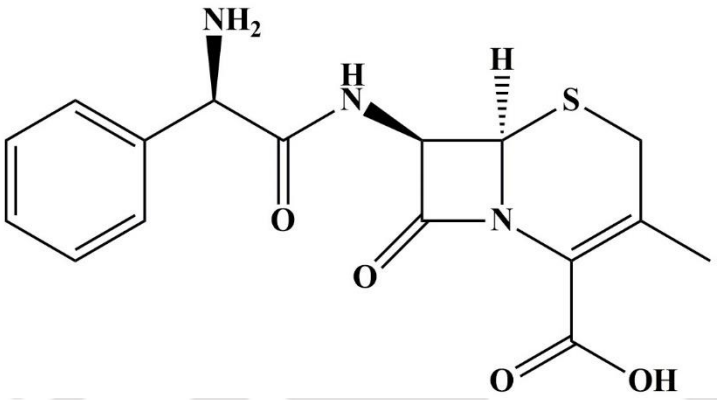

Figure 1.5. Chemical structure of Cephalexin [76].

Cephalexin is the first generation cephalosporin drug which belongs to lactum antibiotics and is having similar fundamental structural requirements like penicillin. It is a semisynthetic antibiotic derived from cephalosporin and is almost completely absorbed from the gastrointestinal tract with a bio availability of 95% [76]. The half-life of Cephalexin is approximately 1.1 hour and is prescribed 3-4 times a day to maintain therapeutic range [77]. The structure of the molecule is similar to the acid-base molecule because of presence of –NH_2, -CONH and –COOH moieties. Cephalosporins are most prescribed antibiotics and are considered as safest and most effective broad spectrum bactericidal antimicrobial agents [77]. By inhibiting the synthesis of essential structural components of bacterial cell wall, they prevent the infections due to gram-positive and gram-negative bacteria. It belongs to lactum antibiotics having similar fundamental structural requirements as penicillin.

Limited studies of release of Cephalexin by hydrogels are being reported in the literature. The Cephalexin delivery of hydrogel formed by 2-hydroxyethyl methacrylate, itaconic acid and poly (alkylene glycol) methacrylates is reported by Tomic et al [78]. Barkhordari and Yadollahi reported enhanced protection and controlled liberation of Cephalexin drug in intestinal tract using CMC encapsulated layered double hydroxide-drug nanohybrids [76].

1.5.2. Delivery of Vitamin B_{12}

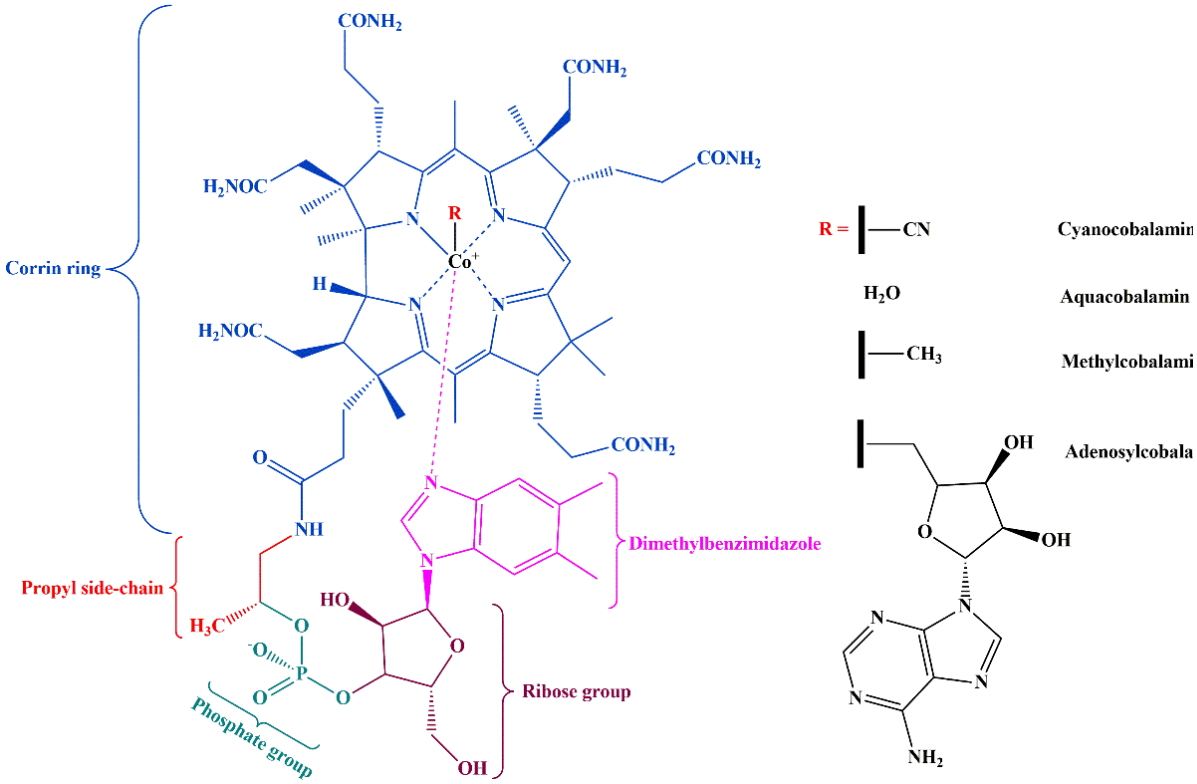

Figure 1.6. Structure of VB_{12}. [79]

Vitamin B_{12} (VB_{12}, cyanocobalamin) is the largest and most complex in the vitamin family. It is an organometallic compound containing cobalt within a corrin ring. The main residues are given as, corrin ring, propyl side-chain, ribose group and dimethylbenzimidazole. Due to its low bioavailability (recommended 1-5 μg per day), it is considered as essential nutrient. Certain bacteria produce VB_{12} in which is available in different forms. The different chemical structures of cyanocobalamin and its derivatives are shown in Figure 1.6. Two of the major active forms are methylcobalamin and adenosylcobalamin. Methylcobalamin is needed by methionine synthase to produce the amino acid methionine from homocyestine whereas adenosylcobalamin is used as a cofactor by methylmalonyl-coenzyme A to produce succinyl coenzyme A. This eventually enters the tricarboxylic acid cycle [79]. Aquacobalamin bears a neutral ligand, that results in a positively charge molecule and is therefore always

accompanied by a counter anion [80]. The deficiency of cobalt in human is treated with the controlled release of VB_{12} which increases the concentration level of cobalt in blood serum and liver. The ribose group plays an importamt role in synthesis of nucleic acid and reduction of ribonucleotides to deoxyribonucleotides. Jin et al. reported that VB_{12} is prescribed to alleviate the symptoms of megaloblastic anemia, allergic asthma and allergic rhinitis [81]. Further, the sustained level of VB_{12} also eases pain associated with carpal tunnel syndrome. The deficiency can lead to weakness, fatigue, constipation and other neurological malfunctions [82].

Moderate number of literature is available for the controlled release of various vitamins including VB_{12}. The earliest reported VB_{12} release is by using poly(*N*-vinyl-2-pyrrolidone) crosslinked polyacrylamide and acrylic acid based hydrogels [83, 84]. More recent investigation on diffusion mechanism of VB_{12} was studied by Jin et al. [81] using poly (acrylic acid) and copolymeric acrylic acid and *N*-vinyl pyrrolidinone based hydrogels. Further Maheswari et al. investigated the release profile of VB_{12} using poly(*N*-isopropylacrylamide-co-*N*-vinyl-2-pyrrolidinone) thermosensitive hydrogels [85]. Carboxymethyl cellulose based hydrogels are recently been explored for the release of VB_{12}. Boruah et al. reported the *in vitro* release of VB_{12} using CMC grafted poly(acrylic acid) and organophilic montmorillonite nanoclay composite hydrogel [86]. Further Nath et al. reported CMC grafted poly(acrylic acid) and layered double hydroxide hydrogels for the *in vitro* release study of VB_{12} [87]. Multiresponsive xylan based hydrogel is also reported by Cao et al. for the release of VB_{12} [88]. The hydrogel is formed with xylan type hemicellulose methacrylate and 4-[(4-acryloyloxyphenyl)azo]benzoic acid using free radical copolymerization method.

1.5.3. Adsorption of Ni (II) and Cd (II)

Industrial wastes contain a large quantity of heavy metals like cadmium, nickel, chromium, lead, mercury, zinc and copper. The toxic nature of heavy metals adversely affects human and animal health. Traditional methods of removing pollutants from wastewater are ion exchange, chemical precipitation, electrochemical removal, membrane separation, coagulation, flocculation and adsorption [89]. Adsorption is a preferable treatment method due to high efficiency, simplicity in design and low cost. Biopolymers such as hydrogels are newest

entrants as adsorbent in wastewater treatment. Presence of various functional groups such as hydroxyls, amines, amides, carboxylates etc. increases the efficiency of metal ion uptake and thus ensures maximum removal. Nickel (Ni (II)) and cadmium (Cd (II)) are toxic contaminants that can cause severe damage in human and aquatic life after being accumulated in high concentrations. Common source of cadmium is battery, coating and painting industry [90-92]. It is carcinogenic, causes iron deficiency [93] and accumulates in liver and kidney [94]. Nickel comes out as pollutant from electroplating, metal finishing and battery industry. Further it causes problems in lungs and kidney. Adsorption behavior depends on the various parameters such as ionic concentration, pH, contact time and temperature. In recent years, acrylate [95], acrylamide [96], alignate [97], PVA [98] and chitosan [99] based hydrogels are used to remove Ni (II) and Cd (II) from wastewater.

Cellulose based hydrogels are widely used for wastewater treatment [100]. Microcrystalline cellulose based hydrogels loaded with Manganese dioxide (MnO_2) are used to remove lead from wastewater [101]. Carboxymethyl cellulose based hydrogels like polyvinyl alcohol – CMC [98], CMC-sodium alignate [97] are used to remove Ni (II). Unlike cellulose, limited studies consisting of O-acetyl galactoglucomannan based hydrogels are available for the removal of heavy metals such as Ni (II) and Cd (II) [102]. βCD based hydrogels such as βCD-acrylic acid and silica-glycidyl methacrylate – βCD acryloyl chloride are reported for the removal of heavy metals, mainly Ni (II) and Cd (II) [103]. Considering the literature, no detailed adsorption study based on polysaccharide-cyclodextrin crosslinked hydrogels are reported. Thus we presume, βCD based hydrogels crosslinked with cellulose and hemicellulose will be an appropriate study for the adsorption of metal ions.

1.6. Objectives of the thesis

(a) Synthesis and characterization of various forms of cellulose and hemicellulose hydrogels as well as copolymerized cellulose-hemicellulose based hydrogels.

(b) Synthesis and characterization of *β*-cyclodextrin based crosslinked hydrogels copolymerized with various forms of cellulose and hemicellulose.

(c) Encapsulation and *in vitro* release of biomolecules by the synthesized hydrogels.

(d) Removal of metal ions from the aqueous solution by the synthesized hydrogels.

1.7. Overview of the chapters

The objectives outlined in the previous section, are performed through the synthesis and purification of hydrogels. The purified hydrogels are characterized by both physical and chemical characterization. Therefore, the hydrogels are employed to encapsulate followed by the *in vitro* release of model vitamin and drug (biomolecules); and adsorption of metal ions. These experiments are described in upcoming three chapters whose summary are given in the ensuing sections.

1.7.1. Chapter 2: Synthesis, characterization of microcrystalline cellulose based hydrogels and *in vitro* release of Cephalexin

In this chapter, three hydrogels namely MCC gel, MCC-CMC gel and MCC-xylan gel are synthesized using EGDE as crosslinker. MCC-CMC gel and MCC-xylan gel are prepared in 1:1 molar ratio. The hydrogels are characterized by Fourier Transform Infra-Red (FT-IR) spectroscopy. Swelling ratio at various pH and gel fraction are determined for the physical characterization of the gel. The morphology of the gels are observed in optical microscope and field emission scanning electron microscope (FESEM). Rheological behavior of the as synthesized hydrogels are further reported at 298 K in cone and plate rheometer. The viscosity of the gels are measured within a wide range of shear rate. Further, gel point of hydrogels are determined by the frequency sweep method. Cephalexin has been used as a model drug to be loaded in the hydrogels. The *in vitro* release of cephalexin is carried out in artificial gastric fluid (AGF, pH = 1.2), artificial intestinal fluid (AIF, pH = 6.8) and phosphate buffer saline (PBS, pH = 7.4).

1.7.2. Chapter 3: Synthesis, characterization of carboxymethyl cellulose-xylan based hydrogels and *in vitro* release of Vitamin B_{12}

In this chapter, pure CMC, pure xylan hydrogels and CMC-xylan hydrogels are synthesized in different molar ratio using EGDE crosslinker. The hydrogels are characterized by FT-IR spectroscopy and morphology of the hydrogels are viewed by optical microscope and FESEM. Rheological behavior of the as synthesized hydrogels is performed at 298 K. By varying the shear rate in wide range, the viscosity of the gels are measured. Frequency sweep is used to observe the detailed viscoelastic behavior of the gels as well as to measure the gel point of hydrogels. Thereafter, temperature sweep is performed to identify the gelation temperature while the time sweep determines the gelation time. Swelling ratio at various pH and gel fraction are determined as physical characteristics of the gel. VB_{12} is used as model vitamin to be loaded in the hydrogels. The *in vitro* release behavior is observed in AGF, AIF and PBS respectively. Further the composite hydrogels are compared with the pure hydrogels in the release of VB_{12}.

1.7.3. Chapter 4: Synthesis, characterization of *β*-cyclodextrin-cellulose/ hemicellulose based hydrogels for the removal of Cd (II) and Ni (II)

In this chapter, four *β*CD-cellulose/hemicellulose based hydrogels, namely *β*CD-xylan, *β*CD-CMC, *β*CD-MCC, *β*CD gel are synthesized using EGDE crosslinker. The synthesized hydrogels are characterized with FT-IR spectroscopy and X-ray Photoelectron Spectroscopy. Further, the physical characterization of hydrogels are performed by swelling study at varying pH and measurement of the gel fraction. Morphology of hydrogels are then visualized though optical microscopy and FESEM instruments. The synthesized hydrogels are used as adsorbent to adsorb Cd (II) and Ni (II) from aqueous solution. The Cd (II) and Ni (II) loaded hydrogels are then visualized by fluorescent microscopy. Atomic Absorption Spectroscopy (AAS) is used to measure the concentration of the metal solutions. The equilibrium concentration data will then reveal the nature of adsorption by comparing the Langmuir and Freundlich isotherms. Time resolved adsorption study will also reveal the kinetics of adsorption i.e. elucidating the adsorption mechanism by hydrogels.

1.7.4. Chapter 5: Concluding remarks & future scope

In this chapter, the key conclusions from the synthesis, characterization and applications using the hydrogels, will be summarized. Apart from the applications attempted in this thesis, the hydrogels can be used in various other applications. These applications will be the key future directions from this thesis.

Chapter 2

Synthesis, characterization of microcrystalline cellulose based hydrogels and *in vitro* release of Cephalexin

---

Highlights

- Synthesis of Microcrystalline cellulose based hydrogels
- Characterization by FT-IR spectroscopy, morphology and swelling studies
- Rheology of hydrogels
- *In vitro* release of Cephalexin in various physiological buffers

Keywords

A. Microcrystalline cellulose;
B. Hydrogel;
C. Rheology;
D. Cephalexin.

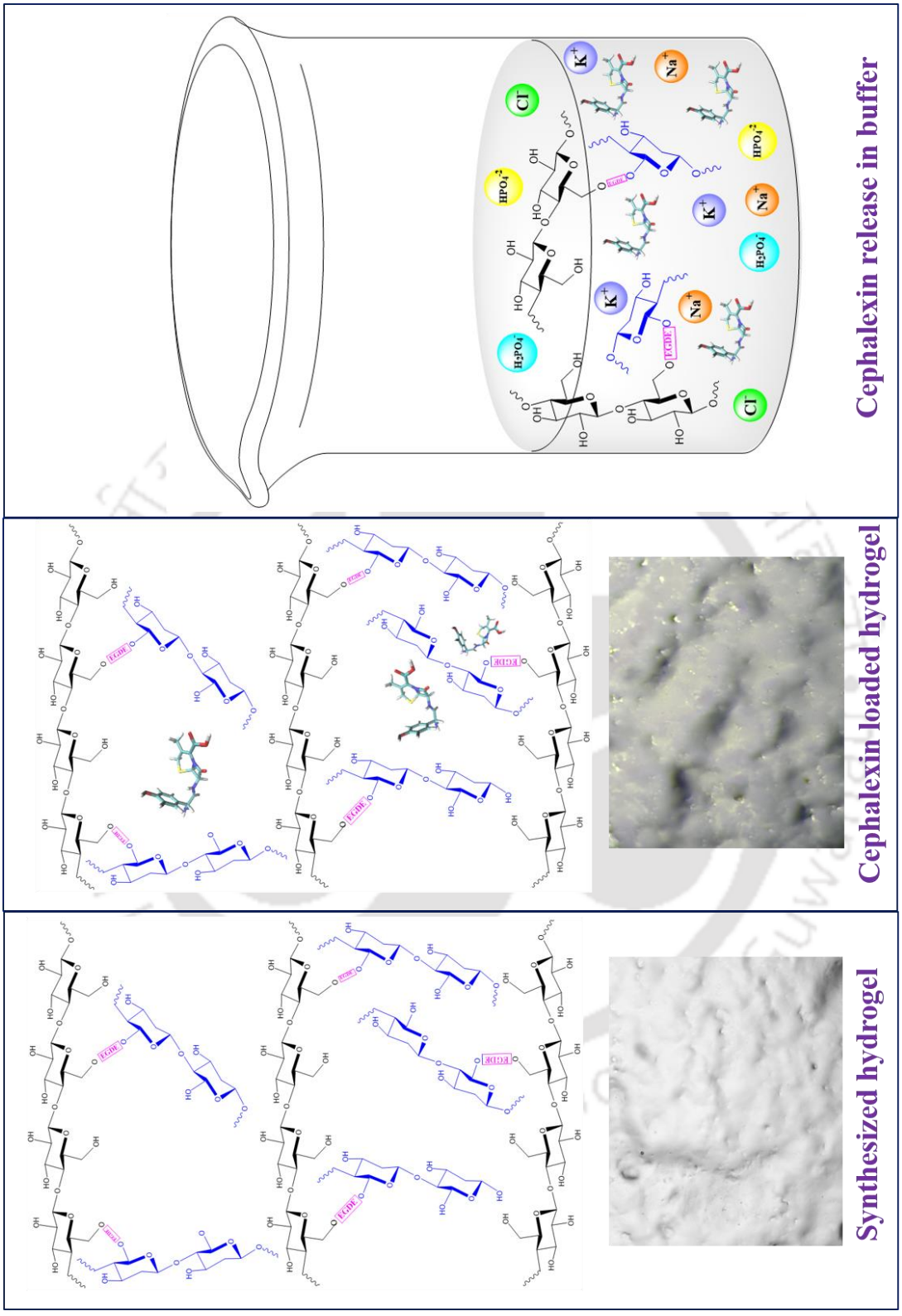

Figure2.1. Pictorial representation of encapsulation of drug followed by its release in buffer solution.

2.1. Chapter summary

Three hydrogels namely, MCC, MCC-CMC and MCC-xylan are synthesized using EGDE as crosslinker. For the chemical characterization, FT-IR spectroscopy is adopted, whereas swelling ratio and gel fraction are used for the physical characterization of the hydrogels. The morphological observation are performed in optical microscope and FESEM. The rheological characterization of the synthesized hydrogels elucidates the flow behavior of the gels in wide shear rate. Further, it determines the gelation point which enlightens the capability of gels to resist permanent deformation. Cephalexin is one of the most prescribed antibiotics and is almost completely absorbed from the gastrointestinal tract with a bio availability of 95%. Cephalexin is used as a model drug to be loaded within the hydrogels and subsequently the *in vitro* release is observed in AGF, AIF and PBS. Further, the *in vitro* release of Cephalexin will be measured in successive buffers i.e. first in AGF followed by AIF and PBS.

2.2. Materials and methods

2.2.1. Materials

Carboxymethyl cellulose sodium salt (CMC), beechwood xylan (xylan) were purchased from Sigma Aldrich. Microcrystalline cellulose (MCC) was purchased from Merck. Auxiliary chemicals such as sodium hydroxide, urea, sodium chloride, potassium dihydrogen phosphate and hydrochloric acid (37 wt%) were purchased from Merck. EGDE and Cephalexin monohydrate were purchased from TCI India. Phosphate buffer saline (PBS) was purchased from Himedia. All the chemicals were used in as received condition. Deionized (DI) water was supplied from in-house Millipore water synthesis unit (make: Millipore, model: ELix-3).

2.2.2. Preparation of hydrogels

The synthesis of hydrogels are divided into three distinct steps, namely; i) preparation of precursors, ii) synthesis of hydrogel by the addition of crosslinker and iii) purification of hydrogel. The schematic of three steps are given in Figure 2.2. In the first step, MCC was dissolved in 60 wt% NaOH and 40 wt% urea solution as reported by Zhou et al [104]. Separately, xylan and CMC were dissolved in 1 mol L^{-1} aqueous NaOH solution. CMC and xylan solutions were mixed with MCC solution in 1:1 molar ratio to prepare MCC-CMC and MCC-xylan precursor solutions. Next the solutions were transferred into a round bottom flask and then heated to 323 K to get homogeneous mixture. There after EGDE crosslinker was added drop wise into the solution. Pure MCC gel was prepared by adding EGDE drop wise into the homogeneous MCC solution. The gelation was seen to complete within 20 min. After the formation of gels, they were thoroughly washed with DI water to remove unreacted precursors. Thereafter the gels were neutralized with 0.1 M HCl solution and subsequently lyophilized (Freeze drier, make: Martin Christ, model: Alpha 2-4 LD) for further characterization. The reaction scheme of all three hydrogels are given in Figure 2.3.

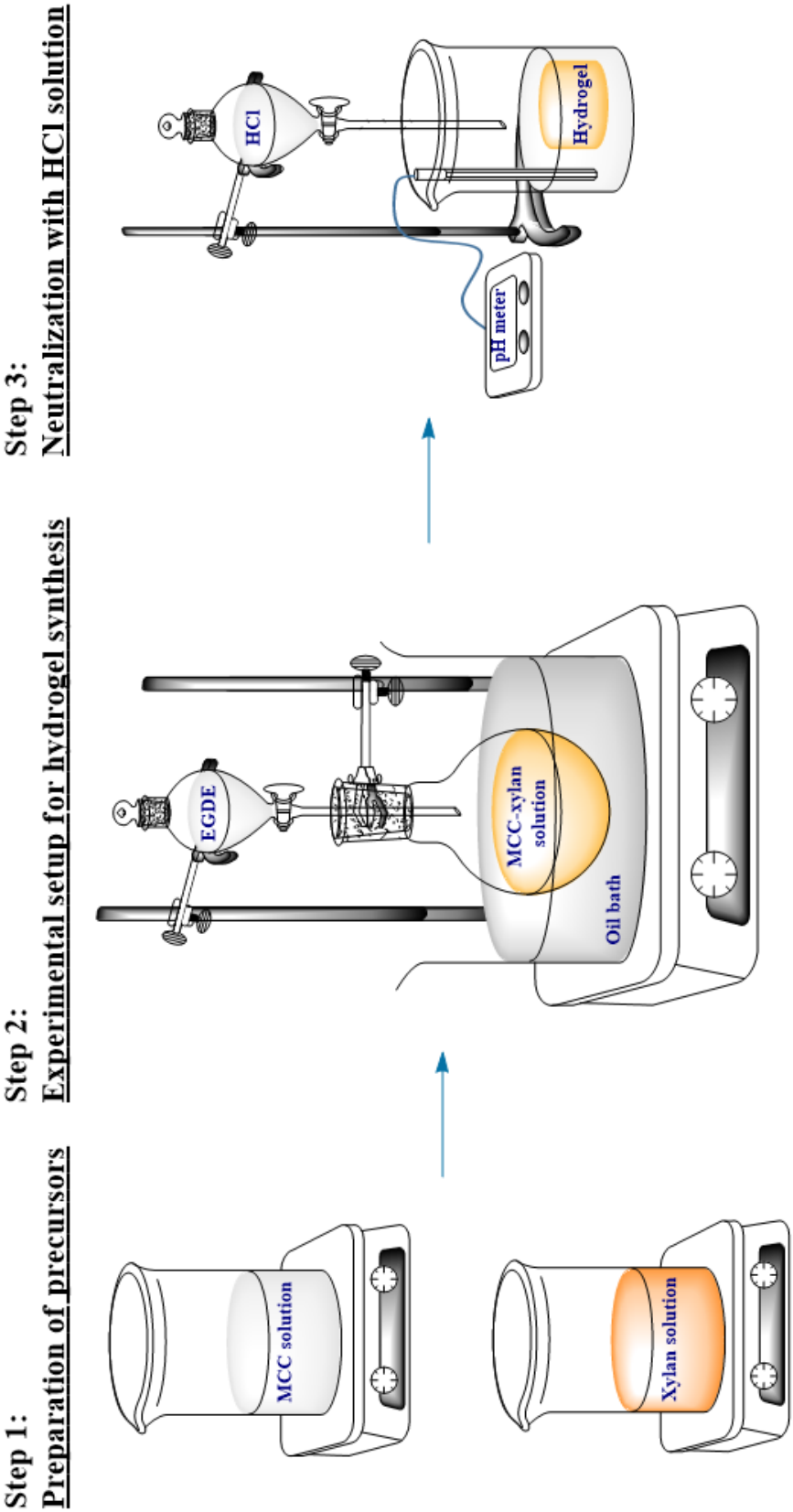

Figure 2.2. Schematic of hydrogel synthesis.

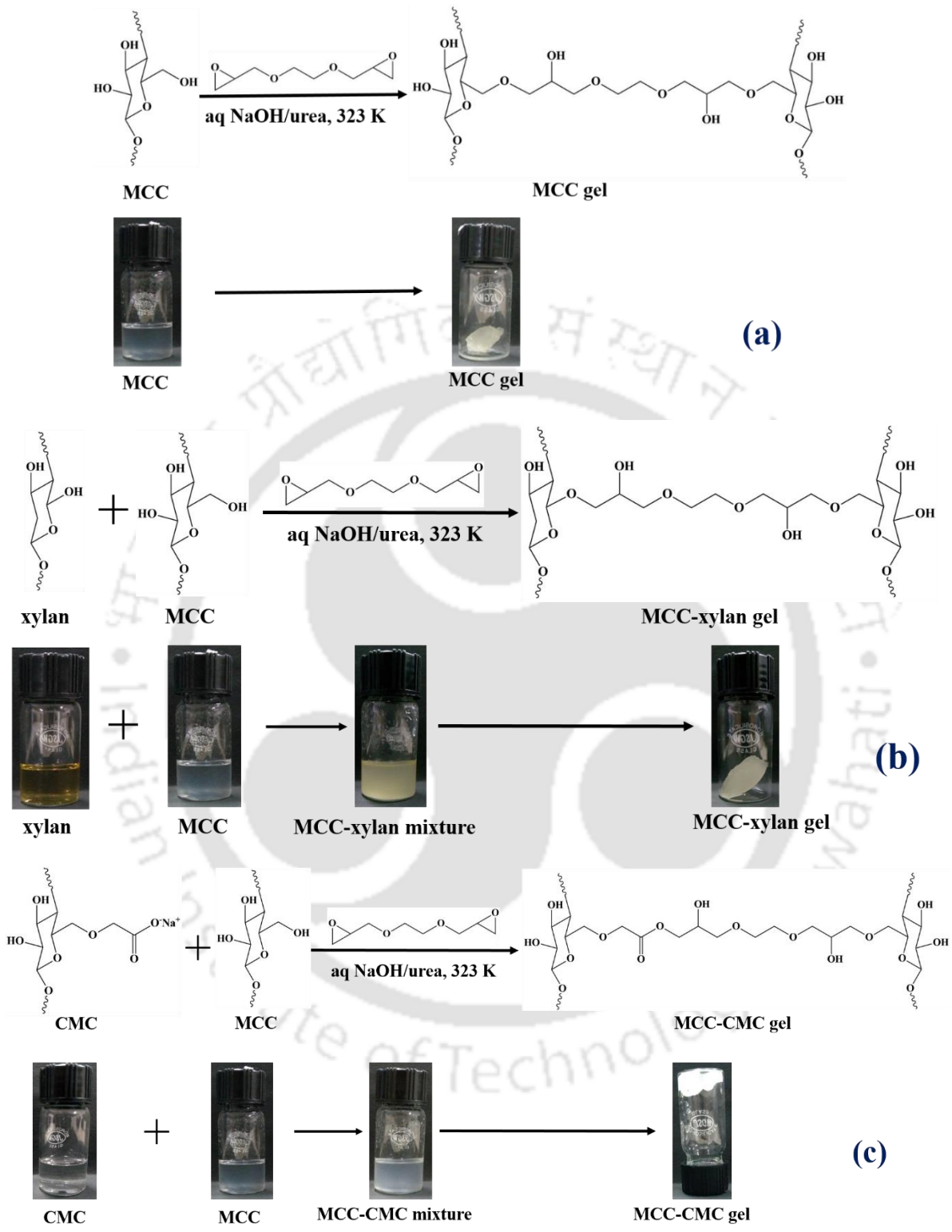

Figure 2.3. Reaction scheme of hydrogel formation. (a) MCC gel, (b) MCC-xylan gel, (c) MCC-CMC gel.

2.2.3. Characterization

2.2.3.1.FT-IR spectroscopy

Freeze dried hydrogels were grinded and mixed with excess amount of dried potassium bromide (KBr). Later the mixed powder was placed in hydraulic press to prepare transparent pellet. The pellets were placed in FT-IR spectrometer (make: Shimadzu, model: IRAffinity-1) and the transmission spectra were recorded within the range of 400 cm^{-1} to 4000 cm^{-1} using 30 scans per sample with a resolution of 4 cm^{-1}.

2.2.3.2.Morphology

The morphology of hydrogels were observed in optical microscope (make: Carl Zeiss, model: Scope A1, AXIO, software: ZEN 2.3) and Field Emission Scanning Electron Microscope (make: Carl Zeiss, model: GeminiSEM 300). Freeze dried hydrogels were placed on a carbon tape that was fixed on a specimen stub. The stub was sputter-coated with gold and the observation was performed with a potential of 3 kV at an optical zoom of 1 μm and 200 nm. For the optical microscopic images, freeze dried hydrogels were placed on a glass slide and covered with coverslip.

2.2.3.3.Rheology

The rheological studies on the developed hydrogels were performed on the rheometer (make: Anton Paar (Austria), model: Physica MCR 301) using cone and plate geometry (diameter: 50 mm, angle: 1°, 0.1 mm gap) at 298 K. The flow behavior of the hydrogels were determined within a shear rate of 1×10^{-2} to 1×10^{3} s^{-1}. To find the storage moduli (G'), loss moduli (G'') and linear viscoelastic region profiles (LVR), amplitude test was performed at a constant angular frequency of 1 Hz and within a strain of 1×10^{-1} % to 1×10^{3} %. From, the amplitude test, LVR is determined at 1% of strain. Frequency sweep test of the gels was performed at constant strain within a frequency of 1×10^{-2} to 1×10^{3} Hz. The constant strain is obtained from LVR. The loss tangent ($\tan\delta$) is determined from the loss and storage moduli obtained from frequency sweep test and is defined as the ratio of viscous to elastic response. The expression is given as;

$$\tan\delta = \frac{G''}{G'} \tag{2.1}$$

2.2.3.4.Equilibrium swelling ratio

Swelling determines the amount of water absorbed by hydrogel within a certain period. We determine the equilibrium swelling ratio of hydrogel i.e. highest amount of water absorbed by hydrogel after attaining equilibrium weight. Briefly a certain amount of freeze dried hydrogel is submerged into pH buffer or DI water for 48 hour at 298 K. The hydrogel is allowed to swell inside buffer or DI water to attain equilibrium. After 48 hour, the hydrogel is filtered to remove excess water after which the weight is measured. The equilibrium swelling ratio (*SR*) is measured as,

$$SR(\%) = \frac{\left(W_{eq} - W_i\right)}{W_i} \times 100\% \tag{2.2}$$

Where, W_i is weight of freeze dried hydrogel and W_{eq} is equilibrium weight of hydrogel. The swelling is measured in artificial gastric fluid (AGF, pH = 1.2) and artificial intestinal fluid (AIF, pH = 6.8), phosphate buffer saline (PBS, pH = 7.4) and deionized (DI) water. The pH of solutions were adjusted by a digital pH meter (make: Eutech Instruments, model: EUTECH pH700).

2.2.3.5.Gel fraction

The constant weight of hydrogel (W_0) was measured after drying at 333 K for 24 hour. Thereafter the hydrogel was immersed in DI water to remove the soluble parts and subsequently heated at 394 K for 4 hour. In the next step, the hydrogel was dried at 333 K for 72 hour with subsequent measurement of weight (W_1). The gel fraction is then given by [58],

$$gel\ fraction(\%) = \left(\frac{W_1}{W_0}\right) \times 100\% \tag{2.3}$$

Both equilibrium swelling ratio and gel fraction measurement were triplicated and standard deviation is represented in terms of error bars.

2.2.3.6.Loading of Cephalexin

Cephalexin is used as model drug to study the loading and *in vitro* release of drug at different physiological buffers. The structure of Cephalexin is given in Figure 2. Freeze dried hydrogel was immersed in 20 mL Cephalexin solution (0.5 mg mL^{-1}) and kept inside an orbital shaker at 120 rpm and 298 K (±0.5 K) for 48 hour. After 48 hour, the tubes were placed in centrifuge at 10,000 rpm to obtain clear supernatant. Later the samples were filtered to separate the drug loaded gels and supernatant. Later, the drug loaded gels were freeze dried. The concentration of Cephalexin in supernatant was measured against the absorbance values obtained from UV-vis spectrophotometer. The amount of Cephalexin loaded into the hydrogel (drug loading) is given by [105],

$$Drug\ loading\,(\%) = \frac{\text{Amount of drug in hydrogel}}{\text{Amount of freeze dried hydrogel}} \times 100 \qquad (2.4)$$

2.2.3.7.Preparation of artificial gastric fluid and artificial intestinal fluid

Artificial gastric fluid (AGF) and artificial intestinal fluid (AIF) were prepared as outlined by Gao et al. [106]. Briefly, 7 mL of hydrochloric acid (37 wt%) and 2 gm of sodium chloride were dissolved in certain volume of water in a 1000 mL volumetric flask. The final volume was adjusted to 1000 mL having a pH of 1.2. AIF was prepared by dissolving 6.8 gm of potassium dihydrogen phosphate in 500 mL DI water. The solution was diluted to 1000 mL solution and pH was adjusted to 6.8.

2.2.2.8.*In vitro* release of Cephalexin

20 mL of AGF, AIF and PBS buffer solutions were added separately in the Cephalexin loaded hydrogels. The sample tubes were kept inside orbital shaker at 310 K (±0.5 K) and 60 rpm. 5 mL aliquot was collected after each hour and subsequently 5 mL fresh buffer solution was added to make up the volume. The method of collection of aliquots has also been adopted from literature [107]. The absorbance of aliquots are measured in UV-vis spectrophotometer and corresponding concentration was calculated against calibration curve. The fraction of Cephalexin release at any certain time (F_t) is given by,

$$F_t(\%) = \frac{M_t}{M_0} \times 100 \qquad (2.5)$$

Where, M_t is the amount of Cephalexin release from hydrogel at a certain time and M_0 is the total amount of Cephalexin loaded initially. All release experiments were performed three times and the standard deviations are reported as error bars in the release profiles.

2.2.3.9.UV-vis spectroscopy

The absorbance of aliquots and supernatant solutions were measured in UV-vis spectrophotometer (make: Shimadzu, model: UV-2600). The concentration of drug in aliquot and supernatant solution were calculated from the absorbance values using calibration curve. The known concentrations were prepared by appropriate dilution of stock drug solution (1 mg mL^{-1}). The calibration curve was prepared from absorbance data of known drug concentrations. Separate calibration curves were plotted for AGF, AIF, PBS buffers (for the aliquots) and DI water (for supernatant).

2.3. Results and discussions

2.3.1. FT-IR spectra

The FT-IR spectra of pure MCC, MCC gel, MCC-CMC and MCC-xylan are given in Figure 2.4. The monomers consist of pyranose ring having characteristic peak of C-H stretching, O-H stretching, C-O stretching, C-C bending and C-H bending. Additionally it has skeletal vibration of C-C and C-O in the pyranose ring and the C-H glycosidic deformation and antisymmetric β-(1→4) glycosidic linkage. Fig. 2.4a represents FT-IR spectra of pure MCC. The O-H and C-H stretching are assigned at 3348 cm^{-1} and 2900 cm^{-1}. The bending of $–CH_2$ is assigned at 1431 cm^{-1}. The skeletal vibrations are recorded at 1371 cm^{-1}. The antisymmetric β-(1→4) glycosidic linkage is reported at 1090 cm^{-1} [108] while the bending of C-C is reported at 1064 cm^{-1} [35]. Here, we observe minor shift in antisymmetric β-(1→4) glycosidic linkage and is assigned at 1112 cm^{-1}. The C-C bending is assigned at 1053 cm^{-1}. C-H glycosidic deformation with ring vibration is assigned to 893 cm^{-1}.

The FT-IR spectra of MCC gel, MCC-CMC, MCC-xylan are given in Fig. 2.4b-d. The characteristic peaks are found in similar positions for all three gels. The O-H stretching is assigned at 3392-3425 cm^{-1}. The doublet peaks at 2912-2914 cm^{-1} and 2875-2877 cm^{-1} are assigned for C-H stretching and bending respectively. The peak at 1454-1460 cm^{-1} represents bending of $–CH_2$, which is present both in monomers and crosslinker. In all of the FT-IR spectra, a broad peak in the range of 1643 – 1654 cm^{-1} is observed. The peak is assigned to the HOH bending of the physically absorb water, since all the precursors and hydrogels are hygroscopic in nature [109, 110]. However, the broad peak is also merged with the asymmetric stretching of COO^- which for CMC in the range of 1600 – 1620 cm^{-1} [35]. However, the asymmetric and symmetric stretching of COO^- is perceived to observe only in Fig. 2.4c. The symmetric stretching of COO^- is reported 1423 – 1446 cm^{-1} which is merged with the bending of $–CH_2$ at 1454 cm^{-1} [111, 112]. The skeletal vibrations of C-O and C-C of pyranose ring are observed at 1354-1363 cm^{-1}. A broad spectra at 1080 cm^{-1} is assigned as collective spectra of antisymmetric β-(1→4) glycosidic linkage and C-C bending mode. The glycosidic C-H deformation with ring vibration is assigned at 842-845 cm^{-1}.

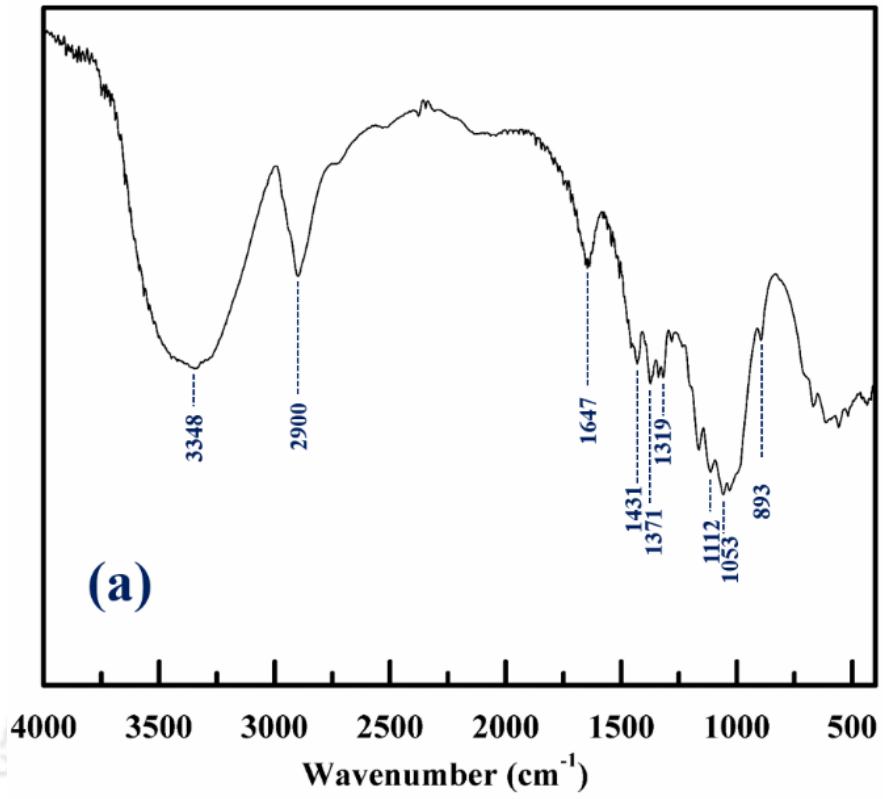

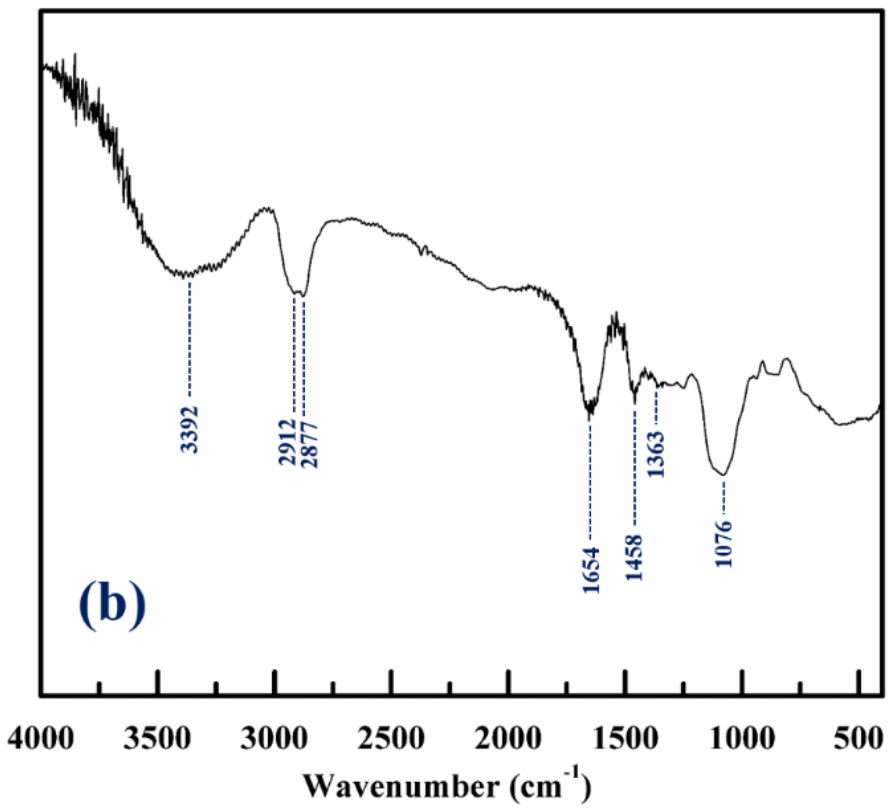

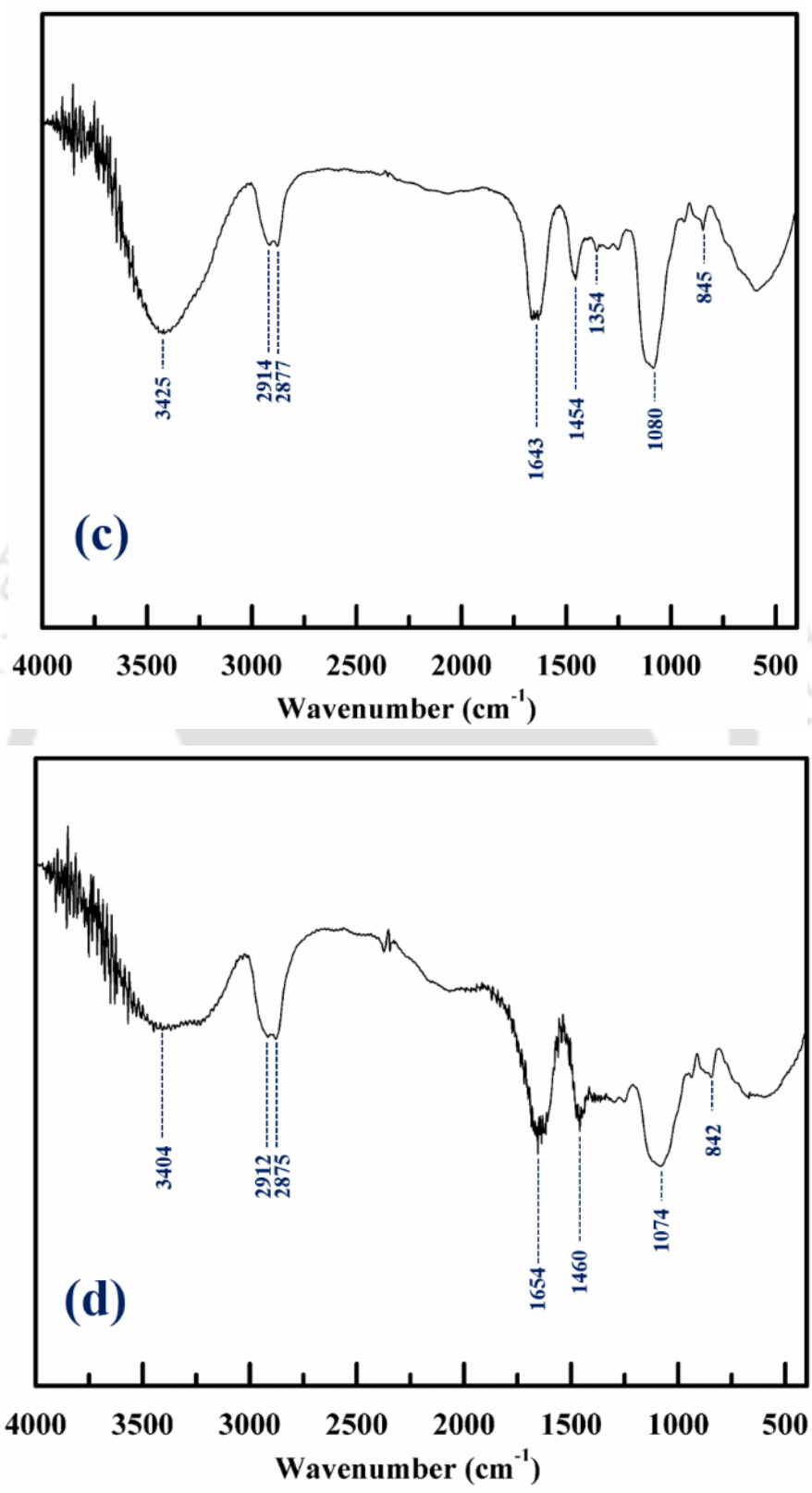

Figure 2.4. FT-IR spectra, (a) MCC pure, (b) MCC gel, (c) MCC–CMC, (d) MCC-xylan.

2.3.2. Morphology of hydrogels

Figure 2.5 and 2.6 represent the morphology of hydrogels, visualized by FESEM and optical microscopy respectively. From FESEM images, all the gels are found to be coarse in nature with uneven surface. The coarse nature of hydrogels are also visible in optical microscope images. The uneven surface creates multilayered morphology of hydrogel and thus pores are visible among layers. Further, the morphology of Cephalexin loaded gels are observed in optical microscope and are given in Figure 2.6d-f. The drug molecules appear to be within the green patches on the surface of the hydrogels. The distribution of drugs are found to be uneven. The random distribution of drug molecules imply that various hydroxyl and carboxyl moieties make ionic bonds with the drug molecules.

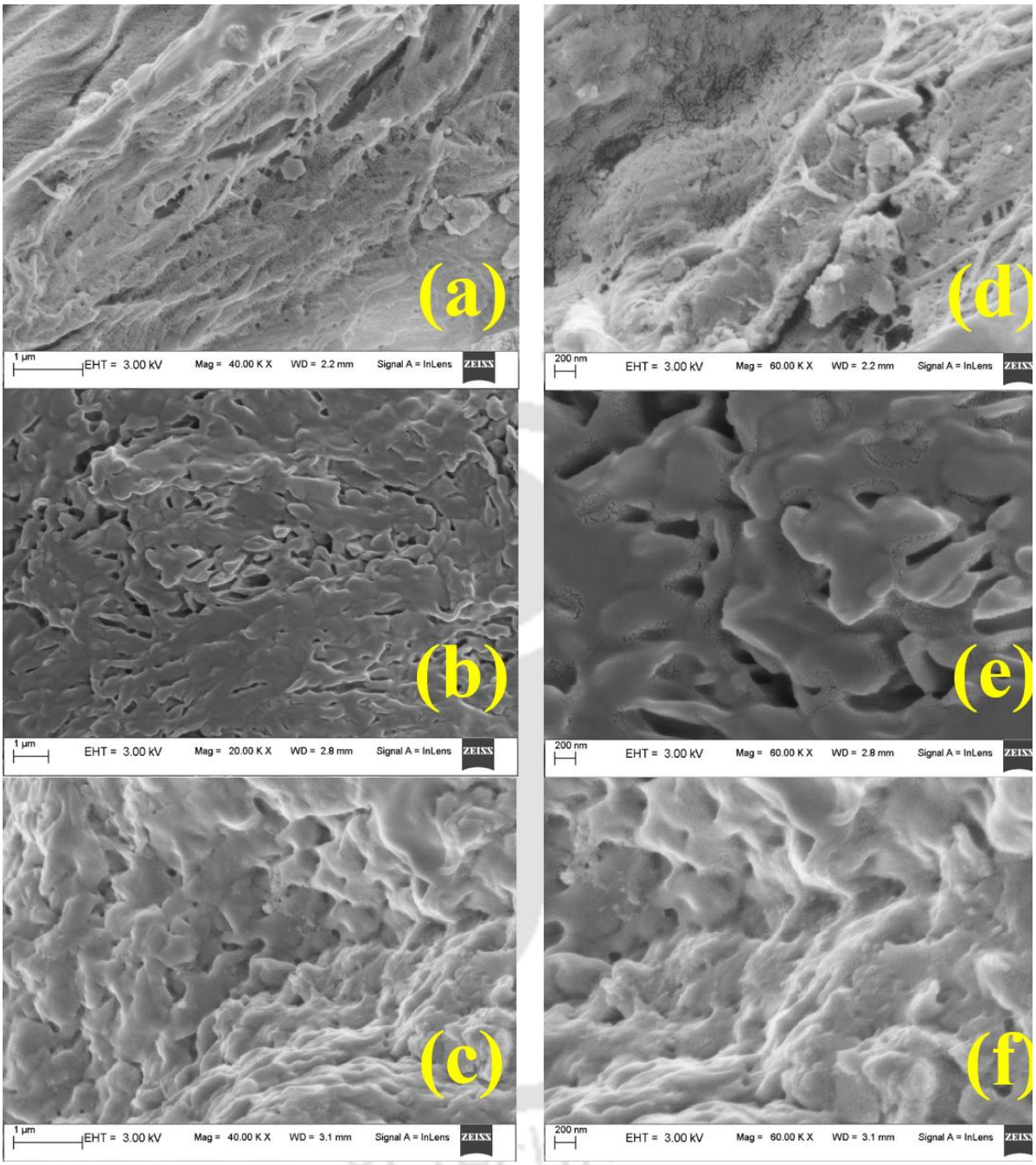

Figure 2.5. FESEM morphology of hydrogels at 1 μm [a-c] and 200 nm [d - f]. (a) and (d) MCC gel, (b) and (e) MCC-xylan, (c) – (f) MCC-CMC.

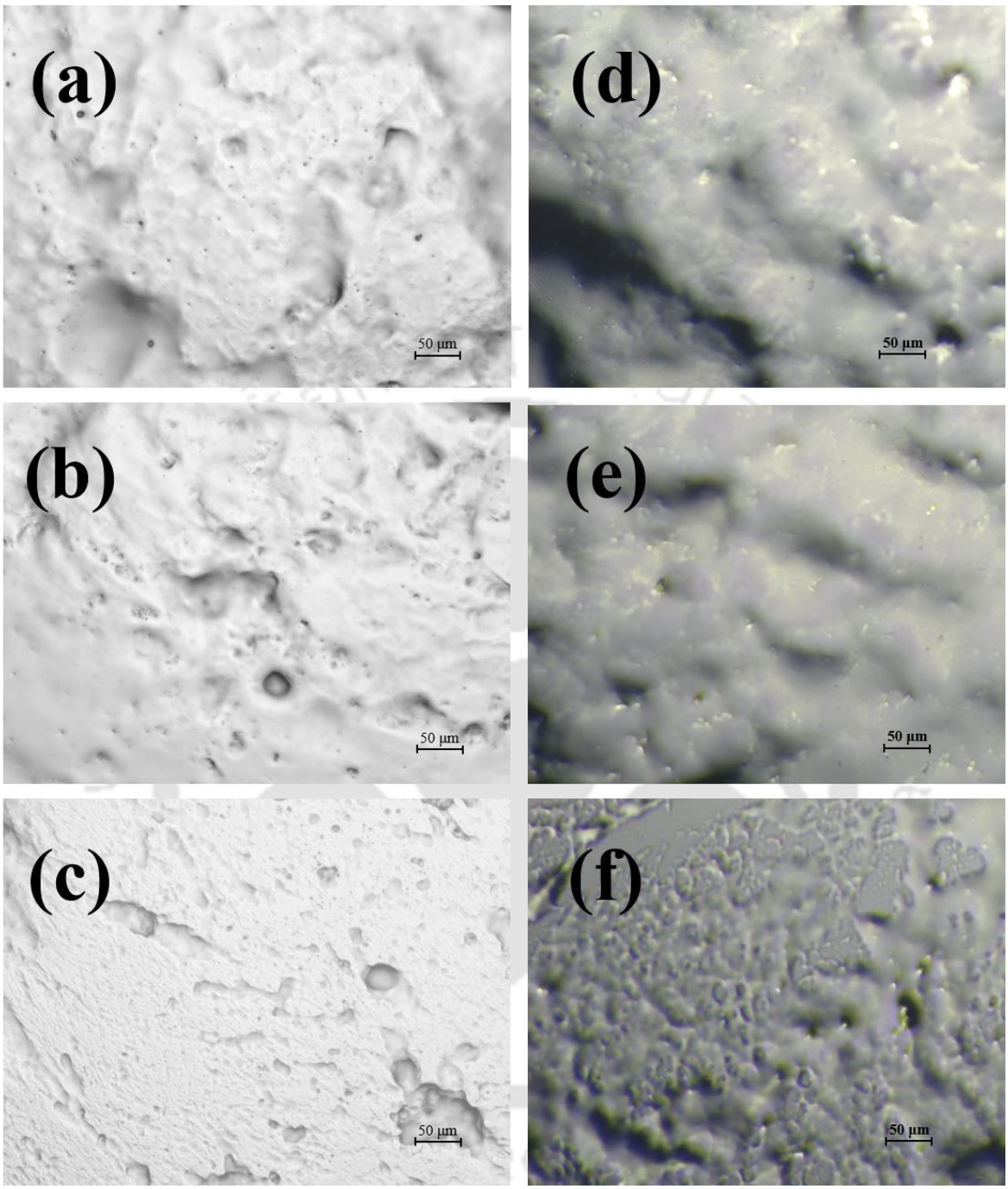

Figure 2.6. Optical microscope images of hydrogels (a-c) and Cephalexin loaded gels (d-f). (a) and (d) MCC gel, (b) and (e) MCC-xylan, (c) – (f) MCC-CMC.

2.3.3. Rheological analysis

The viscosity of the hydrogels are given in Figure 2.7 by varying the shear rate between 0.01-1000 s^{-1}. With the increasing shear rate, we observe a decline in viscosity. The nature of the curves follows shear thinning behavior of the gels which is further confirmed by fitting within a power-law model. Power law equation in terms of apparent viscosity,

$$\eta = m\left(\dot{\gamma}\right)^{n-1} \tag{2.6}$$

Where, η is viscosity, $\dot{\gamma}$ is shear rate, n is power-law index and m is consistency index. Table 2.1 represents the values of parameters of the power law model. The goodness of fit is expressed in terms of correlation coefficient (R^2) whose values are given in Table 1. The R^2 values for all gels are greater than 0.95 which implies the power law model adequately represent the viscosity behavior within the given shear rate. For all three hydrogels, the power law index was less than unity which mathematically confirms the shear-thinning nature of gels with increasing shear rate. Further, we also observe that the viscosity of MCC-CMC is always higher by an order of ten when compared to the remaining hydrogels.

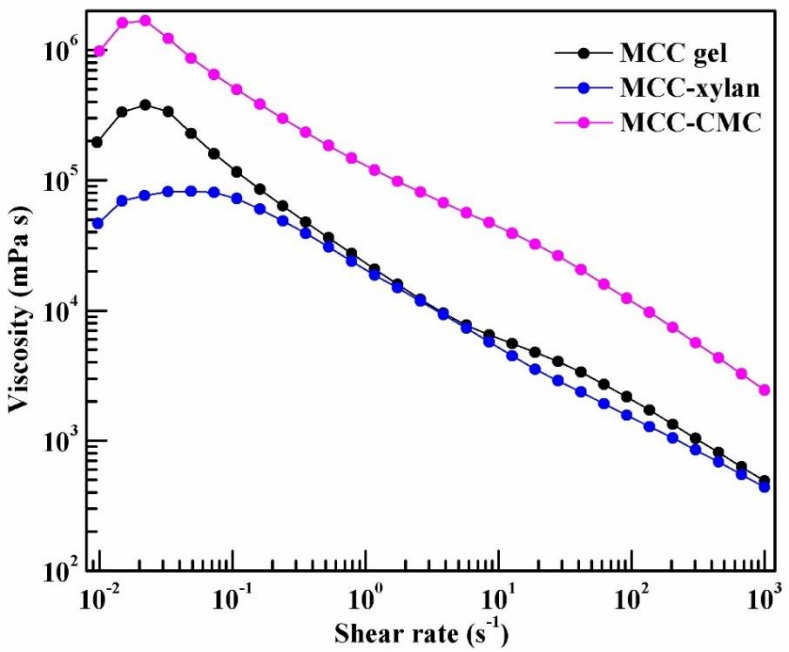

Figure 2.7. Viscosity of hydrogels.

Table 2.1. Power law parameters.

Name of the hydrogel	*m*	*n*	R^2
MCC gel	2.74×10^4	0.414	0.99
MCC-xylan	1.60×10^4	0.507	0.96
MCC-CMC	1.44×10^5	0.442	0.99

Further, we have also examined the viscoelastic properties of the gels by amplitude sweep test in Figure 2.8a by varying the strain from 0.1-1000%. Storage modulus is found to dominate over the loss modulus, until the crossover point. For all three gels, crossover strain lies beyond 100%, reflecting the stability of crosslinked gels. We here observe that the copolymerized MCC-CMC and MCC-xylan gels can sustain higher deformation than MCC gel. From the amplitude sweep test, we further determine the LVR at 5% strain. The dominance of elastic response over viscous response is further examined in frequency sweep (Figure 2.8b) where the frequency is varied from 0.01-100 Hz and at a constant strain of 5%. From Figure 2.8b, we obtain the crossover point for MCC gel at 64 Hz. Although the crossover point of MCC-CMC exceeds when compared to MCC gel, MCC-xylan gel are seen to break early. Upto the crossover point, the elastic response dominates which is a desirable property for hydrogels. We further observe the enhancement of storage and loss moduli of MCC-CMC gel as compared to MCC gel whereas those are reduced for MCC-xylan gel.

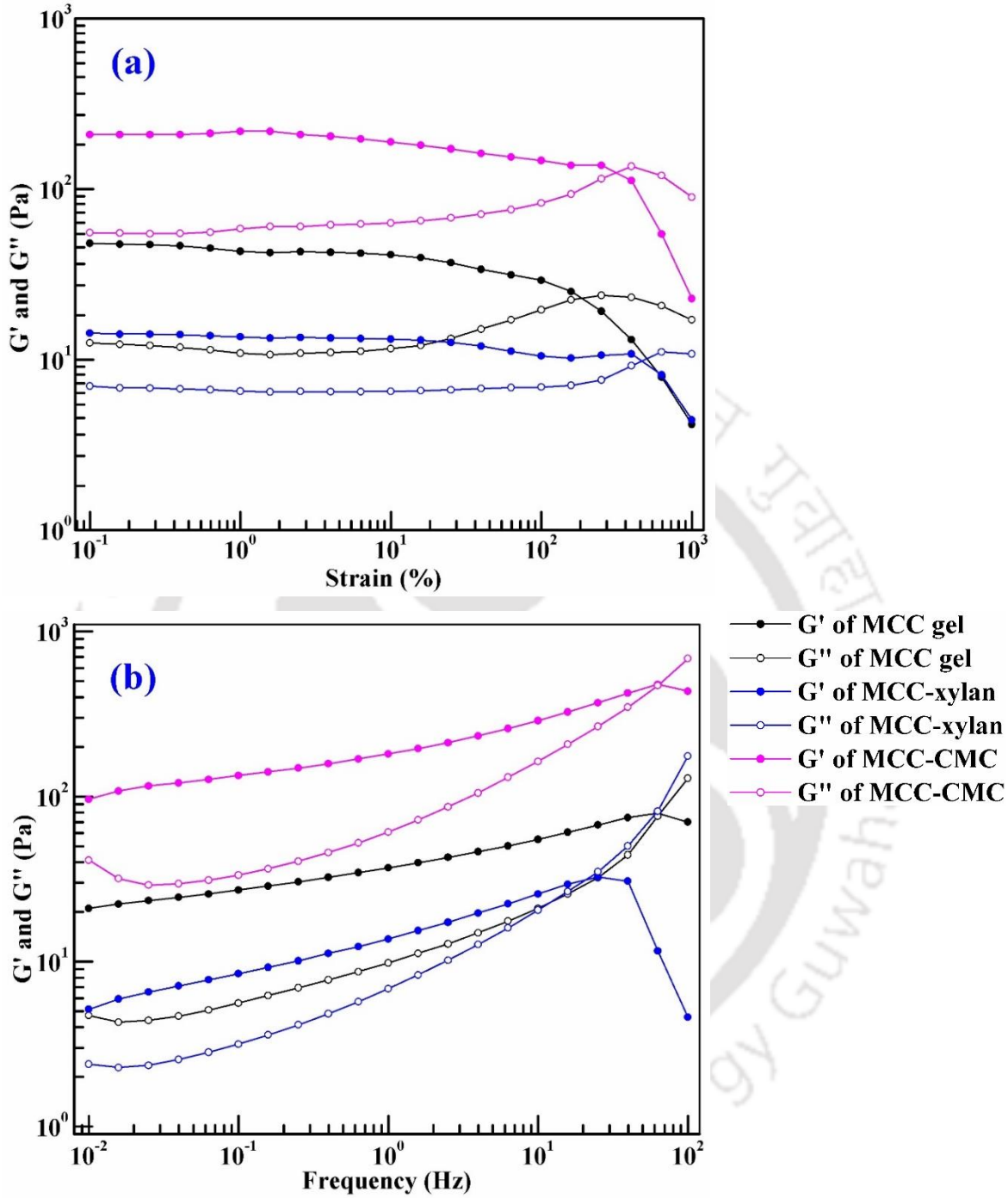

Figure 2.8. Rheology of hydrogels. (a) amplitude sweep, (b) frequency sweep.

Thereafter, we calculate the loss tangent from equation 2.1. The corresponding loss tangent vs frequency plot is given in Figure 2.9. The sol-gel transitions for MCC-CMC and MCC gel are observed after 64 Hz whereas MCC-xylan gel attains it after 20 Hz. Before the sol-gel transition, we observe linear increase of loss tangent i.e. the crosslinked structures losing its elastic nature with increasing frequency and moving towards more liquid like behavior.

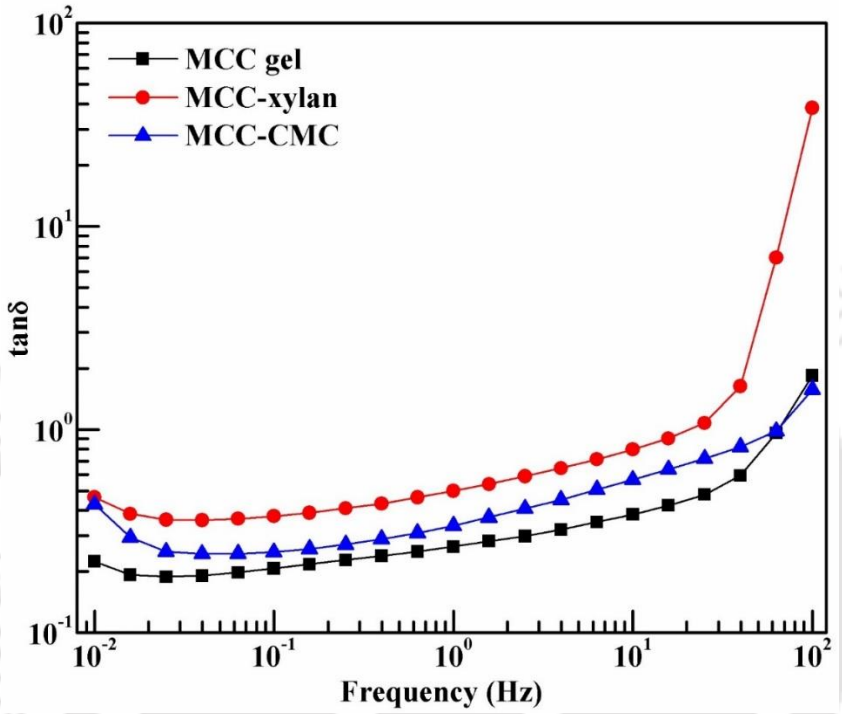

Figure 2.9. Loss tangent of hydrogels

2.3.4. Swelling ratio and gel fraction measurement

The absorbency of water by hydrogels is determined by swelling ratio. The degree of crosslinking is represented by gel fraction. The densely crosslinked hydrogel network has less flexibility to expand. Hence, it entraps lower amount of water and has lower swelling ratio. Here we have performed the swelling of hydrogels in DI water, AGF, AIF and PBS, keeping in mind the Cephalexin uptake and *in vitro* release in physiological buffers. Figure 2.10a represents the swelling ratio of hydrogels as calculated from equation 2.2. The order of swelling for DI water and buffers are found to be MCC-CMC> MCC-xylan > MCC gels.

For all three hydrogels, highest swelling is obtained with DI water and order of swelling is given by: DI water> PBS> AIF> AGF. Hydroxyl (MCC, CMC and xylan) and carboxymethyl moieties (CMC) are dominant charge species of hydrogels. For that, the electrostatic repulsion of the moieties in the side chain of pyranose ring cause swelling. Thus having been in the ion free medium of DI water, the hydrogels swell more than in the buffers. The ionic moieties of hydrogels are readily saturated with free ions of buffers causing less repulsion and less amount of swelling. Further the longer carboxymethyl moiety of CMC gives MCC-CMC network a higher flexibility, resulting in higher swelling over the other two hydrogels. Figure 2.10b represents the gel fraction of hydrogels calculated from equation 2.3. It follows the opposite trend of swelling i.e. MCC gel has a highest gel fraction of 96.98% among all the three hydrogels. Gel fraction here represents the degree of crosslinking. With the increase in crosslinking, the hydrogels has less flexibility to expand, therefore lower swelling. Figure 2.11 represents the images of freeze dried and swelled hydrogels.

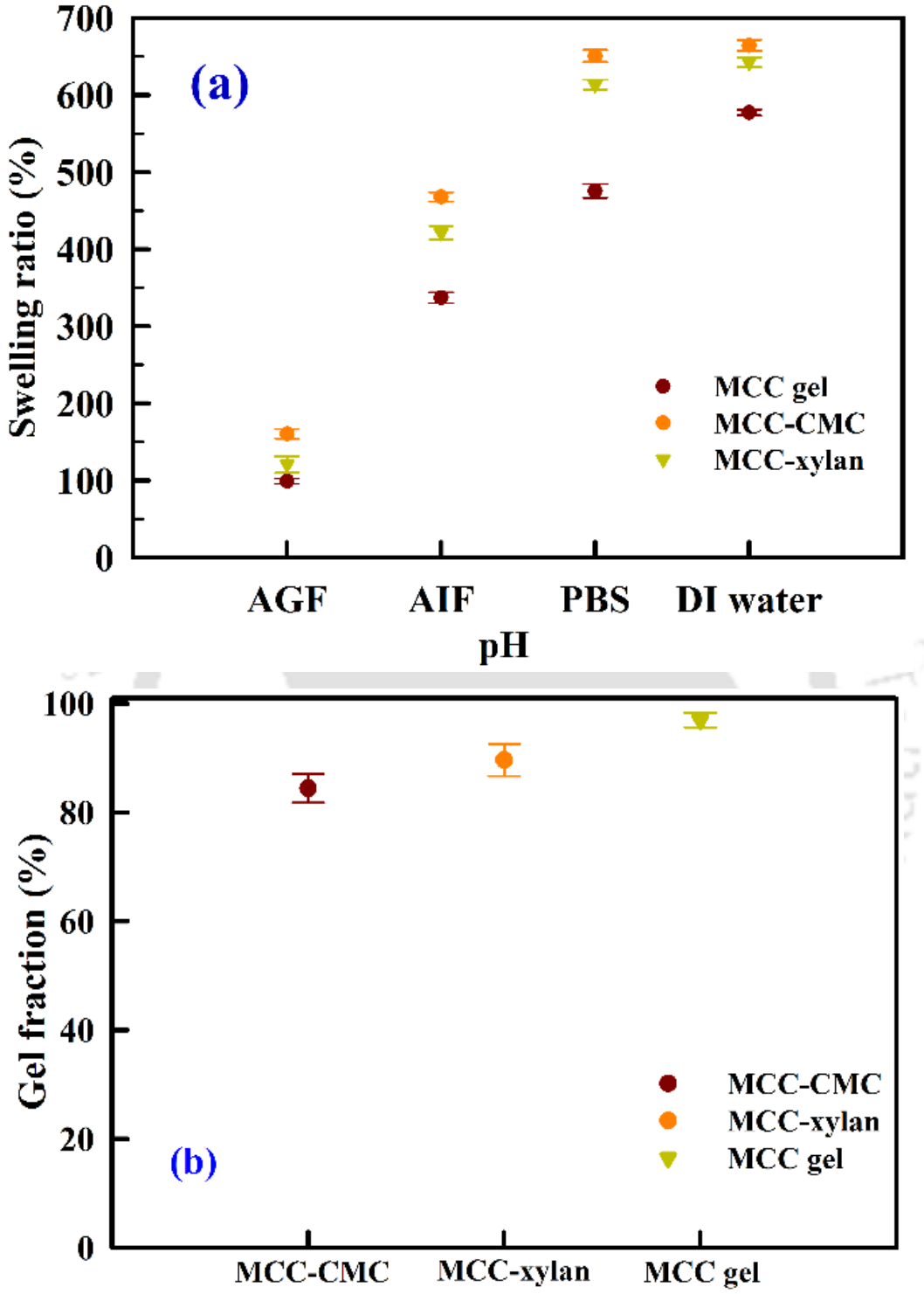

Figure 2.10. (a) Swelling ratio of hydrogels in DI water and various buffers. (b) Gel fraction of hydrogels.

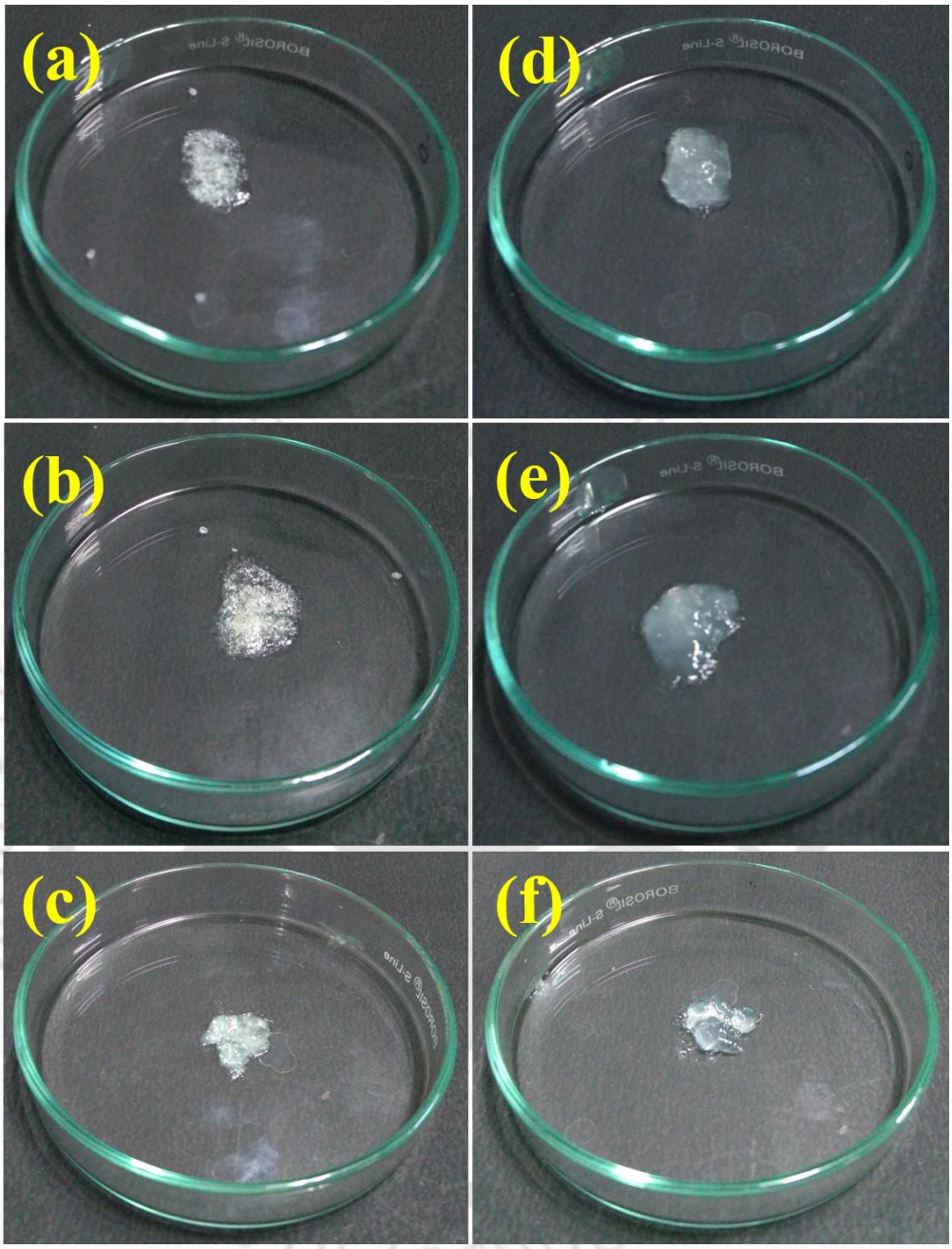

Figure 2.11. Freeze dried (from (a) to (c)) and swelled hydrogels (from (d) to (f)). (a) and (d) MCC gel, (b) and (e) MCC-xylan, (c) and (f) MCC-CMC.

2.3.5. Loading and *in vitro* release of Cephalexin

The loading of MCC gel has been recorded as 19.64% (±0.56%) whereas copolymerized MCC-CMC and MCC-xylan have loading of 26.48% (±1.15%) and 24.25% (±0.91%) respectively. The higher amount of drug loading in MCC-CMC can be attributed to the higher

swelling ratio of hydrogel. The *in vitro* release of Cephalexin at three physiological buffers, namely; AGF, AIF and PBS are performed for 8 hour and given in Figure 2.12a-c. Further Figure 2.12d represents the *in vitro* release study in successive physiological buffers i.e. at AGF for 2 hour, followed by AIF for 2 hour and subsequently in PBS for 6 hour. The mean emptying time in stomach is noted as 1.08 hour (±0.11 hour), followed by the transit time in small intestine as 1.75 hour (±0.25 hour) which leaves the arrival time in colon is 2.83 hour (±0.33 hour) [113]. Therefore, the above mentioned *in vitro* release study in successive buffers (Figure 2.12d) would be sufficient to simulate the release profile in gastrointestinal tract. This will elucidate the efficiency of MCC based hydrogels as an effective carrier for Cephalexin. Further, the pH and composition of AGF, AIF and PBS adequately represent the body fluids inside stomach, small intestine and colon respectively.

The *in vitro* release in AGF produces 14-16% delivery of drug whereas higher delivery of 83-87% and 87-98% are observed in AIF and PBS respectively. The higher amount of release in AIF and PBS are attributed to the high degree of swelling of hydrogels. At pH 1.2, higher amount of H^+ ions are available to protonate the hydroxyl moieties which negate the lower electrostatic repulsion causing lower swelling. Due to the lower swelling, the crosslinked chains are rigid and less flexible to let the Cephalexin diffuse in buffer. However, burst release is observed in AIF and PBS for the first two hour. At higher pH, deprotonated hydroxyl moieties repel each other causing higher swelling and greater diffusion of drug into the media. After two hour, release rate in PBS becomes higher than that in AIF media because of the various ions in PBS when compared to AIF.

Figure 2.12d represents the *in vitro* release of Cephalexin in successive buffers. The release in AGF for first 2 hour resembles the trend of the release in pure AGF. However, the burst release is prevented when the hydrogels are dipped into AIF and PBS buffer respectively because of the already protonated functional moieties of hydrogel. Further, after 4 hour (2 hour in AGF and 2 hour in AIF), the amount of drug release is 45-54%, which is higher than the *in vitro* release in pure AIF buffer. We did not observe any significant drug release after 8 hour for the release in individual buffers (Figure 2.12a-c). But in sequential release, PBS is able to extract ~45% of drug from hydrogels making the cumulative release to 91-98%. Hence, it is concluded that MCC based hydrogels can facilitate the delivery of Cephalexin to 8-9% in

stomach, 37-45% in the small intestine and 37-44% in the colon only when the hydrogels are first exposed to AGF.

Figure 2.12 also draws a comparative study *in vitro* release profile of Cephalexin among MCC, MCC-xylan and MCC-CMC gel. The release of drug in independent buffers primarily depend on the swelling of the gels. Hence, it is expected to have higher release rate from MCC-CMC gel as it consistently produces higher swelling ratio than the other two gels. Further, MCC-CMC hydrogel has an additional carboxyl moiety along with hydroxyl moieties which provide greater number of binding sites for drug. Hence, the sites facilitate affinity towards the cations in buffer and release the drug after the initial burst release. Thus the order of release is MCC-CMC > MCC-xylan > MCC gel for all buffer mediums.

The lower amount of Cephalexin release in AGF followed by the accelerated release in AIF and PBS, can also be attributed to the existence of the drug at various forms. The presence of –COOH, -CONH, NH_2 moieties in the Cephalexin molecule and its inherent acid-base properties resemble to the dipeptide molecules. Depending upon the pH of aqueous medium, Cephalexin (denoted as CPX) can exist as cation (H_2CPX^+), zwitterion ($HCPX^-$) and anion (CPX^-) [114]. The zwitterion form of Cephalexin dominates within a pH range of 2.56-6.88 [115]. Cephalexin is anionic above pH 6.88 and is cationic below 2.56 [76]. Below pH 2.56, the drug exists in cationic form which is repelled by the excess H^+ ions present in AGF medium. This prevents higher amount of release of drug in AGF. However, in zwitterion form, the drug exhibit both acidic and basic properties. Therefore, it can combine with the metal ions and H^+ ions in AIF, resulting in a higher release of drug. Further, in the anionic form (above 6.88 pH), the Cephalexin can bind with the available metal ions in PBS buffer. For this to happen, the initial burst release of Cephalexin is higher in PBS as compared to the *in vitro* release in AIF. For the same reason, PBS buffer facilitates extraction of Cephalexin in AGF-AIF-PBS buffer system.

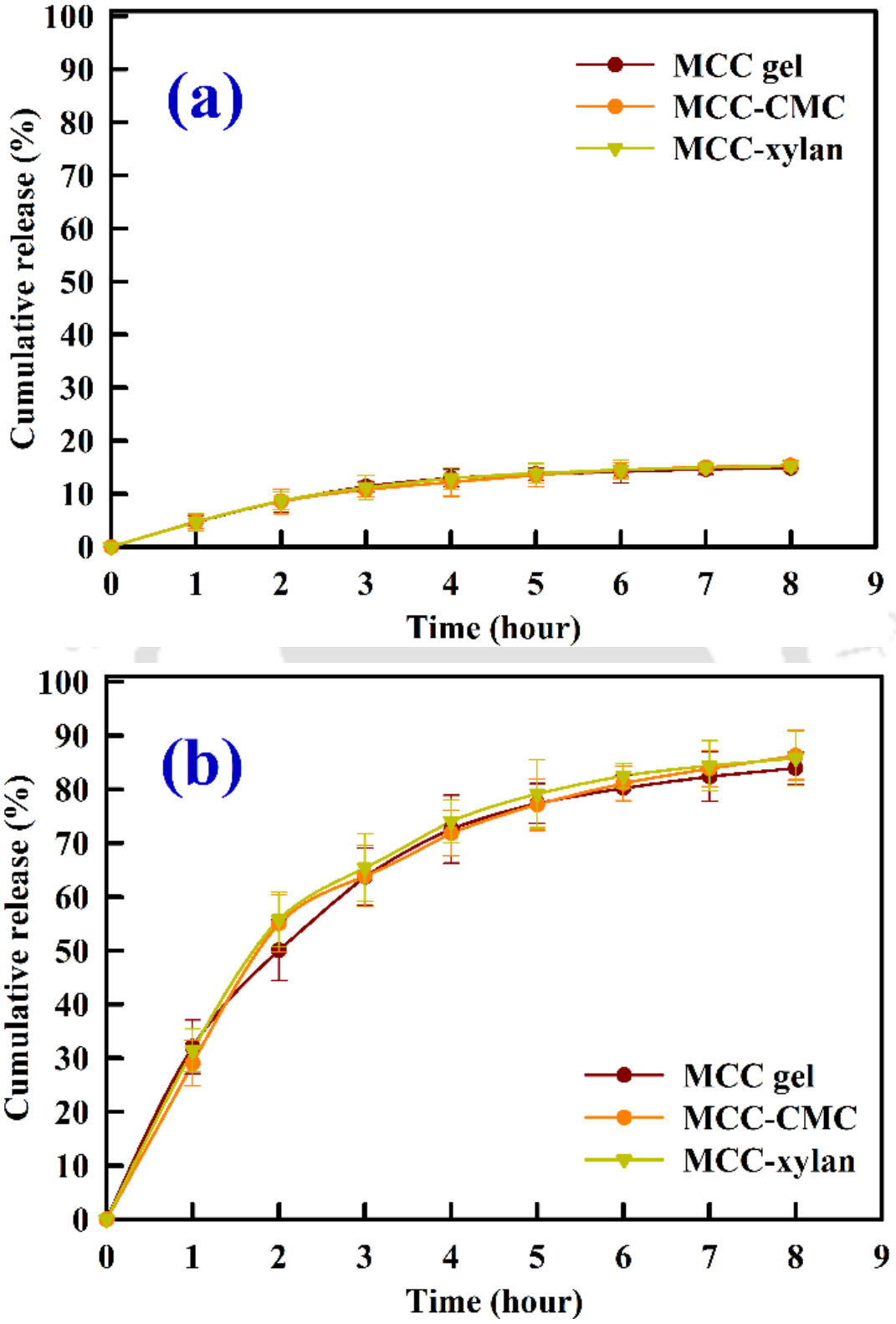

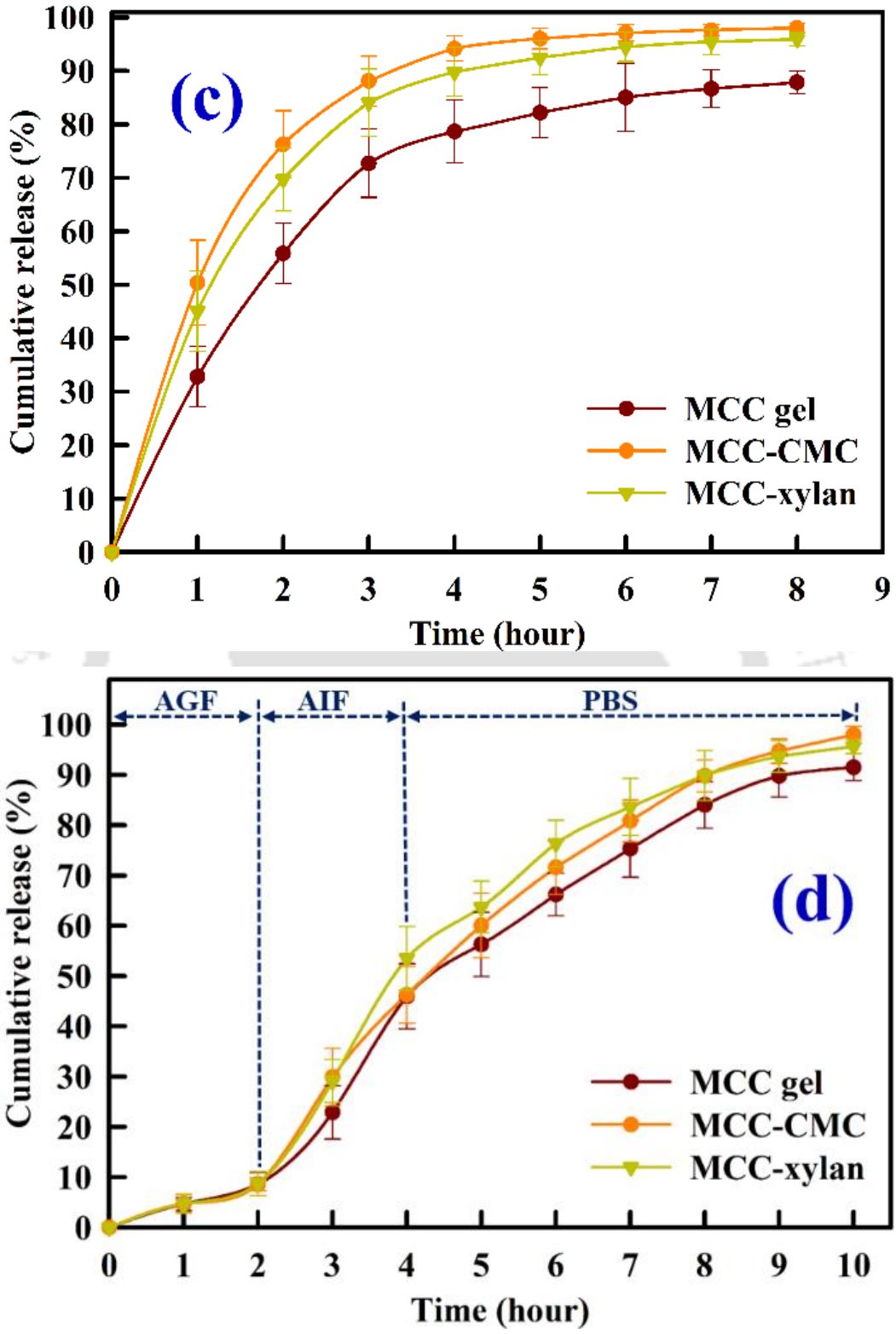

Figure 2.12. *In vitro* release of Cephalexin in physiological buffers. (a) AGF buffer, (b) AIF buffer, (c) PBS buffer, (d) AGF-AIF-PBS buffers.

2.3.6. Comparison of Cephalexin release with literature

Table 2.2. Comparison with literature of *in vitro* release of Cephalexin using hydrogel

Article	Monomers	Drug loading concentration	Release of drug	Refer-ence
Tomić et al.	2-hydroxyethyl methacrylate, itaconic acid and poly (alkylene glycol) (meth)acrylates	7.48×10^{-4} mol dm^{-3}	Less than 80% of drug within 10 hour and ~100% release after 90 hour in PBS buffer at 310 K.	[78]
Barkhordari and Yadollahi	Carboxymethyl cellulose and layered double hydroxide	60 mg of Cephalexin per 100 mL bi-distilled water	Cumulative release of 10% in AGF in 2 hour followed by 60% in AIF for 2 hour followed by 22% in PBS for 4 hour at 310 K.	[76]
Present study	Carboxymethyl cellulose sodium salt, beechwood xylan, Microcrystalline cellulose	0.5 mg mL^{-1} aqueous solution	14-16% release in AGF, 83-87% release in AIF and 87-98% release in PBS within 8 hour at 310 K. 91-98% release in consecutive physiological buffers within 10 hour.	---

The *in vitro* release of Cephalexin in physiological buffers are compared with the previous two reports given in literature (Table 2.2). Barkhordari and Yadollahi reported 0.061 gm of Cephalexin incorporated into per gm of layer double hydroxide – Cephalexin nanohybrid with CMC as protective capsule [76]. The cumulative release of drug is 10% in AGF for 2 hour followed by 60% in AIF for 2 hour and by 22% in PBS for 4 hour. The kinetic mechanism is reported as ion-exchange process followed by the diffusion of Cephalexin into the aqueous medium. Tomić et al. reported the *in vitro* release of Cephalexin in PBS (pH = 7.4) at 310 K.

The 2-hydroxyethyl methacrylate, itaconic acid and poly (alkylene glycol) methacrylates based hydrogels are reported to release less than 80% of drug within 10 hour and ~100% release after 90 hour [78]. For all the reported hydrogels, initial burst release is followed by the steady release. In this work, we have shown the *in vitro* release of Cephalexin in three physiological buffers independently as well as its sequential release in AGF, AIF and PBS. Further the release of Cephalexin in PBS is higher than that reported by Tomić et al. within 10 hour [78]. For the oral delivery route, the carrier will not remain in the gastrointestinal tract for long period as reported by Tomić et al., rather a higher amount of drug release is necessary within a stipulated period. Therefore, a cumulative release of 87-98% in PBS within 8 hour elucidates the effectiveness of MCC based hydrogels as an effective carrier of Cephalexin.

2.4. Conclusions

MCC based homopolymerized and copolymerized gels with CMC and xylan are synthesized using EGDE crosslinker. MCC-CMC gels has swelling ratio of 160%, 468%, 651% and 664% in AGF, AIF, PBS and DI water respectively which are higher among three gels in the respective mediums. The swelling ratio is shown to increase with the pH. The gel fraction follows the opposite trend of swelling ratio whereby MCC gel has the highest gel fraction of 96.98%. A coarse nature is observed in the morphological observation for all hydrogels. Further, the hydrogels produce shear thinning behavior with increasing shear rate. A longer gel point at 64 Hz is observed for MCC-CMC hydrogel, whereas MCC-xylan produces a shorter gel point of 20 Hz. Upto the gel point, elastic nature of hydrogel prevails as determined from the loss tangent. The longer gelation point of MCC-CMC reflects the suitability of MCC-CMC among three gels. Further MCC-CMC gel shows a drug loading capacity of 26.48% (±1.15%) which is highest among the three gels. Further, MCC-CMC releases 15% Cephalexin in AGF, 86% in AIF and 98% in PBS respectively. The *in vitro* release kinetics in AIF and PBS reveal initial burst release of Cephalexin due to the swelling of gels followed by a steady release.

Chapter 3

Synthesis, characterization of carboxymethyl cellulose-xylan based hydrogels and *in vitro* release of Vitamin B_{12}

Highlights

- Synthesis of carboxymethyl cellulose-xylan based hydrogels
- Characterization by FT-IR spectroscopy, morphology and swelling studies
- Rheology of the hydrogels
- *In vitro* release of Vitamin B_{12} in various physiological buffers

Keywords

A. Carboxymethyl cellulose;
B. Xylan;
C. Hydrogel;
D. Rheology;
E. Vitamin B_{12}.

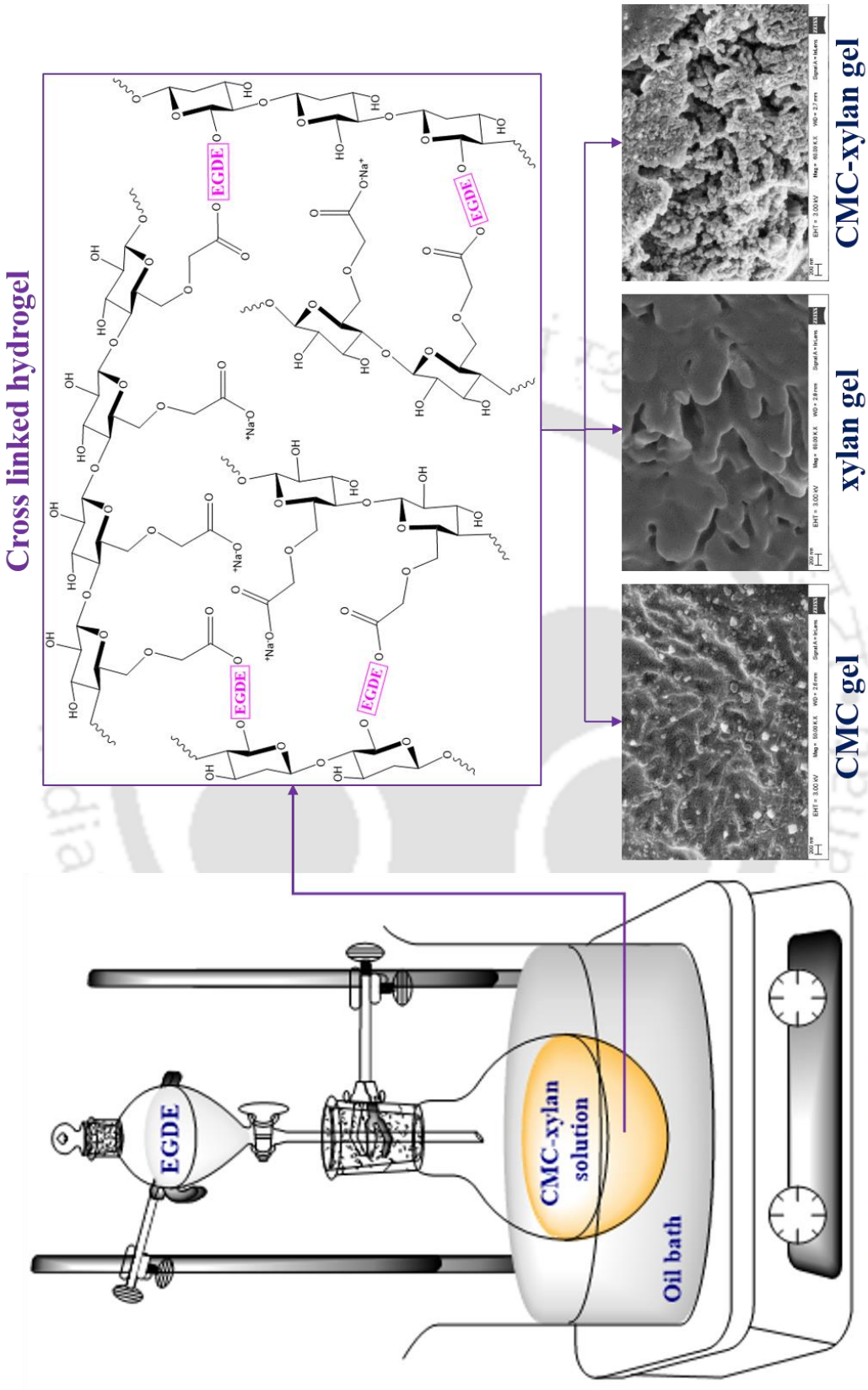

Figure 3.1. Pictorial representation of synthesis, crosslinking structure and morphology of hydrogels.

3.1. Chapter summary

Vitamin B_{12} (VB_{12}) is considered as essential nutrient to human body. With the aim of successful *in vitro* release of VB_{12} in the gastrointestinal tract. The synthesis of CMC and xylan based homopolymerized and copolymerized hydrogels using EGDE crosslinker in alkaline medium is attempted in this chapter. The hydrogels are physically characterized by swelling ratio and gel fraction whereas FT-IR spectroscopy reveals the functional moieties associated with the gels. Morphological observation of hydrogels are performed in FESEM and optical microscope. Flow behavior, gel point, gelation temperature and gelation time are determined from the rheological behavior of the gels. VB_{12} is loaded in the hydrogels and subsequent studies involving the *in vitro* release in AGF, AIF, and PBS. Further, the release study is also attempted in successive buffers i.e. first in AGF, followed by AIF, followed by PBS.

3.2. Materials and methods

3.2.1. Materials

Vitamin B_{12} were purchased from TCI India. All other chemicals required for synthesis of hydrogel, characterization and application to the *in vitro* release of VB_{12}, are given in Section 2.2.1.

3.2.2. Preparation of hydrogels

Precursor solutions of CMC and xylan were separately dissolved in 1 mol L^{-1} aqueous NaOH solution. After obtaining homogeneous solutions, xylan and CMC were mixed in 25 mol% : 75 mol% (XC25), 50 mol% : 50 mol% (XC50) and 75 mol% : 25 mol% (XC75) respectively. Next the solutions were transferred into a round bottom flasks and then heated to 323 K to get homogeneous mixture and EGDE crosslinker was added drop wise into the solution. The gelation was seen to complete within 15 min. After the formation of gels, they were thoroughly washed with DI water to remove unreacted precursors. Thereafter they are neutralized with 0.1M HCl solution and subsequently lyophilized for further characterization. In addition to the copolymerized CMC-xylan gel, EGDE was also added drop wise into pure xylan and pure CMC solutions to prepare pure xylan gel and pure CMC gel respectively. The crosslinking scheme of the hydrogels are given in Figure 3.2.

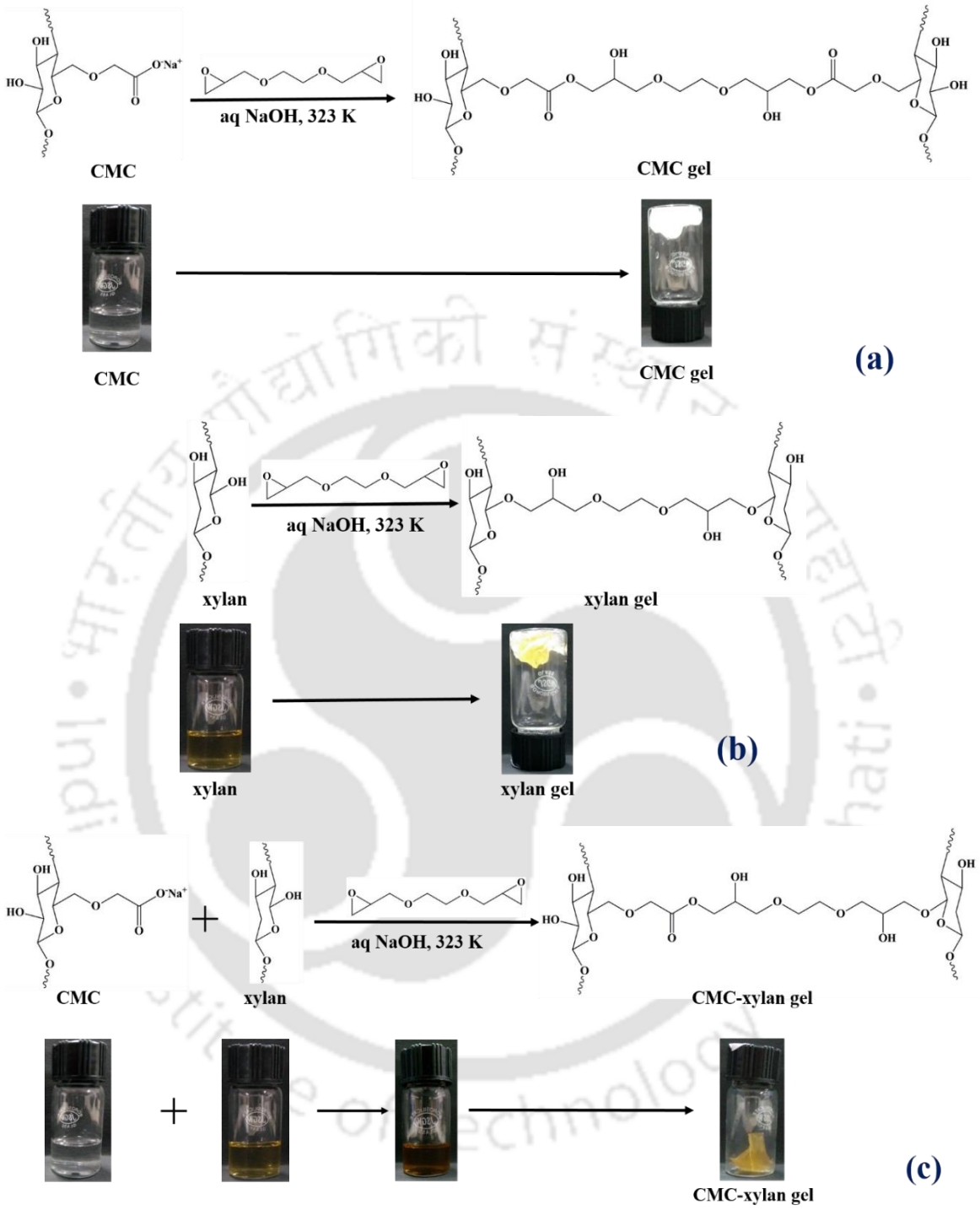

Figure 3.2. Reaction scheme of hydrogel formation. (a) CMC gel, (b) xylan gel, (c) CMC-xylan gel.

3.2.3. Characterization

The characterization procedure of FT-IR spectroscopy, morphology, swelling ratio and gel fraction are similar to that of characterization procedure described in Chapter 2 for the respective techniques.

3.2.3.1.Rheology

The procedure of rheological analysis is similar to the Section 2.2.3.3. From, the amplitude test, LVR is determined at 1% of strain. Further, the temperature sweep of the of the precursor solution is performed at a temperature range of 298-353 K with 1% of strain obtained from LVR and with 1 Hz frequency obtained from frequency sweep test. The time sweep of the precursor solution is performed for 60 min at corresponding gelation temperature with 1% of strain obtained from LVR and with 1 Hz frequency obtained from frequency sweep test.

3.2.3.2.Loading of VB_{12}

Pre-weighed amount of freeze dried hydrogels were immersed in 20 mL VB_{12} solution (0.5 mg mL^{-1}). The sample tubes were kept in the same orbital shaker for 48 hour at 298 K (±0.5 K) and 120 rpm inside dark condition. After 48 hour, the tubes were placed in centrifuge at 10,000 rpm to obtain clear supernatant. Later the samples were filtered to separate the vitamin loaded gels and supernatant. Later, the vitamin loaded gels were freeze dried. Appropriate volume of supernatant was collected and appropriately diluted to measure the concentration of remaining VB_{12} by UV-vis spectroscopy. The amount of vitamin loaded in the hydrogel (*VB_{12} loading*) is calculated by [105],

$$VB_{12}\ loading\,(\%) = \frac{\text{Amount of } VB_{12} \text{ in hydrogel}}{\text{Amount of freeze dried hydrogel}} \times 100 \qquad (3.1)$$

3.2.3.3.Release of VB_{12}

The release of VB_{12} was carried out in three buffers, namely; AGF, AIF and PBS respectively. The VB_{12} loaded dried hydrogels were placed in buffers and 20 mL buffer solution was added. The solutions were placed in the same orbital shaker at 310 K (±0.5 K) at 60 rpm. After each hour, 5 mL buffer solution was collected and replaced by 5 mL fresh buffer solution to

maintain equal volume. The collected aliquots were filtered to remove any fragment of hydrogel. Amount of VB_{12} in the aliquots was determined by UV-vis spectroscopy.

3.3. Results and discussions

3.3.1. FT-IR spectra

Figure 3.3 represents FT-IR characterization of pure CMC, pure xylan, synthesized CMC gel, xylan gel and CMC-xylan gel. Major characteristic peaks of CMC and xylan are O-H stretching, C-H stretching, C-H bending, C-C bending, skeletal vibration of C-O and C-C in pyranose ring, antisymmetric β-(1→4) glycosidic linkage and C-H glycosidic deformation. The FT-IR spectra of pure CMC and pure xylan are given in Figure 3.3a and 3.3b respectively. O-H stretching of pure CMC and pure xylan are assigned at 3568 cm^{-1} and 3449 cm^{-1} respectively. C-H stretching of both are assigned at 2900 cm^{-1}. The bending of $–CH_2$ is assigned at 1420 cm^{-1} for both cases. Skeletal vibrations are also observed at 1320 cm^{-1} and 1338 cm^{-1} respectively. For pure CMC, bending of C-C is assigned at 1057 cm^{-1} and the same for pure xylan is assigned at 1042 cm^{-1}.

The characteristic peaks in FT-IR spectra of CMC gel, xylan gel and CMC-xylan gel (Figure 3.3c-e) are found in similar positions. For the hydrogels, stretching of O-H varies in the range of 3392-3455 cm^{-1}. A doublet peak of 2914-2920 cm^{-1} and 2875-2881 cm^{-1} represents C-H stretching and bending respectively. In all FT-IR spectra, a peak at 1637-1647 cm^{-1} is primarily described as the HOH bending of the physically absorbed water [109, 110] and is merged with the asymmetric stretching of COO^-, generally observed within the range of 1600-1620 cm^{-1} [44]. The symmetric bending of $–CH_2$ is observed at 1420 – 1458 cm^{-1} [112]. However, close proximity to this, the symmetric stretching vibration of COO^- moiety is found in 1423 – 1446 cm^{-1} [35]. Hence, the two are merged in a broad peak at 1458 cm^{-1}. The skeletal vibrations are shifted in the range of 1338-1361 cm^{-1}. Kono et al. report the bending of C-C is at 1064 cm^{-1} and Sekkal et al. report antisymmetric β-(1→4) glycosidic linkage at 1090 cm^{-1} [35, 108]. For that, the broad peak at 1080-1088 cm^{-1} is collectively considered as merger of antisymmetric β-(1→4) glycosidic linkage and bending of C-C. The glycosidic deformation of C-H with ring vibration is assigned at 843-876 cm^{-1}.

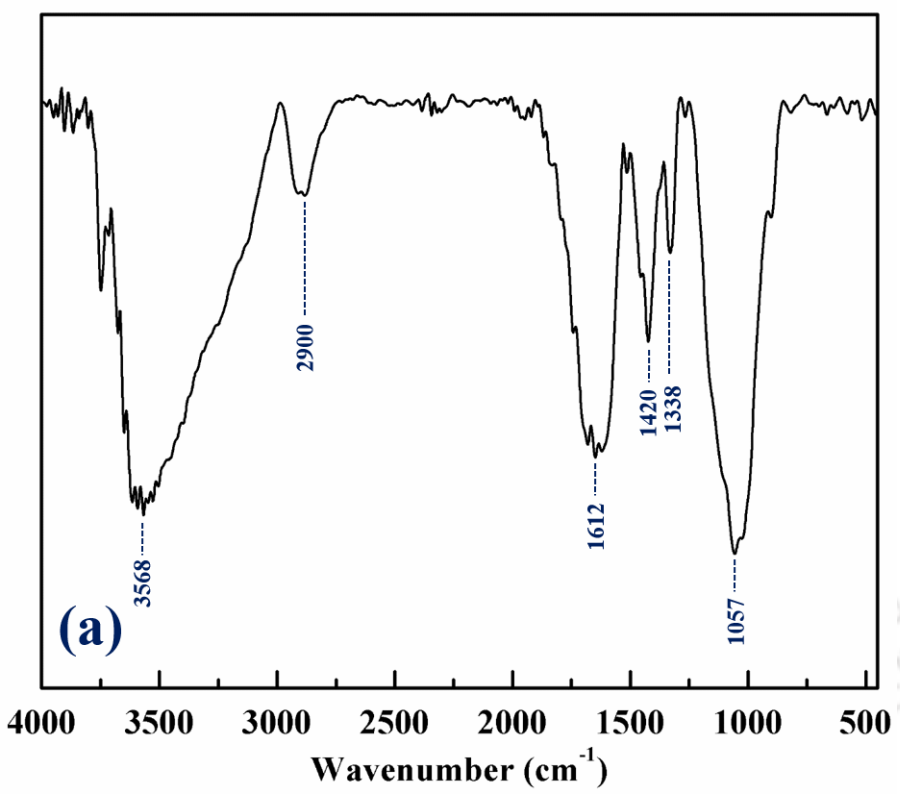

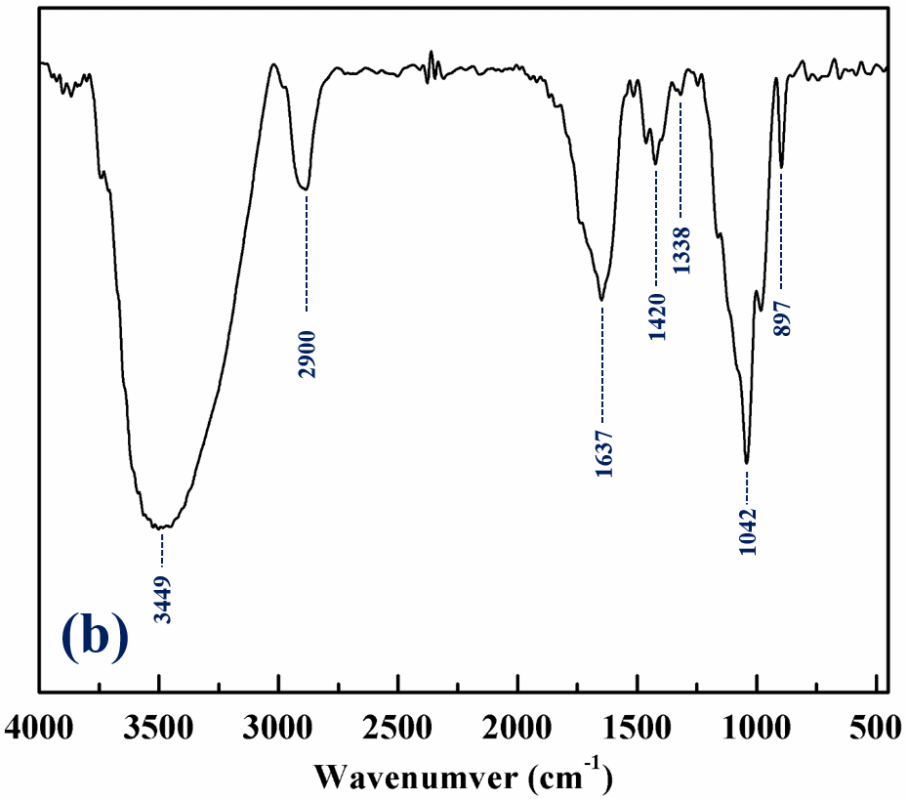

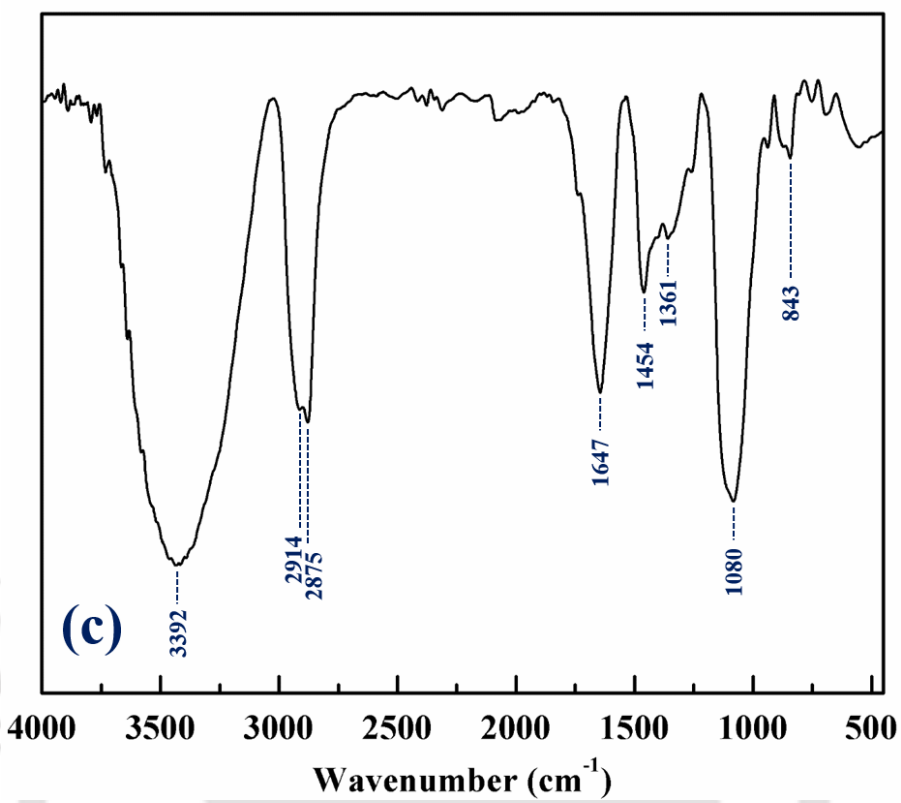

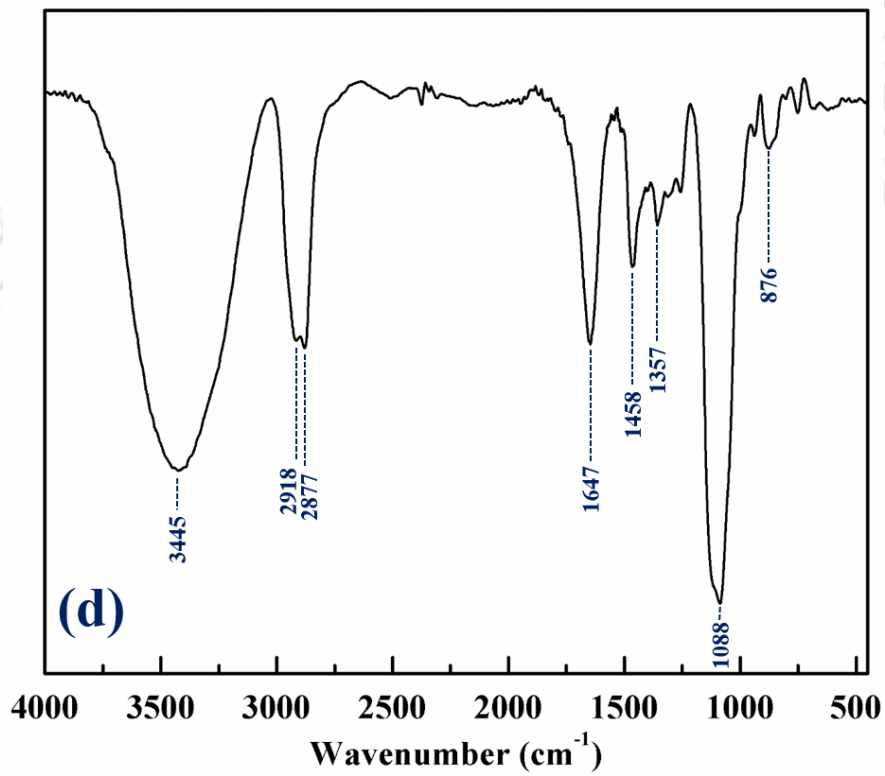

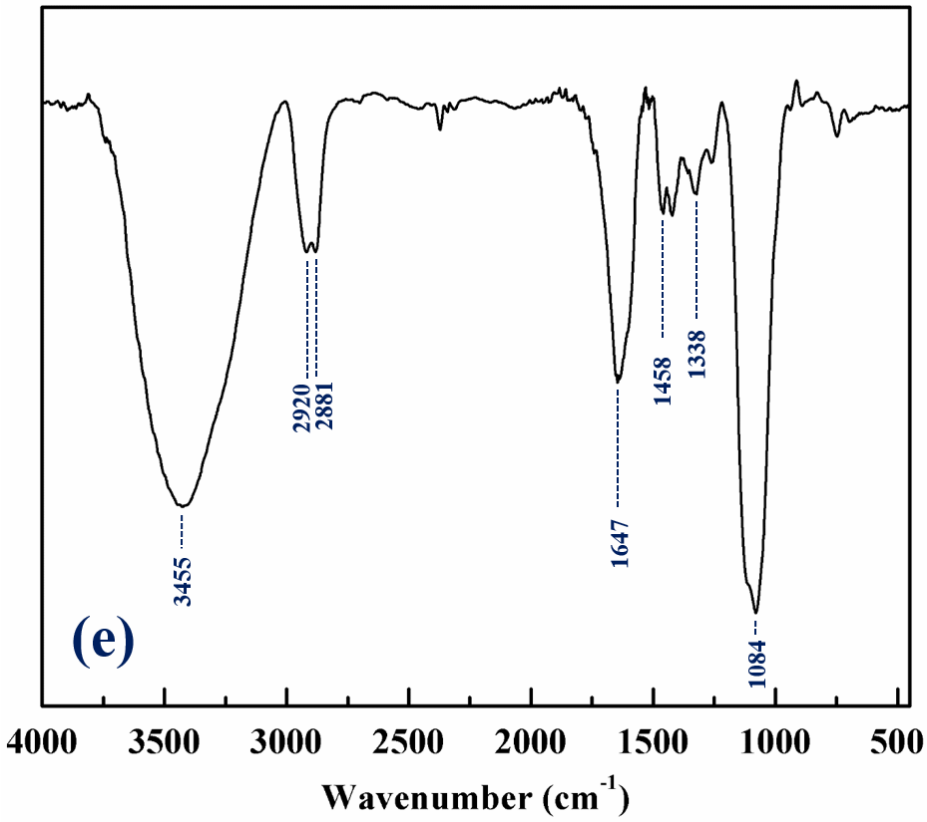

Figure 3.3. FT-IR spectra, (a) CMC pure, (b) xylan pure, (c) CMC gel, (d) xylan gel, (e) CMC-xylan.

3.3.2. Morphology of hydrogels

The morphology of hydrogels are visualized by FESEM and optical microscope and are given in Figure 3.4 and 3.5 respectively. From the FESEM images (Figure 3.4), the microstructure of xylan gel appears to be coarse in nature with random elongations. The random elongations create uneven pores and an increased surface area which may act as possible complex formation sites for VB_{12}. In contrast to xylan gel, CMC gel appears to have uneven surface only. The beads, visible on the surface may be sodium ions of carboxymethyl cellulose sodium salt. The presence of sodium ions on the surface reflects the presence of carboxymethyl chains attached to the pyranose ring of CMC and for this reason VB_{12} easily binds with CMC gel. However, the copolymerized CMC-xylan gel has a porous structure. The pores are well attributed to absorb VB_{12} inside pore wall enabling higher uptake of VB_{12}. The hydrogels appear to be glossy and coarse in the optical microscopic images (Figure 3.5a-c). The VB_{12}

loaded hydrogels are further visualized using optical microscope and are given in Figure 3.5d-f. Upon loading of VB_{12}, the hydrogels do not lose its glossy appearance and the vitamin is seen to absorb throughout the surface.

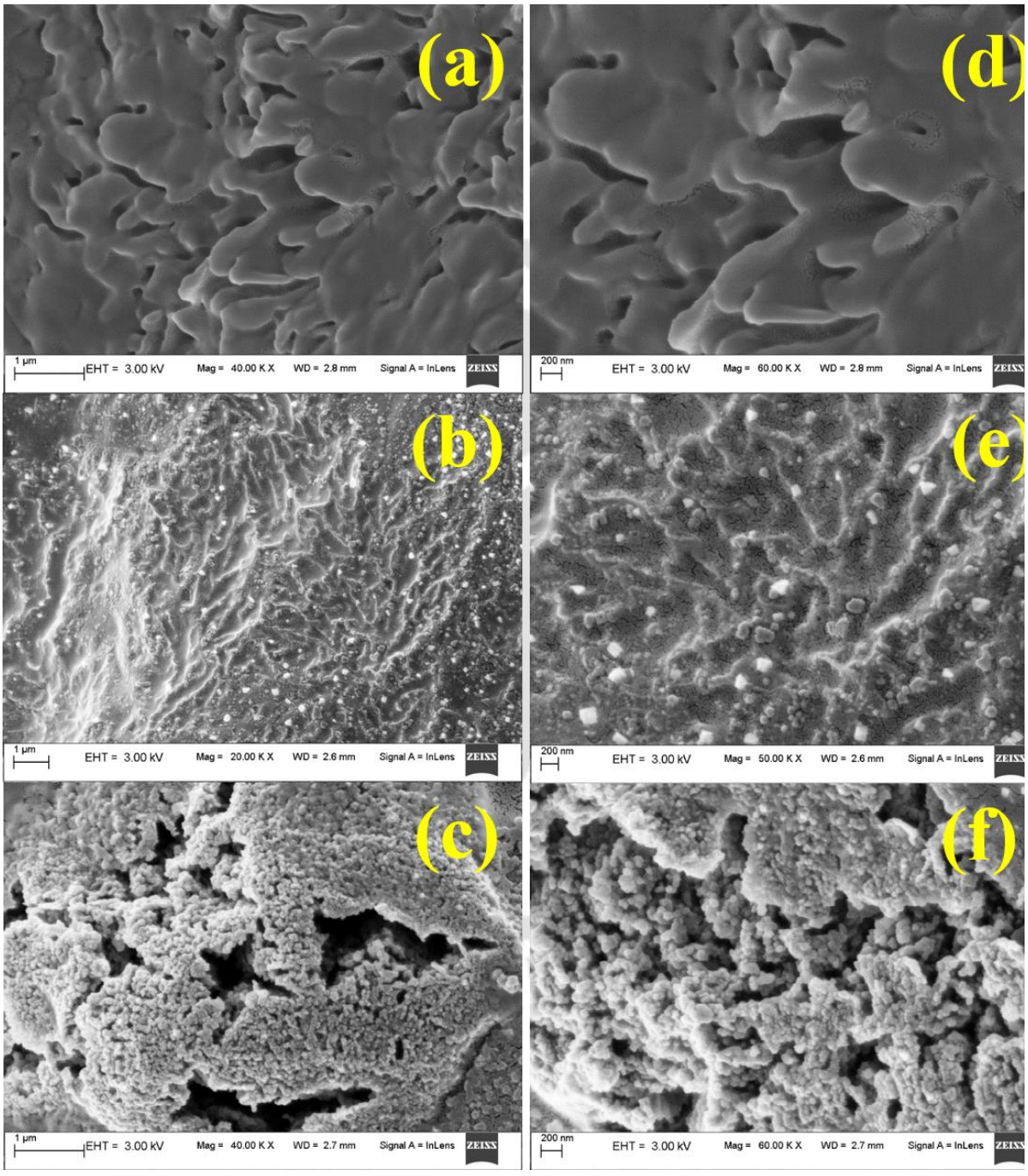

Figure 3.4. FESEM morphology of hydrogels at 1 μm (a)-(c) and 200 nm (d) - (f). (a) and (d) xylan gel, (b) and (e) CMC gel, (c) – (f) CMC-xylan gel.

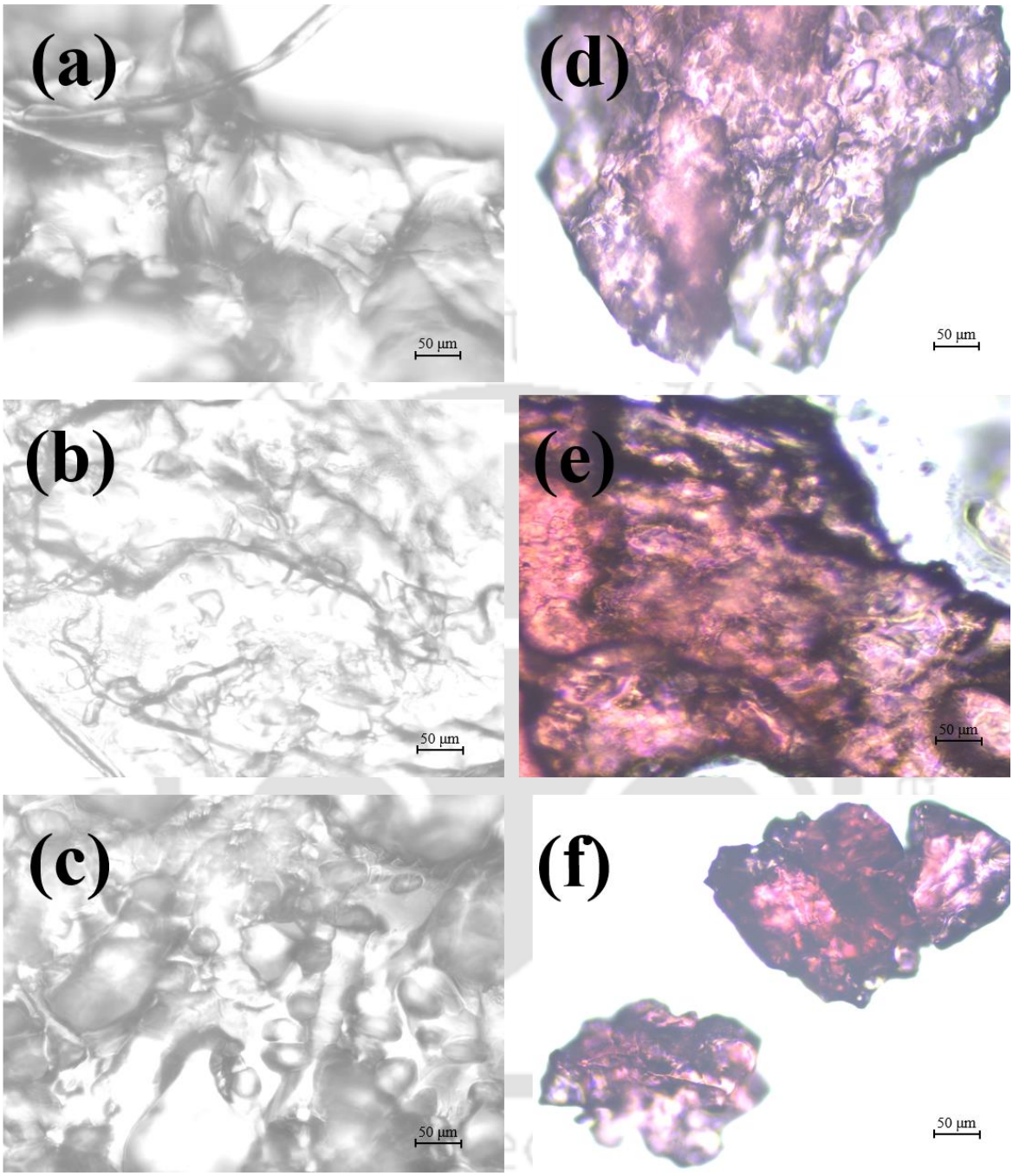

Figure 3.5. Optical microscope images of hydrogels (a-c) and VB_{12} loaded hydrogels (d-f). (a) and (d) xylan gel, (b) and (e) CMC gel, (c) and (f) CMC-xylan gel.

3.3.3. Rheological analysis

The viscosity of the gels are measured at 298 K within a shear rate of 0.01-1000 s^{-1} and is given in Figure 3.6. For all the hydrogels, with the increasing shear rate, the viscosity decreases, referring to the shear thinning behavior of the hydrogel. At high rate (> 100 s^{-1}), the viscosity of all hydrogels is found in similar region although distinct nature of curves are visible at lower shear rate. This is attributed to the loosening of crosslinking structure at high shear rate.

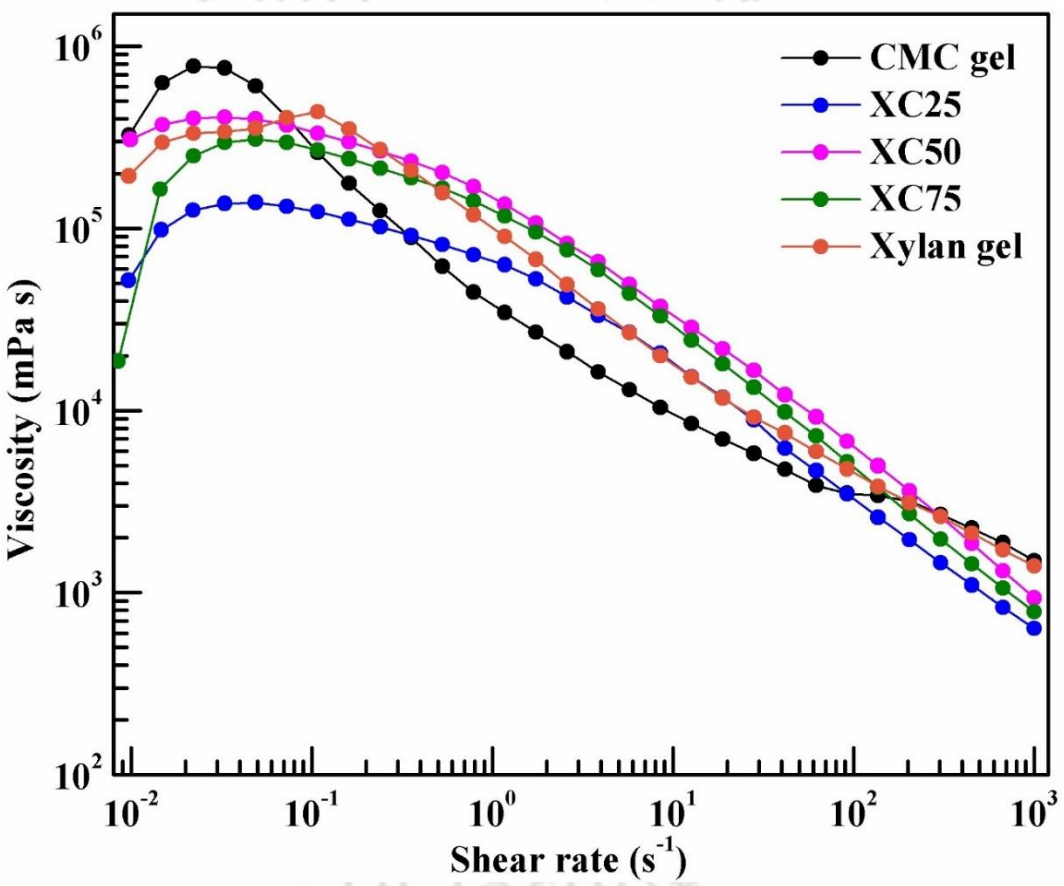

Figure 3.6. Viscosity of hydrogels.

The shear thinning behavior of hydrogels are further confirmed by fitting the flow behavior in power law model. The values of parameters of the power law model are given in Table 3.1. The power law index for all hydrogels are less than unity which mathematically confirms the

shear-thinning nature of gels with increasing shear rate. The goodness of fit is expressed in terms of correlation coefficient (R^2) whose values are given in Table 3.1.

Table 3.1. Power law parameters.

Name of the hydrogel	m	n	R^2
CMC gel	5.23×10^4	0.422	0.96
XC25	3.54×10^4	0.524	0.89
XC50	8.64×10^4	0.451	0.94
XC75	5.86×10^4	0.507	0.80
Xylan gel	6.75×10^4	0.454	0.95

Further the amplitude sweep test of the hydrogels is carried out to find out the storage and loss moduli of the gels. The amplitude sweep is reported at Figure 3.7a within 0.1-1000% strain range at 298 K. For all gels, we observe a crossover at 500% of strain and storage modules dominates over the loss modulus. The linear viscoelastic region (LVR) is determined at 1% strain and to confirm the viscoelastic characteristics, we have performed frequency sweep test keeping 1% strain constant. For the copolymerized gels, the dominance of storage modulus over loss modulus reflects the solid like behavior of the gels within the range of strain considered. Figure 3.7b represents the frequency sweep plot of the gels at 298 K, 1% strain and 0.01-100 Hz frequency range. For all the gels, dominance of storage moduli ($G^{'}$) is observed over loss moduli ($G^{''}$) until crossover point, typically appears after 10 Hz. Among all the gels, XC50 (50 mol% xylan : 50 mol% CMC) shows highest crossover frequency at 54.43 Hz which reflects the structure of this gel can accommodate larger deformation than pure CMC and xylan gel. For all the copolymerized gels, the lesser values of storage and loss modulus have been observed than pure CMC and xylan gels. We have further calculated the loss tangent values of the hydrogels and plotted in Figure 3.8 as a log-log plot with respect to the frequency. At higher frequencies (> 10 Hz), the loss tangent becomes greater than unity i.e. phase transition occurs. After the phase transition, the crosslinked structure breaks down and thereafter the liquid like behavior of the gels are confirmed.

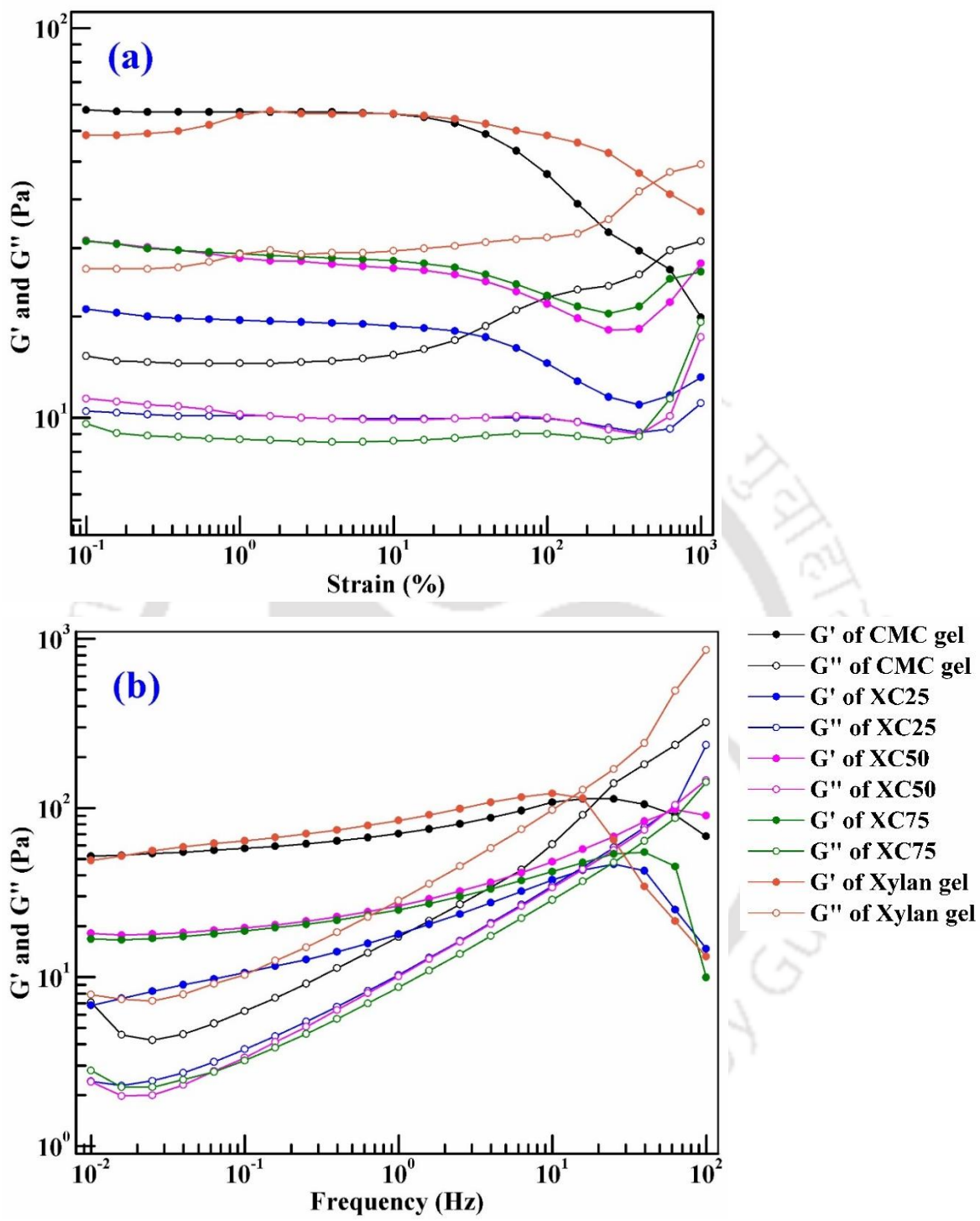

Figure 3.7. Rheology of hydrogels, (a) amplitude sweep, (b) frequency sweep.

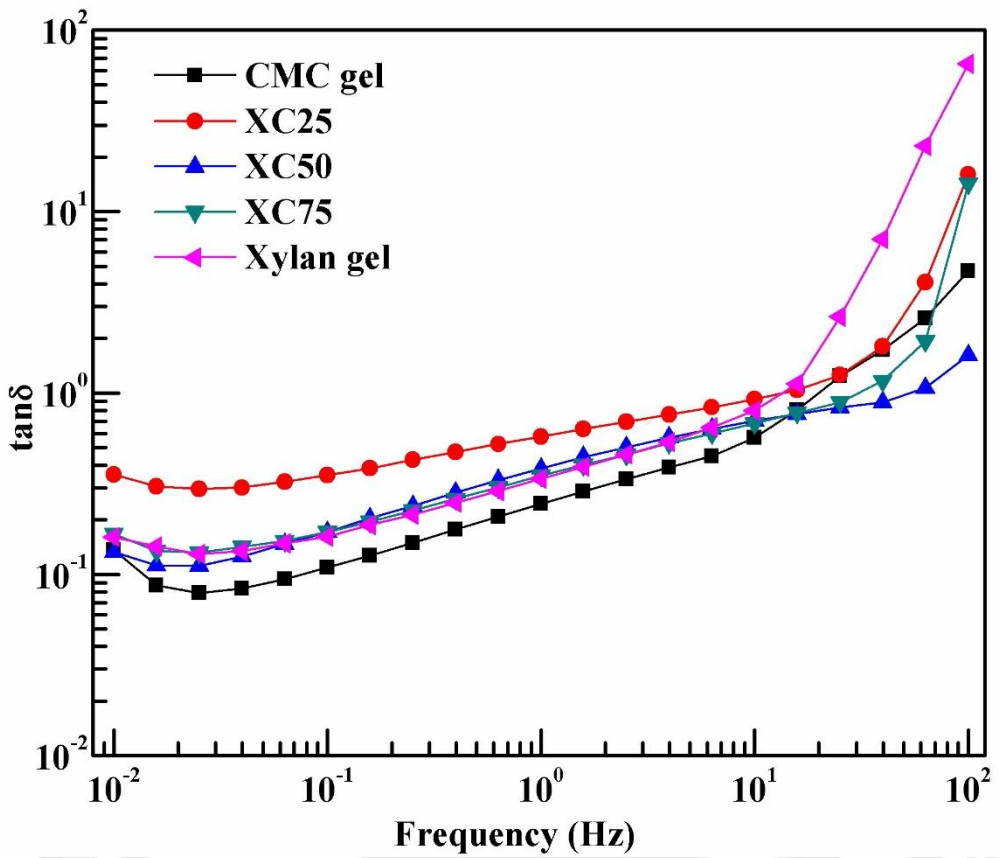

Figure 3.8. Loss tangent of hydrogels

Figure 3.9a represents the temperature sweep measurement of precursor of hydrogels within 298-353 K, with 1 K min^{-1} increment of temperature, 1 Hz frequency and 1% of strain. The gelation point, gelation temperature and gelation time of all the hydrogels are given in Table 3.2. We observe that the viscous nature of the precursors dominates until the gelation temperature. The gelation temperature of all gels are observed within 317-324 K. After the gelation temperature, elastic nature is seen to be prominent i.e. evolution of network. During the evolution of network, sharp rise of storage and loss moduli are observed. The formation of network is completed within 317-330 K. The similar temperature range is also observed during the hydrogel synthesis. Among the five hydrogels, XC50 gel has the narrowest temperature range for the network evolution. For that, 1:1 molar ratio is concluded as ideal mixture to form cellulose-hemicellulose hydrogel. After the gelation, the network stabilizes and no new crossover is observed. This implies the stability of the network is up to 353 K at the LVR. Figure 3.9b represents the time sweep measurement of the precursor solution

measured at the corresponding gelation temperature with 1 Hz frequency and 1% of strain. Like temperature sweep, viscous nature of precursor dominates until the crossover point. The crossover point for every hydrogel appears within 5-11 min, signifying the relative slow nature of gelation after addition of crosslinker. However, once it starts the whole network is built up within 5-7 min and sharp changes in storage and loss moduli are observed. Among the five gels, XC50 produces fastest gelation time of 5 min. After the evolution of network, the network remains stable for long duration which reflects strong network formation and also confirms the elastic behavior when compared to the viscous behavior.

Table 3.2. Values of gelation parameters.

Parameters	Hydrogels				
	CMC gel	XC25	XC50	XC75	Xylan gel
Gel point (Hz)	20.00	13.61	53.82	30.64	13.54
Gelation temperature (K)	318	324	317	321	322
Gelation time (min)	7.5	6.25	5	7	11

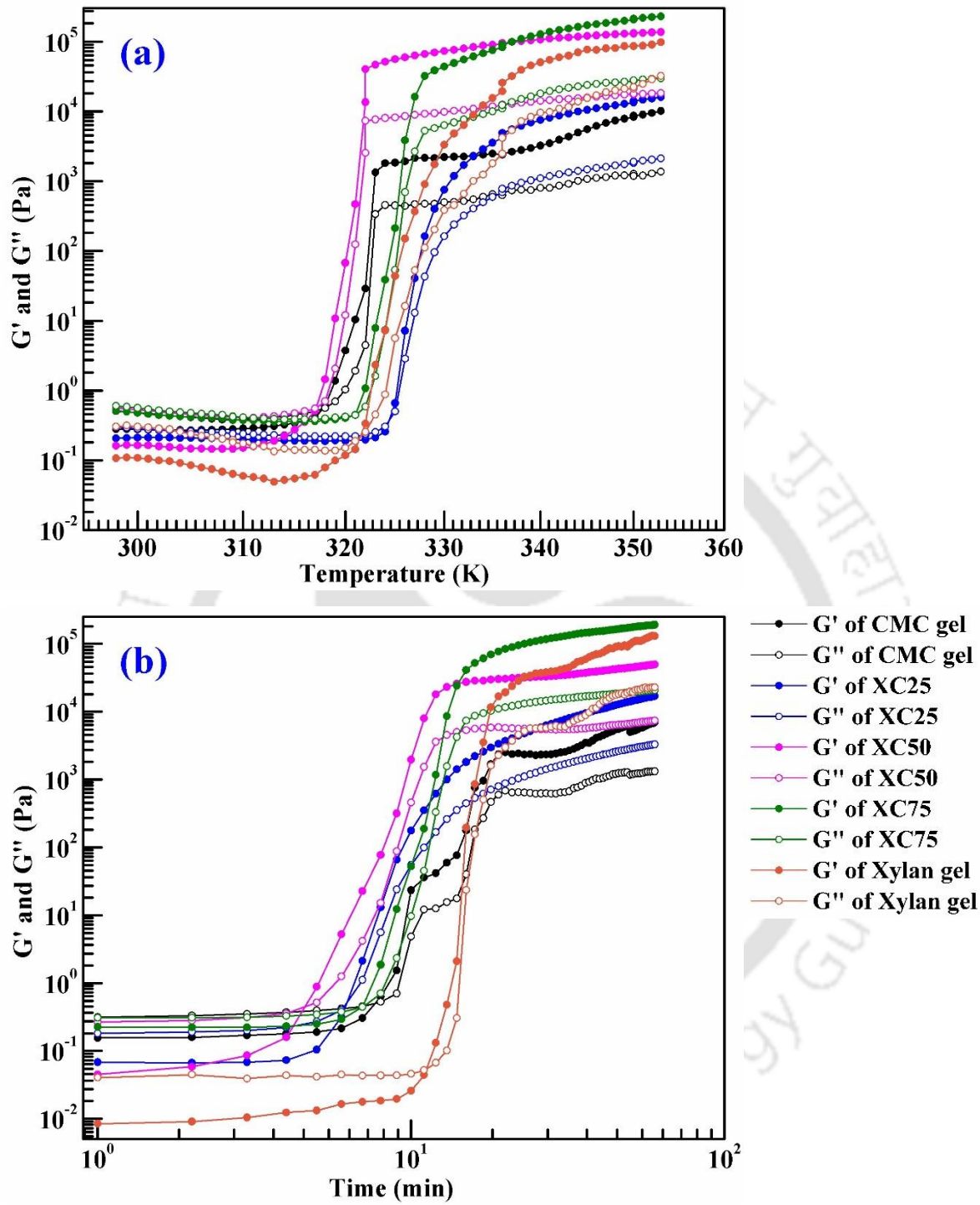

Figure 3.9. Temperature sweep and time sweep of precursor solutions, (a) temperature sweep, (b) time sweep.

3.3.4. Swelling ratio measurement and gel fraction

Figure 3.10a represents the swelling ratio of hydrogels measured in deionized (DI) water, AGF, AIF and PBS buffers. Both CMC and xylan are linear polymers which create network gel by crosslinking. The dominant charge species of polysaccharides i.e. hydroxyl moiety (in CMC and xylan) and carboxymethyl moiety (in CMC) repel each other and expand the network structure in suitable medium. The swelling ratio is determined by the amount of water absorbed to the dry weight of hydrogel. Here, the order of swelling is CMC gel > XC25 > XC50 > XC75 > xylan gel. The long chain carboxymethyl moiety electrostatically repel each other; therefore the swelling ratio increases with the increment of molar ratio of CMC in hydrogel. Further, for all hydrogels, greater swelling is observed in DI water. For buffers, the available free ions readily bind with the deprotonated hydroxyl and carboxymethyl moieties and hinder swelling. For that, least swelling ratio is observed in AGF buffer. For all the hydrogels, the trend of swelling ratio is observed in all buffers and DI water is, DI water > PBS > AIF > AGF. Figure 3.10b represents the gel fraction of hydrogels. The trend of gel fraction follows the trend: CMC gel < XC25 < XC50 < XC75 < xylan gel. As the gel fraction increases, the degree of crosslinking in the network increases. Therefore, the network has less flexibility to swell and absorb more water. For that, the gel fraction follows the opposite trend of swelling ratio [98]. Figure 3.11 represents the images of freeze dried and swollen hydrogels.

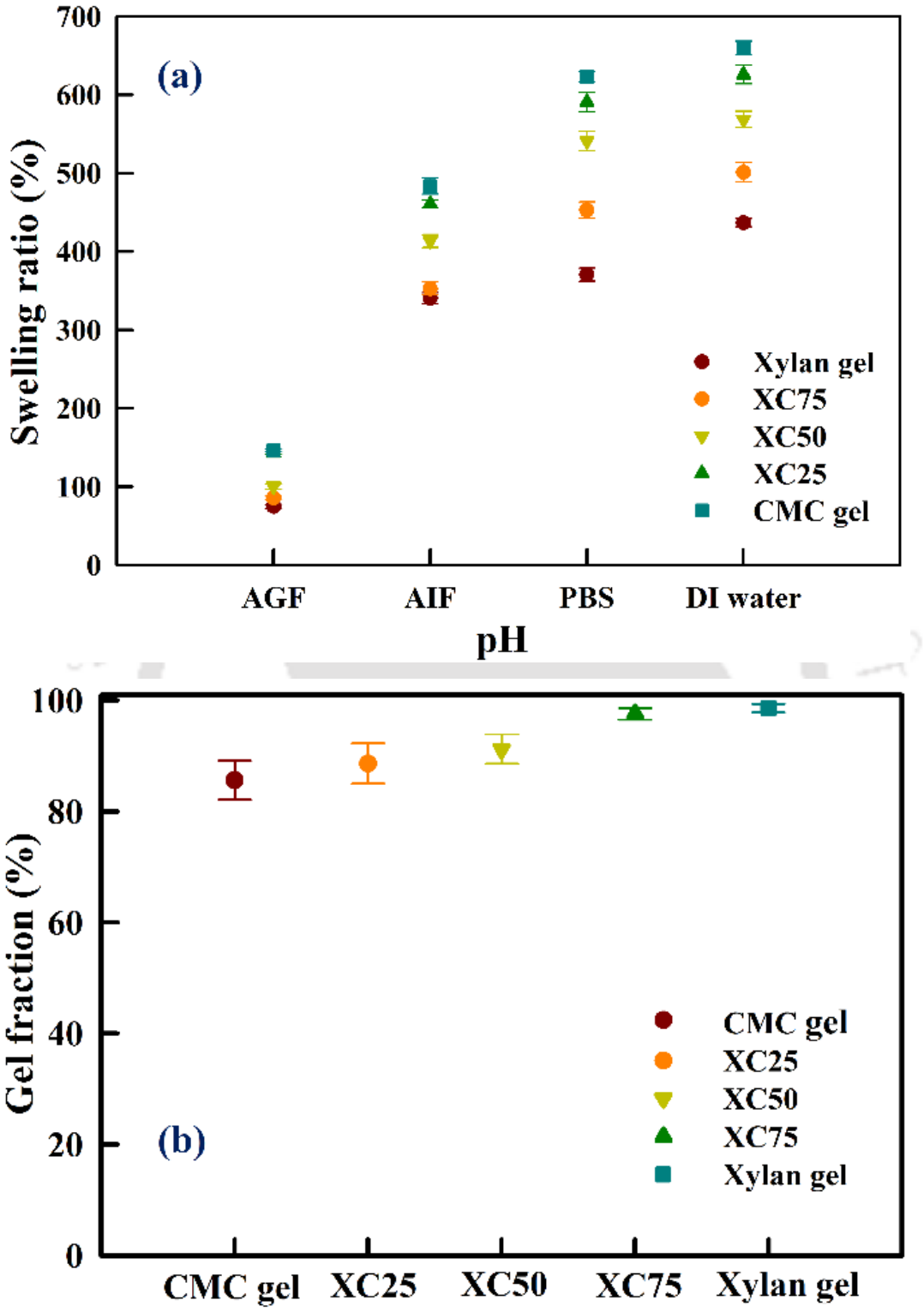

Figure 3.10. (a) Swelling ratio of hydrogels in DI water and various buffers. (b) Gel fraction of hydrogels.

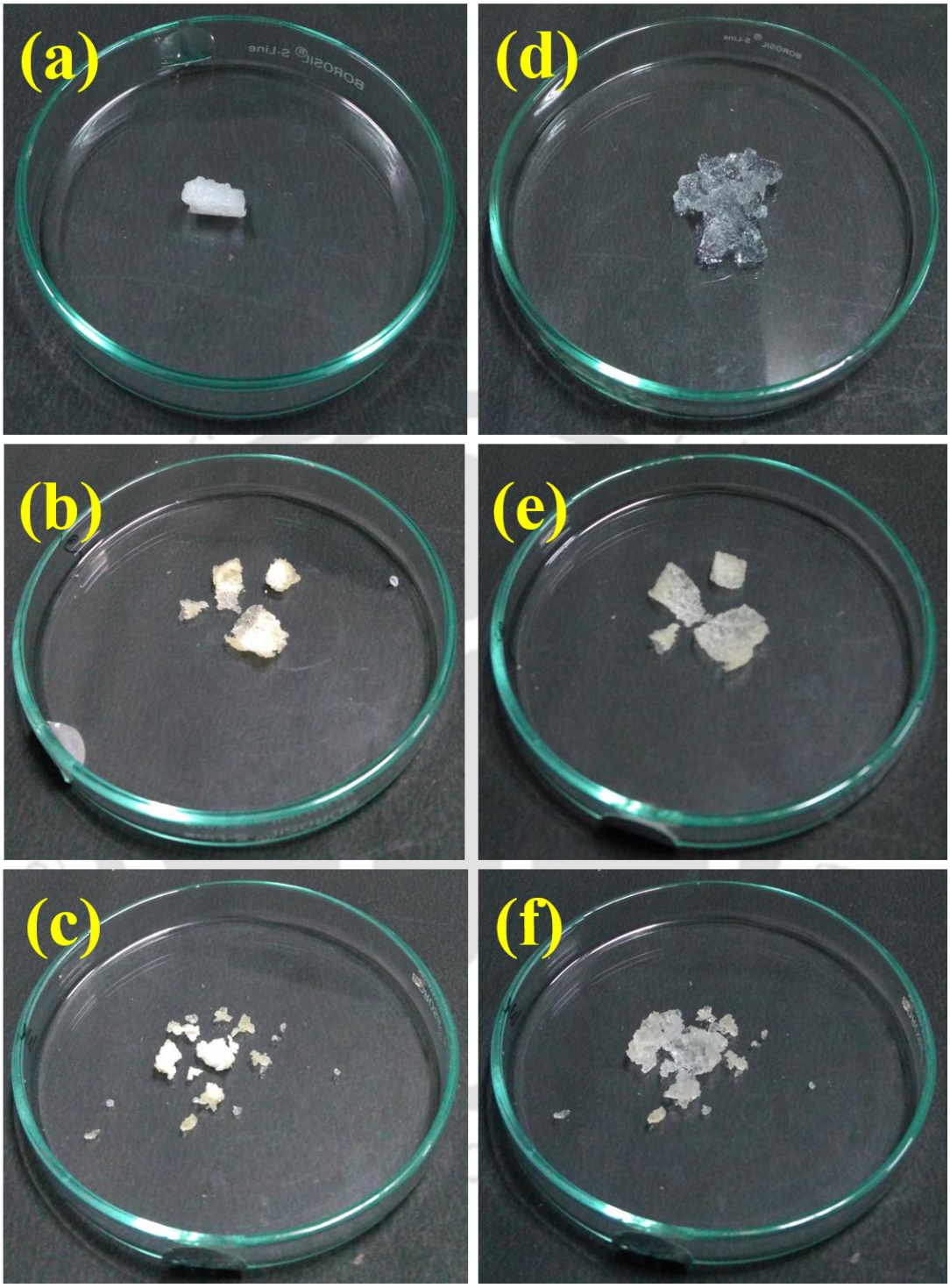

Figure 3.11. Freeze dried (from (a) to (c)) and swelled hydrogels (from (d) to (f)). (a) and (d) CMC gel, (b) and (e) xylan gel, (c) and (f) CMC-xylan gel.

3.3.5. Loading of VB_{12}

Figure 3.12 represents the VB_{12} loading in the hydrogels. CMC gel and xylan gel have 15.46% and 17.75% VB_{12} loading respectively whereas copolymerized gels have greater than 20% loading. XC50 has highest VB_{12} loading of 36.59% among the copolymerized gels. The recorded loading is higher than the reported loading of Bajpai & Dubey [84] and Xu et al [116]. It is presumed that the porous structure of copolymerized gels adsorb higher amount of vitamin than the surface adsorption by pure CMC and xylan gels.

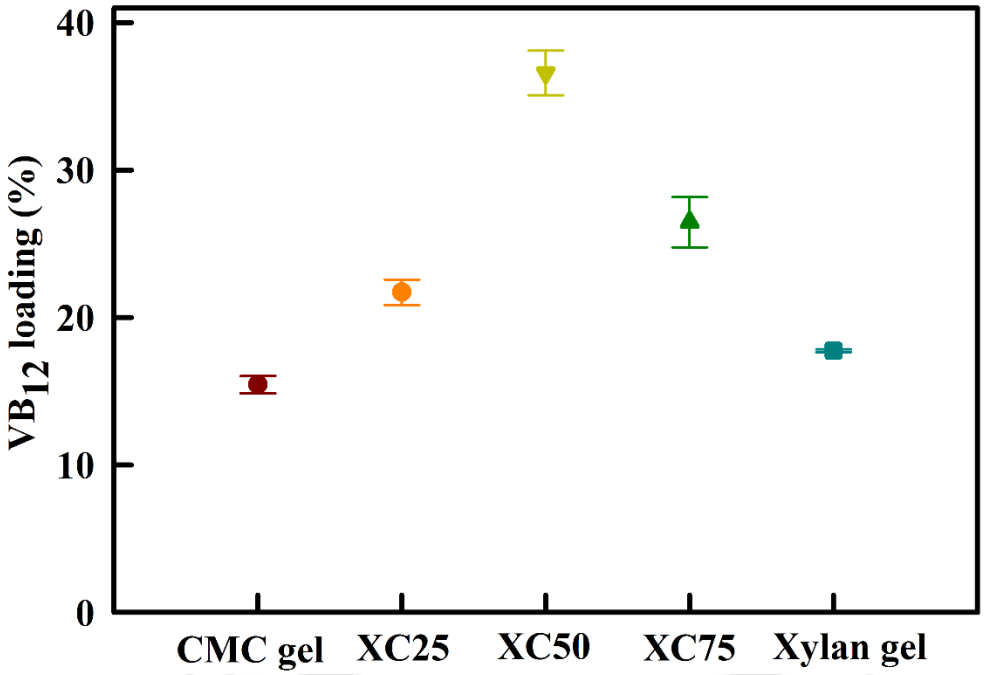

Figure 3.12. *VB_{12} loading* (%) in hydrogels

3.3.6. *In vitro* release of VB_{12}

The *in vitro* release of VB_{12} from the hydrogel network in AGF, AIF and PBS buffers are given in Figure 3.13a-c. AGF mimics the stomach fluid whereas AIF mimics the first zone of intestinal fluid [76]. The pH of the colonic fluid is 7.4 which is adequately represented by PBS [117]. Thus the *in vitro* release of VB_{12} in these buffers will elucidate the vitamin release behavior in simulated physiological fluids. Further, Figure 3.13d represents the *in vitro* release of VB_{12} in consecutive buffers. The mean gastric emptying time is 1.08 hour (±0.11 hour) and mean colonic arrival time is 2.83 hour (±0.33 hour) which reflects the transit time through small intestine as 1.75 hour (±0.25 hour) [113]. Therefore, a residence time of 2 hour in gastric fluid i.e. AGF, 2 hour in intestine fluid i.e. AIF and 6 hour in colonic fluid i.e. PBS would be a realistic effort to simulate the *in vitro* release of VB_{12} in gastrointestinal tract [117].

It is observed, from Figure 3.13a-c that the *in vitro* release of VB_{12} depends on the pH of the medium. Cumulative release of less than 28% is observed in AGF compared to 80-88% in AIF and 93-98% in PBS. The release of guest molecules (here VB_{12}) from hydrogel depend on the available ions in the buffer as well as swelling nature of hydrogels. The swelling of hydrogels happens due to the repulsion of charged moieties which allow them to move away from each other resulting in the loosening of matrix thereby allowing the diffusion of water. However a lower swelling is observed if the negatively charged hydroxyl and carboxyl moieties are quickly protonated. Therefore, for AGF, the higher amount of available H^+ ions quickly occupy the unprotonated sites and thus block the electrostatic repulsion and in turn lower the released amount of VB_{12}. CMC and xylan gels release 19.05% and 19.27% VB_{12} respectively in AGF buffer after 8 hour whereas the copolymerized gels release within 24-28%. A flat plateau is observed for all release profiles in AGF, reflects the tightly bound VB_{12} cannot be released in AGF. Only the loosely surface bound VB_{12} is released in AGF. In AIF and PBS, we observe an initial burst release of VB_{12} (Figure 3.13b-c). The burst release is attributed to the swelling behavior of the gels and dominates for first two hour for all gels. However, after the initial burst, we observe slow and gradual release of VB_{12}. During this time, the ions of respective buffers bind with the hydroxyl moieties facilitating the release of VB_{12} into medium. From Figure 3.13d, we observe a similar amount of VB_{12} release in AGF in first 2 hour as compared to the VB_{12} release in AGF only (Figure 3.13a). However, the

burst releases in AIF and PBS are not observed here as the unprotonated moieties are already been occupied with H^+ ions in AGF. The release of the VB_{12} will mainly depend on the available ions of the AIF and PBS buffers. Therefore, we observe significant amount of VB_{12} which has been delivered by PBS i.e. the hydrogels are capable to release VB_{12} in the colon. Further, the hydrogels are also able to deliver VB_{12} at a longer duration of 10 hour if they are first exposed to AGF.

The *in vitro* release study in different physiological buffers also defines the efficiency of hydrogels as effective carrier of VB_{12}. In all release media, XC50 hydrogel is proven to facilitate highest cumulative release as compared to other gels. Although, CMC and xylan gels produce highest and lowest swelling ratio in all buffers respectively, the cumulative release is lower than the copolymerized gels. This indicates the mere diffusion of water and the resulting relaxation of crosslinking, is not the prime factor for the delivery of VB_{12}. The copolymeric gels have porous morphology as observed from FESEM, providing the ideal binding sites for VB_{12} both at the surface as well as inside the pores. Further, these gels have higher gelation point i.e. can withstand high deformation strain than the pure CMC and xylan gels. Thus they can better hold the crosslinked structure. Further for longer duration, the VB_{12} molecules can be attached to the binding sites.

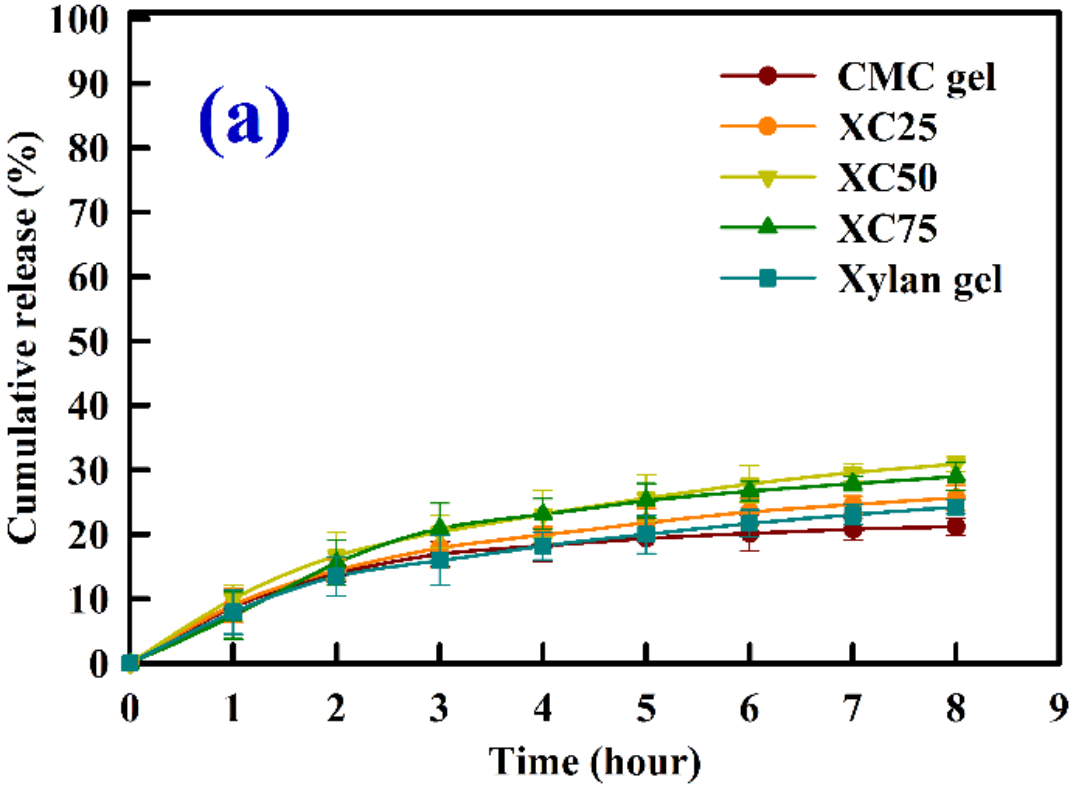

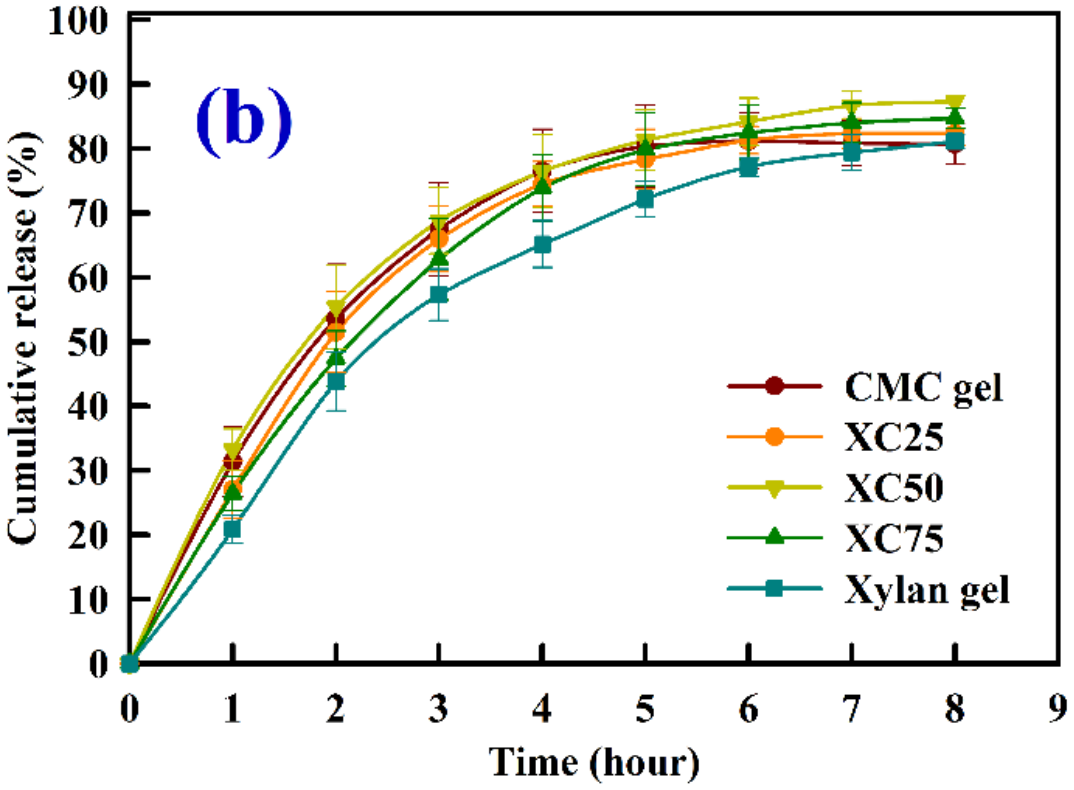

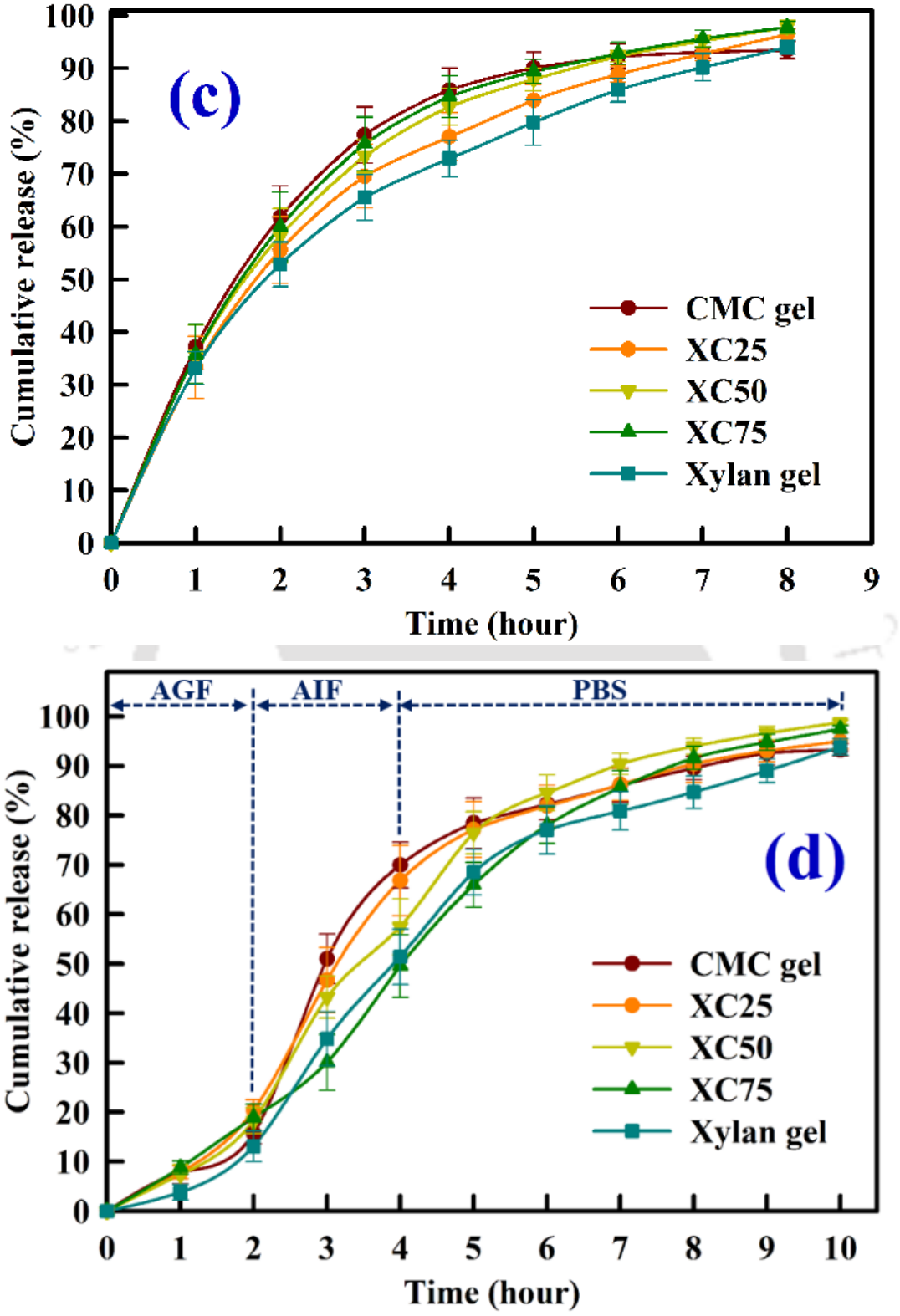

Figure 3.13. *In vitro* release of VB_{12} physiological buffers. (a) AGF buffer, (b) AIF buffer, (c) PBS buffer, (d) AGF-AIF-PBS buffers.

3.3.7. Comparison of VB_{12} release with literature

The *in vitro* release of VB_{12} from hydrogels in physiological buffers are compared with the previously reported two CMC based hydrogel and one xylan based hydrogel reports. The summary of comparison is given in Table 3.3. Boruah et al. reported less than 35% cumulative release of VB_{12} in pH 1.2 and less than 55% cumulative release of VB_{12} in pH 7.4 after 10 hour using CMC grafted poly(acrylic acid) and organophilic montmorillonite nanoclay composite hydrogel [86]. However, the cumulative release increases to 76.2% after 10 hour using lower amount of crosslinker in DI water at room temperature. Nath and Dolui reported VB_{12} loaded CMC grafted poly(acrylic acid) and layered double hydroxide hydrogel [87]. The hydrogel released 66% VB_{12} in pH 7.4 and 50% in pH 1.2 in 6 hour. They further reported the VB_{12} loaded hydrogel without LDH was seen to release a total of 45% in pH 1.2 and 59% in pH 7.4 after 6 hour. Cao et al. also reported *in vitro* release of VB_{12} from multiresponsive xylan hydrogel at pH 2.2 and 7.4 at 310 K for a period of 7 hour [88]. A cumulative release of 78.3% in acidic medium and 89.3% in alkaline medium without UV irradiation have been reported; whereas higher amount of VB_{12} has been released in alkaline medium in presence of UV. Compared to the previous reports, the CMC-xylan copolymerized hydrogels of this work, have higher delivery capacity in AIF and PBS respectively for longer duration. However, lesser amount of VB_{12} is delivered in AGF medium. Unlike the previous reports, we have studied the delivery of VB_{12} in consecutive physiological buffers of gastrointestinal tract. Overall the hydrogels are capable of delivering VB_{12} greater than 90% for 10 hour.

Table 3.3. Comparison with literature of *in vitro* release of VB_{12} using hydrogel

Article	Monomers	VB_{12} loading concentration	Release of VB_{12}	Refer-ence
Boruah et al.	Carboxymethyl cellulose-*g*-poly(acrylic acid) and organophilic montmorillonite nanoclay composite	0.125 wt% in buffer solution of pH=7.0	55% and 34% cumulative release in 10 hour for pH 7.4 and 1.2 respectively.	[86]
Nath and Dolui	Carboxymethyl cellulose-*g*-poly(acrylic acid) and layered double hydroxide	1.25 wt% in buffer solution of pH=7.0	Released in pH=1.2 and 7.4. 59% and 45% cumulative release in 6 hour for pH 7.4 and 1.2 respectively for without LDH. With LDH, 66% and 50% cumulative release in 6 hour for pH 7.4 and 1.2 respectively.	[87]
Cao et al.	Xylan type hemicellulose	0.5 mg mL^{-1} aqueous solution	PBS buffer, with or without presence of UV irradiation of 365 nm, at 310±3 K. Cumulative release is 89.3%.	[88]
Present study	Carboxymethyl cellulose sodium salt and beechwood xylan	0.5 mg mL^{-1} aqueous solution	19-28% release in AGF, 80-88% release in AIF and 93-98% release in PBS within 8 hour at 310 K. 93-99% release in consecutive physiological buffers within 10 hour.	---

3.4. Conclusions

EGDE crosslinked CMC and xylan based homopolymerized hydrogels as well as copolymerized CMC-xylan based gels are synthesized in alkaline medium. Among the five gels, CMC gel possesses highest swelling ratio and xylan gel has the least swelling ratio in AGF, AIF, PBS buffer and DI water. The swelling ratio of CMC gel is 146.58% in AGF buffer and steadily increases to 659.34% in DI water. However, gel fraction follows the opposite trend of swelling ratio i.e. highest gel fraction of 98.63% is obtained with xylan gel while CMC gel produces 85.64% gel fraction. Morphology of CMC and xylan gel appear to be coarse in nature whereas copolymerized CMC-xylan gels are porous in nature. All five hydrogels produce shear thinning behavior upon increasing rate upto 1000 s^{-1}. Further, CMC-xylan gel (1:1 molar ratio) gave lower gel point than CMC gel and xylan gel. The longer gel point proves that the copolymerized structure can withstand more stress than pure hydrogels. Further the loss tangent values are less than unity until gel point signifying the elastic nature of hydrogels which dominates over the viscous nature. The dominance of elastic nature concludes the successful crosslinking with EGDE whereby hydrogels can relax the crosslinking structure upto gel point with an influence of external stimuli. CMC-xylan gel (1:1 molar ratio) has least gelation temperature of 317 K and gelation process starts after 5 min. After the gelation, stable hydrogel network is observed upto 353 K. This hydrogel is further proved to have higher VB_{12} loading of 36.59%. Further, the copolymerized gels release 24-28% VB_{12} in AGF, 82-88% in AIF and 96-98% in PBS which are higher than homopolymerized gels. The *in vitro* release profile reflects the initial burst release of VB_{12} followed by the steady release upto 8 hour.

Chapter 4

Synthesis, characterization of *β*-cyclodextrin-cellulose/hemicellulose based hydrogels for the removal of Cd (II) and Ni (II)

Highlights

- Synthesis of *β*-cyclodextrin-cellulose and *β*-cyclodextrin-hemicellulose based hydrogels
- Characterization by FT-IR spectroscopy, morphology and swelling studies
- Adsorption of Cd (II) and Ni (II) with respect to adsorption dosage, concentration, pH and temperature
- Benchmarking with adsorption isotherm models
- Kinetics of adsorption behavior

Keywords

A. *β*-cyclodextrin;
B. Cellulose;
C. Hemicellulose;
D. Hydrogel;
E. Adsorption.

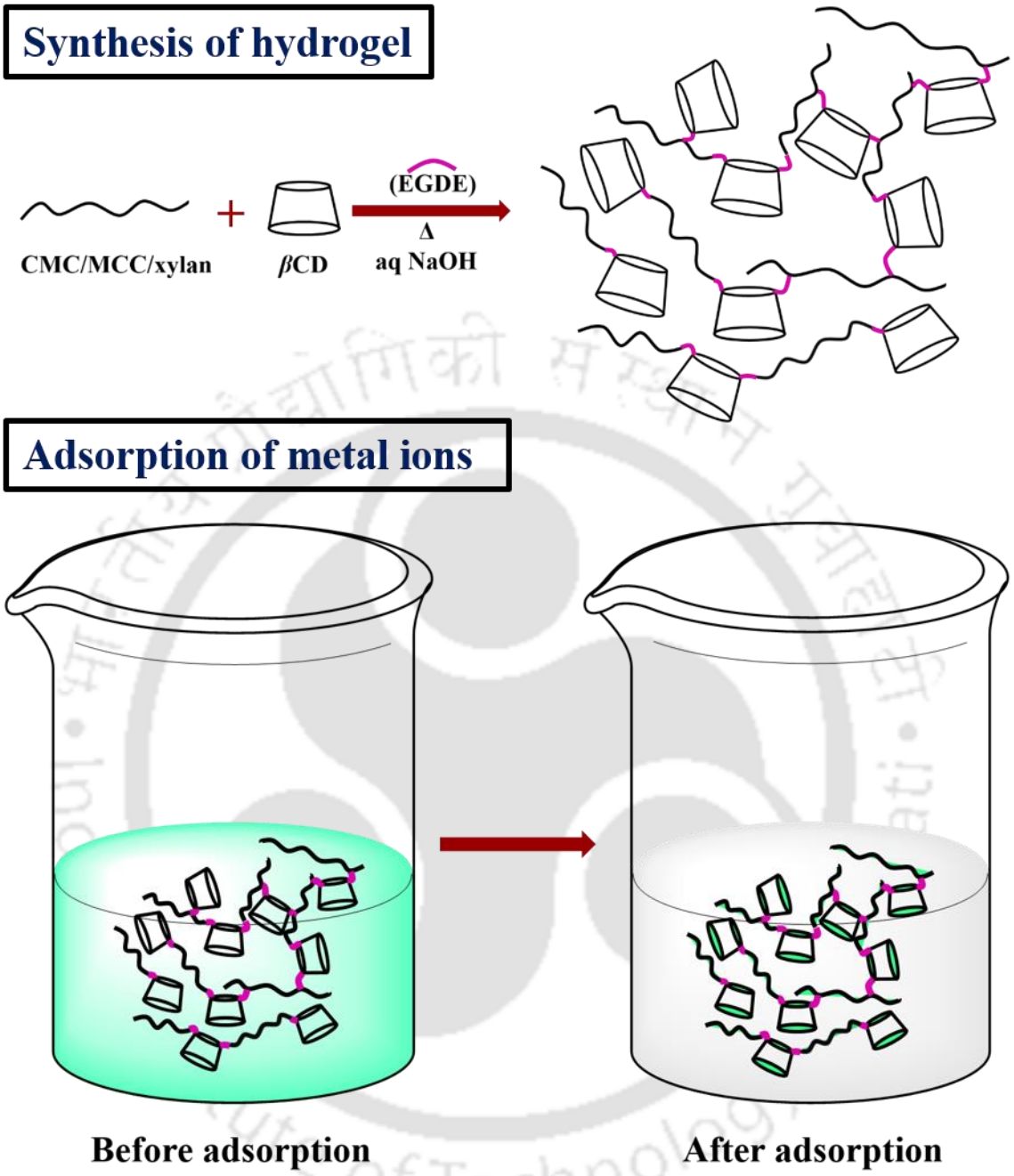

Figure 4.1. Pictorial representation of synthesis of adsorption followed by adsorption of metals.

4.1. Chapter summary

Nickel (Ni (II)) and cadmium (Cd (II)) are two such toxic contaminants that can cause severe damage in human and aquatic life after being accumulated in high concentrations. Therefore, in this chapter, the polysaccharide based hydrogels are employed to adsorb Ni (II) and Cd (II) from aqueous solutions. Four *β*CD based hydrogels are synthesized using EGDE as crosslinker. CMC, MCC, xylan are crosslinked with EGDE to produce hydrogels; namely *β*CD-CMC, *β*CD-MCC and *β*CD-xylan, in alkaline medium at 1:1 mole ratio. Additionally pure *β*CD gels are also prepared in alkaline medium. The synthesized hydrogels are characterized with FT-IR spectroscopy, X-ray Photoelectron spectroscopy, swelling ratio, gel fraction and the morphologies are observed in optical microscope and FESEM. The adsorption studies are carried out by varying adsorbent dosage, concentration, pH and temperature. The equilibrium adsorption data are fitted in Langmuir and Freundlich isotherm model to reveal the nature of adsorption. The time resolved adsorption capacities are fitted to pseudo first order and pseudo second order model to determine the kinetics of adsorption.

4.2. Materials and methods

4.2.1. Materials

Nickel chloride hexahydrate ($NiCl_2.6H_2O$) and cadmium chloride monohydrate ($CdCl_2.H_2O$) were purchased from Merck. All other chemicals required for synthesis of hydrogel, characterization and application are given in Section 2.2.1.

4.2.2. Preparation of hydrogels

*β*CD was dissolved in 1.5 mol L^{-1} aqueous NaOH solution. CMC, xylan and MCC were separately dissolved as described in Chapter 2. After getting a homogeneous mixture, *β*CD was added in all three cases in a 1:1 mole ratio. The mixtures were heated at 323 K and stirred until homogeneous precursor solution is obtained. EGDE crosslinker was added drop wise into the solution. Pure *β*CD based hydrogel was prepared by adding EGDE into homogeneous solution of *β*CD. The gelation was seen to complete within 30 min. The gels were washed with DI water to remove unreacted precursors. Thereafter the alkaline pH of the gels was neutralized with 0.1 M HCl solution and subsequently lyophilized. The schematic diagram of synthesis of gels are given in Figure 4.2-4.5.

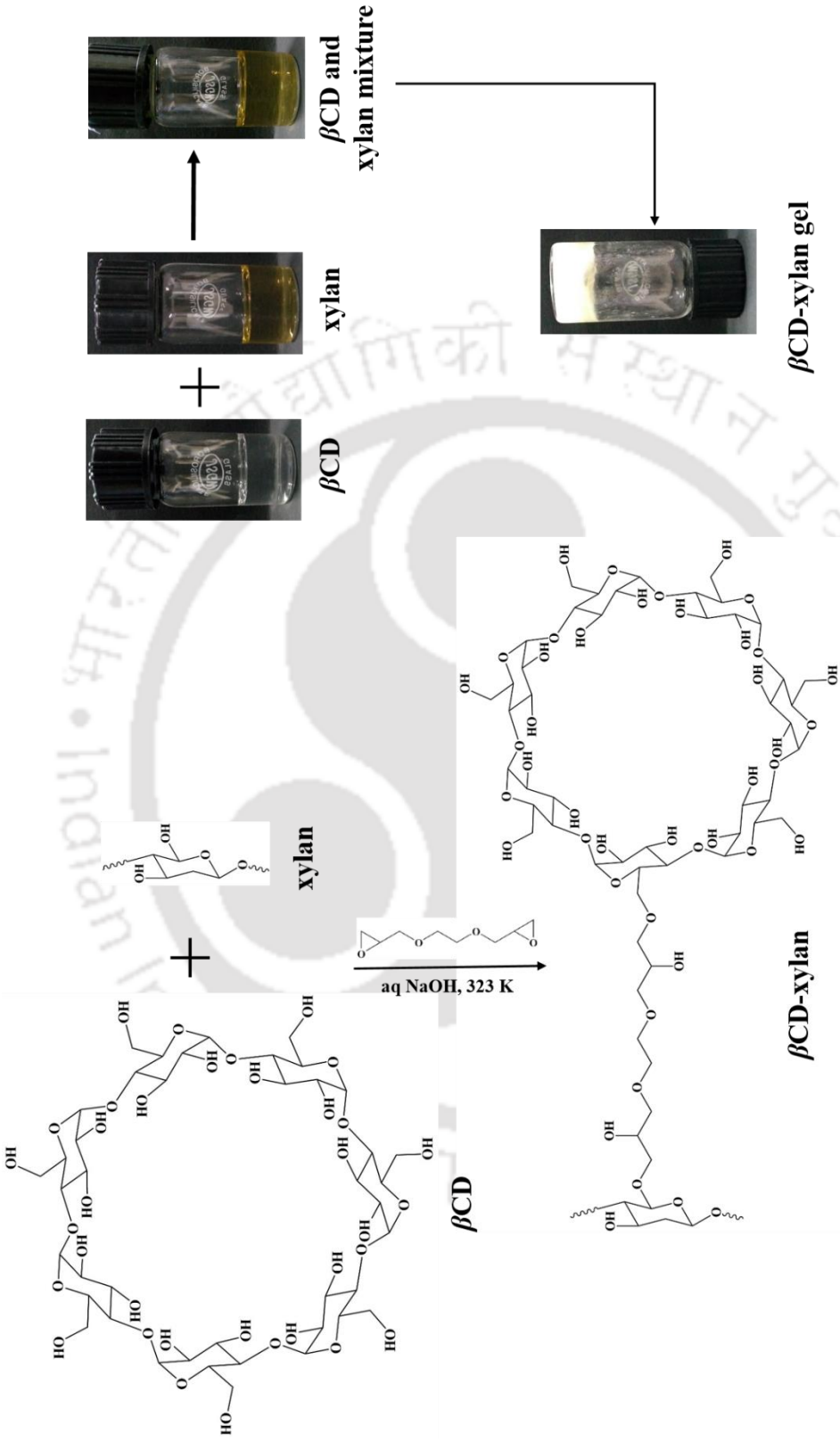

Figure 4.2. Reaction scheme of *β*CD-xylan hydrogel formation

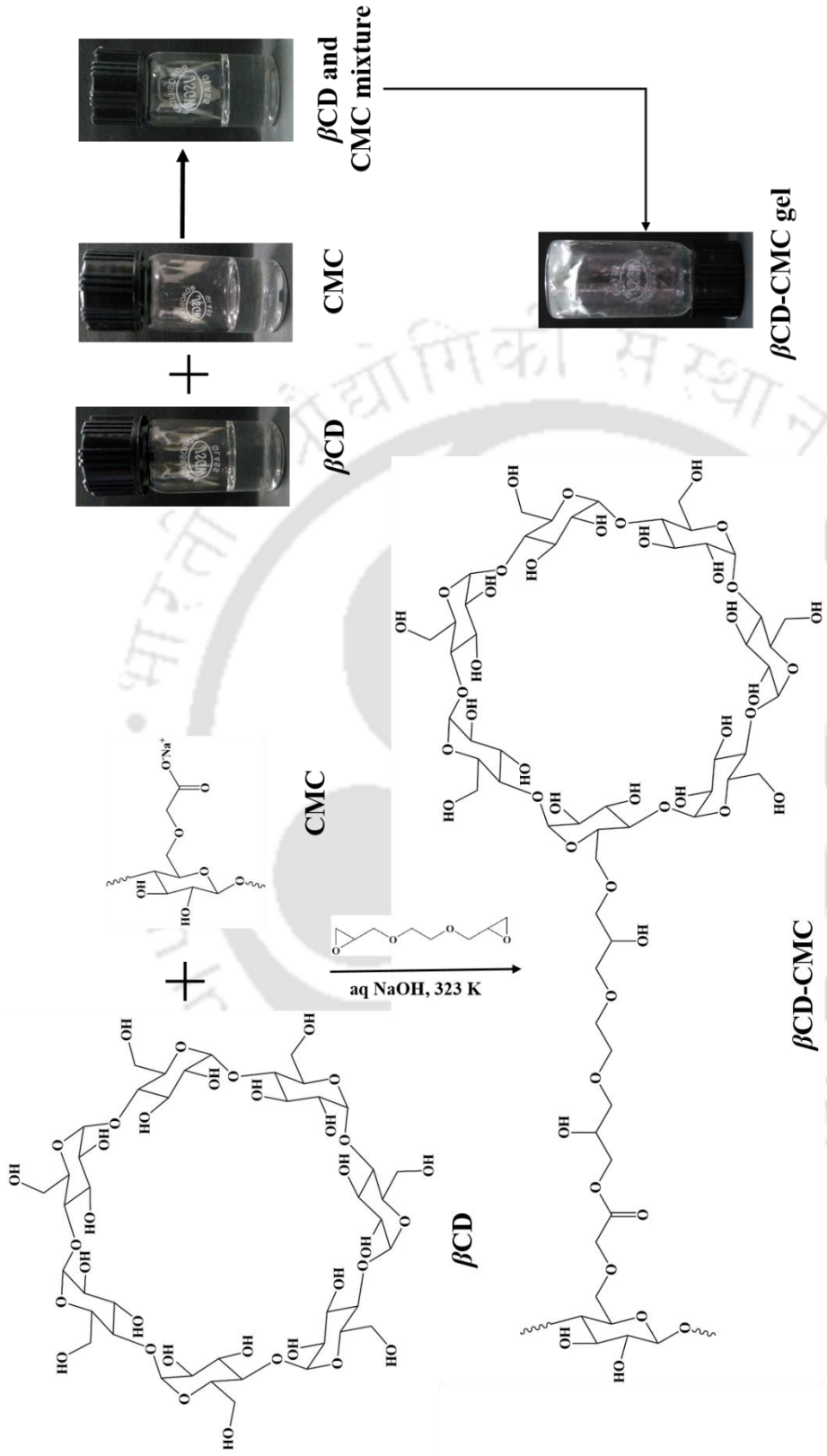

Figure 4.3. Reaction scheme of βCD-CMC hydrogel formation

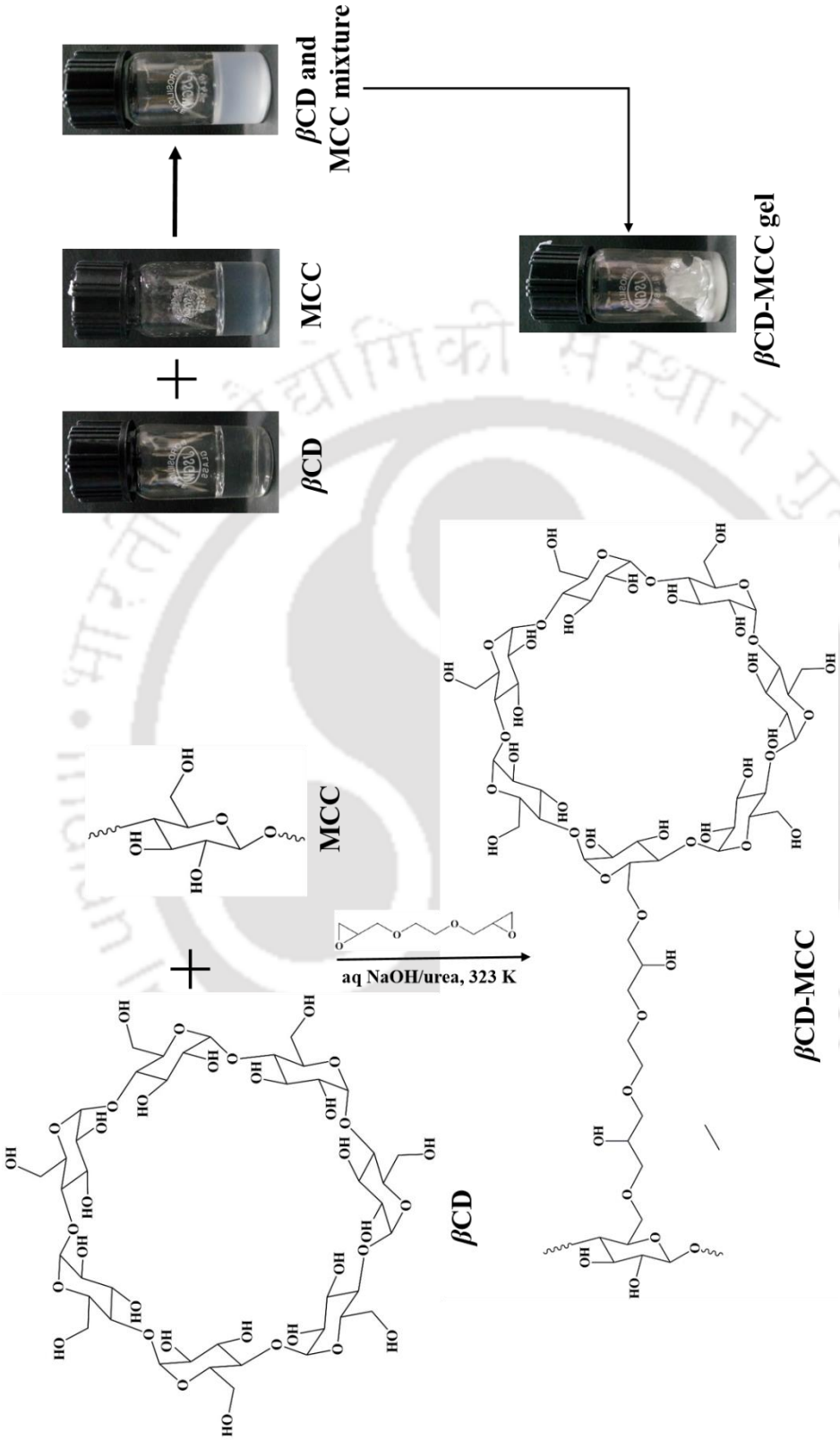

Figure 4.4. Reaction scheme of *β*CD-MCC hydrogel formation

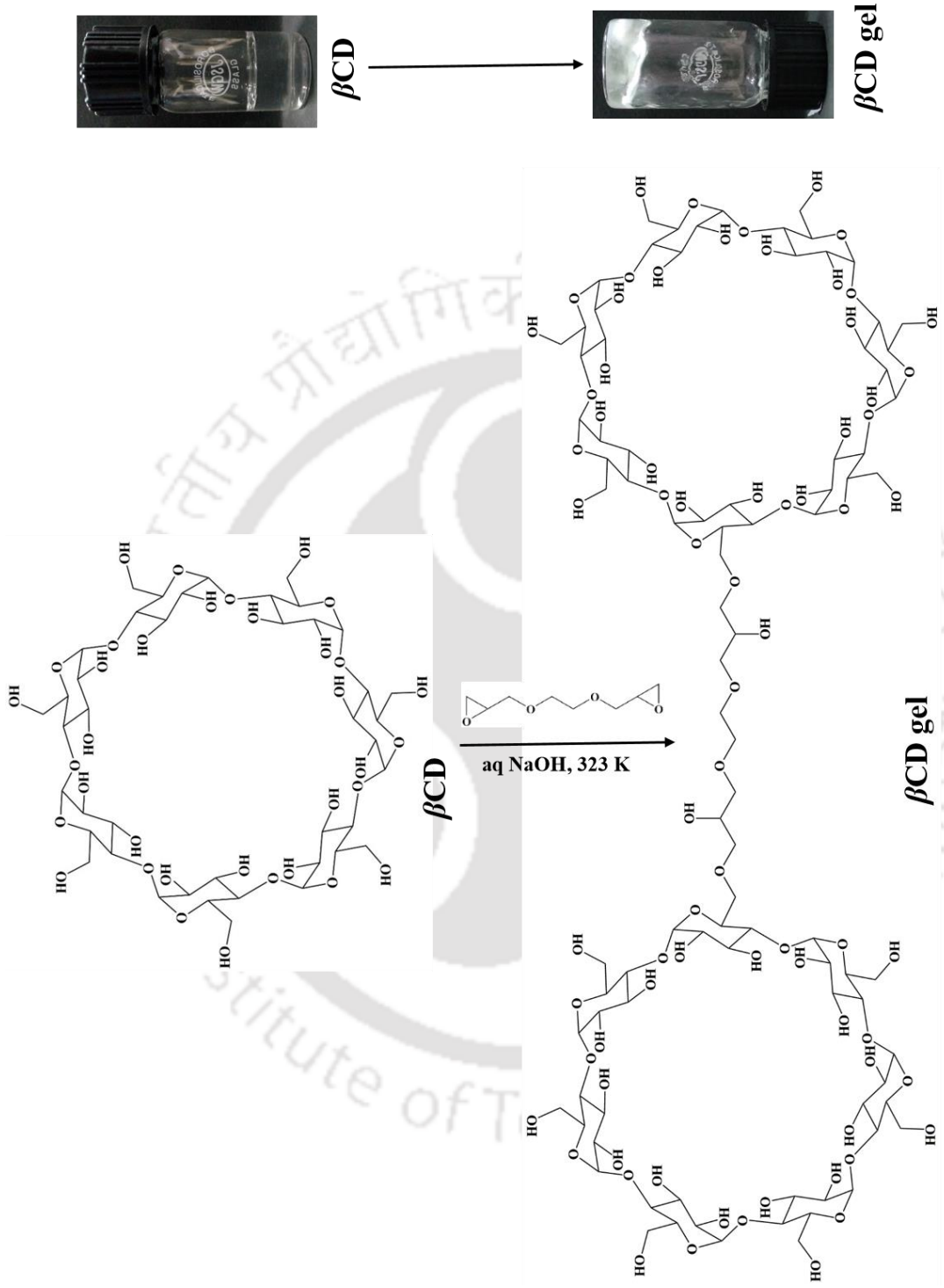

Figure 4.5. Reaction scheme of βCD gel hydrogel formation

4.2.3. Characterization

The characterization procedure of FT-IR spectroscopy, swelling ratio and gel fraction are similar to that of characterization procedure described in Chapter 2 for the respective techniques. The preparation of samples for the morphological observation in optical microscope and FESEM are similar to that described in Section 2.2.3.2. Further, the morphology of Cd (II) and Ni (II) loaded hydrogels in the fluorescence mode within the same microscope at 475 nm wavelength light.

The point of zero charge (PZC) analysis was performed by ΔpH method. The analysis is carried out to determine the surface functionality of the hydrogel with respect to the change of pH of the solution [118]. The difference in pH is calculated by,

$$\Delta pH = pH_i - pH_f \tag{4.1}$$

Where, pH_i is the initial fixed pH maintained by HCl or NaOH solution. After immersing the hydrogel, the pH changes to pH_f. Therefore, ΔpH was plotted against pH_i. PZC of the hydrogel was identified by the point of intersection of the curve at the zero value of ΔpH.

4.2.3.1.X-ray photoelectron spectroscopy

The X-ray photoelectron spectroscopy (XPS) was performed at room temperature on AXIS-ULTRA using Al as the monochromatic source (1.486 keV).

4.2.3.2.Adsorption experiments

The adsorption of metals using hydrogels were performed in aqueous solutions of Cd (II) and Ni (II). The respective solutions were prepared after dissolving a certain amount of salt in deionized water (DI). 1.7909 gm of $CdCl_2.H_2O$ was dissolved in DI water in a one liter volumetric flask. The well shaken solution was made up to one liter with DI water to make 1000 mg L^{-1}, 1000 mL stock solution of Cd (II). Similarly, 4.0499 gm of $NiCl_2.6H_2O$ was dissolved in DI water and final volume was made up to 1 liter to make 1000 mg L^{-1}, 1000 mL Ni (II) stock solution. The adsorption experiments were carried out at varying dosage of adsorbents, concentrations, pH of metal solutions and temperature. The stock solutions were

diluted as per the requirement to prepare various concentrations of metal solutions. A measured amount of hydrogels were put into 100 mL conical flask with 25 mL Cd (II) or Ni (II) solutions at different concentrations. The flasks were kept into an orbital shaker (make: Daihan Labtech, model: LSI 3016R) at 298 K and were rotated at 120 rpm for 12 hour to reach equilibrium. After that the solutions were filtered and the filtrate was taken to AAS to measure the metal concentration. The similar process was followed for pH dependent adsorption and temperature dependent adsorption. The removal efficiency (Removal, %) was calculated as below:

$$\text{Removal}(\%) = \left(\frac{C_0 - C_e}{C_0}\right) \times 100\% \tag{4.2}$$

Where, C_0 and C_e (in mg L^{-1}) are initial and equilibrium concentration of metal ions in solution respectively. The equilibrium adsorption capacities (q_e, mg g^{-1}) and time resolved adsorption capacities (q_t, mg g^{-1}) are calculated by the following equations

$$q_e = (C_0 - C_e) \times \left(\frac{V}{m}\right) \tag{4.3}$$

$$q_t = (C_0 - C_t) \times \left(\frac{V}{m}\right) \tag{4.4}$$

Where, C_0, C_t, C_e are initial, time resolved and equilibrium concentration of metal ions in solution (mg L^{-1}), V is volume of metal ion solution taken for adsorption (in L) and m is the dry weight of hydrogel (gm). All the measurements are triplicated.

4.2.3.3.Atomic absorption spectroscopy

The concentration of metal ions in the solution during adsorption was measured by atomic absorption spectroscopy (or AAS, in abbreviation) (make: Varian Australia, model: AA240FS) using flame mode. Both the concentration of cadmium and nickel were measured separately in cadmium lamp of wavelength 228.8 nm and nickel lamp of wavelength 232.0 nm.

4.3. Results and discussions

4.3.1. FT-IR spectra

The synthesized hydrogels are characterized by FT-IR spectra and given in Figure 4.6. The polysaccharides are composed of pyranose ring. Two pyranose rings are connected by either α-(1→4) glycosydic linkage (βCD) or β-(1→4) glycosidic linkage (MCC, CMC and xylan). Figure 4.6(a) represents FT-IR spectra of pure βCD in pre-gel condition. The O – H stretching is observed as broad peak at 3450 cm^{-1}. The C – H stretching is obtained at 2922 cm^{-1}. The peak at 1456 cm^{-1} is assigned for the bending of $–CH_2$. Skeletal vibrations are also observed at 1338 cm^{-1}. The stretching vibration of α-(1→4) glycosydic linkage is observed at 1159 cm^{-1} and vibration of the same linkage is observed at 937 cm^{-1} [119]. The bending of C – C is assigned at 1082 cm^{-1} while the stretching of C – O, bonded with the two pyranose ring is assigned at 1028 cm^{-1}. The glycosydic deformation of C – H with ring vibration is assigned to 856 cm^{-1}.

The FT-IR characterization of all four gels are given in Figure 4.6(b-e). The characteristic vibrations are mostly in similar positions and assigned as follows. The O – H stretching is assigned as a broad peak from 3417 – 3437 cm^{-1}. The doublet peak at 2912 – 2918 cm^{-1} and 2877 -2878 cm^{-1} are assigned to C – H stretching and bending respectively. The asymmetric stretching of COO^- is generally observed within the range of 1600-1620 cm^{-1} [44]. However, in all FT-IR spectra, a peak at 1645-1647 cm^{-1} is observed. Since the hygroscopic nature of the gels as well as the precursors, this is primarily described as the HOH bending of the physically absorbed water [109, 110]. Therefore, the asymmetric stretching of COO^- in CMC is merged with this spectra. The symmetric $–CH_2$ bending is observed at 1424 – 1452 cm^{-1} [112]. However, close proximity to this, the symmetric stretching vibration of COO^- moiety is found in 1423 – 1446 cm^{-1} [35]. Hence, the two are merged in a broad peak at 1456 cm^{-1} and assigned to the symmetric bending of $–CH_2$ and symmetric stretching vibration of COO^-. The $–CH_2$ moiety here is present in the aliphatic chain of βCD, MCC, CMC as well as in EGDE crosslinker. Hence, this is observed in all FT-IR spectra. The skeletal vibrations of C – O and C – C in the pyranose ring are observed at 1354 and 1338 cm^{-1} respectively. A broad peak is observed at 1086-1088 cm^{-1} which is considered as merger of several peaks.

The antisymmetric β-(1→4) glycosidic linkage is reported at 1090 cm^{-1} [108] while the bending of C – C is reported at 1064 cm^{-1} [35]. Therefore, the broad peak at 1086-1088 cm^{-1} is collectively assigned to the C – C bending and antisymmetric β-(1→4) glycosidic linkage. The α-(1→4) glycosidic linkage of βCD is again observed at 937-942 cm^{-1}. As before the glycosydic deformation of C – H with ring vibration is shifted to 872-874 cm^{-1}.

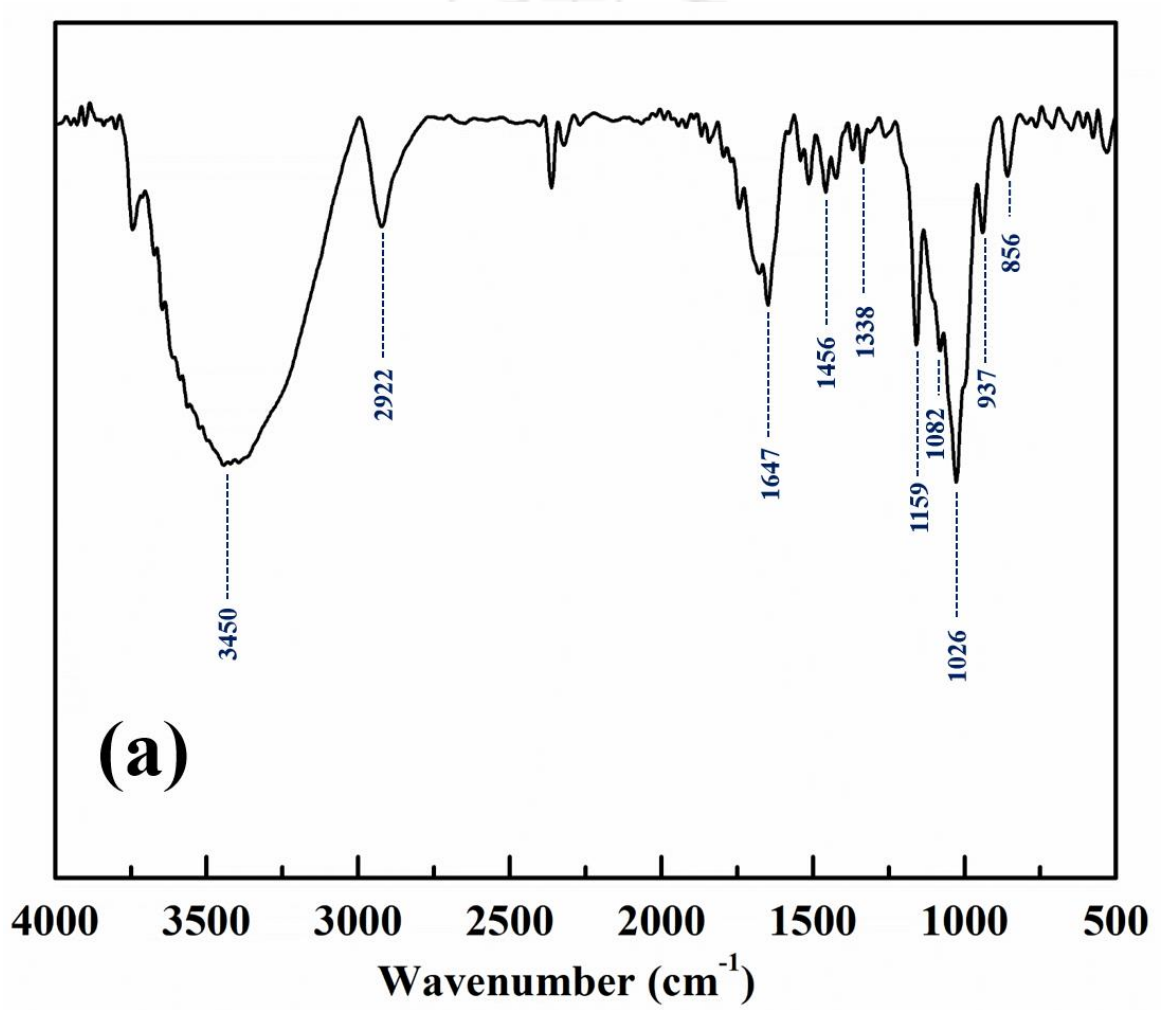

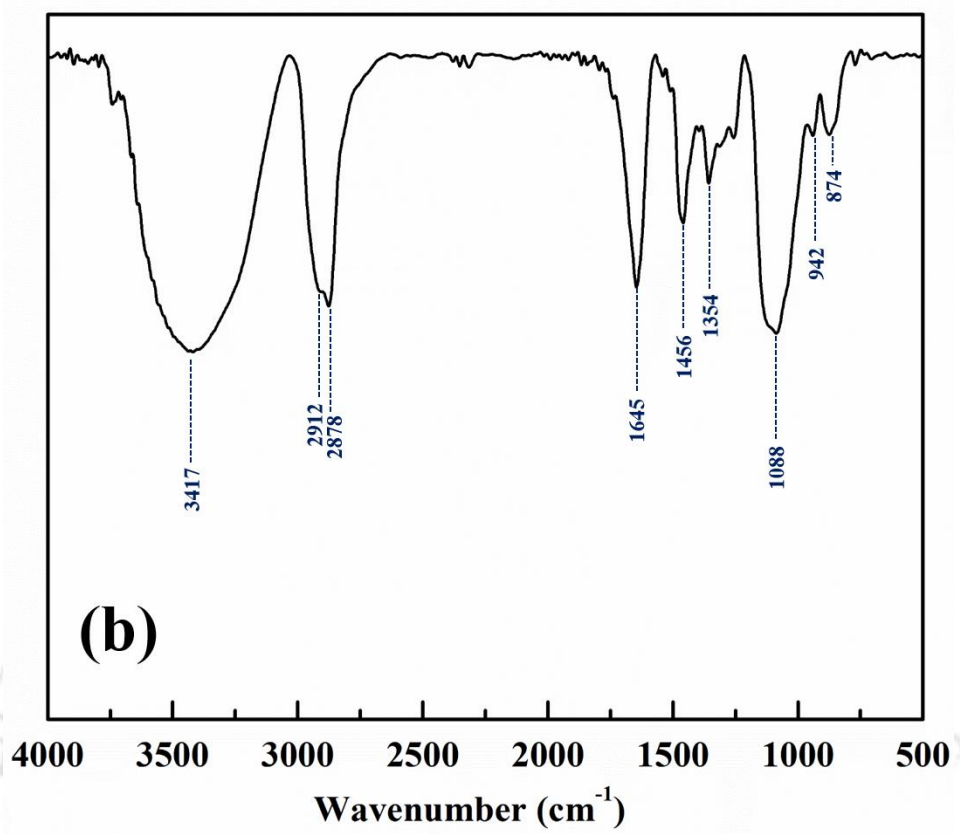

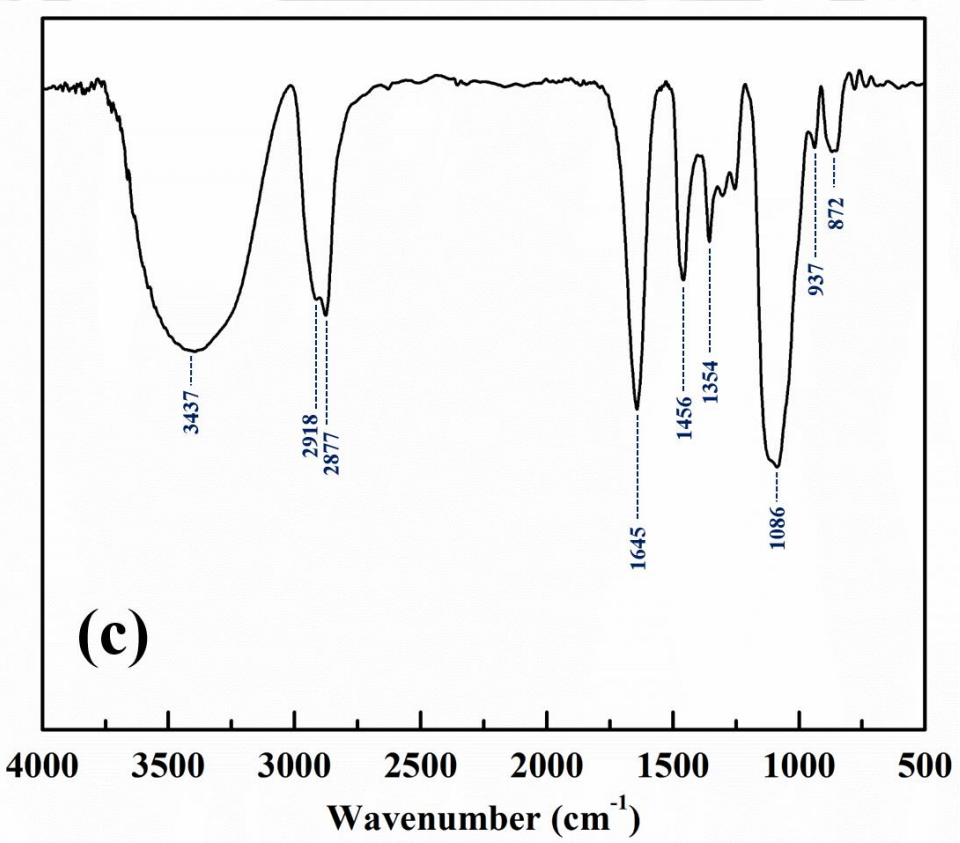

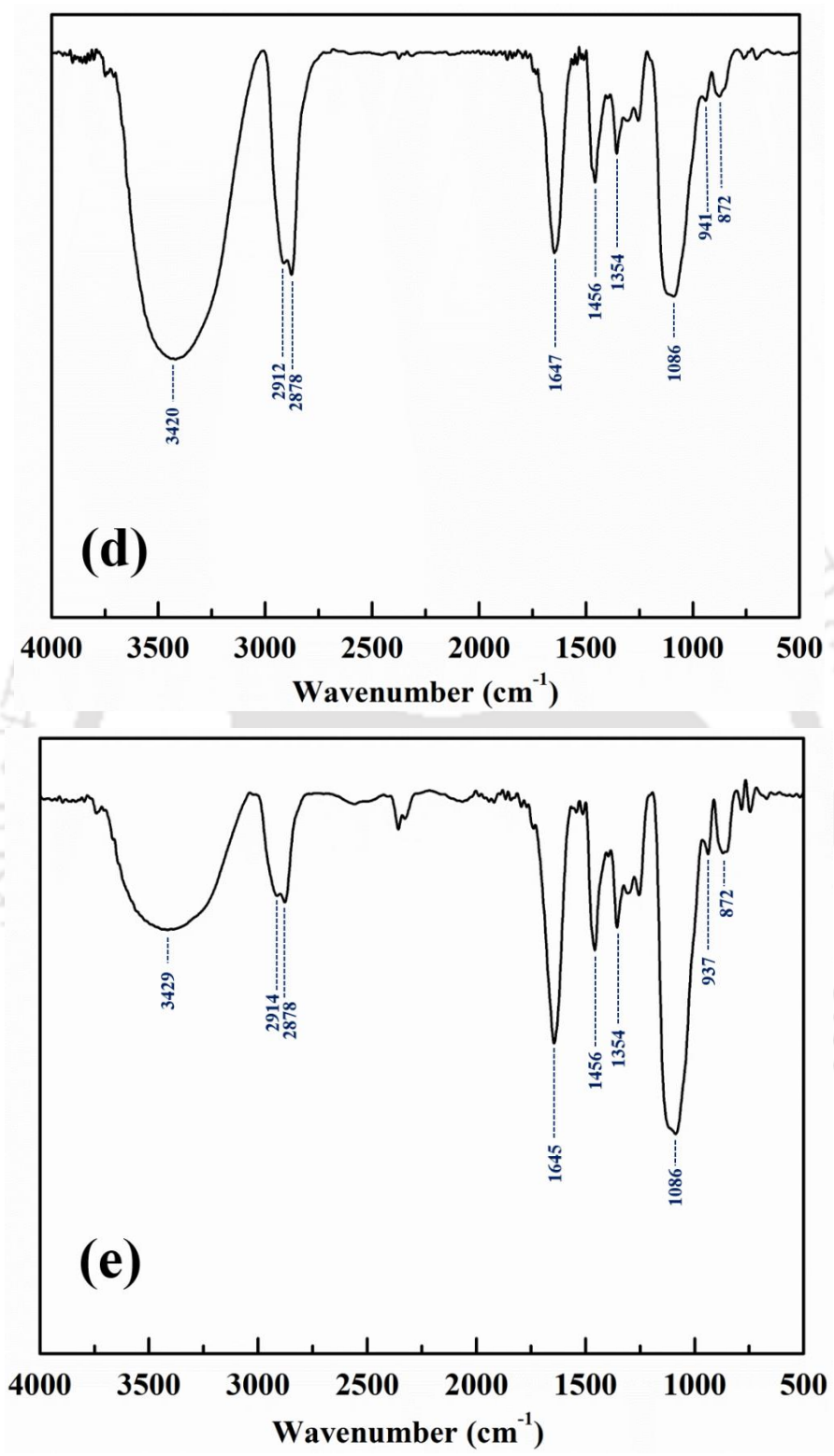

Figure 4.6. FT-IR spectra, (a) *β*CD pure, (b) *β*CD gel, (c) *β*CD –xylan, (d) *β*CD-MCC, (e) *β*CD-CMC.

4.3.2. XPS analysis

Figure 4.7a represents the wide scan XPS spectra of *β*CD –xylan hydrogel. The corresponding deconvoluted C1s and O1s spectra (high resolution) is given in Figure 4.7b and 4.7c respectively. From Figure 4.7b, the C1s curve is deconvoluted to three separate curves having binding energies of 283.1, 284.6 and 285.3 eV. The C-O or C-H aromatic or linear bonds have corresponding binding energies of 283.1 eV whereas C-O is assigned corresponding to the binding energy of 284.6 eV. The C-O-C of pyranose ring is assigned at 285.3 eV. The corresponding assignments matche with the literature reported data of analogous *β*CD and xylan structures [120, 121]. Further, Figure 4.7c refers to the two deconvoluted spectra of O-H, assigned at 530.8 eV and to that of characteristic oxygen in pyranose ring respectively [101].

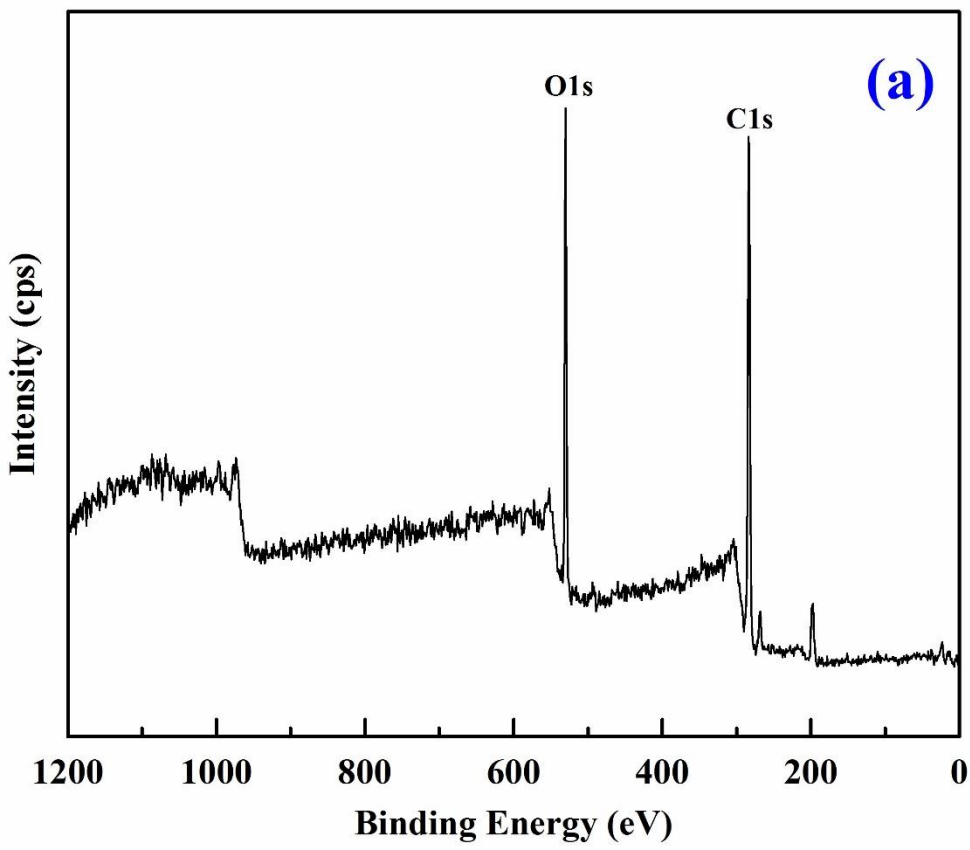

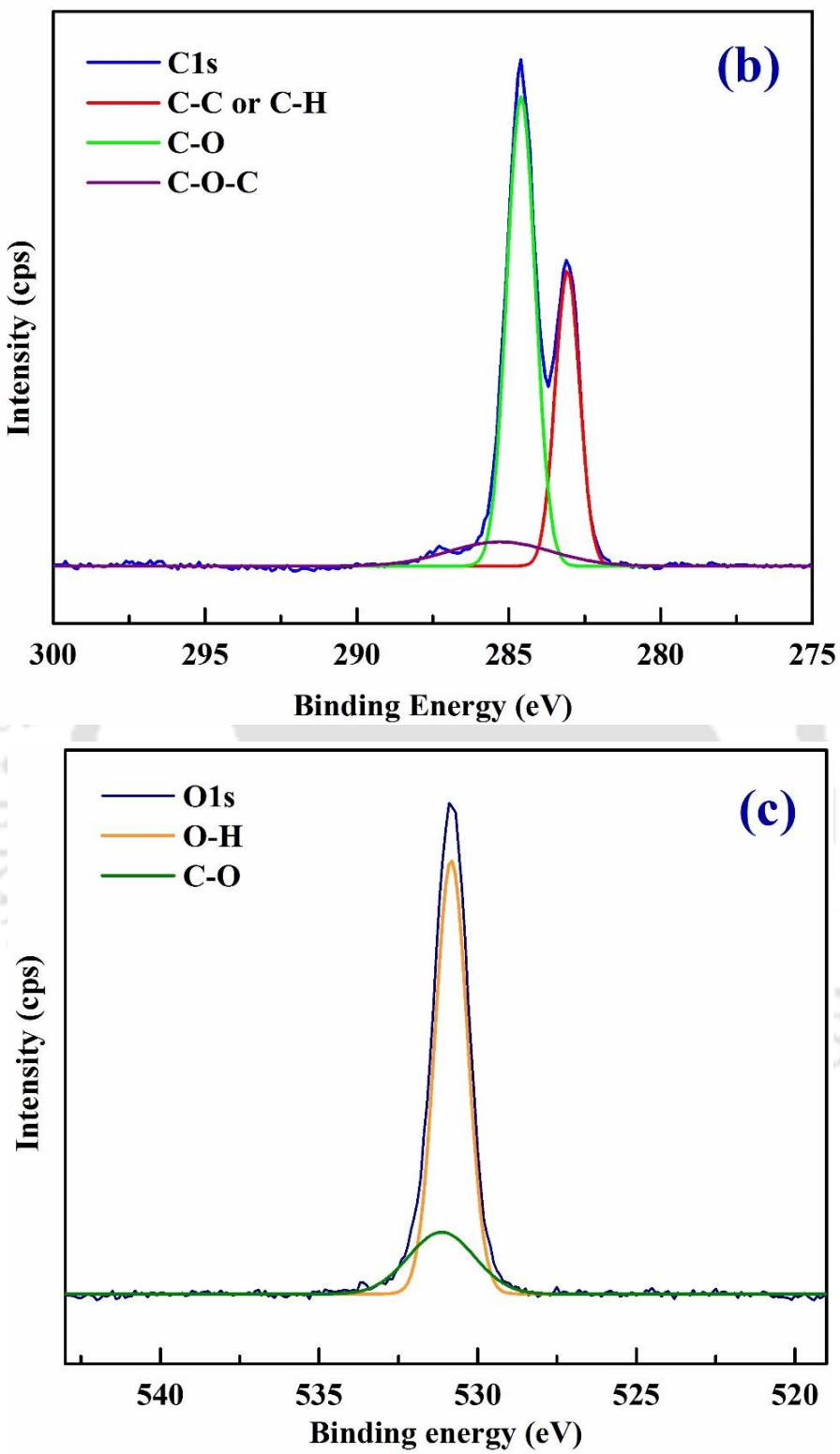

Figure 4.7. (a) Wide scan XPS spectra of *β*CD –xylan, (b) deconvoluted C1s spectra, (c) deconvoluted O1s spectra.

4.3.3. Morphology

The morphology of synthesized hydrogels are visualized through FESEM and optical microscopy and are given in Figure 4.7 and 4.8 respectively. The coarse nature of the gels are visualized further in FESEM images (Figure 4.7). Small discontinuous elongations are visible in the surface which can be presumed as possible binding sites for metal ions. However, coarse gels are also reported to adsorb Cd (II) [96]. Since, adsorption of metal ions happen by binding with hydroxyl and carboxylate ions, the coarse structure will not obstruct the process. The hydrogels appear as glossy structure in optical microscopy. Except *β*CD-MCC gel, others are visible at isolated assemblies whereas *β*CD-MCC gel is an interconnected gel. Figure 4.8 further represents fluorescent microscopic images of the metal adsorbed hydrogel. Here we observe that the surface is adsorbed with metal ions suggesting that uneven surfaces are possible binding sites. Further, concentrated metal spots are observed in the images. These may refer to the trapped Ni (II) and Cd (II) ions inside the network.

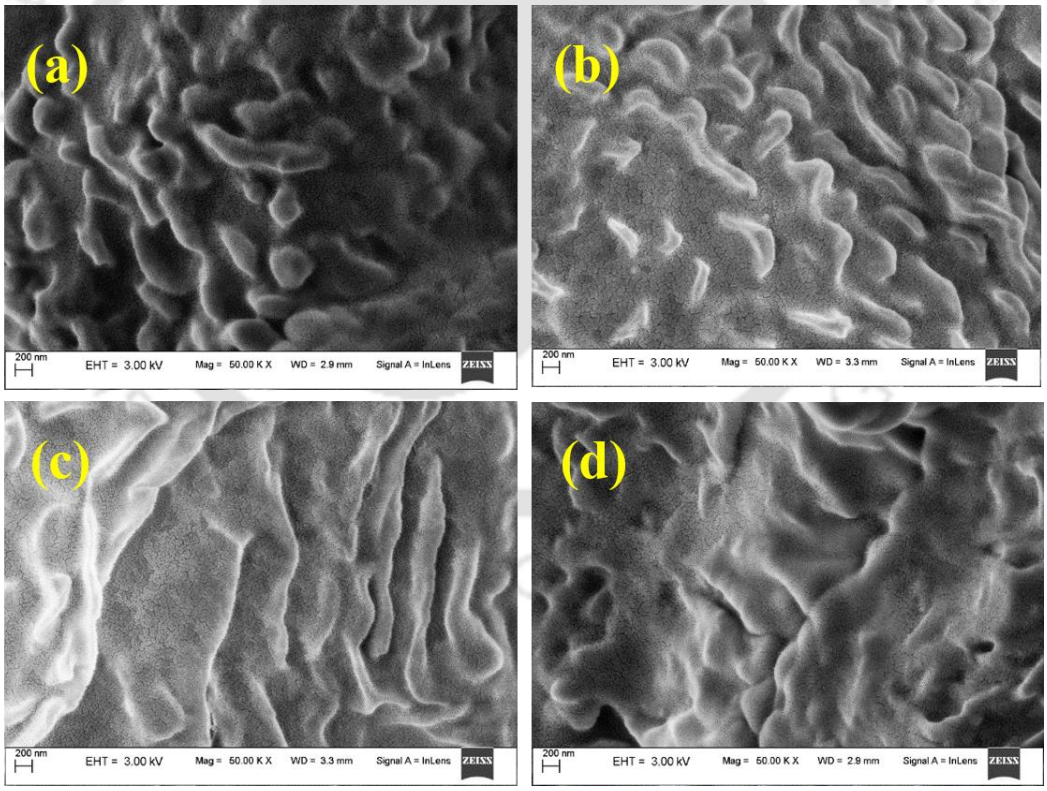

Figure 4.8. FESEM images of hydrogels. (a) *β*CD-xylan, (b) *β*CD-CMC, (c) *β*CD-MCC, (d) *β*CD gel.

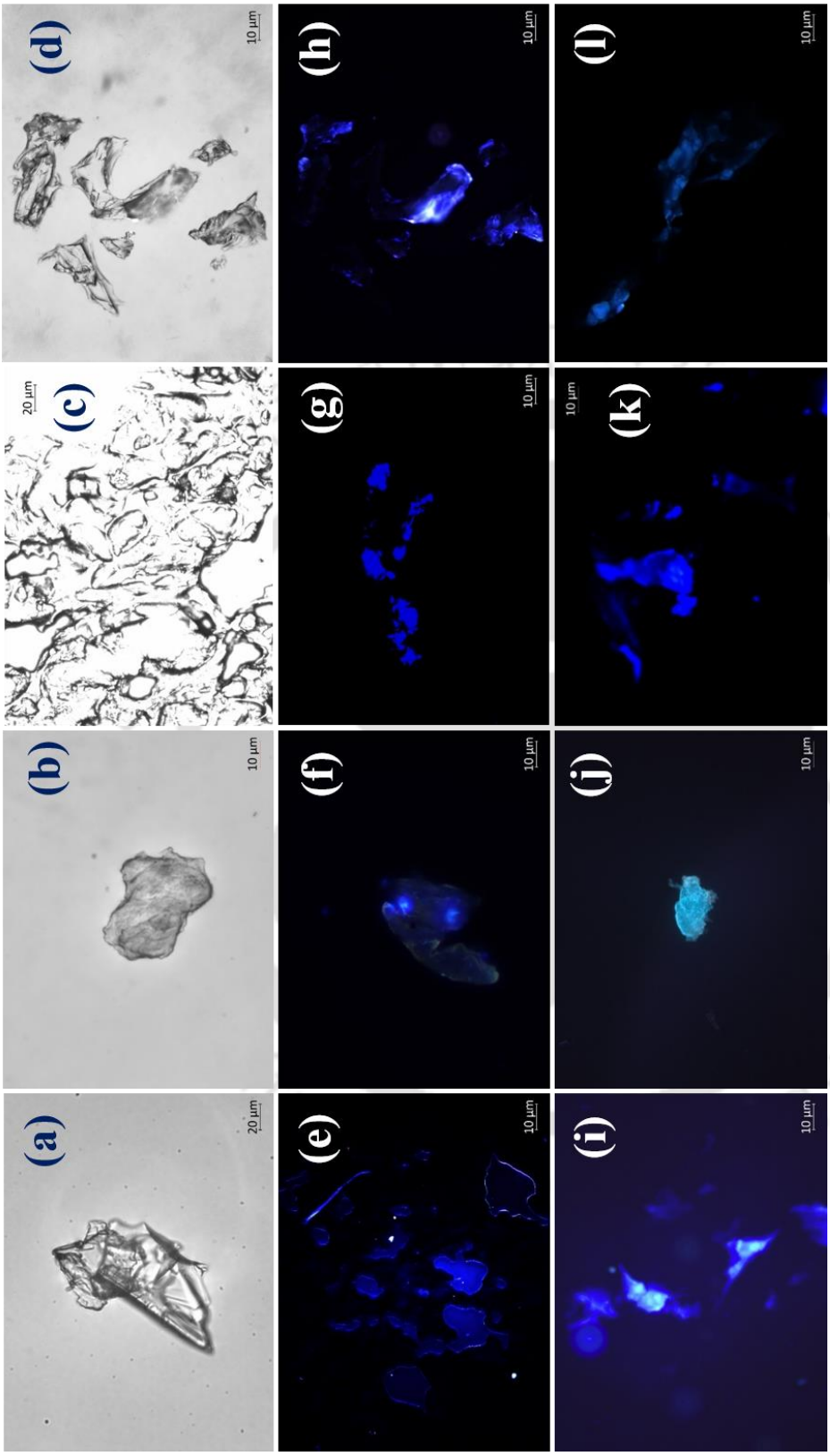

Figure 4.9. Optical microscope images of hydrogels (no metal adsorption), (a) βCD-xylan, (b) βCD-CMC, (c) βCD-MCC, (d) βCD gel. Fluorescent microscopic images of Cd (II) loaded hydrogels [(e) – (h)] and Ni (II) loaded hydrogels [(i) – (l)]. (e) and (i) βCD-xylan, (f) and (j) βCD-CMC, (g) – (k) βCD-MCC, (h) - (l) βCD gel.

4.3.4. Swelling ratio and gel fraction

Swelling represents the amount of water hydrogel can absorb. It is a fundamental physical property of hydrogel which implies that a higher swelling is desired. We present the swelling of four hydrogels at pH = 2, 4, 6, 8 and DI water as given in Figure 4.9a. The toroid shape of *β*CD limits its swelling. The swelling of *β*CD gel initiates through the flexibility of crosslinker. Therefore, it shows least swelling in the pH medium and DI water. The cellulose and hemicellulose consist of pyranose ring and are linear in nature. It should be noted that the gelation procedure for the copolymerized gels creates a network structure where the flexibility of network is more than the *β*CD gel network. Here the individual cellulose and hemicellulose chains can expand, allowing more water to be trapped in the network. Further we observe an increase in swelling ratio for all four hydrogels with the increment in pH. A highest swelling of 362.53% is observed for *β*CD-CMC gel at pH = 8.

The swelling data with the increment of pH can be explained with the electrostatic repulsions of the hydrogel network. The dominant charge species of the synthesized hydrogels are unprotonated hydroxyl (MCC, xylan, *β*CD) and carboxylate anions (CMC). The electrostatic repulsion of these charged moieties causes swelling. Compare to other three hydrogels (*β*CD gel, *β*CD-xylan, *β*CD-MCC), *β*CD-CMC has longer side chain attached to the pyranose ring. Hence it is more flexible to swell. At lower pH, the unprotonated anions get protonated, thereby reducing the ionic repulsions. These lower swelling at pH = 2. Near the neutral (pH=6) or alkaline (pH=8) region, the unprotonated anionic moieties repel more causing higher swelling [35, 98].

Figure 4.9b represents the gel fraction of four hydrogels. *β*CD gel has highest gel fraction of 96.54 % and *β*CD-CMC is having least gel fraction of 47.59 % among four hydrogels. The trend of gel fraction follows the opposite trend of swelling behavior [98]. Higher gel fraction represents densely crosslinked structure. Densely crosslinked structure has less flexibility to expand and thus lower water uptake capability i.e. lower swelling. However, low gel fraction of *β*CD-CMC allows free carboxymethyl moieties to expand and increase water uptake. The images of the freeze dried and swollen gels are given in the Figure 4.10.

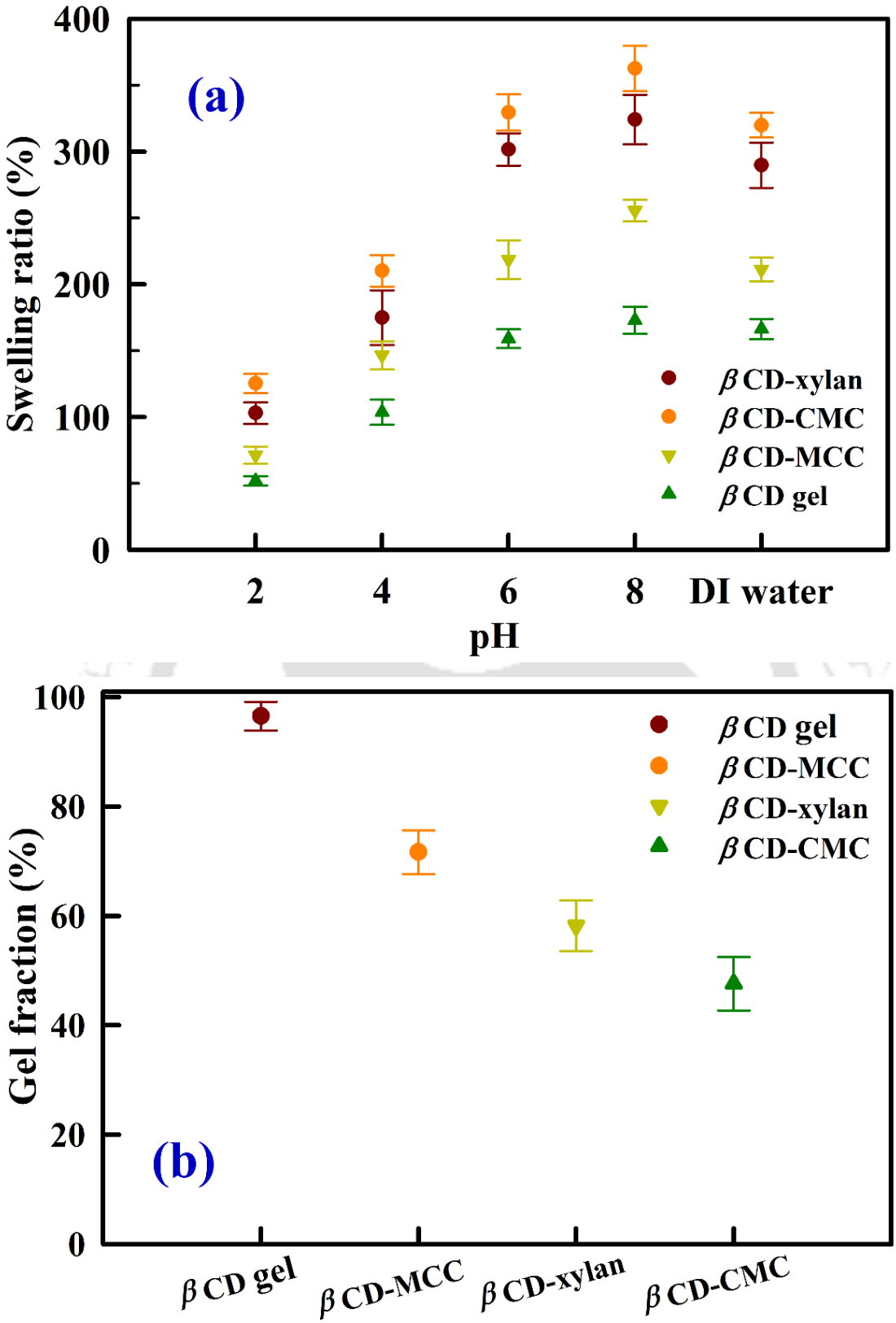

Figure 4.10. (a) Swelling ratio of hydrogels in DI water and pH = 2, 4, 6 and 8. (b) Gel fraction of hydrogels.

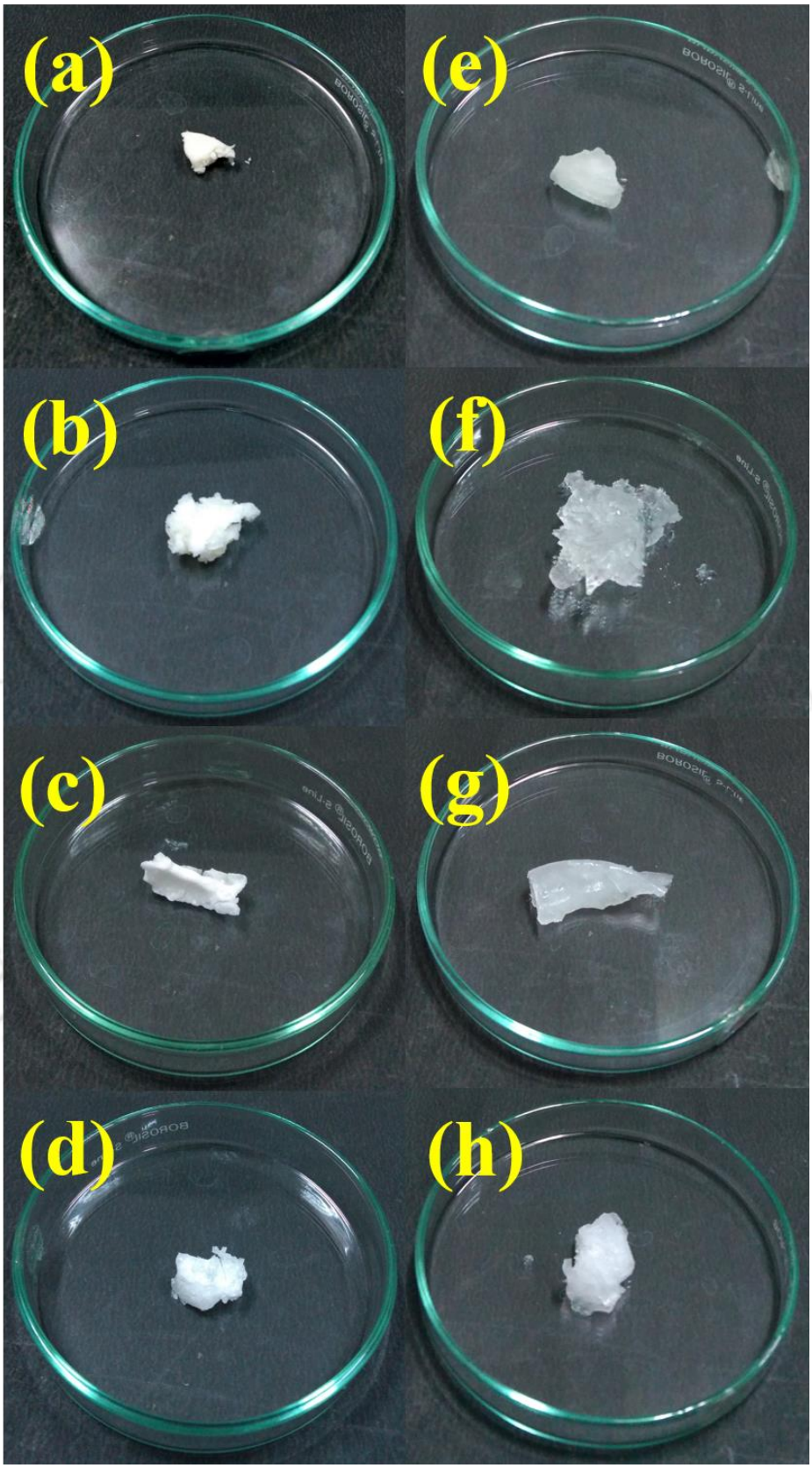

Figure 4.11. Freeze dried (from (a) to (d)) and swelled hydrogels (from (e) to (h)). (a) and (e) *β*CD-xylan, (b) and (f) *β*CD-CMC, (c) and (g) *β*CD-MCC, (d) and (h) *β*CD gel.

4.3.5. Point of zero charge

The PZC of four hydrogels lie within pH = 2.25 – 3.0 ($PZC_{\beta CD\text{-}xylan}$ = 2.66, $PZC_{\beta CD\text{-}CMC}$ = 2.25, $PZC_{\beta CD\text{-}MCC}$ = 2.33, $PZC_{\beta CD\ gel}$ = 3.00). The net charge on the surface of hydrogel turns positive below the PZC. This implies the protonated binding sites on the surface of the hydrogel. However, pH higher than the PZC, the net surface charge of the material is negative i.e. the carboxylate/hydroxyl moieties of βCD based gels are deprotonated. The deprotonated binding sites readily adsorb the metal ions from the aqueous solution. The cellulose/hemicellulose copolymers add more number of anionic binding sites with the βCD and thus reducing the PZC of the copolymerized hydrogels.

4.3.6. Removal of Cd(II) and Ni(II)

The synthesized hydrogels are used to adsorb Cd (II) and Ni (II) ions from aqueous solutions. The parameters of adsorption are optimized with variation of adsorbent dosage, initial concentration of metal ions in solutions, pH of solutions and temperature. The removal efficiency is calculated from equation 4.1 and equilibrium adsorption capacity is determined from equation 4.2. All the adsorption experiment data are triplicated and standard deviation is reported in plots.

4.3.6.1.Effect of adsorbent dosage

The effect of adsorbent dosage on the adsorbent capacity and removal of metal ions is determined at 50 mg L^{-1} initial metal ion concentration solution in DI water at 298 K. The amount of adsorbent varies from 80 to 500 mg which is taken in a 25 mL metal ion solution. The equilibrium adsorption capacities and removal efficiencies are given in Figure 4.11. From Figure 4.11, highest adsorption capacity and removal efficiency are observed for 80 mg adsorbent dosage. With the increase in amount of adsorbent dosage, the binding sites for adsorption increase; hence it can bind with higher number of metal ions. Hence for higher adsorbent dosage, the number of vacant sites are more. Further in the expression of adsorbent capacity (equation 4.3), mass of adsorbent is at denominator. Hence, with the increment of dosage, adsorption capacities are decreasing. However, at 80 mg dosage of hydrogels, the removal efficiency of Cd (II), is more than 80% for Cd (II) and more than 50% for Ni (II). Hence, the 80 mg adsorbent dosage is considered as optimum dosage for further study.

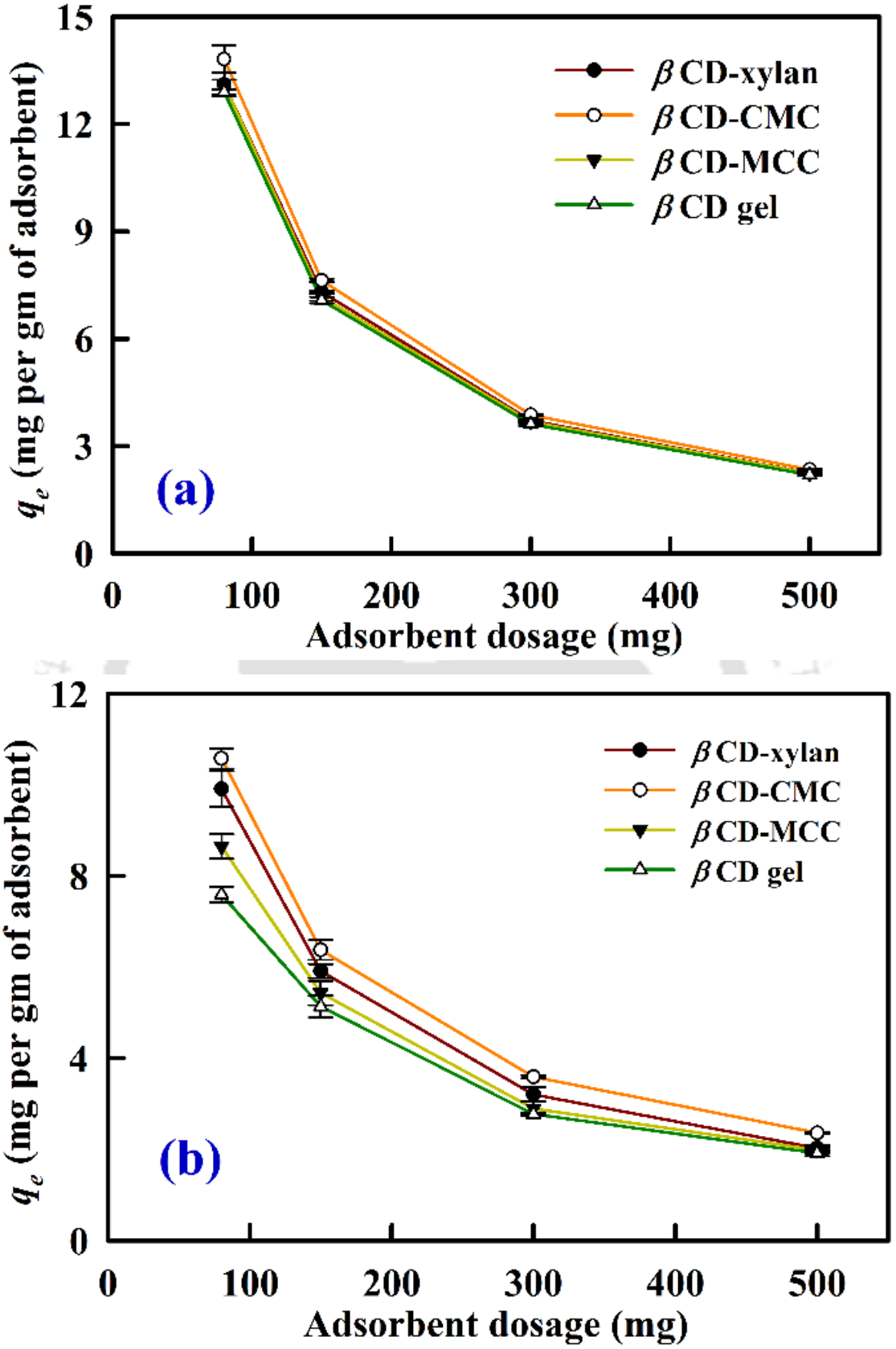

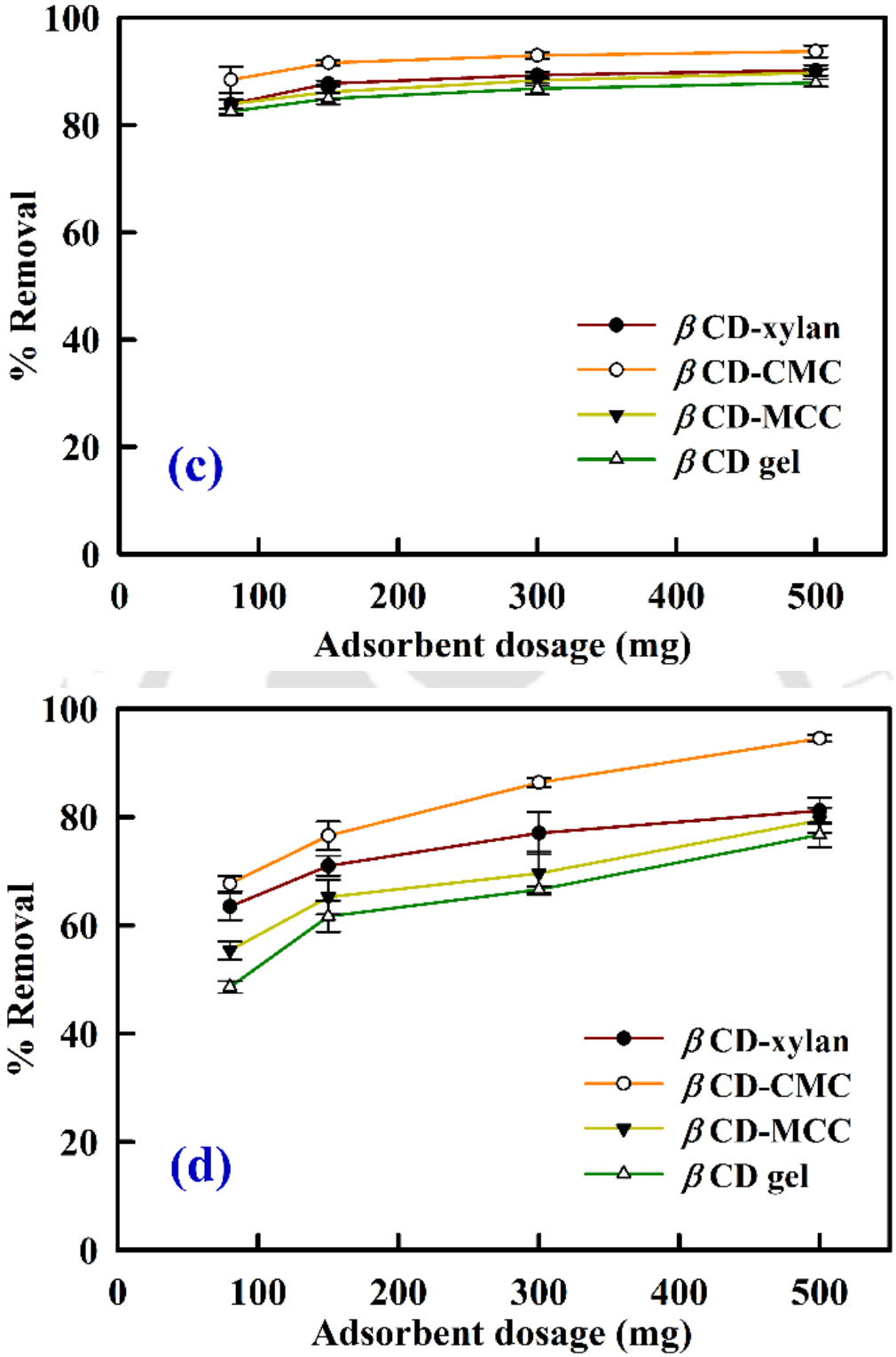

Figure 4.12. Equilibrium adsorption capacity (q_e) and removal of pollutant at various dosage of adsorption at 50 mg L^{-1} initial metal ion concentration. (a) q_e of Cd(II), (b) q_e of Ni(II), (c) removal of Cd (II), (d) removal of Ni (II).

4.3.6.2.Effect of concentration

Figure 4.12 represents the concentration variation adsorption study of both the metals. The initial metal ion concentrations are varied from 5, 15, 25, 50, 100, 300 and 500 mg L^{-1} and are performed at 298 K in DI water. The removal efficiency of the hydrogels decreases over the increase in concentrations which also increases the adsorption capacity. These imply, at lower concentrations, all the adsorption sites are not occupied with the metal ions. However, at 100 mg L^{-1}, a significant change happens in the nature of capacity curve for the adsorption of Ni (II) (Figure 4.12b). Here, after 100 mg L^{-1} initial concentration, the adsorption capacity does not change significantly and the adsorption capacity reaches towards the near saturation adsorption by the gels. For the adsorption of Cd (II), the rate of adsorption slows down after 100 mg L^{-1} initial concentration and thereafter negligible change is observed after 300 mg L^{-1}. Among the four hydrogels, *β*CD-CMC hydrogel has an adsorption capacity 41.06 mg g^{-1} for Cd (II) and 18.44 mg g^{-1} for Ni (II) for 500 mg L^{-1} initial concentration. The order of adsorption capacity for both ions are *β*CD-CMC > *β*CD-xylan > *β*CD-MCC > *β*CD gel. Metal ions are being adsorbed in surface as well as in hydrophobic cavity of *β*CD.

In addition to hydroxyl moieties, CMC based hydrogels have $–COO^-$ moiety which can easily bind with metal ions. Surface adsorption is the likely occurrence in *β*CD-xylan and *β*CD-MCC hydrogels due to the ionic bonding of metal ions with hydroxyl moiety. However, at lower initial concentration, the difference in removal or adsorption capacity is not visible. At 5 mg L^{-1}, all the hydrogels show efficient removal of more than 90% for cadmium and 80% for nickel respectively. The removal efficiency of hydrogels decreases with the increase in initial metal ion concentration. At 100 mg L^{-1} initial concentration, the removal is 78.76% and 50.85% for Cd (II) and Ni (II) respectively with *β*CD-CMC gel. Therefore, we have used these two initial concentrations to measure the effect on adsorption with various pH.

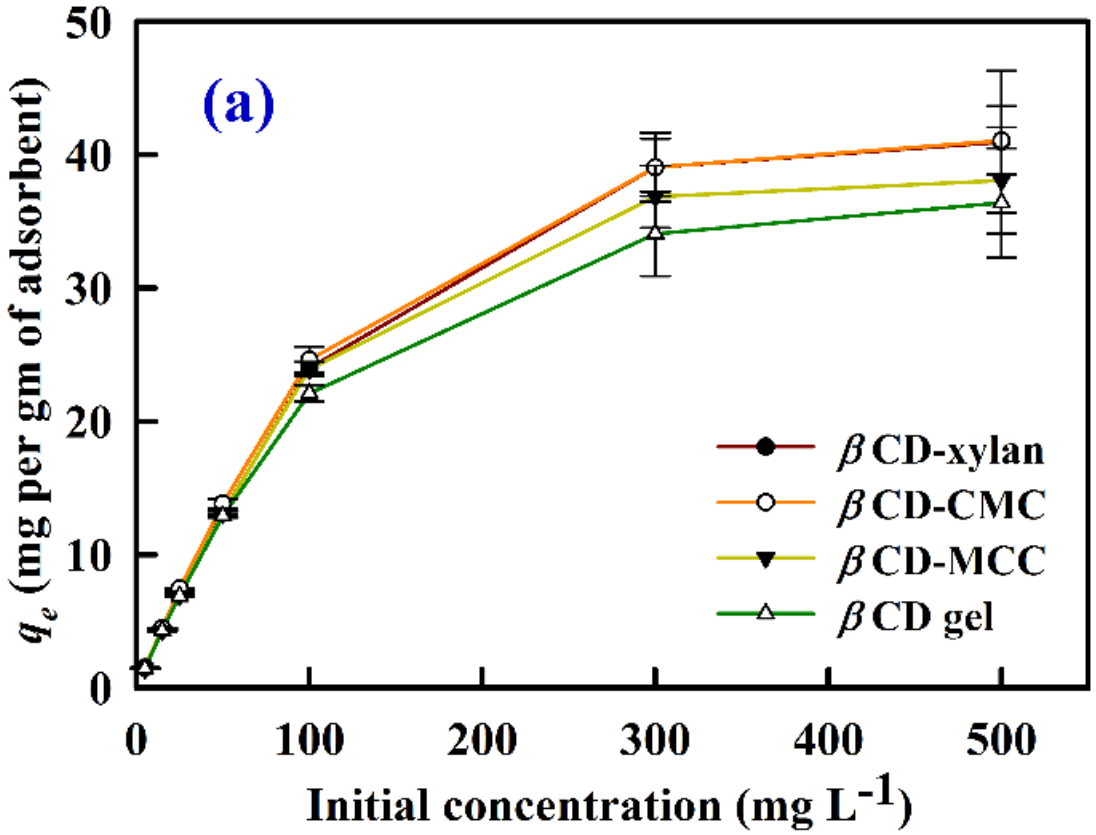

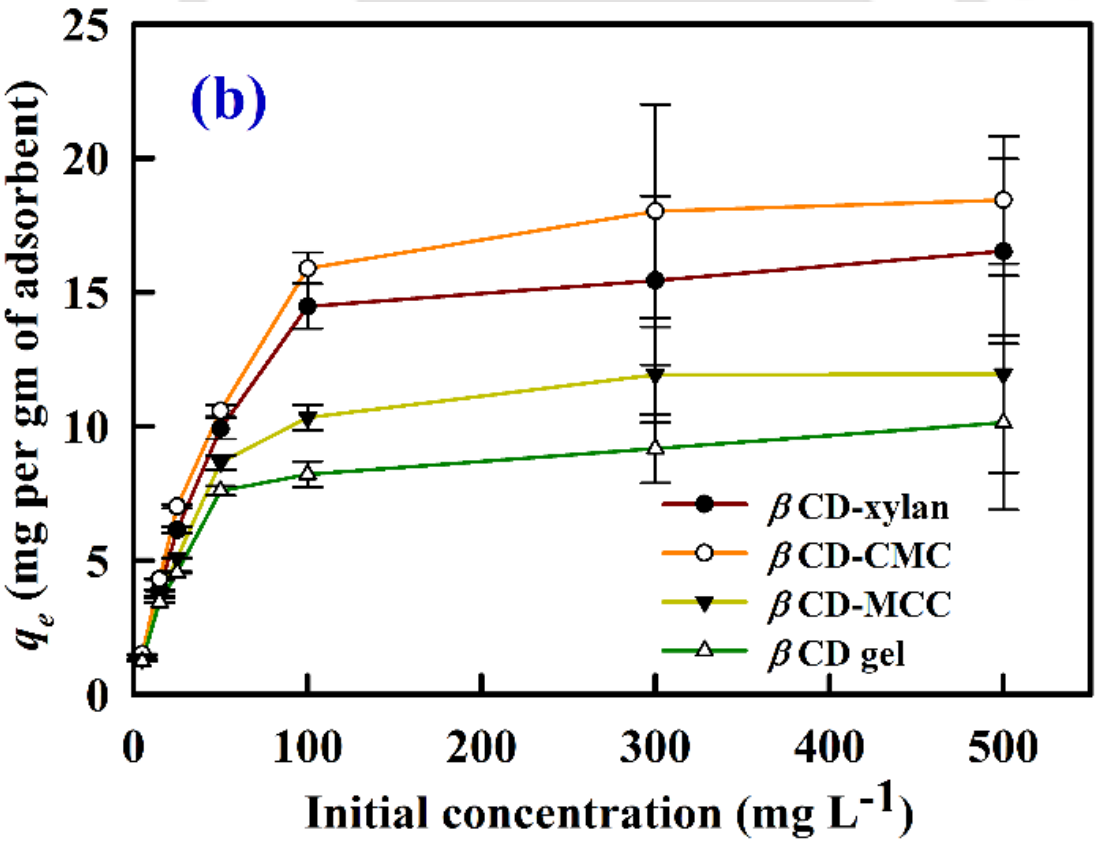

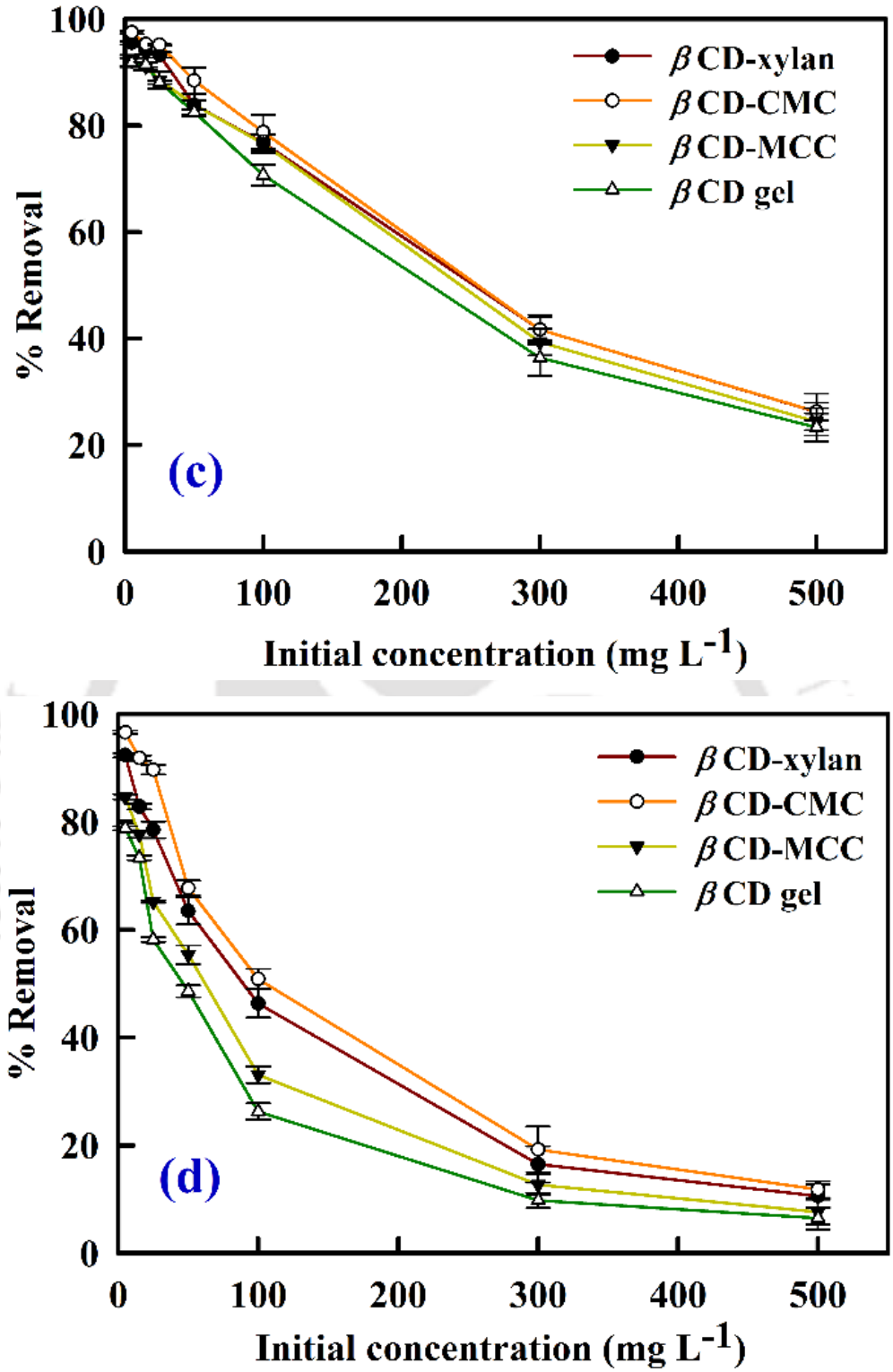

Figure 4.13. Equilibrium adsorption capacity (q_e) and removal of pollutant at various initial metal ion concentrations, (a) q_e of Cd(II), (b) q_e of Ni(II), (c) removal of Cd (II), (d) removal of Ni (II).

4.3.6.3.Effect of pH

The effect of pH on the adsorption capacity and removal efficiency of the metal ions is determined at pH = 2, 4, 6 and 8 for 5 mg L^{-1} and 100 mg L^{-1}; and are reported in Figure 4.13. The removal efficiency is lowest at pH = 2 for all the cases. Removal efficiency increases with the increase in pH and the highest is obtained at pH = 6 for all four hydrogels. In the strong acidic condition, H^+ ions are freely available. Hence H^+ and metal ions compete each other to bind with available carboxylate or hydroxyl moieties of hydrogel resulting in poor removal rate.

The removal efficiency lies in the order of *β*CD-CMC > *β*CD-xylan > *β*CD-MCC > *β*CD gel for both 5 mg L^{-1} and 100 mg L^{-1} initial concentrations. The cyclic structure of *β*CD provides less flexibility to swell and hence lowest rate of removal of metal ions. However a decrease in removal efficiency is observed at pH = 8. The reason is attributed to the metal hydroxide formation in alkaline condition. The formation of $Cd(OH)_2$ and $Ni(OH)_2$ begins at pH 10 and pH 7 respectively [102]. The adsorption capacities follow a similar trend of removal. At pH = 6 and 100 mg L^{-1} initial concentration, the adsorbent capacities of *β*CD-CMC are 24.66 mg g^{-1} and 15.93 mg g^{-1} for Cd (II) and Ni (II) respectively. All four hydrogels adsorb considerably less amount of Ni (II) than Cd (II) ions making the adsorption process favorable for Cd (II) removal using *β*CD-cellulose/hemicellulose based hydrogels.

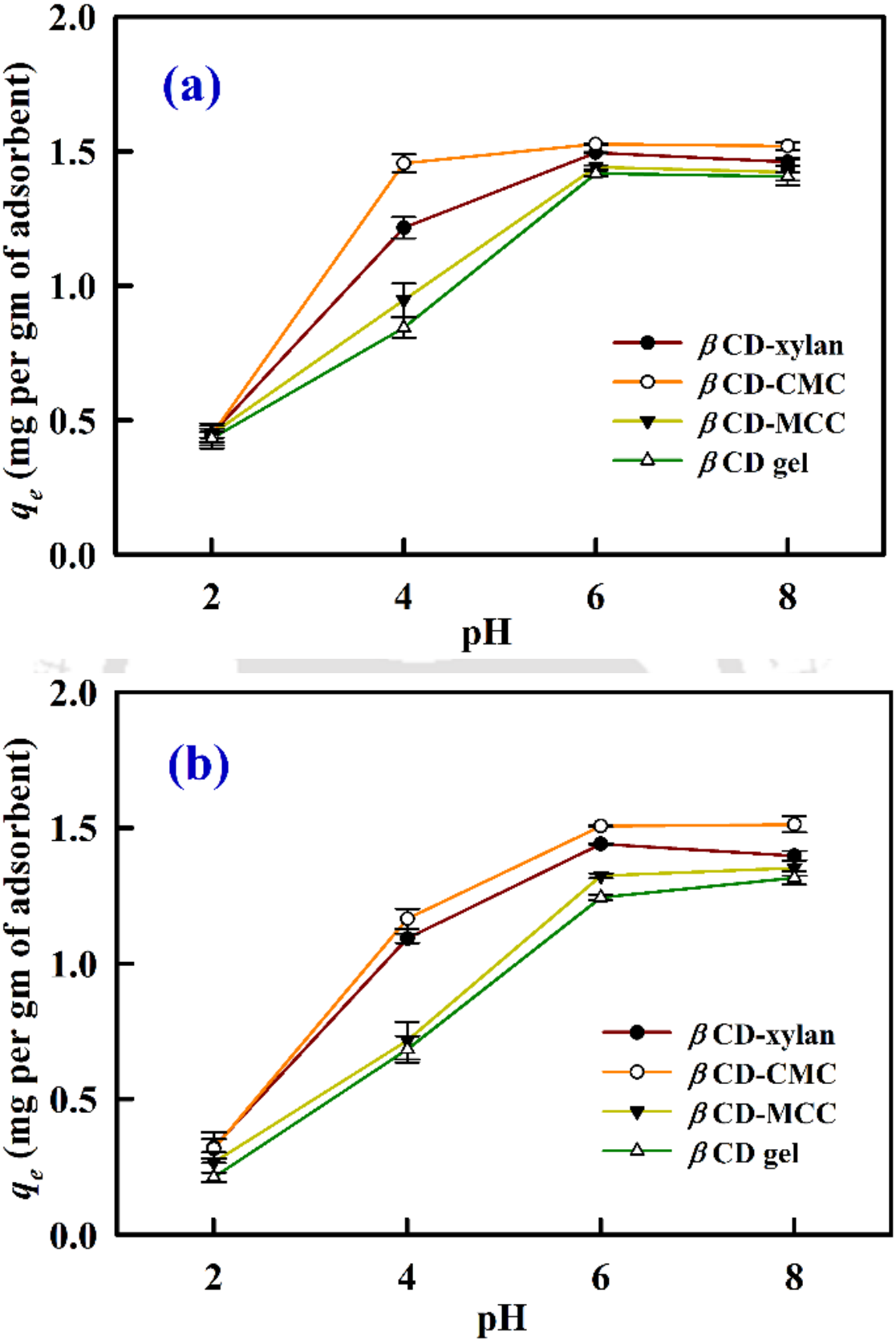

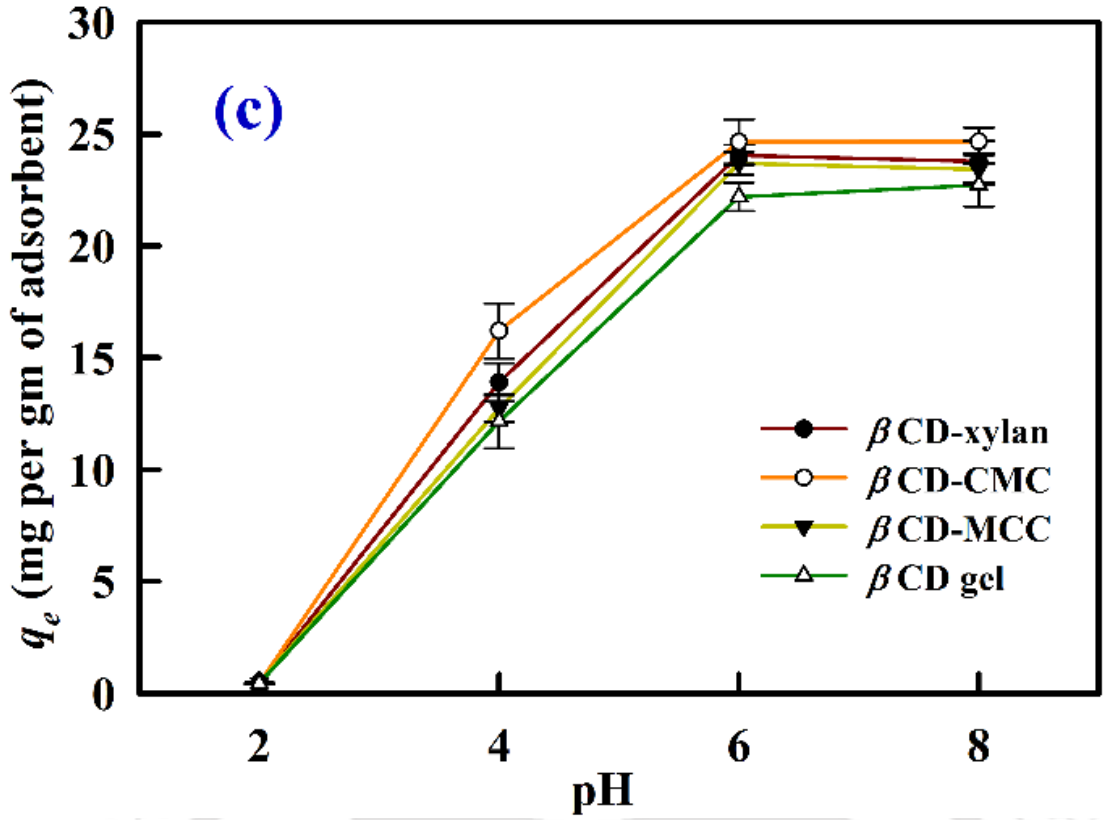

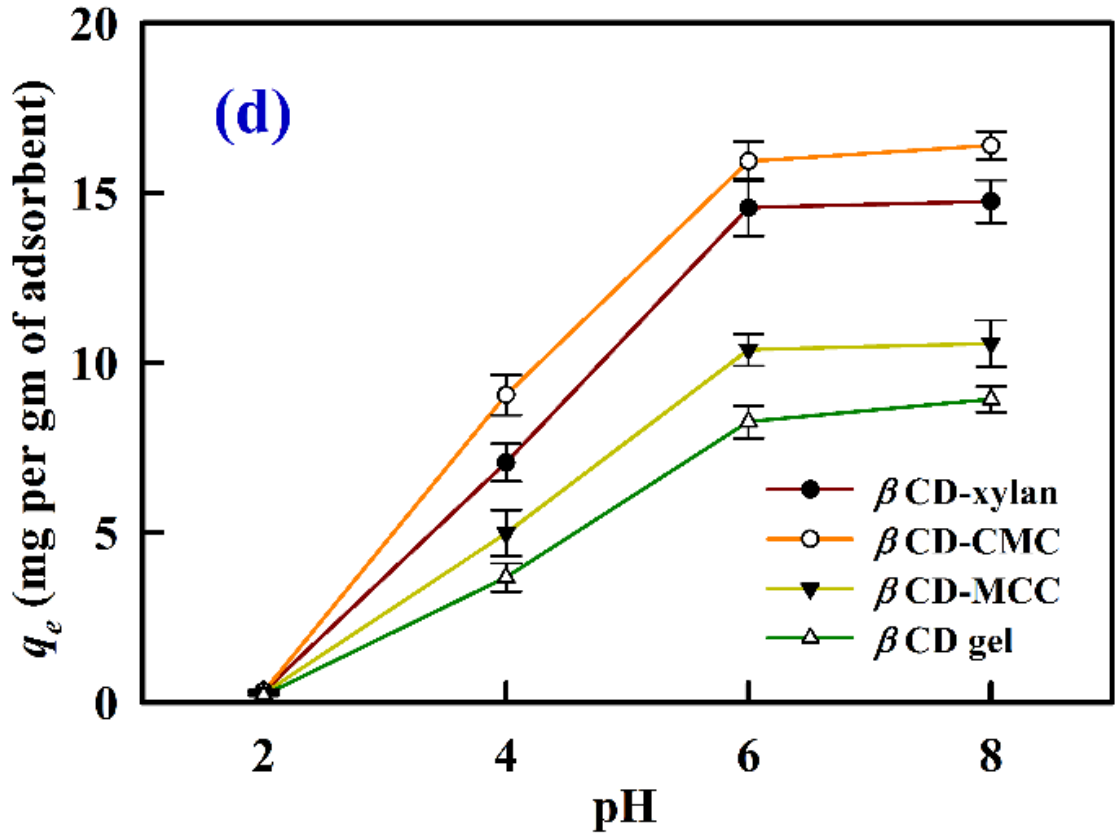

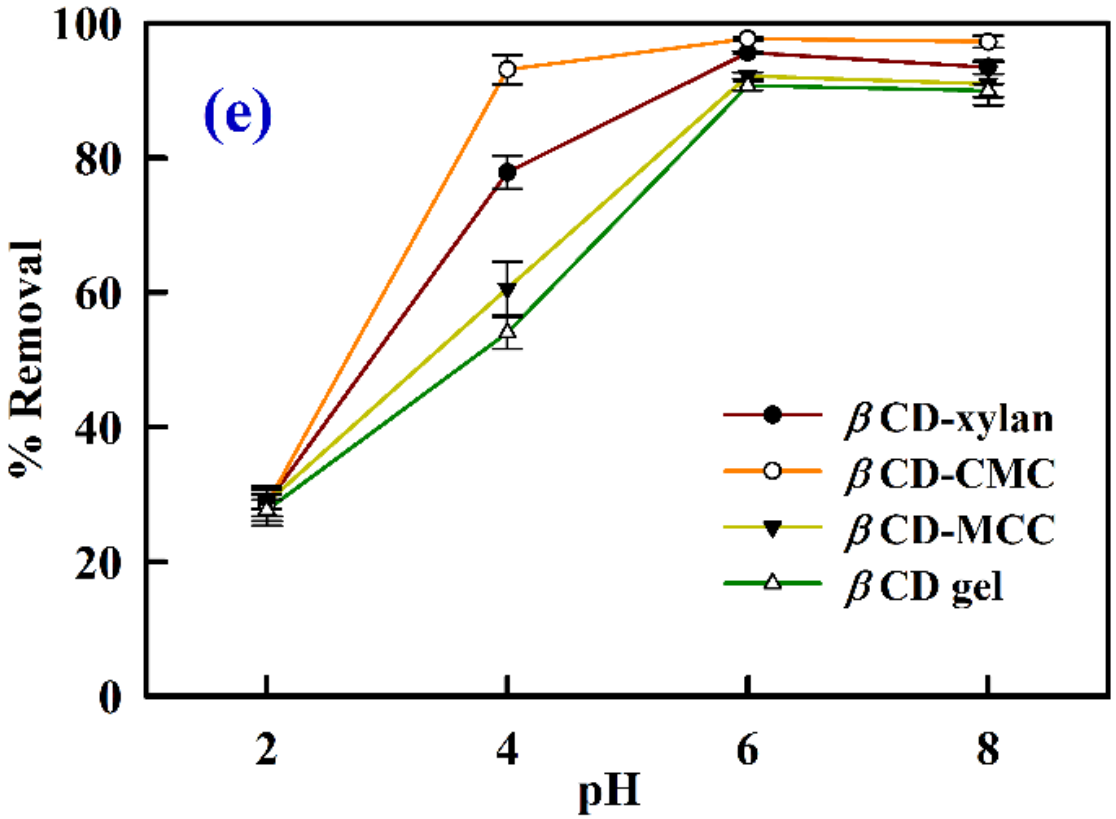

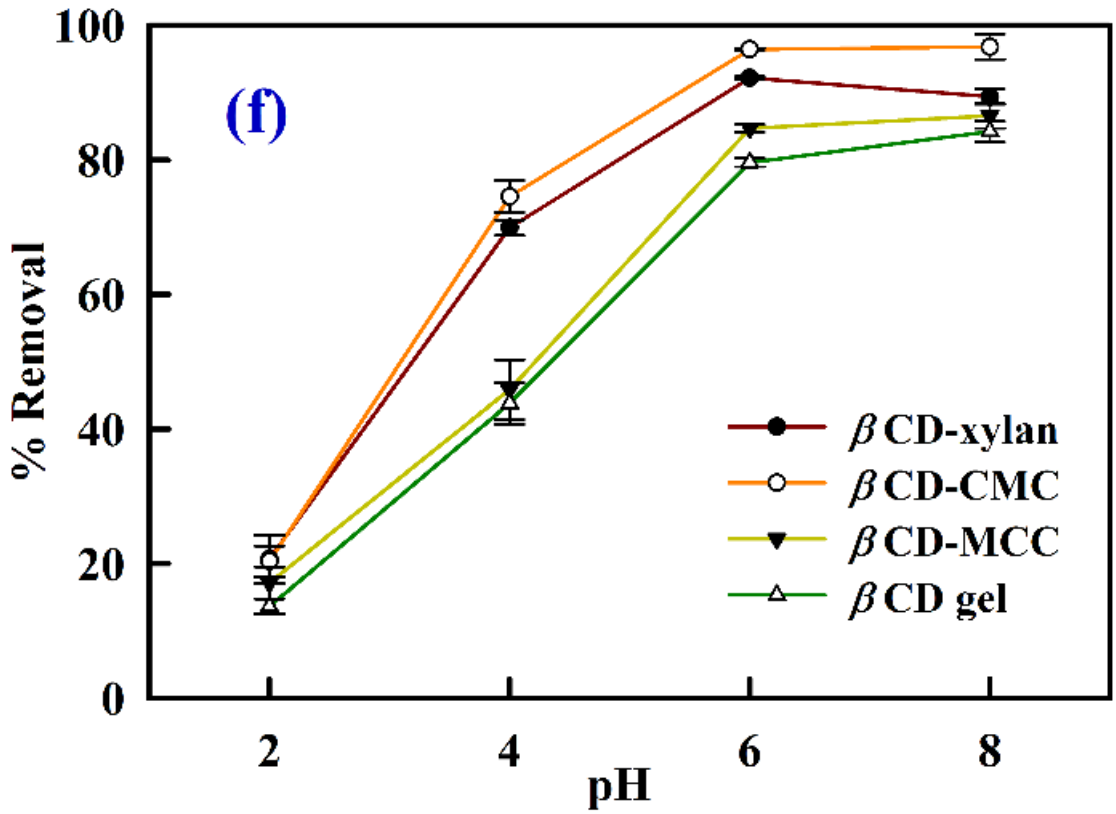

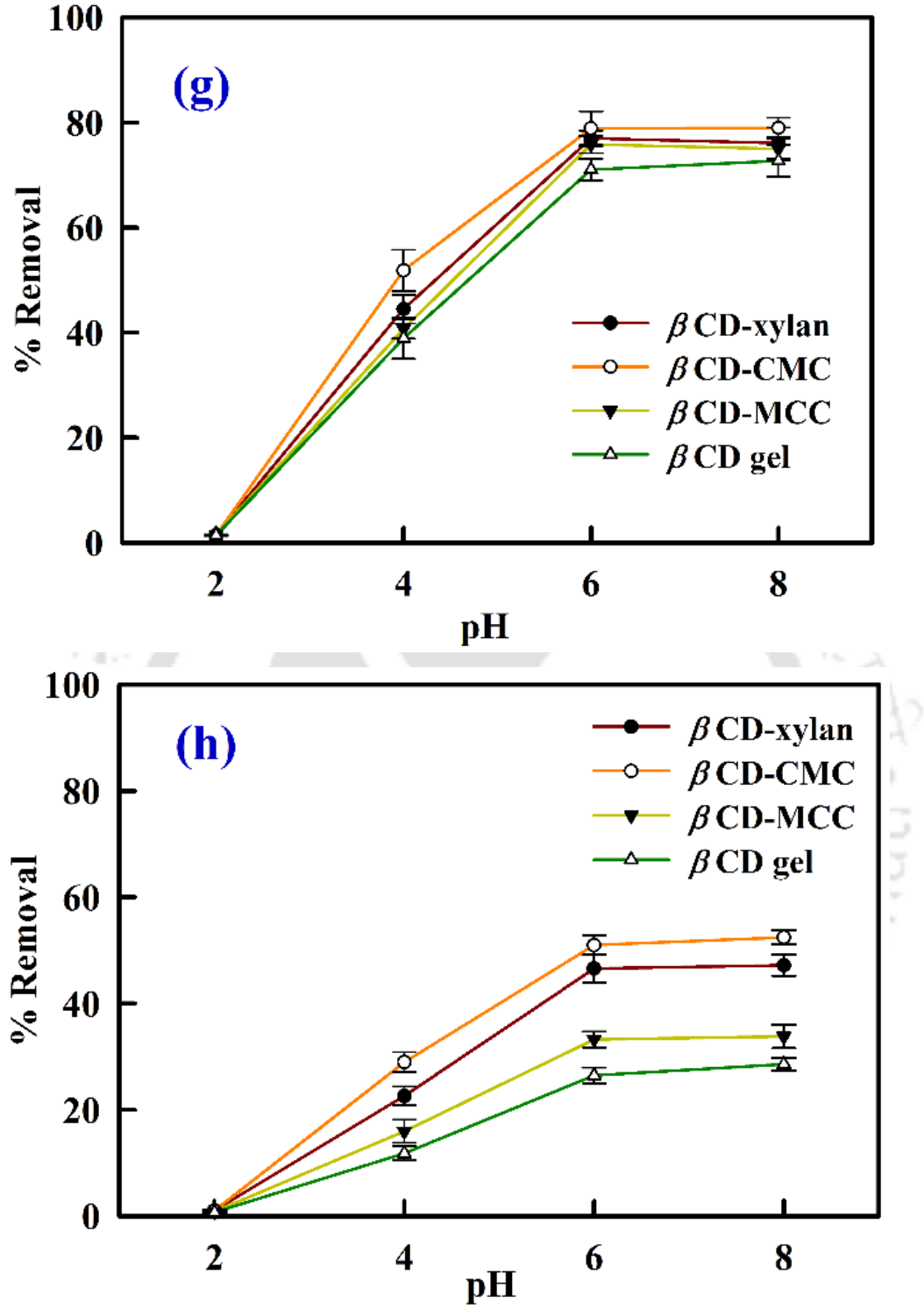

Figure 4.14. Equilibrium adsorption capacity (q_e) [(a)-(d)] and removal of pollutant [(e)-(h)] at various pH for the initial metal ion concentration of 5 mg L^{-1} and 100 mg L^{-1}. (a) and (c) q_e of Cd(II), (b) and (d) q_e of Ni(II), (e) and (g) removal of Cd (II), (f) and (h) removal of Ni (II).

4.3.6.4.Effect of temperature

The effect of temperature of adsorption process is measured by varying the temperature at T = 298, 308, 318, 328 K and reported at Figure 4.14. All temperature variation adsorption experiments are carried out at 80 mg of adsorbent dosage, pH = 6 and 100 mg L^{-1} initial metal ion concentrations. There is a mild increase in adsorption capacities as well as removal efficiencies with the increase in temperature. At higher temperature also, *β*CD-CMC uptakes higher amount of metal ions than the other three. Thus the order of adsorption capacity and removal efficiency becomes *β*CD-CMC > *β*CD-xylan > *β*CD-MCC > *β*CD gel. At higher temperature, hydrogels swell more, allowing a large expose of surface hidden under the top layer. The newly exposed surfaces tend to have more binding sites to adsorb metal ions. The variation in adsorption capacity with all four hydrogels is relatively small for Cd (II) than Ni (II). For both the metals, the adsorption capacities of *β*CD-xylan and *β*CD-MCC lie within the range of *β*CD-CMC and *β*CD gel. The increment in adsorption capacity is attributed to the endothermic nature of adsorption i.e. energy is being consumed during uptake. The removal efficiency for temperature variation follows a similar trend of adsorption capacity. However, as the increment of capacity is very small, we take 298 K temperature as the optimum adsorption temperature for the model fitting of adsorption isotherm and kinetics.

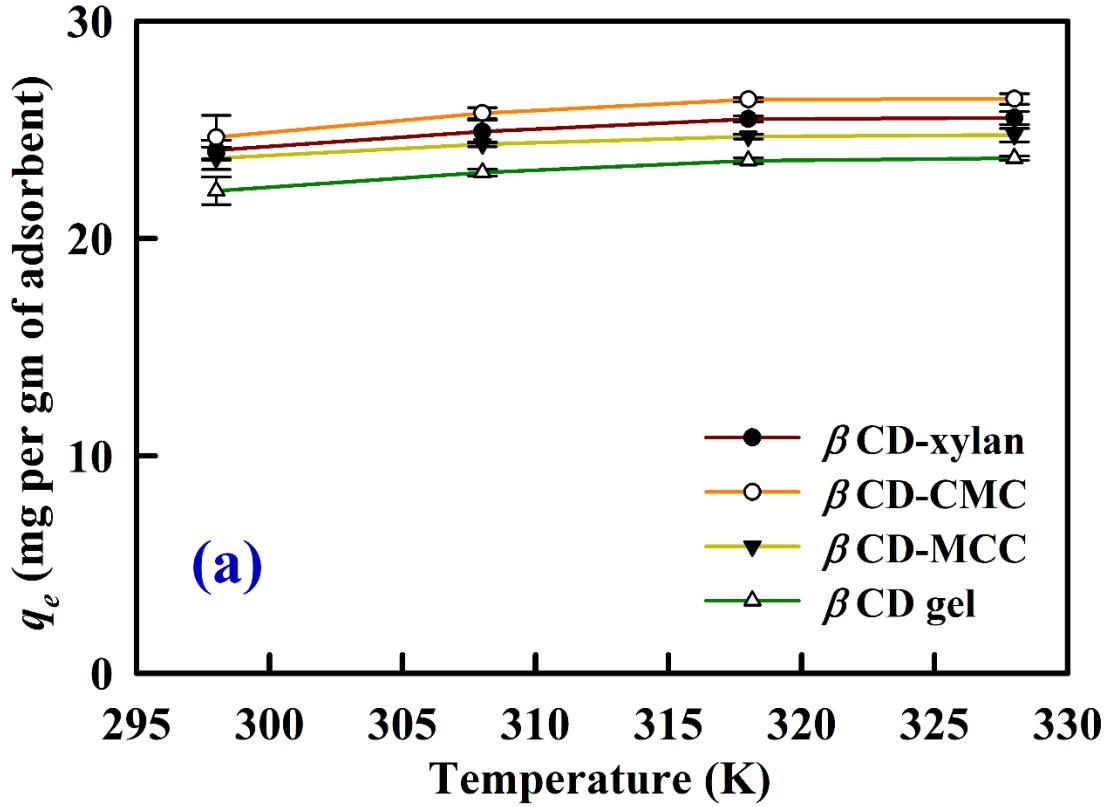

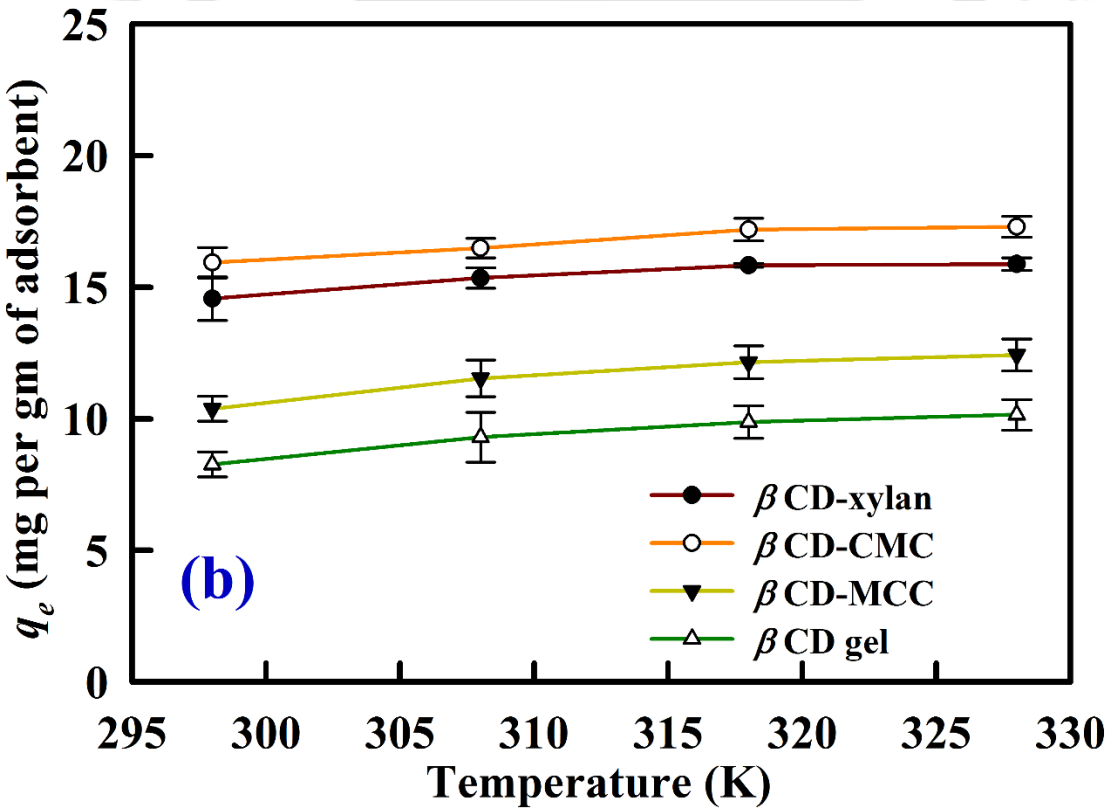

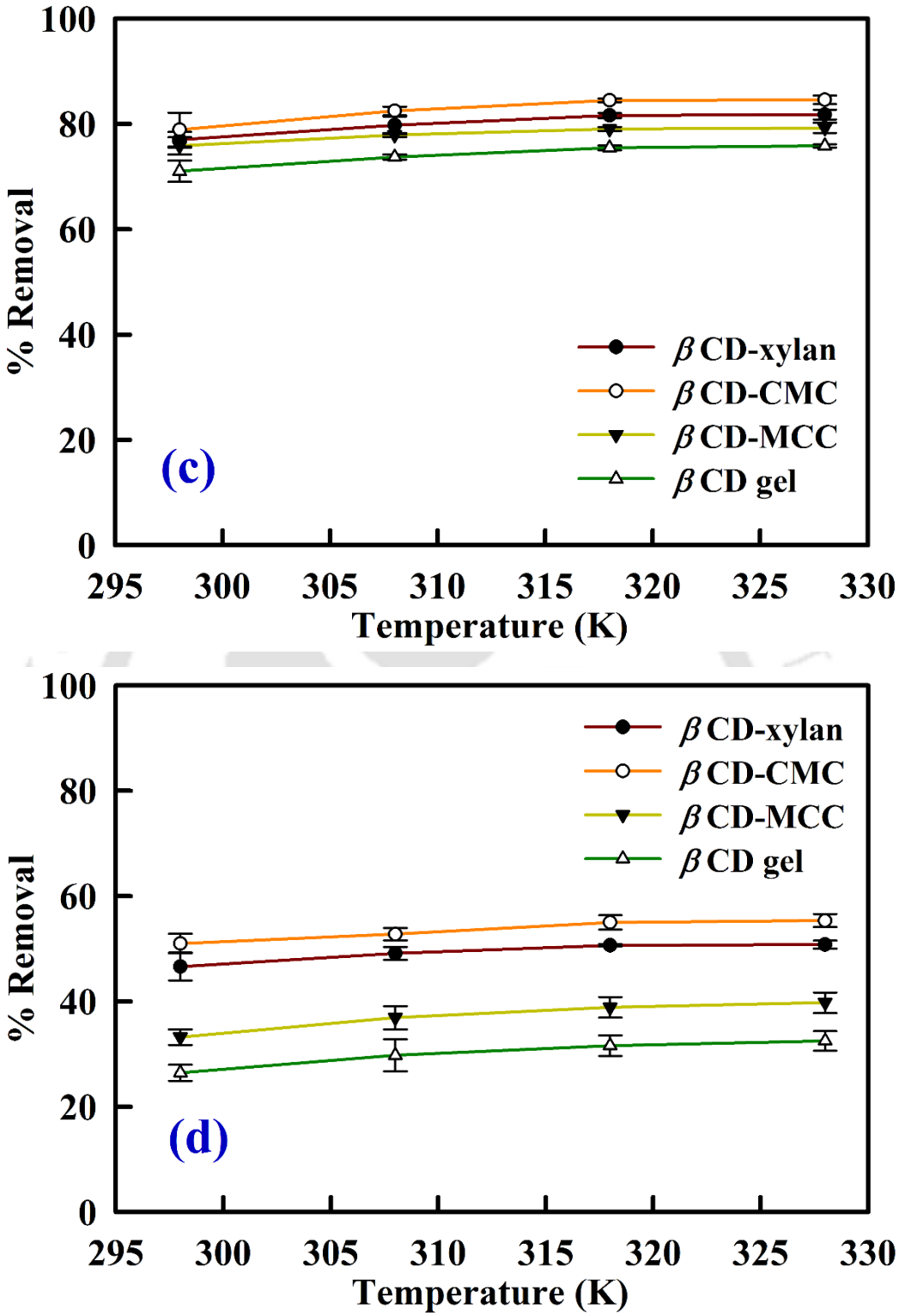

Figure 4.15. Equilibrium adsorption capacity (q_e) and removal of pollutant at temperatures, (a) q_e of Cd(II), (b) q_e of Ni(II), (c) removal of Cd (II), (d) removal of Ni (II).

4.3.6.5. Adsorption of Cd (II) and Ni (II) from mixed feed

After optimizing the adsorption parameters of single metal ion adsorption, we move to the selective adsorption of Cd (II) and Ni (II) from mixed feed. However, the mixed feed stream varies with a possible number of combination of concentration of metal ions, leading to a huge number of dataset which is beyond the scope of this work. Hence, we take the 5 mg L^{-1} individual concentration of Cd (II) and Ni (II), at 80 mg adsorbent dosage, pH = 6 and T = 25 °C. Such lower concentration of metal ions for the mixed feed study is also reported in the literature [44][122]. It is evident from the Figure 4.16, Cd (II) adsorbs at a faster rate than Ni (II) for all hydrogels studied. However, the order of adsorption for hydrogels are consistent, implies the highest adsorption capacity is obtained with βCD-CMC gel and least with βCD gel. Due to the selective adsorption, less amount of Cd (II) and Ni (II) are adsorbed than the adsorption of individual metal ions. The equilibrium adsorption capacity of each metal ion is then calculated with respect to its individual initial concentration.

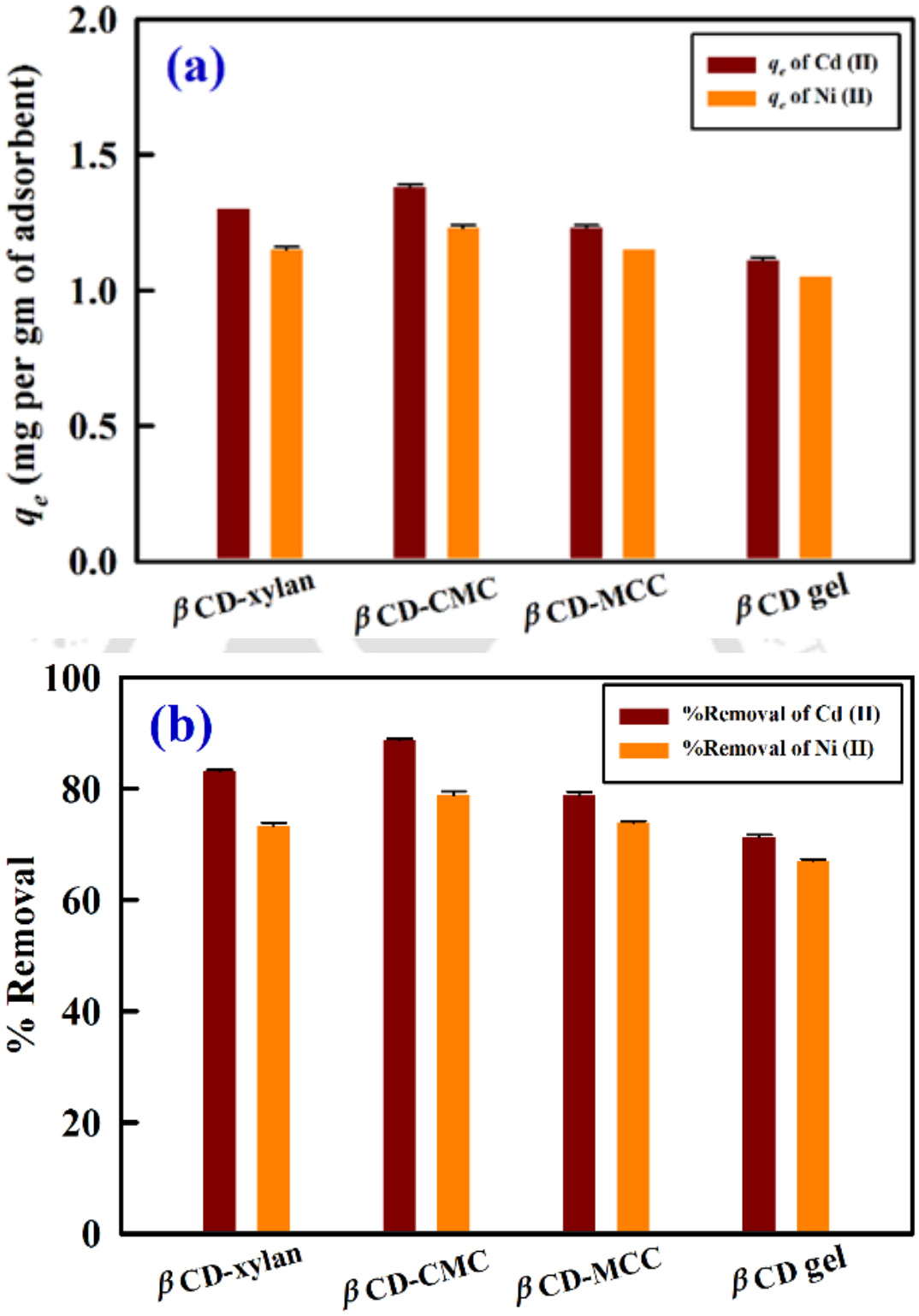

Figure 4.16. Equilibrium adsorption capacity (q_e) and removal of Cd (II) and Ni (II) from mix feed, (a) q_e of metal ions, (b) removal of metal ions.

4.3.6.6.Equilibrium adsorption isotherm

The adsorption isotherm is based on the assumption that every adsorption site is equivalent and that the ability of a particle to bind at adsorption site is independent of whether or not the site is occupied [123]. The isotherms describe the nature of interaction between adsorbate and adsorbent. Further the analysis of data determines maximum adsorption capacity of the adsorbent which in turn optimizes the use of adsorbent. The equilibrium solution concentration is obtained when a dynamic balance of concentration of adsorbate is established with bulk solution to that of liquid-adsorbent interface. In this scenario, adsorption equilibrium is reached. To explore the adsorption mechanism of Ni (II) and Cd (II) by four hydrogels, Langmuir and Freundlich isotherm models shall be adopted. The equilibrium concentrations and equilibrium adsorbent capacities are measured at T = 298 K, pH =6 for the corresponding metal ion concentrations of 5, 15, 25, 50, 100, 300 and 500 mg L^{-1}.

Langmuir isotherm: Langmuir isotherm model assumes monolayer adsorption of solutes on a homogeneous surface [124]. Homogeneous surface refers to finite number of identical sites having homogeneous adsorption energy. Further the identical and equivalent number of localized sites are having monolayer thickness. Thus, once the binding site is occupied with adsorbate, no further adsorption can happen at that site [123]. Therefore, the site poses equal affinity for the adsorbates with uniform energies of ion exchange [125, 126]. The Langmuir isotherm is given by,

$$\frac{C_e}{q_e} = \frac{1}{q_m b} + \frac{1}{q_m} C_e \qquad (4.5)$$

C_e (in mg L^{-1}) is equilibrium concentration of metal ions in solutions and q_e (in mg g^{-1}) is equilibrium adsorption capacities. q_m (in mg g^{-1}) is maximum adsorption capacity. b is the Langmuir constant (in L mg^{-1}). B is related to the energy of adsorption and affinity to binding sites. The dimensionless constant equilibrium parameter (R_L) determines the essential characteristic of Langmuir isotherm. Favorable isotherm is obtained for the values of R_L between 0 and 1 and unfavorable isotherm happens for R_L greater than 1. R_L = 1 indicates irreversible isotherm and R_L = 0 indicates the linear nature. Mathematically it is expressed as,

$$R_L = \frac{1}{1+bC_0} \tag{4.6}$$

Here, C_0 (in mg L^{-1}) is the initial concentration of metal solutions. Table 4.1 represents the model parameters applying Langmuir and Freundlich models for the experimental data of removal of metal ions using four hydrogels. Table 4.2 represents the corresponding model fitted isotherm equations for each case. The goodness of fit of experimental data on the isotherm model is expressed as correlation coefficient value (R^2) and are reported in Table 4.2.

For both the metal ions, the R^2 values are greater than 0.99 for all hydrogels which indicate monolayer adsorption phenomena for metal adsorption. Further we obtain the highest energy of adsorption (b) for βCD-CMC based hydrogel and least for βCD gel. Therefore, the metal ions prefer to bind more on carboxylate (βCD-CMC gel) and hydroxyl (for all gels) moieties than the inner cavity of βCD. The dimensionless constant R_L for all Langmuir isotherm fitting is obtained within 0-1 for all concentrations and decreasing trend of value of R_L is obtained with increasing concentration (Table 4.3). Thus the adsorption is favorable for both the metals with all four hydrogels. The lower values of R_L (approaching 0) indicate an irreversible nature of adsorption. At higher concentration, metal ions readily bind with adsorption sites leaving no site vacant to adsorb further metal ions. Maximum adsorption capacity (q_m) of 18.6 mg g^{-1} is obtained with βCD-CMC hydrogel for Ni (II) removal whereas βCD-xylan gel produces highest q_m of 42.0 mg g^{-1} for Cd (II) removal.

Freundlich isotherm: Freundlich isotherm is used to describe the multilayer adsorption on a heterogeneous adsorbent surface. The surface is assumed to have no uniform distribution of heat of adsorption. The linear form of Freundlich isotherm is expressed by,

$$\log q_e = \frac{1}{n_f}\log C_e + \log K_f \tag{4.7}$$

Where, C_e and q_e are defined previously. K_f and n_f are Freundlich constants and relates to the adsorption capacity and adsorption intensity respectively. Here, n_f indicates the favorability of adsorption. Value of $n_f < 1$, implies poor adsorption, moderate adsorption characteristic lies for a value of n_f between 1 and 2, while a good adsorption lies between 2 to 10. Freundlich model fitted equations and R^2 values are also reported in Table 4.2 and model parameter values are given in Table 4.1. The R^2 values for adsorption of Cd (II) lie

between 0.92-0.95, suggesting the adsorption is not a non-ideal phenomena. Further it rejects multilayer adsorption of metals on heterogeneous surface since metal ions prefer to bind only with carboxylate and hydroxyl moieties. The correlations are even worse for Ni (II) adsorption as R^2 lies between 0.85 to 0.91 although n_f lies in the adsorption region (except for Ni (II) removal with βCD gel).

Comparing the two isotherms, we conclude that the experimental data appropriately fit with Langmuir isotherm, reflecting the monolayer isotherm. The hydrogel surfaces behave like homogeneous surface. The results are understandable as H^+ is not lost during the synthesis or adsorption conditions. However, it is the carboxylate and hydroxyl moieties that donate proton in the solution, making vacant site accessible for metal ions to adsorb.

Table 4.1. Parameters of Langmuir and Freundlich isotherms

Cd (II)								
	q_m (mg g^{-1})				b (L mg^{-1})			
Langmuir isotherm	βCD-xylan	βCD-CMC	βCD-MCC	βCD gel	βCD-xylan	βCD-CMC	βCD-MCC	βCD gel
	42.02	41.84	39.37	37.45	0.09	0.12	0.08	0.07
	K_f				n_f			
Freundlich isotherm	βCD-xylan	βCD-CMC	βCD-MCC	βCD gel	βCD-xylan	βCD-CMC	βCD-MCC	βCD gel
	4.43	5.27	3.62	3.51	2.32	2.49	2.17	2.23
Ni (II)								
	q_m (mg g^{-1})				b (L mg^{-1})			
Langmuir isotherm	βCD-xylan	βCD-CMC	βCD-MCC	βCD gel	βCD-xylan	βCD-CMC	βCD-MCC	βCD gel
	16.67	18.62	12.21	10.17	0.11	0.16	0.11	0.08
	K_f				n_f			
Freundlich isotherm	βCD-xylan	βCD-CMC	βCD-MCC	βCD gel	βCD-xylan	βCD-CMC	βCD-MCC	βCD gel
	2.80	3.81	2.17	1.87	2.96	3.27	3.05	3.19

Table 4.2. Equations of Langmuir and Freundlich isotherms.

Cd (II)			
	Hydrogels	*Isotherm equations*	R^2
Langmuir isotherm	βCD-xylan	$\frac{C_e}{q_e} = 0.0238C_e + 0.2745$	0.9989
	βCD-CMC	$\frac{C_e}{q_e} = 0.0239C_e + 0.2057$	0.9991
	βCD-MCC	$\frac{C_e}{q_e} = 0.0254C_e + 0.3334$	0.9998
	βCD gel	$\frac{C_e}{q_e} = 0.0267C_e + 0.3874$	0.9992
Freundlich isotherm	βCD-xylan	$\log q_e = 0.4318 \log C_e + 0.6464$	0.9412
	βCD-CMC	$\log q_e = 0.4025 \log C_e + 0.7216$	0.9426
	βCD-MCC	$\log q_e = 0.4609 \log C_e + 0.5588$	0.9203
	βCD gel	$\log q_e = 0.4495 \log C_e + 0.5421$	0.9275
Ni (II)			
	Hydrogels	*Isotherm equations*	R^2
Langmuir isotherm	βCD-xylan	$\frac{C_e}{q_e} = 0.06C_e + 0.5621$	0.9990
	βCD-CMC	$\frac{C_e}{q_e} = 0.0537C_e + 0.3384$	0.9996
	βCD-MCC	$\frac{C_e}{q_e} = 0.0819C_e + 0.7557$	0.9998
	βCD gel	$\frac{C_e}{q_e} = 0.0983C_e + 1.2078$	0.9975
Freundlich isotherm	βCD-xylan	$\log q_e = 0.3383 \log C_e + 0.4478$	0.9098
	βCD-CMC	$\log q_e = 0.3054 \log C_e + 0.5810$	0.9145
	βCD-MCC	$\log q_e = 0.3274 \log C_e + 0.3355$	0.8789
	βCD gel	$\log q_e = 0.3131 \log C_e + 0.2726$	0.8548

Table 4.3. R_L values for the adsorption of Cd (II) and Ni (II) on Langmuir model.

Initial metal Concentration (mg L^{-1})	Cd (II)				Ni (II)			
	R_L				R_L			
	*β*CD-xylan	*β*CD-CMC	*β*CD-MCC	*β*CD gel	*β*CD-xylan	*β*CD-CMC	*β*CD-MCC	*β*CD gel
5	0.70	0.63	0.72	0.74	0.65	0.56	0.65	0.71
15	0.44	0.37	0.47	0.49	0.38	0.30	0.38	0.45
25	0.32	0.26	0.34	0.37	0.27	0.20	0.27	0.33
50	0.19	0.15	0.21	0.23	0.16	0.11	0.16	0.20
100	0.10	0.08	0.12	0.13	0.09	0.06	0.09	0.11
300	0.04	0.03	0.04	0.05	0.03	0.02	0.03	0.04
500	0.02	0.02	0.03	0.03	0.02	0.01	0.02	0.02

4.3.6.7.Adsorption kinetics

The time resolved adsorbent capacities and the removal rate of Cd (II) and Ni (II) with all four hydrogels are given in Figure 4.15. For the adsorption of Cd (II), we observe fast adsorption kinetics upto 120 min (Figure 4.15a). More than 75% of Cd (II) is adsorbed within this period by *β*CD-CMC hydrogel and more than 60% is adsorbed with other hydrogels. Further, the initial adsorption capacity of hydrogel is very similar for *β*CD-CMC and *β*CD-xylan hydrogels. For Cd (II), the adsorption capacities of all four hydrogels upto 100 min are very close reflecting strong affinity of Cd (II) towards the hydrogel moieties. For the adsorption of Ni (II), we observe prolonged adsorption period of 200 min. Unlike the adsorption kinetics of Cd (II), time resolved adsorption capacities of Ni (II) are distinctively placed. However, the rate of adsorption is faster for first 100 min and slows down gradually between 100-200 min. The rate of solute uptake by the adsorbent is described by the kinetics of adsorption. The analysis provides valuable information regarding the binding pathways and the mechanism. Here we employ pseudo first order and pseudo second order model to describe the kinetic behavior of adsorption. Like the previous isotherm fit, goodness of fit is also expressed by R^2. The pseudo first order model assumes the rate of adsorption is proportional to the number of unoccupied sites by the solutes and is expressed by Lagergren equation [127]. The model is expressed as,

$$\ln\left(q_e - q_t\right) = \ln q_e - k_1 t \tag{4.8}$$

Where, q_e (in mg g^{-1}) is equilibrium adsorption capacity and q_t (in mg g^{-1}) is time resolved adsorption capacities. k_1 is pseudo first order rate constant (in min^{-1}). The model is primarily used for solid or liquid adsorption based on the adsorbent capacity. It is based on direct proportional relationship between the difference of saturation uptake and time resolved uptake with the time of adsorption. The linear equations for each cases are given in Table 4.5 and R^2 values are less than 0.99. The lower regression values suggest the in capability of pseudo first order model in describing the adsorption of metal ions on the hydrogel surface. The model is particularly suited for very rapid adsorption process. Further, for entire adsorption kinetics, the pseudo first order model may not be suitable to describe total period of adsorption [128].

The pseudo second order model assumes the rate of occupation of solute at the adsorption sites is proportional to the square number of unoccupied sites [129]. Further, the concentration of binding sites on the surface of adsorbent determines the rate of adsorption. It is expressed as,

$$\frac{t}{q_t} = \frac{1}{k_2 q_e^2} + \frac{t}{q_e} \tag{4.9}$$

Here, k_2 is pseudo second order rate constant (in g mg^{-1} min^{-1}). The R^2 values (Table 4.5) lie greater than 0.99 for all cases. For that, the pseudo second order agrees well for the adsorption of Cd (II) and Ni (II) on the hydrogel surface than pseudo first order model.

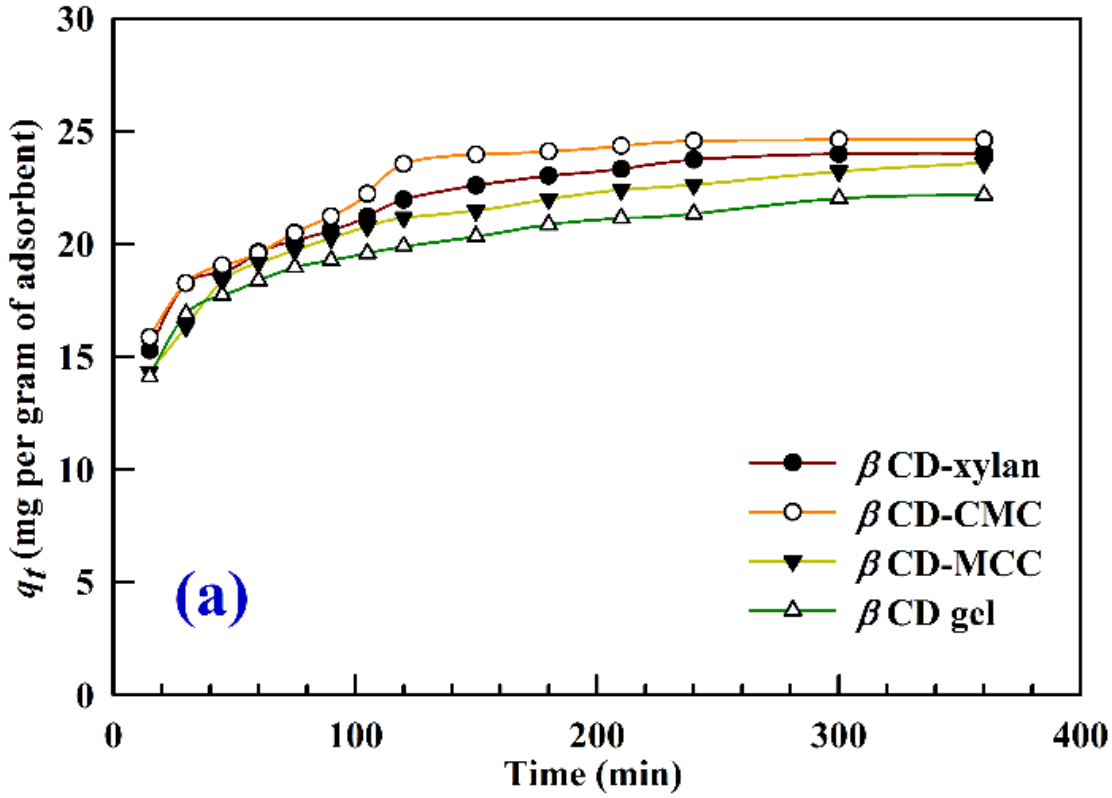

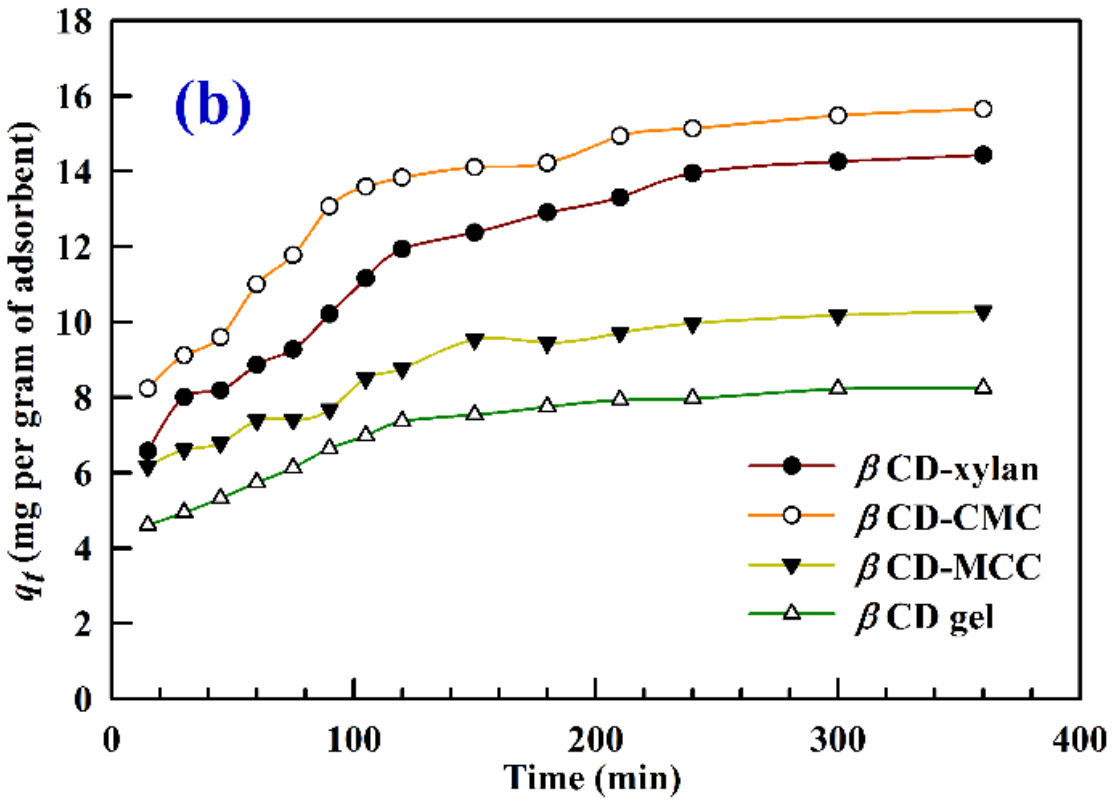

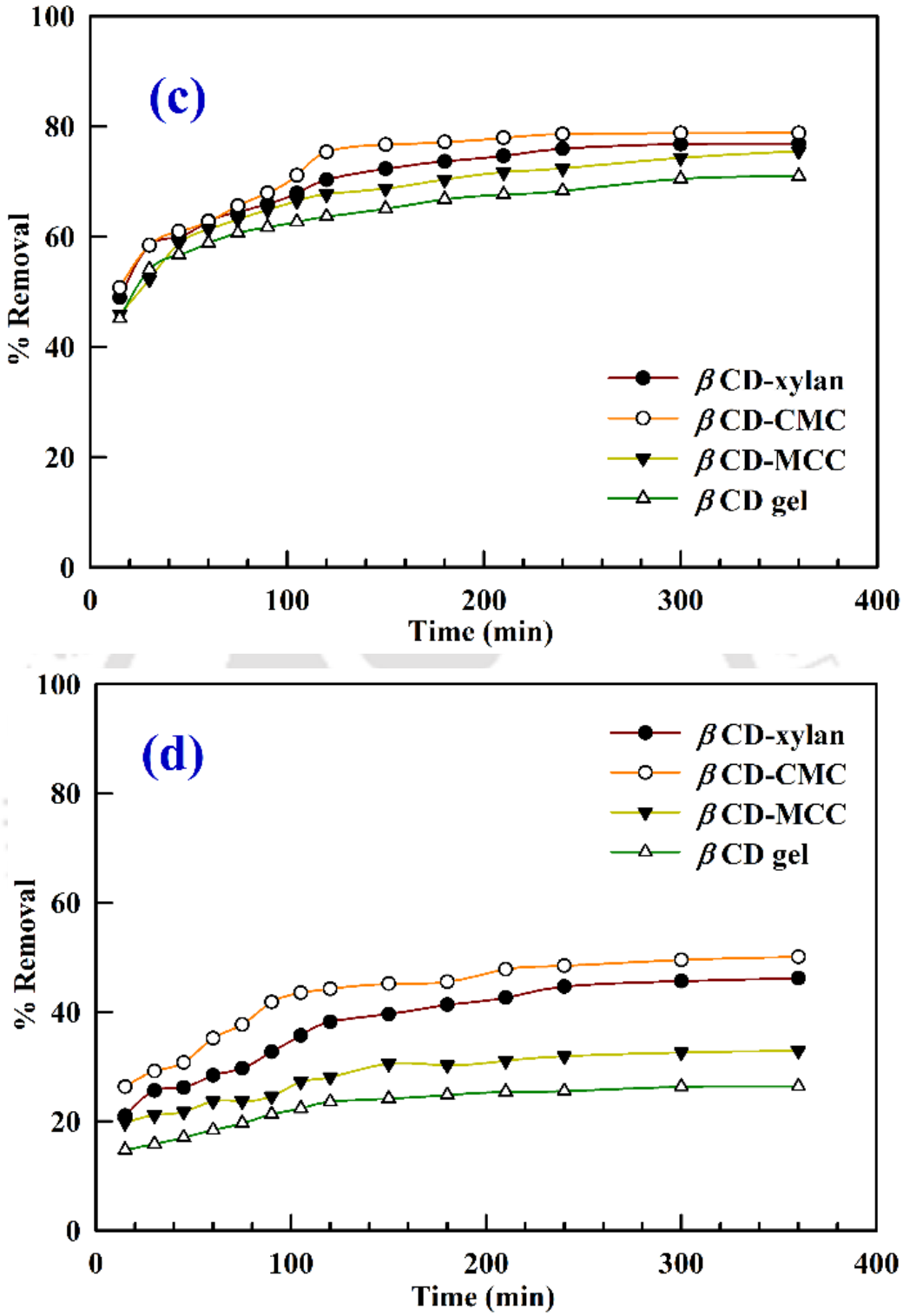

Figure 4.17. Equilibrium adsorption capacity (q_e) and removal of pollutant at various time interval, (a) q_t of Cd(II), (b) q_t of Ni(II), (c) removal of Cd (II), (d) removal of Ni (II).

Table 4.4. Parameters for pseudo first order and pseudo second order models at 298 K.

		Cd (II)				Ni (II)			
	Calculated constants	*β*CD-xylan	*β*CD-CMC	*β*CD-MCC	*β*CD gel	*β*CD-xylan	*β*CD-CMC	*β*CD-MCC	*β*CD gel
Pseudo first order model	k_1 (min^{-1})	1.62×10^{-2}	1.84×10^{-2}	1.12×10^{-2}	1.41×10^{-2}	1.18×10^{-2}	9.70×10^{-3}	1.11×10^{-2}	1.51×10^{-2}
	q_e (mg g^{-1})	13.28	13.13	10.31	11.12	11.45	8.22	5.90	6.12
Pseudo second order model	k_2 (g mg^{-1} min^{-1})	2.59×10^{-3}	2.63×10^{-3}	2.50×10^{-3}	3.00×10^{-3}	1.52×10^{-3}	2.21×10^{-3}	3.36×10^{-3}	4.25×10^{-3}
	q_e (mg g^{-1})	25.06	25.84	24.33	22.83	16.00	16.78	10.99	8.87

Table 4.5. Kinetic equations fitted into pseudo first order model and pseudo second order model

Cd (II)			
	Hydrogels	*Kinetic equations*	R^2
Pseudo first order model	βCD-xylan	$\ln(13.28-q_t)=2.5866-0.0162t$	0.9714
	βCD-CMC	$\ln(13.13-q_t)=2.5752-0.0184t$	0.9785
	βCD-MCC	$\ln(10.31-q_t)=2.3335-0.0112t$	0.9506
	βCD gel	$\ln(11.12-q_t)=2.4085-0.0141t$	0.9053
Pseudo second order model	βCD-xylan	$\frac{t}{q_t}=0.6135+0.0399t$	0.9993
	βCD-CMC	$\frac{t}{q_t}=0.5705+0.0387t$	0.9990
	βCD-MCC	$\frac{t}{q_t}=0.6759+0.0411t$	0.9993
	βCD gel	$\frac{t}{q_t}=0.6398+0.0438t$	0.9991
Ni (II)			
	Hydrogels	*Kinetic equations*	R^2
Pseudo first order model	βCD-xylan	$\ln(11.45-q_t)=2.4380-0.0118t$	0.9859
	βCD-CMC	$\ln(8.22-q_t)=2.1069-0.0097t$	0.9825
	βCD-MCC	$\ln(5.90-q_t)=1.7757-0.0111t$	0.9858
	βCD gel	$\ln(6.12-q_t)=1.8123-0.0151t$	0.9722
Pseudo second order model	βCD-xylan	$\frac{t}{q_t}=2.5750+0.0625t$	0.9935
	βCD-CMC	$\frac{t}{q_t}=1.6053+0.0596t$	0.9981
	βCD-MCC	$\frac{t}{q_t}=2.4657+0.0910t$	0.9959
	βCD gel	$\frac{t}{q_t}=2.9957+0.1128t$	0.9979

4.3.6.8.Thermodynamic parameters

The Gibbs' free energy and change in enthalpy of the adsorption process is calculated from Van't Hoff equation which is given by [130, 131],

$$\frac{d \ln k_{ad}}{dT} = \frac{\Delta H}{RT^2} \tag{4.10}$$

Where R is ideal gas law constant 8.314 J mol^{-1} K^{-1}. K_d is equilibrium constant at constant temperature, and calculated by, $k_{ad} = C_{ad}/C_0$. C_0 and C_{ad} are initial and adsorbed metal ion concentration respectively. ΔH is change in enthalpy (in kJ mol^{-1}). Therefore, integrating equation 4.9 from T_1 to T_2 temperature and assuming, the change in enthalpy during this period is $\Delta H_{T_1 \to T_2}$, we obtain,

$$\Delta H_{T_1 \to T_2} = R \frac{T_2 T_1}{T_2 - T_1} \ln \frac{k_{ad,T_2}}{k_{ad,T_1}} \tag{4.11}$$

However, the Gibbs free energy (ΔG, in kJ mol^{-1}) is calculated from the following equation,

$$\Delta G = -RT \ln k_{ad} \tag{4.12}$$

Here, negative sign is given to express the spontaneity of the process. The calculated values for ΔG and $\Delta H_{T_1 \to T_2}$ are reported in Table 4.6 at 80 mg adsorbent dosage, 100 mg L^{-1} initial concentration of metal ion, pH = 6 of solution and over a temperature range of 298-328 K. For all the adsorption studies, we observe negative values for ΔG which implies, the spontaneous nature of the adsorption process. However, with the increase in temperature, the ΔG decreases upto 318 K. This implies, the adsorption becomes less spontaneous upon increasing temperature and external mechanical shaking is required. However, at 328 K, the increasing trend of ΔG is again observed. We view this as the loosening of the crosslinking structure at this temperature, resulting higher removal. Therefore, it is recommended to perform, the adsorption process at 298 K considering the spontaneity of the process. The calculated change in enthalpy between two successive temperature increments is positive. The endothermic nature of the adsorption of metal ion on the binding sites is established by the positive values of change in enthalpy over the said temperature range [132]. The interaction among the adsorbent sites and adsorbate can

be inferred from the lower value of ΔH. However, the lower values further suggest a physisorption process in adsorption as chemisorption requires an enthalpy change of greater than 40 kJ mol^{-1} [132]. Further, at higher temperature the enthalpy change reduces significantly, implying the possibility of desorption increases at higher temperature. This ensures weak interaction between metal ions and host moieties of hydrogel matrix.

Table 4.6. ΔG and ΔH of adsorption process

		Cd (II)				Ni (II)			
	Temperature (K)	βCD-xylan	βCD-CMC	βCD-MCC	βCD gel	βCD-xylan	βCD-CMC	βCD-MCC	βCD gel
ΔG (kJ mol^{-1})	298	-0.65	-0.59	-0.69	-0.85	-1.89	-1.67	-2.73	-3.30
	308	-0.58	-0.49	-0.64	-0.78	-1.82	-1.64	-2.55	-3.10
	318	-0.54	-0.45	-0.62	-0.75	-1.80	-1.58	-2.50	-3.05
	328	-0.55	-0.46	-0.63	-0.76	-1.85	-1.61	-2.52	-3.07
$\Delta H_{T_1 \to T_2}$ (kJ mol^{-1})	298→308	2.67	3.34	2.04	2.84	4.00	2.60	8.03	8.98
	308→318	1.87	1.97	1.19	1.89	2.53	3.39	4.27	4.90
	318→328	0.18	0.10	0.23	0.43	0.23	0.55	1.90	2.42

4.3.6.9. Proposed adsorption mechanism

The mechanism of adsorption can be formulated from the thermodynamics of the system or kinetics of the adsorption. However, the thermodynamic data is derived from the long term equilibrium dataset whereas the kinetic dataset is derived from the time dependent adsorption study. Based on the thermodynamic calculations, it can be concluded that the adsorption of Cd (II) and Ni (II) in hydrogel is a physisorption process. The lower values of ΔH further support this. On the contrary the kinetic data follows the pseudo second order rate equation which is based on the chemisorption process. The hydrophobic cavity of βCD is capable of hosting Cd (II) and Ni (II) ions inside, making the complexation phenomena feasible. Therefore, it can be concluded that the metal ions first attract to the cavities of βCD which lead to the compliance of pseudo second order model. However, the formation of complex with the metal ions and cavity of βCD is realistic since pure βCD gel adsorbs significant amount of metal ions. Once the cavity is saturated, the metal ions form complex with the hydroxyl/carboxyl moieties of the cellulose/hemicellulose.

A combination of good adsorption capacity and feasible desorption of pollutant from the adsorbent make the adsorbent efficient in large scale usage. However, the desorption technique must be low cost and does not damage the adsorbent. Hence, a 0.1 M HCl solution for the desorption study was prepared as discussed in the literature [6]. Cd (II) and Ni (II) loaded gels were immersed in freshly prepared HCL and inside the orbital shaker for a period of 6 hour. Thereafter the samples are filtered and the concentration of metal ions are measured in AAS. The HCl medium recovered some amount of metal ions which is measured by the regeneration efficiency and given in the Table 6. The regeneration efficiency is given by,

$$\text{Regeneration efficiency}(\%) = \frac{\text{Amount of metal ion released}}{\text{Amount of metal ion adsorbed}} \times 100 \qquad (4.13)$$

Table 4.7. Regeneration efficiency (%) using 0.1 M HCl solution

	Cd (II)	Ni (II)
βCD-xylan	59.03	49.86
βCD-CMC	61.44	55.85
βCD-MCC	30.18	30.30
βCD gel	23.26	19.65

4.3.7. Comparison of metal removal study with literature

Here the comparison in the performance of the adsorption of Cd (II) and Ni (II) using βCD-cellulose/hemicellulose based hydrogels with a few literature reports are reported. The comparison is summarized in Table 4.8. To optimize the adsorption process, a robust variation in parameter is considered and performance of four hydrogels are evaluated in the adsorption process. However, βCD, cellulose and hemicellulose based hydrogels are individually being reported in literature. Here, we have synthesized a new set of hydrogels and are successfully applied for the removal of Cd (II) and Ni (II). The removal of Cd (II) is 24.66 mg g^{-1} is considerably higher than the reported data in literature. The adsorbed capacity of Ni (II) is 15.93 mg g^{-1} which is comparable with that reported in the literature. However, the removal capacity of Ni (II) is considerably less than that reported by Jia et al. for the MCC based hydrogels [95].

Table 4.8. Comparison of metal ion removal study with literature

Article	Monomers	Metal ions adsorbed	Maximum adsorption capacities	Fitted isotherm	Fitted kinetic mechanism	Reference
Wang et al.	*β*CD-acryloyl chloride, Silica-glycidyl methacrylate	Cd (II), Ni (II) and others	15.20 mg g^{-1} at pH 5.5 and 298 K for Cd (II) removal, 11.69 mg g^{-1} at pH 5.5 and 298 K for Ni (II) removal	Langmuir isotherm	Pseudo second order kinetic mechanism	[103]
Wang et al.	Carboxymethyl cellulose, poly(vinyl alcohol)	Ni (II) and others	6 mg g^{-1} at 288 K, DI water for Ni (II) removal	-	-	[98]
Jia et al.	Micro-crystalline cellulose, methyl acrylate	Ni (II) and others	140 mg g^{-1} at pH 4.5 and 301 K for Ni (II) removal	Langmuir isotherm	Pseudo second order kinetic mechanism	[95]
Elgueta et al.	O-acetyl galactogluco-mannan hemicellulose, acrylamido-2-methyl-1-propane - sulfonic acid	Cd (II), Ni (II) and others	19 mg g^{-1} and 23.7 mg g^{-1} Cd (II) and Ni (II) respectively, at pH 3, 298 K.	-	-	[102]
Present study	*β*CD, MCC, CMC and xylan	Cd (II), Ni (II)	24.66 mg g^{-1} and 15.93 mg g^{-1} Cd (II) and Ni (II) respectively, at pH 6, 298 K with 100 mg L^{-1} initial metal concentration.	Langmuir isotherm	Pseudo second order kinetic mechanism	-

4.4. Conclusions

*β*CD based four hydrogels are synthesized from *β*CD, CMC, xylan and MCC oligosaccharides, using EGDE crosslinker in alkaline conditions. The swelling study of synthesized hydrogels are carried out in pH = 2, 4, 6, 8 and DI water where water absorbance increases with pH. A highest swelling ratio of 362.53% is observed with *β*CD-CMC gel at pH = 8. All the hydrogels are shown to have better adsorption abilities toward Cd (II) than Ni (II). Overall the *β*CD-CMC hydrogel has proven to be better candidate for adsorbing Cd (II) and Ni (II) among all studied hydrogels. The parameters of adsorption are studied with the variation of adsorbent dosage, concentration of metal ion solution, pH and temperature. The order of adsorption capacity for both the metals is *β*CD-CMC > *β*CD-xylan > *β*CD-MCC > *β*CD gel with all studied parameters. For Cd (II), *β*CD-CMC based hydrogel gives adsorbent capacities of 13.81 mg g^{-1} at 80 mg adsorbent dosage; 24.61 mg g^{-1} at 100 mg L^{-1} initial metal ion concentration; 24.66 mg g^{-1} at the pH = 6 of metal ion solution; 26.42 mg g^{-1} at the 328 K temperature. Similarly, for Ni (II), *β*CD-CMC based hydrogel gives adsorbent capacities of 10.58 mg g^{-1} at 80 mg adsorbent dosage; 15.89 mg g^{-1} at 100 mg L^{-1} initial metal ion concentration; 15.93 mg g^{-1} at the pH = 6 of metal ion solution and 17.29 mg g^{-1} at the 328 K temperature. The toroid shape of *β*CD prevents it from large swelling and thus giving it lesser amount of surface i.e. active binding sites for adsorption. The surface adsorption of metal ions is confirmed by the Langmuir isotherm model with R_L values are less than 1 for all cases, reflecting favorable condition for adsorption. Pseudo second order is proved to be better fitted model for the adsorption process. Further lower amount of increment in the change in enthalpy values lead to conclude the adsorption process is physisorption process involving weak interaction of complex, formed among metal ions and active binding sites.

Chapter 5

Concluding remarks and future scope

Highlights

- Overall conclusion
- Future direction

5.1. Overall conclusion

Cellulose variants such as microcrystalline cellulose (MCC), carboxymethyl cellulose (CMC) and hemicellulose variant such as xylan are being crosslinked with EGDE to produce cellulose-hemicellulose based hydrogels. Additionally cyclodextrin variant such as β-cyclodextrin (βCD) is also crosslinked with cellulose and hemicellulose to produce hydrogels. Homopolymerized hydrogels as well as copolymerized hydrogels are synthesized in various molar ratios consisting of the precursor monomers. The hydrogels are physically characterized by swelling ratio and gel fractions. Swelling ratios of cellulose-hemicellulose based hydrogels are measured in DI water and physiological buffers, namely, AGF, AIF and PBS. The least swelling ratio for all hydrogels are observed in AGF and this steadily increases with the pH and a highest swelling ratio is obtained for DI water. For βCD-cellulose/hemicellulose based hydrogels, swelling ratio is measured in DI water as well as pH=2 to 8 and is found to follow a similar trend of swelling ratio.

The functional moieties of hydrogels are characterized by FT-IR characterization. In the rheological study, shear thinning behavior is observed for cellulose-hemicellulose based hydrogels within a shear range of 0.01-1000 s^{-1}. The flow behavior of hydrogels follows the power law model. The measurement of loss tangent within a linear viscoelastic region reveals the dominance of elastic nature over the viscous nature of the hydrogels up to the gel point. All the cellulose-hemicellulose based hydrogels can withstand greater than 10 Hz frequency before breaking of their crosslinking structure. From the morphological observation, all hydrogels appear to be coarse in nature with random elongations. The random elongations increase the surface area and thus increases the binding sites for metal ions, drug and protein molecules.

The synthesized hydrogels are successfully applied in three distinct applications.

i. *In vitro* release of Cephalexin drug in various physiological buffers,
ii. *In vitro* release of Vitamin B_{12} in various physiological buffers,
iii. Adsorption of Ni (II) and Cd (II) from aqueous solution.

MCC-CMC based hydrogels have proved to be an effective carrier of Cephalexin drug where ~98% drug is recorded to release in successive buffers for 10 hour (2 hour in AGF followed by 2 hour in AIF followed by 6 hour in PBS). The drug loading capacity is recorded within 19-27% range for all the buffers. Copolymerized CMC-xylan gels have

higher VB_{12} loading than pure CMC and xylan gel. Further CMC-xylan hydrogel in 1:1 molar ratio released ~99% of VB_{12} in successive buffers (2 hour in AGF followed by 2 hour in AIF followed by 6 hour in PBS).

*β*CD-cellulose/hemicellulose based hydrogels are successfully applied to adsorb Cd(II) and Ni(II) from aqueous solution. The adsorption capacity is determined by varying the adsorbent dosage, initial concentration of metal ions, pH of solutions and temperature. *β*CD-CMC hydrogel produces highest adsorption capacity among the four hydrogels for all parameters. Further, the equilibrium adsorption data closely follow the Langmuir isotherm, referring to the monolayer adsorption of metal ions mainly at the surface of hydrogel. The adsorption mechanism follows the pseudo second order rate equations and the adsorption is proved to be spontaneous in nature over the temperature range of 298-328 K.

5.2. Future direction

In this thesis, the synthesized cellulose-hemicellulose hydrogels are applied to deliver model drug (Cephalexin) and model vitamin (Vitamin B_{12}) in physiological buffer *in vitro* condition. Further, another set of hydrogels i.e. cyclodextrin-cellulose/hemicellulose hydrogels are used to adsorb metal ions (Cd (II) and Ni (II)) from aqueous solution. Apart from these applications, the hydrogels can be used in several other applications which are viewed as future directions of this thesis.

Cationic dyes are widely used in paper and leather industries, and are considered to be harmful to aquatic and human life. Hydrogels can act as biosorbent to adsorb the dyes from aqueous solution. The abundance of hydroxyl and carboxymethyl anions in CMC is particularly attractive to bind with the cationic part of dyes with its subsequent removal.

The biocompatibility, biodegradability, soft network formation and water retention capacity of hydrogel, resembles extracellular matrix. For that, cell encapsulation and cytocompatibility of hydrogel is a vast area of application. Previously, the EGDE crosslinked hydrogels were successfully employed for the encapsulation and cytotoxic test of SRA 01/04 cells (Epithelial Cells of Lens) and the COS-7 (isolated cells from the suprarenal African Green Monkey) [59].

Molecular dynamics simulation is an excellent approach to predict the transport properties of hydrogels in various pH medium. Further, the various non-bonded interactions among the guest molecules with the functional moieties of host hydrogel matrix, can be predicted.

The synthesis of novel set of hydrogels coupled with the successful applications in the delivery of biomolecules and adsorption of metal ions, opens up the possibility of scaling up the synthesis process. Hence, it is presumed that an ASPEN plus simulation of scaling up would be the next step forward of this work.

References

1. Khan, F., Tare, R. S., Oreffo, R. O. C. and Bradley, M., "Versatile Biocompatible Polymer Hydrogels: Scaffolds for Cell Growth," *Angew. Chem., Int. Ed.* **48**, 978 – 982 (2009).
2. Bajpai, A. K., Shukla, S. K., Bhanu, S. and Kankane, S., "Responsive Polymers in Controlled Drug Delivery," *Prog. Polym. Sci.* **33**, 1088 – 1118 (2008).

3 Katsoulos, C., Karageorgiadis, L., Vasileiou, N., Mousafeiropoulos, T. and Asimellis, G., "Customized Hydrogel Contact Lenses for Keratoconus Incorporating Correction for Vertical Coma Aberration," *Ophthalmic and Physiological Optics*, **29**,321 – 329 (2009).

4. Lee, Y. J. and Braun, P. V., "Tunable Inverse Opal Hydrogel pH Sensors," *Adv. Mater.*, **15**, 563 – 566 (2003).
5. Muya, F. N., Sunday, C. E., Baker, P. and Iwuoha, E., "Environmental Remediation of Heavy Metal Ions from Aqueous Solution through Hydrogel Adsorption: A Critical Review," *Water Sci. Technol.*, **73**, 983 – 992 (2015).
6. Kurdtabar, M., Peyvand Kermani, Z. and Bagheri Marandi, G., "Synthesis and Characterization of Collagen-based Hydrogel Nanocomposites for Adsorption of Cd^{2+}, Pb^{2+}, Methylene Green and Crystal Violet," *Iran. Polym. J.*, **24**, 791 – 803 (2015).
7. Wichterle, O. and Lim, D., "Hydrophilic Gels for Biological Use," *Nature*, **185**, 117 – 118 (1960).
8. Coviello, T., Matricardi, P., Marianecci, C. and Alhaique, F., "Polysaccharide Hydrogels for Modified Release Formulations," *J. Controlled Release*, **119**, 5 – 24 (2007).
9. Chenite, A., Chaput, C., Wang, D., Combes, C., Buschmann, M. D., Hoemann, C. D.,

   Leroux, J. C., Atkinson, B. L., Binette, F. and Selmani, A., "Novel Injectable Neutral Solutions of Chitosan form Biodegradable Gels In Situ," *Biomaterials*, **21**, 2155 – 2161 (2000).
10. Kosmala, J. D., Henthorn, D. B. and Brannon-Peppas, L., "Preparation of Interpenetrating Networks of Gelatin and Dextran as Degradable Biomaterials," *Biomaterials*, **21**, 2019 – 2023 (2000).

11. Joly-Duhamel, C., Hellio, D. and Djabourov, M., "All Gelatin Networks: 1. Biodiversity and Physical Chemistry," *Langmuir*, **18**, 7208 – 7217 (2002).
12. Šedová, P., Buffa, R., Kettou, S., Huerta-Angeles, G., Hermannová, M., Leierová, V.,
    Šmejkalová, D., Moravcová, M. and Velebný, V., "Preparation of Hyaluronan Polyaldehyde—A Precursor of Biopolymer Conjugates," *Carbohydr. Res.*, **371**, 8 – 15 (2013).
13. Zhu, J., "Bioactive Modification of Poly(ethylene glycol) Hydrogels for Tissue Engineering," *Biomaterials*, **31**, 4639 – 4656 (2010).
14. Buwalda, S. J., Boere, K. W. M., Dijkstra, P. J., Feijen, J., Vermonden, T. and Hennink, W. E., "Hydrogels in a Historical Perspective: From Simple Networks to Smart Materials," *J. Controlled Release*, **190**, 254 – 273 (2014).
15. Ullah, F., Othman, M. B. H., Javed, F., Ahmad, Z. and Akil, H. M., "Classification, Processing and Application of Hydrogels: A Review," *Mater. Sci. Eng., C*, **57**, 414 – 433 (2015).
16. Ahadian, S., Sadeghian, R. B., Salehi, S., Ostrovidov, S., Bae, H., Ramalingam, M. and Khademhosseini, A., "Bioconjugated Hydrogels for Tissue Engineering and Regenerative Medicine," *Bioconjugate Chem.*, **26**, 1984 – 2001 (2015).
17. Bassil, M., Davenas, J. and El Tahchi, M., "Electrochemical Properties and Actuation Mechanisms of Polyacrylamide Hydrogel for Artificial Muscle Application," *Sens. Actuators, B*, **134**, 496 – 501 (2008).
18. Burdick, J. A., Ward, M., Liang, E., Young, M. J. and Langer, R., "Stimulation of Neurite Outgrowth by Neurotrophins Delivered from Degradable Hydrogels," *Biomaterials*, **27**, 452 – 459 (2006).
19. Jain, A., Kim, Y-T., McKeon, R. J. and Bellamkonda, R. V., "In Situ Gelling Hydrogels for Conformal Repair of Spinal Cord Defects, and Local Delivery of BDNF after Spinal Cord Injury," *Biomaterials*, **27**, 497 – 504 (2006).
20. Wang, Y., Adokoh, C. K. and Narain, R., "Recent Development and Biomedical Applications of Self-healing Hydrogels," *Expert Opin. Drug Delivery.*, **15**, 77 – 91 (2018).
21. Laftah, W. A., Hashim, S. and Ibrahim, A. N., "Polymer Hydrogels: A Review," *Polym.-Plast. Technol. Eng.*, **50**, 1475 – 1486 (2011).

22. Herber, S., Olthuis, W., Bergveld, P. and van den Berg, A., "Exploitation of a pH-Sensitive Hydrogel Disk for CO_2 Detection," *Sens. Actuators, B,* **103**, 284 – 289 (2004).
23. Guenther, M., Gerlach, G., Corten, C., Kuckling, D., Sorber, J. and Arndt, K. F., "Hydrogel-based Sensor for a Rheochemical Characterization of Solutions," *Sens. Actuators, B,* **132**, 471 – 476 (2008).
24. Zhang, Y., Ji, H-F., Brown, G. M. and Thundat, T., "Detection of CrO_4^{2-} Using a Hydrogel Swelling Microcantilever Sensor," *Anal. Chem*., **75**, 4773 – 4777 (2003).
25. Beebe, D. J., Moore, J. S., Bauer, J. M., Yu, Q., Liu, R. H., Devadoss, C. and Byung-Ho, J., "Functional Hydrogel Structures for Autonomous Flow Control inside Microfluidic Channels," *Nature*. **404**, 588 (2000).
26. Van Tran, V., Park, D. and Lee, Y-C., "Hydrogel Applications for Adsorption of Contaminants in Water and Wastewater Treatment," *Environ. Sci. Pollut. Res*., **25**, 24569 – 24599 (2018).
27. Gopinath, V., Saravanan, S., Al-Maleki, A. R., Ramesh, M. and Vadivelu, J., "A Review of Natural Polysaccharides for Drug Delivery Applications: Special Focus on Cellulose, Starch and Glycogen," *Biomed. Pharmacother*., **107**, 96 – 108 (2018).
28. Zhu, H., Luo, W., Ciesielski, P. N., Fang, Z., Zhu, J. Y., Henriksson G, Himmel, M. E. and Hu, L., "Wood-Derived Materials for Green Electronics, Biological Devices, and Energy Applications," *Chem. Rev*., **116**, 9305 – 9374 (2016).
29. Ebringerová, A., "Structural Diversity and Application Potential of Hemicelluloses. *Macromol. Symp*.," **232**, 1 – 12 (2006).
30. Petzold, K., Schwikal, K., Günther, W. and Heinze, T., "Carboxymethyl xylan – Control of Properties by Synthesis," *Macromol. Symp.* **232**, 27 – 36 (2006).
31. Van de Manakker, F., Vermonden, T., Van Nostrum, C. F. and Hennink, W. E., "Cyclodextrin-Based Polymeric Materials: Synthesis, Properties, and Pharmaceutical/Biomedical Applications," *Biomacromolecules*, **10**, 3157 – 3175 (2009).
32. Buschmann, H. J., and Schollmeyer, E., "Applications of Cyclodextrins in Cosmetic Products: A review," *J. Cosmet. Sci*., **53**, 185 – 191 (2002).

33. Pinho, E., Grootveld, M., Soares, G. and Henriques, M., "Cyclodextrin-based Hydrogels toward Improved Wound Dressings," *Crit. Rev. Biotechnol*,. " **34**, 328 – 337 (2014).
34. Pahimanolis, N., Kilpeläinen, P., Master, E., Ilvesniemi, H. and Seppälä, J., "Novel Thiol- Amine- and Amino Acid Functional Xylan Derivatives Synthesized by Thiol–ene Reaction," *Carbohydr. Polym.*, **131**, 392 – 398 (2015).
35. Kono, H., Onishi, K. and Nakamura, T., "Characterization and Bisphenol A Adsorption Capacity of *β*-Cyclodextrin–carboxymethylcellulose-based Hydrogels," *Carbohydr. Polym.*, **98,** 784 – 792 (2013).
36. Hu, H., You, J., Gan, W., Zhou, J. and Zhang, L., "Synthesis of Allyl Cellulose in NaOH/urea Aqueous Solutions and Its Thiol–ene Click Reactions," *Polym. Chem*., **6,** 3543 – 3548 (2015).
37. Trache, D., Hussin, M. H., Hui Chuin, C. T., Sabar, S., Fazita, M. R. N., Taiwo, O. F. A., Hassan, T. M. and Haafiz, M. K. M., "Microcrystalline Cellulose: Isolation, Characterization and Bio-composites Application—A Review," *Int. J. Biol. Macromol.* **93**,789 – 804 (2016).
38. Shen, X., Shamshina, J. L., Berton, P., Gurau, G., and Rogers, R. D., "Hydrogels Based on Cellulose and Chitin: Fabrication, Properties, and Applications," *Green Chem.*, **18**, 53 – 75 (2016).
39. Fakrul Alam, A. B. M., and Mondal, M. I. H., "Utilization of Cellulosic Wastes in Textile and Garment Industries. I. Synthesis and Grafting Characterization of Carboxymethyl Cellulose from Knitted Rag," *J. Appl. Polym.*, **128**, 1206 – 1212 (2013).
40. Roy, N., Saha, N., Kitano, T. and Saha, P., "Development and Characterization of Novel Medicated Hydrogels for Wound Dressing," *Soft Mater*., **8**, 130 – 148 (2010).
41. Sadiasa, A., Franco, R. A., Seo, H. S. and Lee, B. T., "Hydroxyapatite Delivery to Dentine Tubules Using Carboxymethyl Cellulose Dental Hydrogel for Treatment of Dentine Hypersensitivity," *J. Biomed. Sci. Eng*., **6**, 9 (2013).
42. Reza, A. T. and Nicoll, S. B., "Characterization of Novel Photocrosslinked Carboxymethyl Cellulose Hydrogels for Encapsulation of Nucleus Pulposus Cells," *Acta Biomater*., **6**, 179 – 186 (2010).

43. Chang, C. and Zhang, L., "Cellulose-based hydrogels: Present Status and Application Prospects," *Carbohydr. Polym.*, **84**, 40 – 53 (2011).
44. Barbucci, R., Magnani, A. and Consumi, M., "Swelling Behavior of Carboxymethyl Cellulose Hydrogels in Relation to Cross-Linking, pH, and Charge Density," *Macromolecules*, **33**, 7475 – 7480 (2000).
45. Nerurkar, N. L., Elliott, D. M. and Mauck, R. L., "Mechanical Design Criteria for Intervertebral Disc Tissue Engineering," *Journal of Biomechanics*, **43**, 1017 – 1030 (2010).
46. Sood, S., Gupta, V. K., Agarwal, S., Dev, K. and Pathania, D., "Controlled Release of Antibiotic Amoxicillin Drug Using Carboxymethyl Cellulose-cl-poly(lactic acid-co-itaconic acid) Hydrogel," *Int. J. Biol. Macromol.*, **101**, 612 – 620 (2017).
47. Teleman, A., Larsson, P. T. and Iversen, T., "On the Accessibility and Structure of Xylan in Birch Kraft Pulp," *Cellulose*, **8**, 209 – 215 (2001).
48. Bigand, V., Pinel, C., Da Silva Perez, D., Rataboul, F., Huber, P., and Petit-Conil, M., "Cationisation of Galactomannan and Xylan Hemicelluloses," *Carbohydr. Polym.*, **85**, 138 – 148 (2011).
49. Hansen, N. M. L. and Plackett, D., "Sustainable Films and Coatings from Hemicelluloses: A Review," *Biomacromolecules*, **9**, 1493 – 1505 (2008).
50. Peng, X-W., Ren, J-L., Zhong, L-X., Peng, F. and Sun, R-C., Xylan-rich "Hemicelluloses-graft-Acrylic Acid Ionic Hydrogels with Rapid Responses to pH, Salt, and Organic Solvents," *J. Agric. Food Chem.*, **59**, 8208 – 8215 (2011).
51. Sun, X-F., Wang, H-H., Jing, Z-X. and Mohanathas, R., "Hemicellulose-based pH-sensitive and Biodegradable Hydrogel for Controlled Drug Delivery," *Carbohydr. Polym.*, **92**, 1357 – 1366 (2013).
52. Sun, X-F., Gan, Z., Jing, Z., Wang, H., Wang, D. and Jin, Y., "Adsorption of Methylene Blue on Hemicellulose-based Stimuli-responsive Porous Hydrogel," *J. Appl. Polym.*, 132 (2015).
53. Dax, D., Chávez, M. S., Xu, C., Willför, S., Mendonça, R. T. and Sánchez, J., "Cationic Hemicellulose-based Hydrogels for Arsenic and Chromium Removal from Aqueous Solutions," *Carbohydr. Polym.*, **111**, 797 – 805 (2014).
54. Ebringerová, A. and Hromádková, Z., "Xylans of Industrial and Biomedical Importance," *Biotechnol. Genet. Eng. Rev.*, **16**, 325 – 346 (1999).

55. Ebringerová, A. and Heinze, T., "Xylan and Xylan Derivatives – Biopolymers with Valuable Properties, 1. Naturally Occurring Xylans Structures, Isolation Procedures and Properties," *Macromol. Rapid Commun.*, **21**, 542 – 556 (2000).
56. Tan, S., Ladewig, K., Fu, Q., Blencowe, A. and Qiao, G. G., "Cyclodextrin-based Supramolecular Assemblies and Hydrogels: Recent Advances and Future Perspectives," *Macromol. Rapid Commun.*, **35**, 1166 – 1184 (2014).
57. Vargas, G., Acevedo, J. L., López, J. and Romero, J., "Study of Cross-linking of Gelatin by Ethylene Glycol Diglycidyl Ether," *Mater. Lett.*, **62**, 3656 – 3658 (2008).
58. Alshehri, S. M., Aldalbahi, A., Al-hajjim A. B., Chaudhary, A. A., Panhuis, M. I. H., Alhokbany, N. and Ahamad, T., "Development of Carboxymethyl Cellulose-based Hydrogel and Nanosilver Composite as Antimicrobial Agents for UTI Pathogens," *Carbohydr. Polym.*, **138**, 229 – 236 (2016).
59. Almeida, J. F., Fonseca, A., Baptista, C. M. S. G., Leite, E. and Gil, M. H., "Immobilization of Drugs for Glaucoma Treatment," *J. Mater. Sci.: Mater. Med.*, **18**, 2309 – 2317 (2007).
60. Choe, D., Kim, Y. M., Nam, J. E., Nam, K., Shin, C. S. and Roh, Y. H., "Synthesis of High-strength Microcrystalline Cellulose Hydrogel by Viscosity Adjustment," *Carbohydr. Polym.*, **180**, 231 – 237 (2018).
61. Liang, X., Qu, B., Li, J., Xiao, H., He, B. and Qian, L., "Preparation of Cellulose-based Conductive Hydrogels with Ionic Liquid," *React. Funct. Polym.*, **86**, 1 – 6 (2015).
62. Davidson, D. W., Verma, M. S. and Gu, F. X., "Controlled Root Targeted Delivery of Fertilizer Using an Ionically Crosslinked Carboxymethyl Cellulose Hydrogel Matrix," *SpringerPlus*, **2**, 318 (2013).
63. Sarkar, D. J. and Singh, A., "Base Triggered Release of Insecticide from Bentonite Reinforced Citric Acid Crosslinked Carboxymethyl Cellulose Hydrogel Composites," *Carbohydr. Polym.*, **156**, 303 – 311 (2017).
64. Wu, S., Yu, F., Dong, H. and Cao, X., "A Hydrogel Actuator with Flexible Folding Deformation and Shape Programming via Using Sodium Carboxymethyl Cellulose and Acrylic Acid," *Carbohydr. Polym.*, **173**, 526 – 534 (2017).
65. Wang, C., Fadeev, M., Zhang, J., Vázquez-González, M., Davidson-Rozenfeld, G., Tian, H. and Willner, I., "Shape-memory and Self-healing Functions of DNA-

based Carboxymethyl Cellulose Hydrogels Driven by Chemical or Light Triggers," *Chem. Sci*., **9**, 7145 – 7152 (2018).

66. Fei, B., Wach, R. A., Mitomo, H., Yoshii, F. and Kume, T., "Hydrogel of Biodegradable Cellulose Derivatives. I. Radiation-induced Crosslinking of CMC," *J. Appl. Polym.*, **78**, 278 – 283 (2000).
67. Ibrahim, S. M., El Salmawi, K. M., and Zahran, A. H., "Synthesis of Crosslinked Superabsorbent Carboxymethyl Cellulose/Acrylamide Hydrogels through Electron-Beam Irradiation," *J. Appl. Polym.*, **104**, 2003 – 2008 (2007).
68. Shang, J., Shao, Z. and Chen, X., "Electrical Behavior of a Natural Polyelectrolyte Hydrogel: Chitosan/Carboxymethylcellulose Hydrogel," *Biomacromolecules*, **9**, 1208 – 1213 (2008).
69. Bajpai, A. K. and Mishra. A., "Carboxymethyl Cellulose (CMC) Based Semi-IPNs as Carriers for Controlled Release of Ciprofloxacine: An In Vitro Dynamic Study," *J. Mater. Sci.: Mater. Med.*, **19**, 2121 – 2130 (2008).
70. Gabrielii, I. and Gatenholm, P., "Preparation and Properties of Hydrogels Based on Hemicellulose," *J. Appl. Polym.*, **69**, 1661 – 1667 (1998).
71. Guan, Y., Zhang, B., Bian, J., Peng, F. and Sun, R-C., "Nanoreinforced Hemicellulose-based Hydrogels Prepared by Freeze–thaw Treatment," *Cellulose*, **21**, 1709 – 1721 (2014).
72. Calvert, P., "Hydrogels for Soft Machines," *Adv. Mater.*, **21**, 743 – 756 (2009).
73. Maleki, L., Edlund, U. and Albertsson, A-C., "Synthesis of Full Interpenetrating Hemicellulose Hydrogel Networks," *Carbohydr. Polym.*, **170**, 254 – 263 (2017).
74. Maleki, L., Edlund, U. and Albertsson, A-C., "Thiolated Hemicellulose As a Versatile Platform for One-pot Click-Type Hydrogel Synthesis," *Biomacromolecules*, **16**, 667 – 674 (2015).
75. Concheiro, A. and Alvarez-Lorenzo, C., "Chemically Cross-linked and Grafted Cyclodextrin Hydrogels: From Nanostructures to Drug-eluting Medical Devices," *Adv. Drug Delivery Rev*., **65**, 1188 – 1203 (2013).
76. Barkhordari, S. and Yadollahi, M., "Carboxymethyl Cellulose Capsulated Layered Double Hydroxides/Drug Nanohybrids for Cephalexin Oral Delivery," *Appl. Clay Sci.*, **121** – **122**, 77-85 (2016).

77. Legnoverde, M. S., Simonetti, S. and Basaldella, E.I., "Influence of pH on Cephalexin Adsorption onto SBA-15 Mesoporous Silica: Theoretical and Experimental Study," *Appl. Surf. Sci.*, **300**, 37 – 42 (2014).
78. Tomić, S. L., Babić, M. M., Antić, K. M., Jovašević Vuković, J. S., Malešić, N. B. and Filipović, J. M., "pH-sensitive Hydrogels Based on (Meth)acrylates and Itaconic Acid," *Macromol. Res.*, **22**, 1203 – 1213 (2014).
79. Pettenuzzo, A., Pigot, R. and Ronconi, L., "Vitamin B_{12}–Metal Conjugates for Targeted Chemotherapy and Diagnosis: Current Status and Future Prospects," *Eur. J. Inorg. Chem.*, **2017**, 1625 – 1638 (2017).
80. Giedyk, M., Goliszewska, K. and Gryko, D., "Vitamin B_{12} Catalysed Reactions," *Chem. Soc. Rev.*, **44**, 3391 – 3404 (2015).
81. Jin, L., Lu, P., You, H., Chen, Q. and Dong, J., "Vitamin B_{12} Diffusion and Binding in Crosslinked Poly(acrylic acid)s and Poly(acrylic acid-co-N-vinyl pyrrolidinone)s," *Int. J. Pharm.*, **371**, 82 – 88 (2009).
82. Okuda, K., "Discovery of Vitamin B_{12} in the Liver and Its Absorption Factor in the Stomach: A Historical Review," *J. Gastroenterol. Hepatol.*, **14**, 301-308 (1999).
83. Dengre, R., Bajpai, M. and Bajpai, S. K., "Release of Vitamin B_{12} from Poly(N-vinyl-2-pyrrolidone)-crosslinked Polyacrylamide Hydrogels: A Kinetic Study," *J. Appl. Polym.*, **76**, 1706 – 1714 (2000).
84. Bajpai, S. K. and Dubey, S., "In Vitro Dissolution Studies for Release of Vitamin B_{12} from Poly(N-vinyl-2-pyrrolidone-co-acrylic acid) Hydrogels," *React. Funct. Polym.*, **62**, 93 – 104 (2005).
85. Maheswari, B., Jagadeesh Babu, P. E. and Agarwal, M., "Role of N-vinyl-2-pyrrolidinone on the Thermoresponsive Behavior of PNIPAm Hydrogel and its Release Kinetics Using Dye and Vitamin-B_{12} as Model Drug," *J. Biomater. Sci., Polym. Ed.*, **25**, 269 – 286 (2014).
86. Boruah, M., Gogoi, P., Manhar, A. K., Khannam, M., Mandal, M. and Dolui, S. K., "Biocompatible Carboxymethyl cellulose-g-poly (acrylic acid)/OMMT Nanocomposite Hydrogel for In Vitro Release of Vitamin B_{12}," *RSC Adv.*, **4**, 43865 – 43873 (2014).

87. Nath, J. and Dolui, S. K., "Synthesis of Carboxymethyl Cellulose-g-poly(acrylic acid)/LDH Hydrogel for In Vitro Controlled Release of Vitamin B_{12}," *Appl. Clay Sci.*, **155**, 65 – 73 (2018).

88. Cao, X., Peng, X., Zhong, L. and Sun, R., "Multiresponsive Hydrogels Based on Xylan-type Hemicelluloses and Photoisomerized Azobenzene Copolymer as Drug Delivery Carrier," *J. Agric. Food Chem.*, **62**, 10000-10007 (2014).

89. Jang, S. H., Min, B. G., Jeong, Y. G., Lyoo, W. S. and Lee, S. C., "Removal of Lead Ions in Aqueous Solution by Hydroxyapatite/Polyurethane Composite Foams," *J. Hazard. Mater*., **152**, 1285 – 1292 (2008).

90. Månsson, N., Bergbäck, B. and Sörme, L., "Phasing Out Cadmium, Lead, and Mercury," *J. Ind. Ecol.*, **13**, 94 – 111 (2009).

91. Martinková, E., Chrastný, V., Francová, M., Šípková, A., Čuřík, J., Myška, O. and Mižič, L., "Cadmium Isotope Fractionation of Materials Derived from Various Industrial Processes," *J. Hazard. Mater*., **302**, 114 – 119 (2016).

92. Choi SB, Yun Y-S. "Biosorption of Cadmium by Various Types of Dried Sludge: An Equilibrium Study and Investigation of Mechanisms," *J. Hazard. Mater*., **138**, 378 – 383 (2006).

93. Gobrecht, J., McDyre, C., Comotto, J. and Reynolds, M., "Induction of Cytotoxic and Genotoxic Damage Following Exposure of V79 Cells to Cadmium Chloride," *Mutation Research/Genetic Toxicology and Environmental Mutagenesis*, **816-817**, 12 – 17 (2017).

94. Karbarz, M., Khalil, A. M., Wolowicz, K., Kaniewska, K., Romanski, J. and Stojek, Z., "Efficient Removal of Cadmium and Lead Ions from Water by Hydrogels Modified with Cysteine," *J. Environ. Chem. Eng.*, **6**, 3962 – 3970 (2018).

95. Jia, Q., Li, D., Gao, X., Yan, J., Ma, Q. and Meng, F., "Hydrazinolyzed Cellulose-g-polymethyl Acrylate as Adsorbent for Efficient Removal of Cu(II) and Ni(II) ions from Aqueous Solution," *J. Chem. Technol. Biotechnol.*, **91**, 1378 – 1386 (2016).

96. He, S., Zhang, F., Cheng, S. and Wang, W., "Synthesis of Sodium Acrylate and Acrylamide Copolymer/GO Hydrogels and Their Effective Adsorption for Pb^{2+} and Cd^{2+}," *ACS Sustainable Chem. Eng.*, **4**, 3948 – 3959 (2016).

97. El-Naggar, A. A., "Radiation Synthesis of Superabsorbent Hydrogels Based on Carboxymethyl Cellulose/sodium Alginate for Absorbent of Heavy Metal Ions from Waste Water," *J. Thermoplast. Compos. Mater.*, **29**, 16 – 27 (2016).

98. Wang, L-Y. and Wang, M-J., "Removal of Heavy Metal Ions by Poly(vinyl alcohol) and Carboxymethyl Cellulose Composite Hydrogels Prepared by a Freeze–Thaw Method," *ACS Sustainable Chem. Eng.*, **4**, 2830 – 2837 (2016).

99. Zhu, Y., Zheng, Y., Wang, F. and Wang A., "Fabrication of Magnetic Macroporous Chitosan-g-poly(acrylic acid) Hydrogel for Removal of Cd^{2+} and Pb^{2+}," *Int. J. Biol. Macromol.*, **93**, 483 – 492 (2016).

100. Mohamed, M. A., Abd Mutalib, M., Mohd Hir, Z. A., M. Zain, M. F., Mohamad, A. B., Jeffery Minggu, L., Awang, N. A. and Salleh, W. N. W., "An Overview on Cellulose-based Material in Tailoring Bio-hybrid Nanostructured Photocatalysts for Water Treatment and Renewable Energy Applications," *Int. J. Biol. Macromol.*, **103**, 1232 – 1256 (2017).

101. Jiao, C., Tao, J., Xiong, J., Wang, X., Zhang, D., Lin, H. and Chen, Y., "In Situ Synthesis of MnO_2-loaded Biocomposite Based on Microcrystalline Cellulose for Pb^{2+} Removal from Wastewater," *Cellulose*, **24**, 2591 – 2604 (2017).

102. Elgueta, E., Sánchez, J., Dax, D., Xu, C., Willför, S., Rivas, B. L. and González, M., "Functionalized Galactoglucomannan-based Hydrogels for the Removal of Metal Cations from Aqueous Solutions," *J. Appl. Polym.*, 133 (2016).

103. Wang, F. P., Li, G. F., Zhou, Q. Q., Yang, C. X. and Wang, Q. Z., "Removal of Metal Ions from Aqueous Solution with *β*-Cyclodextrin-based Hydrogels," *Mater. Express*, **6**, 394 – 402 (2016).

104. Zhou, J., Zhang, L., Deng, Q. and Wu, X., "Synthesis and Characterization of Cellulose Derivatives Prepared in NaOH/Urea Aqueous Solutions," *J. Polym. Sci., Part A: Polym. Chem.*, **42**, 5911 – 5920 (2004).

105. Swamy, B. Y. and Yun, Y-S., "In Vitro Release of Metformin from Iron (III) Cross-linked Alginate–carboxymethyl Cellulose Hydrogel Beads," *Int. J. Biol. Macromol.*, **77**, 114 – 119 (2015).

106. Gao, X., Cao, Y., Song, X., Zhang, Z., Zhuang, X., He, C. and Chen, X., "Biodegradable, pH-Responsive Carboxymethyl Cellulose/Poly(acrylic acid) Hydrogels for Oral Insulin Delivery," *Macromol. Biosci.*, **14**, 565 – 575 (2014).

107. Dutta, S., Samanta, P. and Dhara, D., "Temperature, pH and Redox Responsive Cellulose Based Hydrogels for Protein Delivery," *Int. J. Biol. Macromol.*, **87**, 92 – 100 (2016).

108. Sekkal, M., Dincq, V., Legrand, P. and Huvenne, J. P., "Investigation of the Glycosidic Linkages in Several Oligosaccharides Using FT-IR and FT Raman Spectroscopies," *J. Mol. Struct*., **349**, 349 – 352 (1995).

109. Sun, X. F., Sun, R. C., Fowler, P. and Baird, M. S., "Isolation and Characterization of Cellulose Obtained by a Two-stage Treatment with Organosolv and Cyanamide Activated Hydrogen Peroxide from Wheat Straw," *Carbohydr. Polym.* **55**, 379-391 (2004).

110. Na, N., Hu, Y., Ouyang, J., Baeyens, W. R. G., Delanghe, J. R., Taes, Y. E. C., Xie, M., Chen, H. and Yang, Y., "On the Use of Dispersed Nanoparticles Modified with Single Layer *β*-cyclodextrin as Chiral Selecor to Enhance Enantioseparation of Clenbuterol with Capillary Electrophoresis" *Talanta*, **69**, 866-872 (2006).

111. Ahemen, I., Meludu, O., Odoh, E., "Effect of Sodium Carboxymethyl Cellulose Concentration on the Photophysical Properties of Zinc Sulfide Nanoparticles," *Br. J. Appl. Sci. Technol.*, **3**, 1228-1245 (2013).

112. Yin, Y., Berglund, L. and Salmén, L., "Effect of Steam Treatment on the Properties of Wood Cell Walls," *Biomacromolecules*, **12**, 194-202 (2011).

113. Krishnaiah, Y. S. R., Satyanarayana, S., Rama Prasad, Y. V. and Narasimha Rao, S., "Gamma Scintigraphic Studies on Guar Gum Matrix Tablets for Colonic Drug Delivery in Healthy Human Volunteers," *J. Controlled Release*, **55**, 245 – 252 (1998).

114. Alekseev, V. G., Nikiforova, A. A. and Markelova, S. V., "Reaction of Cefalexine with Manganese(II), Cobalt(II), Nickel(II), Zinc(II), and Cadmium(II) ions," *Russ. J. Gen. Chem.*, **76**, 1468 – 1470 (2006).

115. Nazari, G., Abolghasemi, H. and Esmaieli, M., "Batch Adsorption of Cephalexin Antibiotic from Aqueous Solution by Walnut Shell-based Activated Carbon," *J. Taiwan Inst. Chem. Eng.*, **58**, 357 – 365 (2016).

116. Xu, X., Fu, S., Wang, K., Jia, W., Guo, G., Zheng, X., Dong, P., Guo, Q. and Qian, Z., "Preparation and Characterization of Vitamin-12 Loaded Biodegradable pH-Sensitive Microgels," *J. Microencapsulation*., **26**, 642 – 648 (2009).

117. Bajpai, S. and Dubey, S., "Modulation of Dynamic Release of Vitamin B_2 from a Model pH-sensitive Terpolymeric Hydrogel System," *Polym Int*., **53**, 2178 – 2187 (2004).
118. Maity, J. and Ray, S. K., Competitive Removal of Cu (II) and Cd (II) from Water Using a Biocomposite Hydrogel," *J. Phys. Chem. B*, **121**, 10988-11001 (2017).
119. Nikonenko, N. A., Buslov, D. K., Sushko, N. I. and Zhbankov, R. G., "Investigation of Stretching Vibrations of Glycosidic Linkages in Disaccharides and Polysaccarides with Use of IR Spectra Deconvolution," *Biopolymers*, **57**, 257 – 262 (2000).
120. Kistamah, N., Carr, C. M. and Rosunee, S., "X-ray Photoelectron Spectroscopic Study of Tencel Treated with a Cationic *β*-Cyclodextrin Derivative," *Surf. Interface Anal*., **41**, 710 – 713 (2009).
121. Jing, Z., Zhang, G., Sun, X-F., Shi, X. and Sun, W., "Preparation and Adsorption Properties of a Novel Superabsorbent Based on Multiwalled Carbon Nanotubes–xylan Composite and Poly(methacrylic acid) for Methylene Blue from Aqueous Solution," *Polym. Compos*., **35**, 1516 – 1528 (2014).
122. Bhatluri, K. K., Manna, M. S., Ghoshal, A. K. and Saha, P., "Supported Liquid Membrane Based Removal of Lead (II) and Cadmium (II) from Mixed Feed: Conversion to Solid Waste by Precipitation," *J. Hazard. Mater*., **299**, 504-512 (2015).
123. Langmuir, I., "The Adsorption of Gases on Plane Surfaces of Glass, Mica and Platinum," *J. Am. Chem. Soc*., **40**, 1361 – 1403 (1918).
124. Ali, S. A., Al Hamouz, O. C. S. and Hassan, N. M., "Novel Cross-linked Polymers Having pH-responsive Amino Acid Residues for the Removal of Cu^{2+} from Aqueous Solution at Low Concentrations," *J. Hazard. Mater*., **248-249**, 47 – 58 (2013).
125. Kundu, S. and Gupta, A. K., "Arsenic Adsorption onto Iron Oxide-coated Cement (IOCC): Regression Analysis of Equilibrium Data with Several Isotherm Models and Their Optimization," *Chem. Eng. J.*, **122**, 93 – 106 (2006).
126. Vijayaraghavan, K., Padmesh, T. V. N., Palanivelu, K. and Velan, M., "Biosorption of Nickel(II) Ions onto Sargassum Wightii: Application of Two-parameter and Three-parameter Isotherm Models, " *J. Hazard. Mater.*, **133**, 304 – 308 (2006).

127. Lagergren, S., "About the theory of so called adsorption of soluble substances," *K. Sven. Vetenskapsakad. Handl.*, **24**, 1 – 39 (1898).

128. Ho, Y. S., Wase, D. A. J. and Forster, C. F., "Kinetic Studies of Competitive Heavy Metal Adsorption by Sphagnum Moss Peat, " *Environ. Technol.*, **17**, 71 – 77 (1996).

129. Ali, R. M., Hamad, H. A., Hussein, M. M. and Malash, G. F., "Potential of Using Green Adsorbent of Heavy Metal Removal from Aqueous Solutions: Adsorption Kinetics, Isotherm, Thermodynamic, Mechanism and Economic Analysis," *Ecological Engineering*, **91**, 317 – 332 (2016).

130. Rajesh, Y., Pujari, M. and Uppaluri, R., "Equilibrium and Kinetic Studies of Ni (II) Adsorption Using Pineapple and Bamboo Stem Based Adsorbents," *Sep. Sci. Technol.*, **49**, 533 – 544 (2014).

131. Jossens, L., Prausnitz, J. M., Fritz, W., Schlünder, E. U. and Myers, A. L., "Thermodynamics of Multi-solute Adsorption from Dilute Aqueous Solutions," *Chem. Eng. Sci*., **33**, 1097 – 1106 (1978).

132. Gusain, D., Srivastava, V. and Sharma, Y. C., "Kinetic and Thermodynamic Studies on the Removal of Cu(II) Ions from Aqueous Solutions by Adsorption on Modified Sand," *J. Ind. Eng. Chem.*, **20**, 841 – 847 (2014).

Appendix A: List of publications & conference presentations

List of publications

1. ***Debashis Kundu*** and Tamal Banerjee. Carboxymethyl cellulose-xylan hydrogel: Synthesis, characterization and *in vitro* release of Vitamin B_{12}. **ACS Omega** 2019, 4, 4793−4803.
2. ***Debashis Kundu***, Supriyo Kumar Mondal and Tamal Banerjee. Development of *β*-cyclodextrin-cellulose/hemicellulose based hydrogels for the removal of Cd (II) and Ni (II): Synthesis, Kinetics and Adsorption Aspects**. Journal of Chemical and Engineering Data** 2019, 64, 2601-2617.
3. ***Debashis Kundu*** and Tamal Banerjee. Development of microcrystalline cellulose based hydrogels for the *in vitro* release of Cephalexin. (under review)

List of conference presentations

1. ***Debashis Kundu*** and Tamal Banerjee. Development of Carboxymethyl Cellulose-xylan Based Hydrogels. ***International Conference on Complex and Functional Materials*** (ICCFM 2018), 13th - 16th December, 2018, S. N. Bose Centre for Basic Sciences, Kolkata, West Bengal, India. (**Poster presentation**)
2. ***Debashis Kundu*** and Tamal Banerjee. Development of Microcrystalline Cellulose Based Hydrogels. ***International Conference on Synthetic Potent Molecule and Its Application*** (ICSPMIA- 2018), 30th - 31st October, 2018, Sikkim Manipal Institute of Technology, Majhitar, Sikkim, India. (**Oral presentation**)
3. ***Debashis Kundu*** and Tamal Banerjee. Development of Cyclodextrin-cellulose/hemicellulose Based Hydrogels for the Removal of Cd(II) and Ni(II). ***International Conference on Advancement in Science & Technology*** (ICAST-2018), 3rd - 4th September, 2018, Visva-Bharati University, Santiniketan, West Bengal, India. (**Poster presentation**)

ACS OMEGA

Article

Cite This: ACS Omega 2019, 4, 4793−4803

http://pubs.acs.org/journal/acsodf

Carboxymethyl Cellulose−Xylan Hydrogel: Synthesis, Characterization, and in Vitro Release of Vitamin B_{12}

Debashis Kundu and Tamal Banerjee*

Department of Chemical Engineering, Indian Institute of Technology Guwahati, Guwahati 781039, Assam, India

Supporting Information

ABSTRACT: The current work reports the synthesis of carboxymethyl cellulose (CMC) and xylan-based homopolymerized as well as copolymerized hydrogels using an ethylene glycol diglycidyl ether cross-linker in alkaline medium. The hydrogels are physically characterized by the swelling ratio and gel fraction. The morphological observation of hydrogels reveals the porous structure for the copolymerized gels. The rheological behavior of the gels elaborates that the copolymerized CMC−xylan gel synthesized in a 1:1 molar ratio has superior strain-bearing ability and possesses the shortest gelation temperature and time. Vitamin B_{12} here is used as the model vitamin to be loaded in the hydrogels and subsequent studies involving the in vitro release in artificial gastric fluid (AGF, pH = 1.2), artificial intestinal fluid (AIF, pH = 6.8), and phosphate-buffered saline (PBS, pH = 7.4). The synthesized gels show a cumulative release of 19−28% in AGF, 80−88% in AIF, and 93−98% in PBS, independently. Further, the highest cumulative release of 93−99% is recorded for all gels when in vitro release is performed in successive buffers, that is, first in AGF, followed by AIF and PBS.

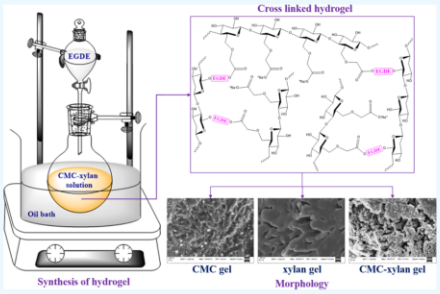

1. INTRODUCTION

Hydrogels are physical or chemical cross-linked three-dimensional polymer networks which swell upon absorbing water but do not dissolve in it. The network often mimics the extracellular matrix and is thus widely used in drug delivery, tissue engineering, and other biological applications.[1] The shape and volume of hydrogels can be reversibly changed upon various external stimuli such as pH, temperature, light, electric and magnetic fields. Polysaccharides are renewable natural polymers bearing the advantages which include nontoxicity, biocompatibility, biodegradability, and natural abundance. The ease of functionalization or chemical cross-linking of the hydroxyl moieties present in the backbone of polysaccharides make them attractive precursors for hydrogels.

Carboxymethyl cellulose (CMC) is a water-soluble derivative of cellulose in which some of the hydroxyl moieties are replaced by carboxymethyl moiety. It is conveniently produced by the alkali-catalyzed reaction between cellulose and chloroacetic acid. It is widely used as thickener, viscosity modifier, emulsion stabilizer, and water retention agent in paint, cosmetic, and food industries. Low immunogenicity, high biocompatibility, and biodegradability make it a potential carrier for controlled release or site-specific drug delivery.[2,3] For this, it got approval from FDA for biomedical applications.[4] CMC is also used as a precursor for stimuli-responsive hydrogels. The carboxymethyl group adds a negative charge to the pyranose backbone, and it significantly increases the cross-linking points and reactive sites. Thus, thermal radical reactions are often employed with the cross-linker to prepare CMC-based homopolymer and copolymer hydrogels.[5,6] Overall, the CMC-based hydrogels are used as carriers for drugs and biological macromolecules.[7]

Xylan is a heteropolysaccharide consisting of pentoses and hexoses. It belongs to the hemicellulose family and found in most abundant quantity in the family. Xylan consists of 80−200 D-xylopyranosyl residues as backbone, which are connected by β-(1 → 4) glycosidic bonds.[8] The backbone is linked with the *O*-acetyl, glucoronic acid side groups.[9] Xylan is obtained from hardwood by the alkali extraction method. Like cellulose, hemicellulose as well as xylan can be easily functionalized because of the abundance of the hydroxyl moiety. The various subclasses of hemicellulose are used as thickeners, emulsifiers, coatings, and additives in paper, food, and pharmaceutical industries.[10,11] Recently, xylan-based hydrogels have gained attention because of the multiresponsive behavior toward pH, organic solvents, and ions. A good number of literature is available for the xylan-based hydrogels as carriers for drug and biological macromolecules[12] and sorbents for heavy metal ions and organic dyes.[13,14]

Vitamin B_{12} (VB_{12}, cyanocobalamin) is the largest and the most complex in the vitamin family. It is an organometallic compound containing cobalt within a corrin ring. The main residues are corrin ring, propyl side chain, ribose group, and dimethylbenzimidazole. Because of its low bioavailability (recommended 1−5 μg per day), it is considered as an essential

Received: December 30, 2018
Accepted: February 20, 2019
Published: March 4, 2019

DOI: 10.1021/acsomega.8b03671
ACS Omega 2019, 4, 4793−4803

Journal of chemical & engineering data

Article

Cite This: J. Chem. Eng. Data 2019, 64, 2601−2617

pubs.acs.org/jced

Development of β-Cyclodextrin-Cellulose/Hemicellulose-Based Hydrogels for the Removal of Cd(II) and Ni(II): Synthesis, Kinetics, and Adsorption Aspects

Debashis Kundu, Supriyo Kumar Mondal, and Tamal Banerjee*

Department of Chemical Engineering, Indian Institute of Technology Guwahati, Guwahati 781039, Assam, India

Supporting Information

ABSTRACT: Carboxymethyl cellulose (CMC), microcrystalline cellulose (MCC), and xylan are cross-linked with β-cyclodextrin (βCD) using ethylene glycol diglycidyl ether cross-linker to produce hydrogels, namely, βCD-CMC, βCD-MCC, and βCD-xylan, in alkaline medium at 1:1 mole ratio. Additionally pure βCD gel is also prepared in alkaline medium. The synthesized hydrogels are characterized by Fourier transform infrared spectroscopy, and the swelling ratio, gel fraction, and the morphologies are observed by a microscope. The hydrogels are used to adsorb cadmium (Cd(II)) and nickel (Ni(II)) ions from aqueous solution. The adsorption studies are carried out by varying adsorbent dosage from 80 to 500 mg, concentration from 5 to 500 mg L^{-1}, pH from 2 to 8, and temperature from 25 to 55 °C. The equilibrium adsorption data closely follow the Langmuir model, suggesting the monolayer adsorption of metal ions by the hydrogels. The adsorption kinetics are found to closely follow the pseudo-second-order model.

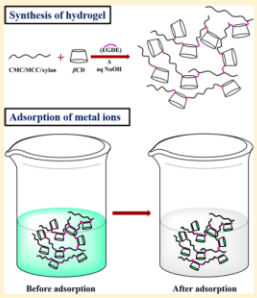

1. INTRODUCTION

Hydrogel is three-dimensional network containing a large amount of water. Natural or synthetic biopolymers often initiate via physical or chemical cross-linking to create network gel. The components are often biocompatible, resulting in widespread use of hydrogel in tissue engineering,[1] drug delivery,[2] biomedical applications,[3] etc. Apart from the conventional applications, hydrogels are used in sensors and actuators,[4] metal-ion removal,[5] and dye removal.[6] Polysaccharides and oligosaccharides are considered as suitable materials for hydrogel because of abundance of hydroxyl groups, which can be either physically cross-linked via van der Waals or hydrogen-bonding interaction or functionalized for chemical cross-linking. Being naturally abundant, biocompatible, and biodegradable, polysaccharides hold advantages over synthetic polymers with respect to the preparation of hydrogel.[7]

Cellulose, homopolysaccharide in nature, exhibits low density, high strength, and high stiffness due to the inherent crystallinity.[8] However, crystallinity of cellulose limits its application due to its insolubility in water and common organic solvents. Several solvents, namely, polar solvent, ionic liquid, deep eutectic solvent, and alkali aqueous system,[9] have been employed to solubilize cellulose. This enables cellulose-based hydrogel to be prepared from cellulose solution via chemical or physical cross-linking process. Carboxymethyl cellulose (CMC) is a water-soluble derivative of cellulose and is a linear polymer. Low immunogenicity, high biocompatibility, and biodegradability make CMC an attractive material for biomedical and pharmaceutical applications.[10,11] Cross-linked CMC is known to absorb a large amount of water to form biocompatible and pH-sensitive hydrogel.[12] Hemicellulose is a heteropolysaccharide with various types of hexose and pentose sugar and is amorphous in nature. Xylan constitutes 25−35% of hemicellulose class[13] and is found in hard wood species. It consists of β-1,4-D-xylopyranosyl unit as a backbone with a low degree of polymerization of 200.[14] Further, it contains 10% 4-*O*-methyl-D-glucoronic acid and β-1,4-D-xylopyranosyl units as backbone.[15] Cyclodextrin (CD) is a toroid-shaped oligosaccharide with 6, 7, and 8 D-glucose units covalently connected by α-1,4-glucosidic linkages. Depending upon the number of units, it is classified as α- (6 units), β- (7 units), and γ- (8 units) CD. Primary hydroxyl groups of CD are located at the narrower, i.e., primary, face, and secondary hydroxyl groups are located at the wider, i.e., secondary, face.[16] This structural formation makes the exterior of CD hydrophilic and interior hydrophobic. CDs have found extensive applications in pharmacy, textile, food, and packaging industries. CD-based hydrogel can be synthesized by facile functionalization or chemical cross-linking with primary or secondary hydroxyl moieties.

Nickel (Ni(II)) and cadmium (Cd(II)) are toxic contaminants that can cause severe damage in human and aquatic life after being accumulated in high concentrations. Cadmium is commonly used in batteries, and coating and painting industries.[17−19] It is carcinogenic, causes iron deficiency,[20] and accumulates in liver and kidney.[21] Nickel comes out as pollutant from electroplating, metal finishing, and battery

Received: January 27, 2019
Accepted: May 17, 2019
Published: May 30, 2019

DOI: 10.1021/acs.jced.9b00088
J. Chem. Eng. Data 2019, 64, 2601−2617